The American Mineralogist

Journal of the Mineralogical Society of America

VOL. 46 SEPTEMBER–OCTOBER, 1961 Nos. 9 and 10

Contents

(*Continued on Cover 2*)

Published bi-monthly by the Society

Mineralogical Society of America

The enlarged issues of this journal for 1961 are made possible by a grant from the Penrose Fund of the Geological Society of America.

The American Mineralogist—Journal of the Mineralogical Society of America

The journal, containing articles on mineralogy, crystallography, and allied sciences, is issued every two months. Contributions are invited.

The general conduct of the journal is in the hands of the editor, Lewis S. Ramsdell, Department of Mineralogy, University of Michigan, to whom all manuscripts should be submitted.

Second class postage paid at Menasha, Wis., under Act of March 3, 1879. Acceptance for mailing at the special rate of postage provided for in section 1103, Act of Oct 3, 1917, paragraph 4 section 429 P. L. & R. authorized March 13, 1922.

Notice of change of address, orders, and remittances should be sent to Marjorie Hooker, c/o U. S. Geological Survey, Washington 25, D. C.

Printed by George Banta Company, Inc., Menasha, Wisconsin
Printed in the United States of America

IRST: LOOK AT UNITRON'S NEW POLARIZING MICROSCOPE

Here is a precision measuring instrument for both orthoscopic and conoscopic observations, designed to meet the exacting requirements of science, education, and industry. Its many features make it ideal for work in chemistry, crystallography, mineralogy and biology as well as in the technology of paper, glass, textiles and petroleum.

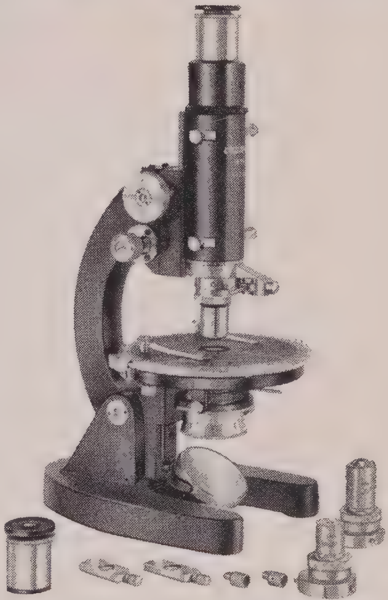

IECK THESE OPTICAL & MECHANICAL FEATURES

Note that UNITRON'S new Model MPS comes complete with optics and accessories and includes features usually associated only with much more costly models.

- **EYEPIECES:** Micro 5X providing measurements to 0.0025mm. and cross-hair 10X. The eye lenses focus to produce sharp reticle images and are keyed to prevent rotation.
- **OBJECTIVES:** 4X(N.A.0.1), 10X(N.A.0.25), 40X(N.A.0.65), achromatic, strain-free, each with centerable mount.
- **NOSEPIECE:** quick-change type for critical centering.
- **CONDENSER and POLARIZER:** three-lens condenser with upper elements on a swing-out mounting, provides either parallel or convergent light. A dovetail-slide focusing mount and iris diaphragm insure optimum illumination and resolution.
- **POLAROID POLARIZER:** rotatable through 360° and graduated every 45°. Plano-concave mirror.
- **ANALYZER:** Polaroid, in sliding metal mount.
- **BERTRAND LENS:** for the study of interference figures, fixed-focus lens is centerable and mounted in a slideway.
- **STAGE:** diameter 115mm., revolves through 360°, graduated in degrees and reads to 6' with vernier. The top is calibrated in mms. in two directions and is drilled and tapped for an accessory mechanical stage. Stage clips.
- **COMPENSATORS:** two compensators are included; a quarter-wave plate and first order red plate. These fit into a slot above the objective lens.
- **FOCUSING:** coarse and micrometric fine adjustments.
- **STAND:** heavy stand, arm inclines to horizontal position.

1 Iris diaphragm
2 Polarizer
3 Swing-out lever
4 Focusing lock
5 Focusing slide

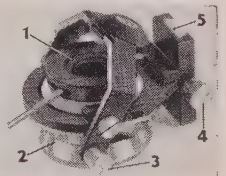

Condenser and Polarizer

IEN: LOOK AT THE PRICE!

Model MPS complete as described, in fitted cabinet.	$269 FOB BOSTON
Quantity prices on three or more.	
Accessory mechanical stage. . . .	$14.75

AVAILABLE ON FREE 10 DAY TRIAL

Send for complete catalog on UNITRON Microscopes.

UNITRON

Instrument Company, Microscope Sales Division
66 Needham St., Newton Highlands 61, Mass.

Please rush UNITRON Catalog on Microscopes. 41

Name ____________________
Company ____________________
Address ____________________
City ____________ State ____________

HE TREND IS TO UNITRON


Leitz

The Mineralogical Society of America, in sorting out its stock of back issues of the AMERICAN MINERALOGIST, finds that it has a few copies of out-of-print issues. These are listed below and are available at the prices given. Postage is additional.

Older issues:

Volume	1, no. 6 (with index to volume), December 1916	$ 2.00
	2, no. 9, September 1917	2.00
	3, no. 6, (Renée—Just Haüy issue), June 1918	3.00
	3, no. 12 (with index to volume), December 1918	2.00
	5, nos. 1, 2, 3, 4, 5, 7, 10, 11, 12, 1920	2.00 each

Complete volumes:

Volume	20, 1935	$25.00
	21, 1936	25.00
	22, 1937 (includes Palache issue)	35.00
	23, 1938	25.00
	32, 1947	25.00

Separate issues:

Volume	22, no. 5, May 1937 (Palache issue)	$20.00
	29, no. 9-10, September-October 1944	5.00
	11-12, November-December 1944	5.00
	30, no. 7-8, July-August 1945	5.00
	31, no. 3-4, March-April 1946	5.00
	32, no. 3-4, March-April 1947	5.00

Complete sets of the American Mineralogist are available with out-of-print issues supplied in microtext, with the exception of the special Palache issue (May, 1937, Vol. 22) which is available only on special order in a full size Xerox reproduction. See page xii in the March-April, 1961, issue for prices.

Send your order to the Treasurer, Marjorie Hooker
Mineralogical Society of America
U. S. Geological Survey
Washington 25, D.C.

'HE AMERICAN MINERALOGIST

JOURNAL OF THE MINERALOGICAL SOCIETY OF AMERICA

ol. 46 SEPTEMBER–OCTOBER, 1961 Nos. 9 and 10

IDENTIFICATION OF CLAY MINERALS BY SINGLE CRYSTAL ELECTRON DIFFRACTION*

G. W. BRINDLEY AND C. DE KIMPE,† *Department of Ceramic Technology, The Pennsylvania State University, University Park, Pennsylvania.*

ABSTRACT

Procedures for identifying clay minerals by means of single crystal electron diffraction tterns obtained with electron microscope-electron diffraction equipment without tilt ijustment of the crystals, are examined critically. In a few special but highly important es, E.D. patterns and micrographs are characteristic of particular minerals. Generally, ys and related layer silicates give closely similar hexagonal patterns. It is shown that ntification is not feasible from observations of intensity distributions nor on the basis of gular relations, but partial identification is possible from accurate measurements of *b* ameters. By using aluminum metal as an internal standard, parameters accurate to ?% are obtained.

INTRODUCTION

Although electron microscopy has been applied extensively to morphogical studies of clay minerals, electron diffraction is seldom used as a neral tool, probably because *x*-ray powder techniques provide adequate entification procedures. In particular centers of research, electron ffraction studies of minerals, including clay minerals, have been underken and references to this work will be made later. In the field of clay ineralogy, electron diffraction and particularly single crystal diffracon has important advantages over other methods of investigation, as e following examples illustrate:

(*a*) In all cases where the identity of an individual clay crystal is imrtant, electron diffraction provides the only method for its identificaon. For example, in the synthesis of clay minerals from gels the develment of crystalline forms can be observed microscopically at a stage uch earlier than crystalline products can be detected by *x*-rays (Gasche and De Kimpe, 1959).

* Contribution No. 60-26 from the College of Mineral Industries, The Pennsylvania ate University, University Park, Pa.

† On leave of absence from the Laboratoire des Colloides des Sols Tropicaux, Institut ronomique, Louvain, Belgium.

(*b*) Correlation of crystal growth and morphology with crystal structure for micron-sized particles can be studied by combined electron microscopy and electron diffraction. Such information is very rarely accessible to *x*-ray study.

(*c*) In studying the thermal decomposition reactions of fine-grained minerals, E.D. patterns may supply clear information when *x*-ray powder diffraction yields poor and inconclusive results. Studies of partially crystallized phases often yield clearer results by electron diffraction than by *x*-ray powder diffraction. An early study of this type was made by Eitel *et al.* (1944), and the work of Roy *et al.* (1955) on metakaolin, and o Brindley and Choe (1961) on the decomposition products of alumina hydrates provides further illustrations.

(*d*) Crystal structure analysis from single crystal E.D. patterns ha been developed particularly by Cowley and by Russian workers. The following papers may be cited as being representative of work in thi area: Cowley (1953), Cowley and Rees (1958), Pinsker (1949, 53) Vainshtein (1956), Pinsker and Vainshtein (1957, 58), Zviagin (1957 58), Popov and Zviagin (1958, 60), Zviagin (1960), Zviagin and Mishchenko (1960).

(*e*) A further application of single crystal E.D. methods to clay mineral study lies in the identification of minor impurities. Contaminant present to the extent of about 1% or less will seldom be recognized in *x*-ray powder diagrams. If the impurities have a distinctive appearance in the electron microscope, then identification by electron diffraction may be possible. Even when impurities are present in clays to a considerably greater extent than 1%, they may still escape detection in *x*-ray identification. Probably as much as 10% of halloysite, or even a higher percentage, in the presence of kaolinite could escape detection by *x*-ray method because of the similarity and overlapping of the patterns but electron microscope and diffraction techniques would give a clear identification (See Brindley and Comer, 1956).

In view of the numerous potential applications of electron diffractio to the study of clay mineral crystals, an investigation was undertaken o methods for identifying single crystals of clay minerals by means of E.D patterns. The results show that although there are considerable difficulties arising from the structural similarities of many of the clay minerals, certain features of the patterns permit a partial identification.

Experimental Procedures

Since it will usually be desirable to examine the morphology of cla particles and to select particular crystals for diffraction study, an instrument which combines the possibilities of electron microscopy wit

selected area diffraction will generally be preferred. On the other hand, nstruments designed primarily as diffraction cameras with little or no provision for use as microscopes may have advantages for tilting and adusting the crystals under examination, but it is a serious disadvantage if he individual crystal cannot be selected visually. These techniques have been discussed recently by Ross and Christ (1958) and by Ross (1959) n relation to mineral studies.

In the present investigation, an R.C.A. electron microscope, type EMU-2D, fitted with a diaphragm for selected area study, has been employed. There was no provision for precise orientational adjustment of he crystals, which were examined in the orientation they adopted on the tage of the instrument, *i.e.*, essentially normal to the electron beam. The ecorded patterns are 5×5 cm. in size and can be measured to give attice spacings accurate to about 0.2% from single crystal spot patterns when an internal calibration standard is employed.

Specimen preparation is essentially the same as for the electron micros-opy of clays, but to obtain isolated crystals it is desirable to have well ispersed samples somewhat more dilute than those generally used for microscopy. Aluminum metal has been used as an internal standard; 2.4 g. of pure aluminum is evaporated under vacuum on to the sample mounted on a collodion film at a distance of about 10–11 cm. The estimated thickness of the metal is about 60 Å. The resulting photographs how a spot pattern from the clay crystal with a superimposed ring pat-ern from the aluminum. The patterns are measured directly after en-rgement to about 50×50 cms. by projection. The positions of individual pots cannot be fixed directly with any accuracy, but when the entire net-ork of spots is carefully ruled out, the pattern can be measured accu-tely and (with certain reservations discussed later) spacings can be ob-ined to within 0.2%.

Identification Procedures

) *Clay minerals giving easily recognized E.D. patterns*

A few clay minerals give patterns which are immediately diagnostic. alloysite has a characteristic tubular or rolled sheet morphology and e E.D. pattern often resembles an *x*-ray rotation diagram. These pat-rns have been discussed by Honjo *et al.* (1954). However, it appears at hexagonal spot patterns may also be obtained from halloysite, posoly from fractured tubes or from thin portions of tubes lying more or s normal to the electron beam. Sepiolite has a fibrous morphology and E.D. pattern differs from those of other clay minerals (Brindley, 59). An unusual E.D. pattern for a chlorite has been reported by khardt (1958), but most chlorites appear to give hexagonal spot pat-

terns (c.f. Figure 2). Antigorite is platy or lath-like, and single crystal patterns are characterized by a long a parameter ranging from about 33 to 43 Å; for some crystals values of 90–110 Å have been obtained. These features of antigorite are easily recognized in single crystal E.D. patterns, but are not easily recognized by x-ray powder diagrams, (Zussman, Brindley, and Comer, 1957). Such highly characteristic E.D. patterns, which are recognizable at sight, are notable exceptions to the results obtained generally for clay minerals.

(*b*) *Identification based on diffracted intensities*

Different clay minerals, having different crystal structures, would be expected to give characteristic distributions of diffracted intensities. In fact, most clay minerals and related layer lattice silicates give very similar hexagonal spot patterns with the experimental conditions employed. Figures 1 and 2 show some typical results.

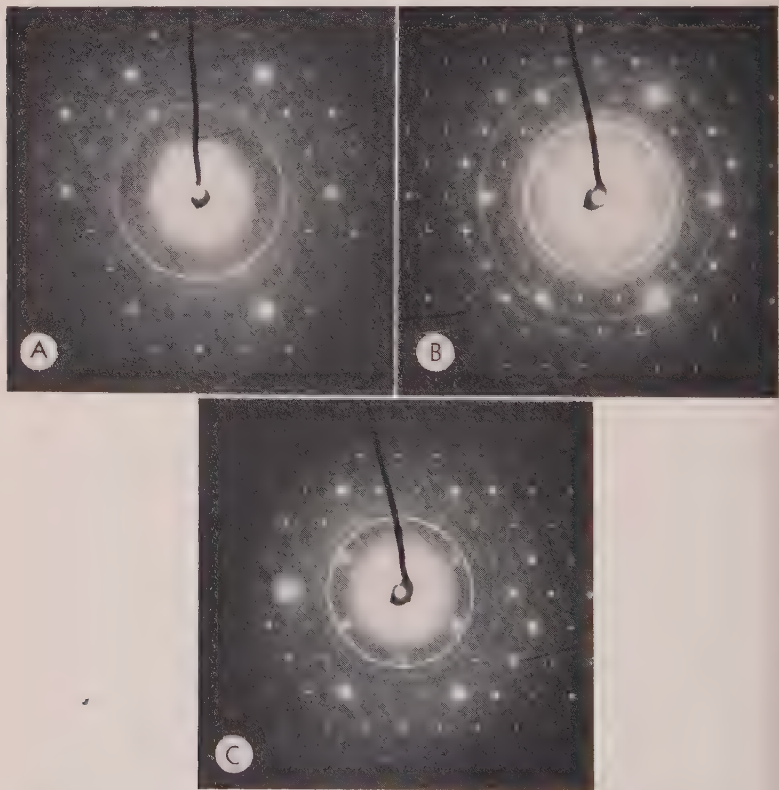

FIG. 1. Single crystal electron diffraction diagrams of (a) kaolinite, (b) dickite, (c) nacrite, with calibration rings from aluminum metal.

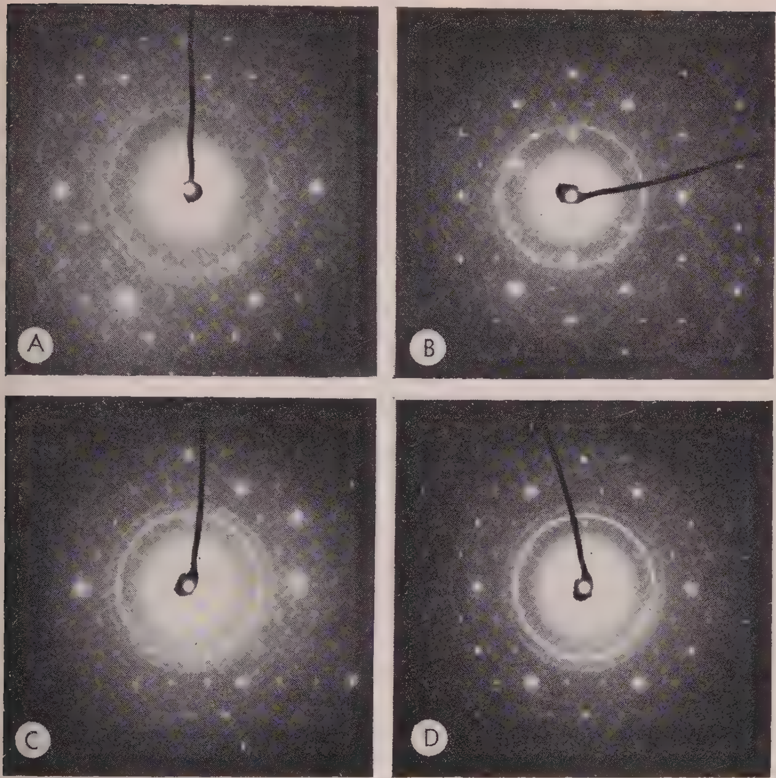

FIG. 2. Single crystal electron diffraction diagrams of (a) muscovite, (b) biotite, (c) clinochlore, (d) daphnite, with calibration rings from aluminum metal.

This lack of discrimination calls for careful consideration. In the first ꞌace, the orientation of the crystals excludes the basal reflections which re important in x-ray identification. Secondly, the $(hk0)$ reflections are ssentially similar for the various layer silicates because of structural milarities, particularly in projections on the basal plane. Such variaons as occur in figures 1 and 2 are largely erratic from one crystal to anther of the same mineral and may arise from uncontrollable variations f thickness, tilt, mosaic character, or similar variables.

It is evident that if a monoclinic crystal (most clay minerals are monoinic or approximately monoclinic) lies with (001) on the collodion subrate, then the a^*b^* reciprocal net is not parallel with the plane of the hotograph, and a series of Laue zones rather than a continuous spot patrn will be produced. In the present experiments, such zonal patterns ave been seen for dickite crystals prior to grinding the material. Genrally, however, zonal patterns have not been observed and one is led to

consider a diffusion of the reciprocal lattice points parallel to c^*, such tha
the recorded diagrams do not show strictly $(hk0)$ reflections but inter
sections of the Ewald sphere with (hk) lines.

Diffusion parallel to c^* due to extreme thinness of the crystals is un
likely even though very thin crystals tend to be selected preferentially
X-ray powder diagrams do not show greatly broadened $(00l)$ lines. Diffu
sion may arise from stacking faults parallel to (001) and undoubtedly th
prevalence of such faults in layer silicates must have an important influ
ence on the E.D. patterns of most clay minerals. Another source of diffu
sion parallel to c^* has been suggested by Cowley (1960) who consider
that if the structural layers have appreciable curvature, the electro
scattering from the component sheets of atoms will be incoherent, *i.e*
the diffraction process will be essentially two-dimensional in character.

It has to be recognized, however, that three-dimensional diffractio
data are obtainable from layer silicate minerals, including clay mineral
The "texture method" used particularly by many Russian workers, whic
utilizes a large number of crystals oriented with respect to the sul
strate but disoriented in the plane of the substrate, gives three-dimer
sional data from which structure analyses have been made, and by th
technique it should be possible to distinguish and identify clay mineral
It is not, however, a single crystal method, and it requires equipment i
which tilting of the specimen can be made. Oberlin (1957) and Oberl
and Tchoubar (1959) reported a close agreement between observed ar
calculated electron diffraction intensities for single crystals of kaolinit
but it is not clear how crystals were selected or adjusted with exactly tl
required orientation to record correctly the $(hk0)$ zone of reflections.

It must be concluded that most clay crystals give rise to sufficient di
fusion of the $hk0$ diffractions parallel to c^* so that hexagonal spot pa
terns can be obtained from crystals lying flat on the substrate and wit
out precise tilt adjustment. Under these conditions, identification on t
basis of electron diffraction intensity distributions is not general
feasible.

(*c*) *Identification on the basis of the β-angle*

A second potential method of identification rests on a determination
the β-angle for those clay minerals which are monoclinic or approximate
monoclinic. This method also requires a true recording of the a^*b^* r
ciprocal net, and from the discussion in the previous section it seems u
likely that these conditions can be readily satisfied. However, the meth
deserves brief consideration.

For a monoclinic structure,

$$a^* = 1/d(100) = 1/(a \sin \beta)$$
$$b^* = 1/d(010) = 1/b$$

and the reciprocal axial ratio is given by

$$a^*/b^* = b/(a \sin \beta)$$

For the layer lattice silicates, the crystal axial ratio b/a is always very close to $\sqrt{3}$ and therefore one can write

$$a^*/b^* = \sqrt{3}/\sin \beta$$

An important consequence of this result is that the true a^*b^* reciprocal net is not precisely hexagonal. As is well-known, an hexagonal array can be represented by a centered rectangular cell with axial ratio *exactly* equal to $\sqrt{3}$.

Kaolinite is a good example to consider, for although not strictly monoclinic, since $\alpha = 91.6°$, it has a β-angle of 104.8° which is larger than that for any other clay mineral. The calculated value of a^*/b^* is *1.797*. A series of careful measurements have been made on ten well-defined single crystal diagrams of kaolinite, which yielded an axial ratio of $1.734_5 \pm 0.001_6$. A similar result was obtained previously by Gastuche and De Kimpe (1959), though with less precision because they did not use an internal standard. Such a standard is desirable even for ratio determinations in order to correct for any optical or electron-optical aberrations.

This result provides further evidence that the E.D. patterns do not record the true a^*b^* reciprocal net under the conditions of the experiment. The observed pattern can be considered as a projection of the true a^*b^* net made possible by the diffusion of the reciprocal lattice nodes parallel to c^*. The recorded parameters are therefore $a^* \cos(\beta - 90°)$, and b^*, and their ratio is given by

$$\frac{a^* \cos(\beta - 90°)}{b^*} = \frac{b}{a} \simeq \sqrt{3}$$

This agrees exactly with the experimental results for kaolinite.

It is evident that, under the conditions employed, the β-angle cannot be determined and that clay mineral identification on this basis is not feasible.

(d) *Identification on the basis of the b-parameter*

Values of the b parameter of a number of clays and related minerals are listed in Table I. They fall into several groups. The dioctahedral minerals generally have smaller b parameters than the trioctahedral minerals, but the extent of ionic substitution in the lattice also determines the precise parameter values.

Among the *dioctahedral* minerals, the 1:1 kaolin minerals have $b = 8.95$ with little or no variation in the value.

For the 2:1 minerals, the smallest b parameters are shown by those minerals with mainly Al ions in the octahedral positions. Montmoril-

TABLE I. VALUES OF b-PARAMETERS FOR CLAYS AND RELATED LAYER SILICATE MINERALS FROM X-RAY DATA

		b(Å)
1. *Dioctahedral minerals*		
1:1 type	Kaolin minerals	8.95
2:1 type	Montmorillonite, Beidellite	8.95–9.00
	Muscovite	9.00–9.02
	Glauconite	9.07–9.12
	Nontronite	9.13
2. *Trioctahedral minerals*		
1:1 type	Serpentine minerals	9.20–9.26
	Amesite	9.19
	Chamosite (ferrous)	9.33–9.38
	Cronstedtite	9.52
	Greenalite	9.61
2:1 type	Phlogopite	9.20–9.23
	Biotite	9.25
	Hectorite	9.09
2:2 type	Chlorites	9.20–9.35

lonites and beidellites have $b \simeq 8.95$–9.00 Å and muscovite and simila micas have $b \simeq 9.00$–9.02 Å. Substitution of iron and magnesium fo aluminum leads to larger values of b, approximately 9.07–9.12 Å fo glauconites (Warshaw, 1957) and about 9.13 Å for nontronite. Very ap proximately, the b parameter, in Å, appears to be related to compositio by the equation:

$$b = 9.00 + 0.06_0 y$$

where y is the number of Fe+Mg ions replacing 2 Al ions in octahedr positions.

Among the *trioctahedral* minerals, the 1:1 serpentine minerals hav values of b in the range 9.20–9.26 Å. Chamosite with an octahedral catio population approximately ($Fe_{1.8}^{2+}$ $Mg_{0.2}$ $Al_{0.8}$) has $b \simeq 9.33$–9.38 Å, but the oxidized ferric form, $b \sim 9.10$ Å. Amesite, with approximately (M Al) in octahedral positions, has $b \simeq 9.19$ Å. The mineral greenalite wi approximate octahedral composition ($Fe_{2.3}^{2+}$ $Fe_{0.5}^{3+}$) has $b \simeq 9.61$ Å ar cronstedtite with octahedral cation composition (Fe_2^{2+} Fe^{3+}) and tetr hedral cation composition (Si Fe^{3+}) has $b \simeq 9.52$ Å, (Steadman ar Youell, 1957, 1958).

Among the 2:1 mica-type minerals, phlogopite has $b \simeq 9.20$–9.23 (Smith and Yoder, 1956), biotite has $b \simeq 9.25$ Å (Walker, 1949). Hecto ite, with octahedral cation composition approximately ($Mg_{2.7}$ $Li_{0.3}$) h $b \simeq 9.09$ Å.

Among the chlorites, the b parameters range from about 9.20–9.35 Å and this variation has been studied several times in relation to (Fe, Mn) substitution. The results can be represented by the following relations:

$b = 9.21 + 0.032(\text{Fe}) \cdots$ (based on data by Engelhardt, 1942)

$b = 9.202 + 0.028(\text{Fe, total}) + 0.047(\text{Mn}) \cdots$ (Hey, 1954)

$b = 9.210 + 0.037(\text{Fe}^{2+}, \text{Mn}) \cdots$ (based on data by Shirozu, 1958)

The variation with Fe content (number of Fe ions replacing Mg in octahedral positions) is considerably less than in the 2:1 minerals where Al is the replaced cation.

It is obvious that on the basis of b parameter measurements alone, the identification of clay minerals is restricted in scope. However, it can be expected that E.D. techniques will be applied to problems of a more specialized kind than those to which x-ray diffraction is routinely applied. Also, electron diffraction will not be applied except in conjunction with electron microscopy. In special circumstances, accurate b parameter measurements in conjunction with electron microscope observations can be expected to be a very useful identification aid.

The following results will show the degree of accuracy which can be achieved by using an internal calibration standard and an instrument of the electron microscope type.

Experimental Results

An R.C.A. electron microscope, type EMU-2D, has been used to measure the b parameters of typical clay minerals, with thin vaporized layers of aluminum metal as an internal calibration for all E.D. patterns.

The results obtained are given in Table II. For each mineral, the arithmetic mean value and the mean deviation are given. Each individual observation is believed to be accurate to 0.2–0.3%; the mean deviations

Table II. Single Crystal Electron Diffraction Measurements of b Parameters of Some Clays and Layer Silicate Minerals

Mineral	Patterns measured	b(Å)
Kaolinite	10	8.946 ± 0.008
Dickite	12	8.945 ± 0.014
Nacrite	14	8.935 ± 0.010
Muscovite	10	9.000 ± 0.009
Biotite	5	9.240 ± 0.007
Chlorite	5	9.200 ± 0.007
Clinochlore	5	9.207 ± 0.027
Corundophilite	5	9.180 ± 0.017
Daphnite	5	9.240 ± 0.060

are slightly better than 0.2% in most cases, but for daphnite, a chlorite, the results are somewhat poorer. The variation of the results for the last-named mineral may represent a real variation among the crystals examined; three mica crystals were measured from this sample.

It is evident from this tabulation, and from the data in Table I, that it is quite practicable to distinguish the following mineral groups: (1) the kaolin minerals, (2) muscovite and similar minerals, (3) the ferro-magnesian layer silicates. Within the latter group, however, distinction of particular minerals is not possible without additional information.

Summary and Conclusions

Single-crystal electron diffraction has many applications within the field of clay mineralogy if a satisfactory identification procedure can be developed. Apart from the special, but very important, cases in which the E.D. patterns are highly characteristic of individual minerals or varieties the majority of clay minerals have similar structures and give similar E.D. patterns when the crystal lies flat on a substrate without precise orientational adjustment; this limitation is inherent in many types of equipment designed primarily for electron microscopy. It is shown that identification on the basis of characteristic intensity distributions or on the basis of the β-angle, is not generally feasible with such instruments. From accurate measurements of b parameters, using aluminum metal as an internal standard, it is possible to obtain at least partial identification of clays and related layer lattice silicates. The variation of b with iron content in minerals is discussed.

Acknowledgments

This work forms part of the program of Project 55, sponsored by the American Petroleum Institute. One of us, (C. De K.), wishes to express his thanks to Professor J. J. Fripiat, Director of the Laboratoire des Colloides des Sols Tropicaux, Louvain, Belgium, for leave of absence to participate in this program. We desire also to thank Dr. G. Honjo and Dr. N. Kitamura, of the Tokyo Institute of Technology, for valuable discussion of this paper.

References

Brindley, G. W., (1959). X-ray and electron diffraction data for sepiolite. *Am. Mineral.* **44**, 495–500.

Brindley, G. W., and Comer, J. J., (1956). Structure and morphology of a kaolin clay from Les Eyzies (France). *Proc. Fourth Nat. Conf. Clays and Clay Minerals, Nat. Acad. Sci.-Nat. Res. Coun., Publn.* **456**, pp. 61–66.

Brindley, G. W., and Choe, J. O., (1961). The reaction series, gibbsite→chi alumina →kappa alumina→corundum, *Am. Mineral.*, **46**, 771–785.

Cowley, J. M., (1953), Structure analysis of single crystals by electron diffraction. I. Techniques, Acta Cryst., **6**, 516–521. II. Disordered boric acid structure. *Acta Cryst.*, **6**, 522–529.

Cowley, J. M., (1960), Coherent diffraction intensities from distorted crystals. *Fifth International Congress, Int. Union of Crystallography, Abstracts* p. 16.

Cowley, J. M., and Rees, A. L. G., (1958), Fourier methods in structure analysis by electron diffraction. *Rep. Progress in Physics*, **21**, 165–225.

Eckhardt, F.-J., (1958), Elektronoptische Untersuchungen an Einkristallen aus tonigen Sedimenten. *Neues Jb. Mineral.*, Mh., 1–17.

Eitel, W., Radczewski, O. E., Kedesdy, H., (1943), Elektronen-Mikroskopie und-Beugung Silikatischer Metaphasen. *Abh. Preuss. Akad. Wiss., Math.-Nat. Kl.*, No. 5, pp. 5–45.

Engelhardt, W. v., (1942), Die Strukturen von Thuringit, Bavalit, und Chamosit und ihre Stellung in der Chloritgruppe. *Z. Krist.*, **104**, 142–159.

Castuche, M. C., and de Kimpe, C., (1959), Tentative de synthèse des argiles du groupe du kaolin dan les conditions normales de temperature et de pression. *Acad. Roy. Belg., Bull. Cl. Sciences*, **45**, 1087–1104.

Hey, M. H., (1954), A new review of the chlorites. *Mineral. Mag.*, **30**, 277–292.

Honjo, G., Kitamura, N., and Mihama, K., (1954), A study of clay minerals by means of single-crystal electron diffraction diagrams—The structure of tubular kaolin. *Clay Min. Bull.*, **2**, 133–141. See also *Acta Cryst.*, **7**, 511–513, (1954).

[illegible]berlin, A., (1957), Altérations des cristaux de kaolinite; détermination par microdiffraction électronique, de la structure des produits altérés. *C. R. Acad. Sc.*, (*Paris*), **244**, 1658-1661.

[illegible]berlin, A., and Tchoubar, C., (1959), Reconnaissance de certains minéraux du groupe de la kaolinite par microdiffraction électronique. *C. R. Acad. Sc.*, (*Paris*), **248**, 3184–3186.

[illegible]nsker, Z. G., (1949, 1953), "Electron Diffraction", Russian edition, 1949; English translation, 1953, by J. A. Spink and E. Feigl, Butterworths Scientific Pubs., London. See especially pp. 281–287.

[illegible]insker, Z. G., and Vainshtein, B. K., (1957, 1958), A survey of electron diffraction structural analysis. *Kristallografiia*, **2**, 552, (1957) Russian Edn.; *Sov. Phys. Crystallography* **2**, 551–571, (1958) American Edn.

[illegible]pov, N. M., and Zviagin, B. B., (1958, 1960), Application of a 400 Kev. electron-diffraction apparatus to the study of single crystals. *Kristallografiia*, **3**, 700, (1958), Russian Edn.; *Sov. Phys. Crystallography*, **3**, 712–715, (1960), American Edn.

[illegible]oss, M., and Christ, C. L., (1958), Mineralogical applications of electron diffraction. *Am. Mineral.*, **43**, 1157–1178.

[illegible]oss, M., (1959), Mineralogical applications of electron diffraction. II. Studies of some vanadium minerals. *Am. Mineral.*, **44**, 322–341.

[illegible]oy, Rustum, Roy, D. M., and Francis, E. E., (1955), New data on thermal decomposition of kaolinite and halloysite. *J. Am. Ceram. Soc.*, **38**, 198–205.

[illegible]hirozu, H., (1958), *X*-ray powder patterns and cell dimensions of some chlorites in Japan. *Miner. J.*, (*Japan*), **2**, 209–223.

[illegible]ith, J. V., and Yoder, H. S., (1956), Experimental and theoretical studies of the mica polymorphs. *Mineral. Mag.*, **31**, 209–225.

[illegible]eadman, R., and Youell, R. F., (1957), Crystallography and thermal transformations of cronstedtite. *Nature* **180**, 1066–67.

[illegible]eadman, R., and Youell, R. F., (1958), Mineralogy and crystal structure of greenalite. *Nature* **181**, 45.

Vainshtein, B. K., (1956), Structure analysis by electron diffraction. *Nuovo Cimento*, Supplement to vol. **3**, 773–797.

Walker, G. F., (1949), Decomposition of biotite in the soil. *Mineral. Mag.*, **28**, 693–703.

Warshaw, C. M., (1957). "The Mineralogy of Glauconite". Ph.D. Thesis, The Pennsylvania State University.

Zussman, J., Brindley, G. W., and Comer, J. J., (1957), Electron diffraction studies of serpentine minerals. *Am. Mineral.*, **42**, 133–153.

Zviagin, B. B., (1957, 1958), Determination of the Structure of celadonite by electron diffraction. *Kristallografiia*, **2**, 393, (1957), Russian Edn.; *Sov. Phys. Crystallography*, **2**, 388–394, (1958), American Edn.

Zviagin, B. B , (1969), Electronographic determination of the structure of kaolinite. *Kristallografiia*, **5**, 40–50.

Zviagin, B. B., and Mishchenko, K. C., (1960), Electronographic refinement of the structure of muscovite. *Kristallografiia*, **5**, 600–604.

Manuscript received September 24, 1960.

THE AMERICAN MINERALOGIST, VOL. 46, SEPTEMBER-OCTOBER, 1961

VEIN MINERALS FROM THE TAMWORTH AND PARRY GROUPS (DEVONIAN AND LOWER CARBONIFEROUS), N.S.W.

KEITH A. W. CROOK, *University of New England, Armidale, N.S.W., Australia.**

ABSTRACT

Veins in the Tamworth and Parry Groups bear the following minerals: calcite, laumontite, stilbite, heulandite, prehnite, pumpellyite, epidote, axinite, chlorite, muscovite, quartz, albite, bytownite, and amphibole. The stratigraphic distribution of each species is different. Mineral assemblages are characteristic of the albite-epidote mineral facies, the prehnite-pumpellyite facies, and the laumontite subfacies and heulandite-analcite subfacies of the zeolite facies. Those characteristic of the first two facies occur in irregular veins, those of the heulandite-analcite subfacies in joints, and those of the laumontite subfacies in bedding veins, faults and shear zones.

Comparison with the stratigraphic distribution of diagenetic minerals indicates the irregular veins are diagenetic. Later the zeolite facies veins formed under lower P-T conditions, those in the joints being earliest and characteristic of the lowest P-T conditions.

A quartz-bytownite-amphibole vein in a hornfels, thought to be a metamorphosed laumontite-chlorite vein, is described.

INTRODUCTION

The Tamworth and Parry Groups, which are the lowest units in the Tamworth Trough sequence of western New England, New South Wales (Fig. 1) have been described stratigraphically and petrographically by the author (Crook, 1961 *a*, *b*, *c*). An outline of their stratigraphic subdivision is presented in Table 1.

In the Tamworth-Nundle district, and westwards the two groups exhibit a depth sequence of diagenetic minerals (Crook, 1961*c*), in which three diagenetic facies are represented –the laumontite, the prehnite-pumpellyite, and the albite-epidote. In addition, veins bearing calcium-aluminium silicates are common in the sequence, seventy-odd having been examined. These are described herein.

Optical data, incorporated in Table 2, have been obtained from mineral fragments in most cases, although thin sections were utilized for quartz-rich veins (R964–R970). Refractive indices were measured by the immersion method, using Cargille oils checked on an Abbe refractometer. Accuracy is ± 0.002 for values below 1.600 and generally somewhat poorer for values above this. Specimen numbers of the W-series are the author's field numbers (series KCW . . . . /56, 57 or 58). Those of the R-series are University of New England collection numbers (old series). All material is housed in the University of New England.

* Now at Geology Dept., Australian National University, Canberra, A.C.T., Australia.

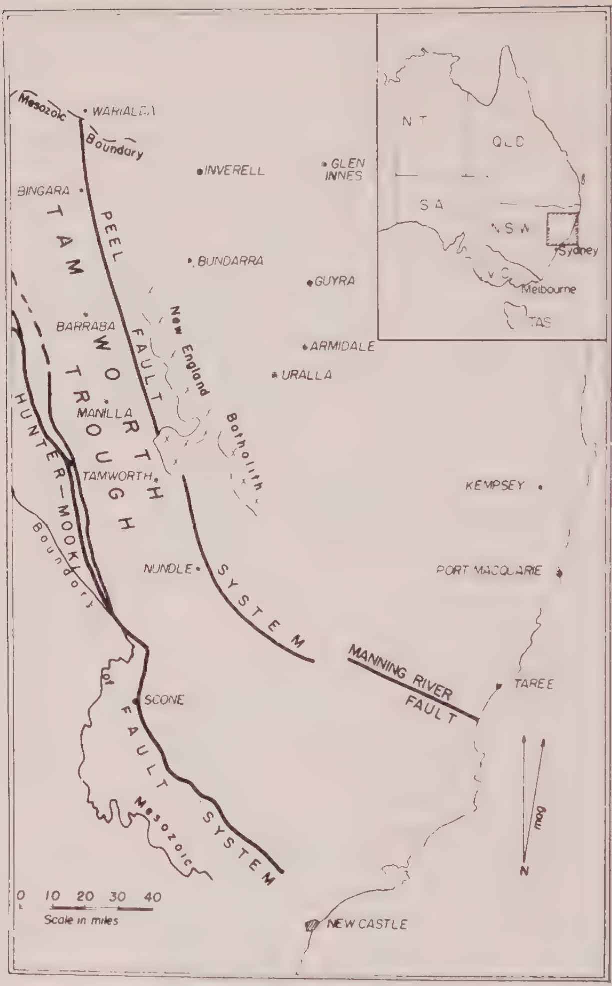

FIG. 1. Locality map (geological data from Voisey, 1959).

The veins occur in several different ways:

(*a*) straight or irregular macroscopic or microscopic veins apparently unrelated to any structural features of the rock.

(*b*) joint fillings

(*c*) bedding veins

(*d*) in fault planes, along the margins of dykes which occupy faults, or in shear zones in dykes.

Those of type (*a*) are the earliest, being cut by joints. As will be shown elsewhere, jointing was the earliest structure formed during deformation

TABLE 1. STRATIGRAPHIC SUBDIVISIONS OF THE TAMWORTH AND PARRY GROUPS

Series	Stage	Group	Eastern and Southern Regions		Western and Northern Regions	
Lower Carboniferous	Visean		(not preserved)		"Lower Kuttung Group" (CK)	
Lower Carboniferous	Tournaisian	PARRY GROUP	Pyramid Hill Arenite Members (Clp) –1 –2 –3 –4 –4a –5 –6 –7	Goonoo Goonoo Mudstone (Clg)	Goonoo Goonoo Mudstone (Clg)	–Boiling Down Sandstone Member (Clbs)
			P– Q– R– S– T– U– V– Va–			–Gowrie Sandstone Member (Clgs)
			W– –8 X– –9 Y– –10 Z–			–Turi Graywacke Member (Clt)
			–Benama Graywacke Member (Clbg) –Wombramurra Formation (Clw)			–Garoo Conglomerate Member (Clgc)
			–Scrub Mountain Conglomerate Member (Cls)			–Scrub Mountain Conglomerate Member (Cls)
			–Hyde Graywacke Member (Clh)			–Kiah Limestone Member (Duk)
Upper Devonian			Baldwin Formation (Dub)		Baldwin Formation (Dub)	
Middle Devonian		TAMWORTH GROUP (DT)	Yarrimie Formation (Dmy) Silver Gully Formation (Dms)		Yarrimie Formation including Levy Graywacke Member (Dmlg) Silver Gully Formation (Dms)	
Lower Devonian		TAMWORTH GROUP (DT)	Wogarda Argillite (Dlw) Drik-Drik Formation (Dld) Cope's Creek Keratophyre (Dlc) Pipeclay Creek Formation (Dlp) - - - - - - Hawk's Nest Beds (Dh) Stratigraphic position unknown)		Seven Mile Formation (Dls)	

of the area, pre-dating the folding. Thus the joint fillings (*b*) post-date type (*a*). The bedding veins (*c*), which are clearly later than the joint fillings, where intersections occur, are probably related to the folding, as relief of load pressure would be necessary for material to be deposited along bedding planes.

The veins of type (*d*) are probably also related to the folding. In another place the faults and shears in which they occur will be shown to be related to the folding or to be later than it. Veins of type (*d*) may therefore be considered as roughly contemporaneous with those of type (*c*).

TABLE 2. PROPERTIES OF VEIN MINERALS

No.	Formation and Position	Vein Type	CO_3	Laumontite		Stilbite		Epidote	Prehnite	Quartz p (present) m (minor)
			ω	β	$Z\wedge c$	α	γ	β	β	
W5	Clg below Clp$_5$	d	1.658	1.516	13°					
W106	Clg above Clp$_4$	c		1.520	10°					
W111	Clg above Clp$_4$	b[3]								
W112	Clg above Clp$_4$	c	1.658	1.520	—					
W125	Clg below Clp$_6$	b				1.494	1.503			
W145	Clg below Clp$_7$	b				1.494	1.505			
W146	Clg below Clp$_7$	–[1]	1.658	1.515	36°					
W152	Clg below Clp$_5$	–	1.658							
W153	Clg below Clp$_5$	–	1.658			1.492	1.505			
W154	Clg below Clp$_5$	–	1.658							
W160a	Clg above Clp$_5$	d	1.658 and also anom. biaxial $\beta=1.632$; $\gamma=1.640$ (strained)							
W160b	Clg above Clp$_6$	d	1.658	1.517	50°					
W174	Clg above Clp$_4$	d	1.658			1.489	1.503			m
W177	Clg above Clp$_{5a}$	–		1.517	36°					
W180	Clg above Clp$_6$	b				1.489	1.505			
W183	Clg bet. CK & Clp$_4$	b				1.489	1.503			
R964	Dmy	a						1.764		p
W282a	Clg below Clp$_5$	d		1.517	46°					
R965	Clp$_9$?	–[3]	pres.						1.620	p
W331	Clg above Clbg	d	1.658							
W340b	Clbg	–	1.658					1.764		p
W353a	Clbg	–							1.620	p
W369	Clg (low)	–						v. minor		p
W402	Dmy	–	1.682							p
W487	Clw	a	1.658						1.621	p
W489	Clw	a						1.748		p
W498	Clw	a						1.753		p
W583	Dmy	a								p
W608	Clg below Clp$_5$	b		1.514	41°	1.489	1.505			
W615	Clg above Clp$_8$	c		1.517	41°					
W623	Clg above Clp$_{4a}$	b				1.489	1.504			
W626	Clg below Clgc	–		1.517	41°					
W630	Clg below Clgc	c	1.658	1.517	16°; 43°					
W658	Clg below Clp$_x$	–	1.658							
W661	Clg below Clp$_x$	a	1.658							p
W673	Clg below Clp$_9$	--	1.658	1.517	36°					
W682	Clp$_7$	d							1.621	p
W691	Clg below Clp$_8$	c		1.517	16°; 36°					
W700	Clg below Clp$_8$	b[3]								
W701	Clg below Clp$_8$	c	1.658	1.517	26°; 53°					p
W705	Clg below Clp$_8$	b	1.658	1.517	16°	1.490	1.505			
W706	Clg above Clp$_8$	d	1.658							
W707	Clg below Clp$_8$	d		1.517	49°					
W726	Clg above Clgs	–	1.658						1.621	
W730	Clg above Clgs	d[3]	1.658	1.517	16°; 42°	1.489	1.504			
R966	Clg above Clgs	d	1.658	1.517	45°				1.634	p
W879	Clp$_x$	c								p
W876	Clp$_8$	d	{1.658 / 1.704							
W898	Cls	–							1.621	p
W909	Clg below Cls	b	1.658							
W917	Dms	a	1.658							
W932	Dmy	–		1.517	40°					
W941	Dlw	a						1.750		
W949	Clg below Clp$_R$	d	1.658	1.517	45°					
R967	DT (?Dms)	a[3]	1.658					1.750		
W956	DT (?Dms)	a[3]								
R968	DT (?Dms)	a	1.658[2]					present	present	p
W1051	Dub	–	1.658	1.517	43°					
W1098	Dmy	–	1.658							p
R970	Dub	a	1.658	minor				present		p
W1106	Dub	b				1.489	1.506			
W1114	Clg above Duk	–[3]								p
W1116	Clg sl. above Duk	–							1.615	p
W1141	Clpy?	–	1.658							
W1142	Clg below Cls	d	1.658	1.517	41°					
W1143	Clg below Clp$_{6a}$	–	1.658	1.517	45°	1.489	1.505			
W1147	Clpz	–	1.658					1.751		p
W1147a	Clpz	–						1.752	1.617	p
W1147b	Dms	–	1.658							
W1151	Clw	a							1.615	p
W1155	Dld	–				?altered-agg. pol. $n=1.53$				
W1167	Clg below Clp$_{10}$	a						1.755		p

[1] "–" indicates data on type not recorded in field-book.
[2] Also contains chlorite and muscovite.
[3] Axinite present as follows: R967, $\beta=1.680$; W956, $\beta=1.684$.
Heulandite present in W111, $\beta=1.502$, W700, $\beta=1.505$; W1114, $\beta=1.497$.
Pumpellyite present in R965, and in R966; $\beta=1.690$–1.700.

Mineralogy

The following minerals have been encountered in the veins, and will be discussed in order:

carbonates	epidote
laumontite	axinite
stilbite	chlorite
heulandite	muscovite
prehnite	quartz
pumpellyite	albite
	bytownite

Carbonates: Calcite is by far the most common carbonate, and is remarkably pure. It is usually white en masse, and colorless and transparent in crushed fragments. Thirty-seven determinations give $\omega = 1.658 \pm 0.002$. In one case (W160*a*) optically anomalous carbonate occurs with calcite. This shows $\beta = 1.632 \pm 0.002$, $\gamma = 1.640 \pm 0.002$ and $2V(-)$ *ca.* 10°. It has wavy extinction, and the anomalous optics are apparently due to strain.

In only two cases have carbonates other than calcite been encountered. These are W876 from Member 9 of the Pyramid Hill Arenite (a brown carbonate) and W402 from the Yarrimie Formation. These have

W876 $\omega = 1.704 \pm 0.003$ (occurs with calcite)

W402 $\omega = 1.682 \pm 0.002$.

Both are uniaxial negative. The refractive index determinations suggest dolomite.

Carbonate occurs throughout the sequence, having been encountered as far down as the Silver Gully Formation.

Laumontite is also widespread, usually in bedding veins or faults. It occurs as silky white columnar prismatic crystals, showing good cleavage, and often forms acicular clumps. It is usually associated with calcite. Twenty-three determinations give $\beta = 1.514$ to 1.520, $2V(-)$ ca. 30°.

The extinction angle ($Z \wedge c$) varies between 10° and 53°. Usually the central parts of grains give lower values, about 16°, whilst the margins give values about 42°. The junction between the optically different materials is irregular, but sharp. At times the two types of material are arranged so as to simulate complex twinning, giving a patchy extinction.

This variation in optical properties has been discussed by Coombs (1952) with whose data the present data are in good agreement. He has shown that the variation is due to the laumontite becoming modified to leonhardite by loss of water. Laumontite is characterized by higher refractive indices and a much smaller extinction angle than its leonhardite

equivalent. In this study the mineral is termed laumontite in general discussion, regardless of its state of hydration, following Coombs (1952, p. 819), who points out that the hydration state of the mineral may vary with the weather.

Laumontite extends down the sequence to the upper part of the Yarrimie Formation, but is most common in the upper parts of the sequence.

Stilbite occurs as regular aggregates of pink, or rarely white, columnar crystals in joint planes, the aggregates being oriented with their long axes perpendicular to the joint surfaces. It rarely has associated minerals.

Stilbite has one good cleavage parallel to the optic axial plane, and as the mineral tends to lie on this cleavage in the crush, determination of 2V or β is well-nigh impossible without resorting to a U-stage. In cases where rough estimation has been possible 2V$(-)$ is small. Refractive indices (12 determinations) give: α: 1.489 ± 0.002 to 1.494 ± 0.002; γ: 1.503 ± 0.002 to 1.506 ± 0.002.

Stilbite is almost completely restricted to the upper part of the sequence, although an isolated occurrence in the Baldwin Formation has been noted.

In the Drik Drik Formation, joints are filled with a pink mineral of similar morphology to the stilbite. Optical examination (W1155) however shows it to be an aggregate polarizing mass with low D.R. and $n = ca.$ 1.53. An x-ray powder photograph suggests albite.

Heulandite occurs in joints, usually as salmon pink to red plates lying on the joint surfaces. Only three examples have been noted.

Since heulandite has one good cleavage normal to the optic axial plane ($\perp$ to Z), most grains give good Bx_a figures. Data obtained are: 2V$(+)$ small, $\beta = 1.497 \pm 0.002$, 1.502 ± 0.002, 1.505 ± 0.002.

Because of the few occurrences, the stratigraphic distribution of heulandite is rather ill-defined. The lowest occurrence is below the Scrub Mountain Conglomerate Member.

Prehnite occurs as dull white usually fibrous masses often associated with quartz. It is largely confined to veins of type (*a*).

Refractive index values (10 determinations) range from $\beta = 1.615 \pm 0.003$ to 1.634 ± 0.003, indicating a somewhat variable composition with an upper limit of about 3% Fe_2O_3. Birefringence is moderate to low with 2V$(+)$ large and straight extinction. Cleavage is good; absorption is variable and may be strong.

In one case (R966) optically anomalous prehnite (cf. Winchell, 1951, p. 360) was encountered. This has $\beta = 1.634 \pm 0.003$, 2V$(+)$ small, $r < v$ strong, and wavy extinction. Other parts show anomalous blue interference colors, 2V$(+)$ *ca.* 30° and $r > v$ very strong.

Prehnite in megascopic veins extends from near the horizon of Member 6 of the Pyramid Hill Arenite to below the Scrub Mountain Conglomerate Member, with an isolated occurrence in the Tamworth Group. Evidence from microveins, however, extends this distribution to range from Member 3a of the Pyramid Hill Arenite to the upper part of the Silver Gully Formation.

Pumpellyite has been encountered only in three veins in the middle of the sequence.* One is in a sheared dyke above the Gowrie Sandstone Member (R966). The others are in veins of type (*a*), one megascopic, the other microscopic, from lower in the sequence. The mineral is deep green, and occurs in granular aggregates of small subhedral crystals.

Pumpellyite from R966, accompanied by prehnite, quartz, and later laumontite and calcite, gives:

X = almost colorless	$\gamma-\alpha=$ ca. 0.018
Y = bright green	$\beta=1.690-1.700$, apparently variable
Z = almost colorless	

2V(−) large $r>v$ strong, wavy extinction
fine prismatic crystals (0.02×0.004 mm.) elongated parallel to b, $Y\|b$.

These data suggest a pumpellyite containing 6–7 wt.% of Fe_2O_3, using the graphs of Coombs (1953, p. 131).

An *x*-ray powder photograph of this pumpellyite gave data which agree closely with the pumpellyite examined by Coombs (1953, p. 121) from Calumet, Michigan.

Epidote characteristically forms apple-green granular aggregates associated with quartz, and usually occurs in veins of type (*a*).

X = Z = colorless	$\beta=1.748\pm0.004$ to
Y = pale yellow green	1.764 ± 0.004
2V(−) ca. 70° to 2V(+) large	$r>v$, slight.

The refractive indices suggest a range of from 25 mol.% to 35 mol.% of $HCa_2Fe_3Si_3O_{13}$. In one case (W1104), possible zoisite was encountered.

Epidote ranges downwards from below Member 10 of the Pyramid Hill Arenite, and has been encountered as low as the Wogarda Argillite.

Axinite occurs as purple plates in veins in spilites in the Tamworth Group at Bowling Alley Point (cf. Benson 1913, p. 577). Data follow:

2V(−) ca. 70°; $r<v$ strong, $\beta=1.680\pm0.004$, again 1.684 ± 0.002, D.R. low; pleochroic: pale violet (fast) to colourless (R967, W956).

Axinite from Bowling Alley Point was described crystallographically by Anderson (1906, p. 133). The exact stratigraphic position of the local-

* This was the first known recognition of pumpellyite in Australia. It has since been recognized by Wilshire (pers. comm.) in the Prospect Lopolith near Sydney, and elsewhere.

ity is uncertain, but it is close to the junction of the Yarrimie and Silver Gully Formations.

Chlorite occurs rarely in veins of type (*a*). Three occurrences, two in microveins, of pale green chlorite have been noted in the Tamworth Group.

Muscovite: One example of this, associated with epidote, quartz, calcite, prehnite and chlorite, occurs in a vein in the Tamworth Group.

Quartz occurs as milky white aggregates, usually unstrained and without crystal form. Veins of type (*a*) are the most common. It is distributed through the sequence from below Member 5*a* of the Pyramid Hill Arenite downwards, although traces occur in a vein above Member 4 of the same unit (W174). This accords reasonably with the observations of Carey (1937, p. 339), and Engel (1954, p. 20) who noted that quartz veins in the areas examined by them (northwest of the present area) are restricted to the Barraba Mudstone (*i.e.* the lower parts of the Parry Group, herein). They did not examine the Tamworth Group.

Albite has been noted only in microveins in the Tamworth Group. It occurs as small, albite-twinned laths often associated with quartz (R921, 937) or calcite (R919, 921, 933) and occasionally prehnite or chlorite. Both lithic and feldspathic labile graywackes may carry these veins.

Bytownite: R957, a hornfelsed argillite from the Hawk's Nest Beds, contains a thin quartz-bytownite-amphibole vein of type (*a*) with minor sphene and apatite. The bytownite is clear, with multiple twinning and moderate relief, $\beta = 1.576 \pm 0.002$ giving a composition of An_{82} (mol.%) derived from the graph of Poldervaart (1950).

Parageneses of Vein Minerals

Determinations of parageneses on several multicomponent veins are shown in Table 3. Sequences have been determined by noting the order of deposition in the case of open space fillings, and also by the relationships between the minerals shown in the case of intersecting veins. Development of crystal facies has also been used as a criterion. In some cases contemporaneous deposition appears to have occurred. The most common sequence of deposition follows: epidote, pumpellyite, prehnite, quartz, stilbite, laumontite, calcite. This paragenetic sequence is similar to the major trend observed for the cement in the sediments (Crook, 1961*c*), except that quartz in the vein paragenetic sequence is somewhat later. In the vein paragenetic sequence, as in the cements, the earliest minerals to form are those characteristic of the lower portions of the stratigraphic sequence.

Two veins amongst those described deserve further comment. W1155,

TABLE 3. PARAGENESES OF VEIN MINERALS

—— Order of deposition ——→						
epidote,		prehnite, muscovite, chlorite,		quartz,		calcite
epidote,				quartz		
	pumpellyite,	prehnite,		quartz,	laumontite,	calcite
		prehnite,				calcite
				quartz		calcite
					laumontite,	calcite
					stilbite,laumontite,	calcite
			heulandite,	quartz		
					stilbite,	calcite, laumontite
		prehnite,	calcite,	quartz		
quartz, epidote,			calcite			
	pumpellyite			quartz	prehnite	calcite

Underlined pairs represent contemporaneous deposition.

which bears probable albite pseudomorphous after stilbite, occurs as a joint-filling, an occurrence unknown for albite elsewhere in the sequence It may have formed as a stilbite vein, and later been metasomatized by the addition of NaAl and loss of Ca, SiO_2 and H_2O, during the period of formation of the laumontite facies veins in the upper part of the sequence (see below).

R957 bears the extraordinary assemblage quartz-bytownite-amphibole and occurs in the contact aureole of the post-orogenic Mt. Ephraim Granite in a biotite-actinolite hornfels. This vein can scarcely be genetically related to the granite magma. The most likely origin would seem to lie in thermal metamorphism of a pre-existing laumontite-chlorite vein. At temperatures characteristic of the albite-epidote hornfels facies, laumontite will form anorthite-quartz according to the reaction:

$$\underset{\text{laumontite}}{CaAl_2Si_4O_{12}\cdot 4H_2O} \rightarrow \underset{\text{anorthite}}{CaAl_2Si_2O_8} + \underset{\text{quartz}}{2SiO_2} + 4H_2O$$

As laumontite usually bears some Na, the resultant plagioclase will not be pure anorthite. The amphibole could have formed from a chlorite by the usual metamorphic reaction.

STRATIGRAPHIC DISTRIBUTION OF THE VEIN MINERALS

Figure 2 shows the stratigraphic distribution of the more common vein minerals. Carbonate occurs throughout. Laumontite, stilbite and heulandite tend to be confined to the middle and upper portions, pumpellyite to the middle portions, quartz and prehnite to the basal-upper portions and below, epidote to the lower-middle and lower portions, and albite to the lower portions.

Comparison of these results with the results obtained for the same species (or related species) occurring as diagenetic modifications (Fig. 3) (see also Crook, 1961*c*) is instructive. In each, calcite occurs throughout the sequence. Prehnite, epidote and albite have roughly the same distribution in each, and quartz has a distribution resembling that of the quartz cement in the feldspathic labile arenites, but appears slightly higher in the sequence. Pumpellyite apparently occurs slightly higher in the sequence as veins, but data are meager.

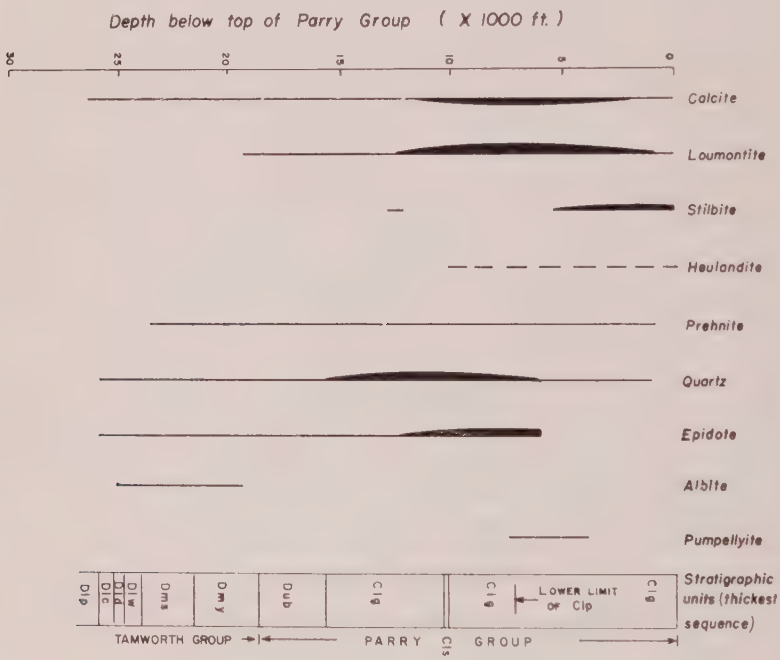

FIG. 2. Stratigraphic distribution of vein minerals.

The zeolites show the most noticeable differences. In comparison with the zeolitic modifications of the detrital feldspar, which range further downward than zeolitic cements, the vein laumontite, heulandite, and and possibly also the stilbite range still further downward, extending into the Yarrimie Formation in the case of laumontite.

Mineral Facies Represented

Analysis of Table 2 and the data from microveins shows that the following assemblages can be recognized in the veins:

1. stilbite ± calcite (+quartz)
2. heulandite (+quartz)
3. laumontite ± calcite (+stilbite, quartz)
4. prehnite ± pumpellyite ± quartz ± calcite
5. epidote ± quartz ± calcite (+prehnite)
6. axinite ± epidote ± calcite
7. albite ± quartz ± calcite (+prehnite, chlorite)
8. calcite ± quartz
9. quartz

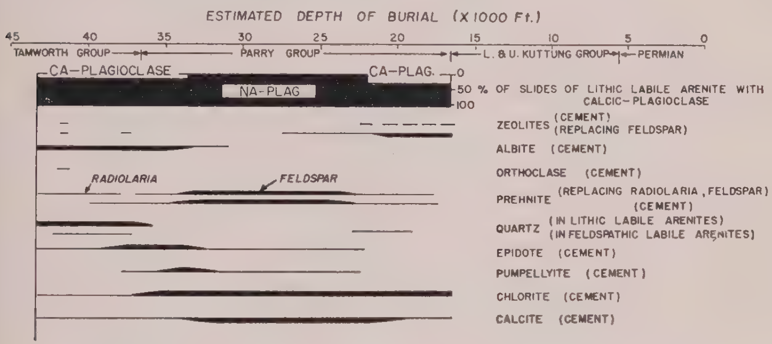

FIG. 3. Stratigraphic distribution of diagenetic minerals.

In the above list species which appear in brackets occur rarely. Some veins listed in Table 2 bear laumontite and calcite together with either prehnite or epidote. In these cases the laumontite and calcite is clearly later, and the veins may be considered as a combination of assemblages 3 and 4 or 5.

The above assemblages may be divided into four groups: 1–3 which represent the zeolite facies of Coombs *et al.*, (1959); 4 representing the prehnite-pumpellyite mineral facies; 5 and 6 representing the albite-epidote mineral facies; and 7–9 which do not bear diagnostic minerals. The two stages of the zeolite facies described by Coombs *et al.* (1959) are present: 1 and 2 represent the heulandite-analcite stage (or subfacies) and 3 the laumontite stage.

The minerals of assemblages 4 to 7 occur in veins of type (2) which are pre-deformational. They are also the early minerals in the paragenetic sequence. Their stratigraphic distributions are similar to those of the same species occurring as diagenetic modifications. There seems little doubt, therefore, that the veins of the albite-epidote and prehnite-pumpellyite mineral facies are of diagenetic origin. As noted by Ellis and Fyfe (in Coombs *et al.*, 1959), quartz becomes a prominent component in the veins only in the prehnite-pumpellyite and higher-grade facies.

The veins representing the zeolite facies are of types (*b*), (*c*) and (*d*), and are syn- or post-deformational. Their minerals come late in the paragenetic sequence, and have stratigraphic distributions different from those of the same species occurring as diagenetic modifications. Veins of this facies, therefore, are probably not related to the diagenesis of the sequence, but to a later, and different, P-T regime.

Veins of the heulandite-analcite subfacies are of type (*b*), and are older than those of the higher grade laumontite subfacies, which occurs as veins of types (*c*) and (*d*). This indicates a reversal of the trend towards lower-grade modifications, and it apparently occurred during and after folding, as the bedding and fault veins (*c* and *d*) formed at this time.

Ellis and Fyfe (in Coombs *et al.*, 1959, p. 83) have pointed out that where $P_{load} = P_{H_2O}$ in the rock, decrease in water pressure in open fissures due to osmotic conditions enables the formation of higher grade assemblages in the fissures than those being formed in the rock. In the Tamworth Trough sequence the vein minerals are either of the same facies as those formed in the rock, or of lower-grade facies. This suggests that, whatever the P-T conditions operating during vein formation, they could not have arisen simply by lowering of P_{H_2O}; temperatures must have dropped as well.

In summary the veins in this sequence indicate the following history. After modification at the temperatures and pressures obtaining during diagenesis (see Crook, 1961*c*), there was a decrease in temperature, and probably of water-pressure also, allowing the deposition of minerals of the heulandite-analcite subfacies on the joints in the sediments. Later, during folding, and particularly during subsequent faulting, there was an increase in water-pressure, or in temperature, or both, permitting the deposition of the veins of the laumontite subfacies along bedding planes and in faults.

CaAl-silicates in veins cutting diagenetically modified sediments and other rocks are probably of common occurrence, although they are not often noted. Niggli *et al.*, 1940, p. 576 record prehnite and later laumontite in the "Alpine Cleft" deposits of Switzerland. The author has noted heulandite, analcite, and laumontite-bearing veins filling joints and fractures in Cretaceous and Lower Tertiary labile sandstones in the Rocky Mountains Foothills of Alberta. Coombs (Coombs *et al.*, 1959) has described prehnite, pumpellyite, laumontite and stilbite veins in New Zealand sediments, pointing out that they are later than the metamorphic maximum, and have a retrogressive significance being correlated "with the filling of fractures under conditions of progressively decreasing load and temperature during denudation." The Tamworth Trough zeolite-facies veins also have a retrogressive significance, but show a reversal of

the trend to lower P and T, in that the higher grade laumontite postdates the stilbite.

Acknowledgments

The author is indebted to Prof. C. E. Marshall for the use of *x*-ray equipment at the University of Sydney, to Dr. G. H. Packham for taking *x*-ray photographs, and to Prof. D. S. Coombs for helpful discussion of the problem. Miss J. Forsyth assisted with the drafting. This work was completed for publication during the tenure of a National Research Council of Canada Post-doctoral Fellowship at the University of Alberta.

References

Anderson, C. (1906), Mineralogical Notes: No. III—Axinite, petterdite, crocoite and datolite. *Aust. Mus. Rec.*, **6**, 132–144.

Benson, W. N. (1913), The geology and petrology of the Great Serpentine Belt of New South Wales. Part II. The geology of the Nundle district. *Proc. Linn. Soc. N.S.W.*, **38**, 569–596.

Carey, S. W. (1937), The Carboniferous sequence in the Werrie Basin. *Proc. Linn. Soc. N.S.W.*, **62**, 341–376.

Coombs, D. S. (1952), Cell-size, optical properties and chemical composition of laumontite and leonhardite with a note on regional occurrences in New Zealand. *Am. Mineral.*, **37**, 812–830.

——— (1953), The pumpellyite mineral series. *Mineralog. Mag.*, **30**, 113–135.

———, Ellis, A. J., Fyfe, W. S., and Taylor, A. M. (1959), The zeolite facies; with comments on the interpretation of hydrothermal syntheses. *Geochem. Cosmochem. Acta*, **17**, 53–107.

Crook, K. A. W. (1960a), Petrology of Tamworth Group, Lower & Middle Devonian, Tamworth-Nundle district, New South Wales, *J. Sedim. Petrol.*, **30**, 353–369.

——— (1960b), Petrology of Parry Group, Upper Devonian-Lower Carboniferous, Tamworth-Nundle district, New South Wales. *J. Sedim. Petrol.*, **30**, 538–552

——— (1961a), Stratigraphy of the Tamworth Group (Lower and Middle Devonian), Tamworth-Nundle District, N.S.W. *J. Proc. Roy. Soc. N.S.W.*, **94**, 173–188.

——— (1961b), Stratigraphy of the Parry Group (Upper Devonian-Lower Carboniferous), Tamworth-Nundle district, N.S.W. *J. Proc. Roy. Soc. N.S.W.*, **94**, 189–207.

——— (1961c), Diagenesis in the Tamworth and Parry Groups (Devonian and Lower Carboniferous), Tamworth-Nundle district. In preparation.

Engel, B. A. (1954), The geology of the south-eastern portion of the County of Darling. B.Sc. Honours Thesis, University of New England.

Niggli, P., Koenigsberger, J., and Parker, R. L. (1940), Die Mineralien der Schweizeralpen. Bd II., 307–661, Wepf and Co., Basel.

Poldervaart, A. (1950), Correlation of physical properties and chemical composition in the plagioclase, olivine and ortho-pyroxene series. *Am. Mineral.*, **35**, 1067–1079.

Voisey, A. H. (1959), Tectonic evolution of north-eastern New South Wales, Australia. *J. Proc. Roy. Soc. N.S.W.*, **92**, 191–203.

Winchell, A. N. and Winchell, H. (1951), Elements of optical mineralogy. Part II. Description of minerals. 4th ed. J. Wiley and Sons, New York.

Manuscript received September 24, 1960.

THE AMERICAN MINERALOGIST, VOL. 46, SEPTEMBER-OCTOBER, 1961

POLYMORPHISM OF ABO_3 TYPE RARE EARTH BORATES*

ERNEST M. LEVIN, ROBERT S. ROTH AND JERRY B. MARTIN,†
National Bureau of Standards, Washington, D. C.

ABSTRACT

Polymorphic relationships as a function of temperature and ionic radius were investigated for thirteen ABO_3-type borates, including all of the normally trivalent rare earth ions as well as La^{+3}, Y^{+3}, In^{+3}, and Mn^{+3}. The melting points of the compounds varied irregularly from 1660° C. for $LaBO_3$ to 1540° C. for $EuBO_3$. In general, the borate compounds exhibited the same structure types as the three forms of $CaCO_3$, *i.e.*, aragonite, vaterite, and calcite. Compounds of the larger ions, $LaBO_3$ and $NdBO_3$, showed the aragonite-type structure at low temperature. These compounds were found to have a reversible transformation at 1488° C. and 1090° C., respectively. The high-temperature forms were different from each other, and both exhibited low symmetry. The following borates showed a stable vaterite-type phase: $SmBO_3$, $EuBO_3$, $GdBO_3$, $DyBO_3$, YBO_3, $HoBO_3$, $ErBO_3$, $TmBO_3$, $YbBO_3$, and $LuBO_3$. Above 1285° C., $SmBO_3$ inverted to the high-$NdBO_3$ type polymorph. Below 1310° C., $LuBO_3$ formed the calcite-type structure. No polymorphism was observed in the eight intermediate borates. Indium borate showed only the calcite-type structure. A discussion of the factors affecting polymorphism, such as radius ratio, density, and pressure, in addition to interpretation of infrared and structure data may explain why the vaterite-type structure is more stable in the borates than in the carbonates. Unit cell dimensions are listed for indexed *x*-ray diffraction powder patterns, together with limited optical data. Published *x*-ray powder data for vaterite are compared.

INTRODUCTION

The increasing availability of purified rare earth oxides has served as an impetus to the study of systems containing these oxides. The lanthanide series is significant from a crystal chemical standpoint because it consists of a large, nearly homologous chemical group within the periodic table, in which ionic radius varies from 1.15 Å for lanthanum to 0.85 Å for lutecium. Thus the effect of ionic radius can be studied on such properties as compound formation, solid solution and immiscibility.

Compounds equimolar in R_2O_3 and B_2O_3 are of the ABO_3 type. The classic study on the "Isomorphism of Borates and Carbonates" was made by Goldschmidt and Hauptmann (1931 32). They studied the lanthanum, indium, scandium, and yttrium borates. Lanthanum borate was found to have the $CaCO_3$-aragonite type structure, whereas the other borates were found to be of the $CaCO_3$-calcite type structure, with YBO_3 possibly possessing a $CaCO_3$-vaterite polymorph.

In a major study of the double oxides of trivalent elements, Keith and Roy (1954) included a few experiments on equimolar mixtures of

* Presented at 17th Annual Pittsburgh Diffraction Conference, Nov. 11, 12 and 13, 1959, Mellon Institute, Pittsburgh, Pa.

† Guest worker, summer 1959, from Vanderbilt University, Tenn.

lanthanum, yttrium, indium, and chromium oxides with boric oxide. They noted a high form of $LaBO_3$ but no calcite polymorph of YBO_3.

None of the compounds mentioned are true rare earth borates. Thus it is evident that phase studies in the rare earth borate systems offer a relatively unexplored field. Such studies, along with crystal chemical implications might prove helpful, moreover, in interpreting the complex polymorphic relationships among the carbonates of divalent cations.

The primary objective of this study, therefore, was to investigate the equimolar compositions of boric oxide and the normally trivalent rare earth oxides. In addition, because of ionic radii considerations, Y_2O_3, In_2O_3, and Mn_2O_3 were included. The information on ABO_3 polymorphs was to serve also as a starting point for the more complete study of selected rare earth oxide-boric oxide systems (Levin, *et al.*, 1961).

Materials and Methods

Starting Materials

Starting materials for the preparation of mixtures consisted of reagent grade boric acid powder and thirteen high-purity oxides obtained either commercially or from the Bureau of Mines. The results of general qualitative spectrochemical analyses of these oxides are given elsewhere (Schneider and Roth, 1960; Schneider, 1960). The purity of the oxides, except for Y_2O_3 (99.7%), was better than 99.9%.

Preparation of Mixtures

Calculated amounts of boric acid and of the respective oxides sufficient to yield 1, 2, or 3- g batches of the 1:1 composition were weighed into plastic containers and thoroughly blended for $\frac{1}{2}$ hr. with a high-speed mechanical mixer. In the preparation of mixtures, 0.3 (wt. %) excess of the calculated amount of boric acid (equivalent to about 0.2% excess B_2O_3) was added to compensate for possible volatilization during heating. Mixtures were pressed at approximately 20,000 psi into discs, $\frac{5}{8}$ in. in diameter; fired slowly to 600° or 700° C., in covered platinum crucibles; and ground in an agate mortar. The process of pressing, heating, and grinding was repeated twice at successively higher temperature intervals, up to a maximum of 900° C. Subsequent "quenching" experiments were done in sealed platinum tubes.

The following representative samples were analyzed by the Chemistry Division of the National Bureau of Standards: $LaBO_3$, $NdBO_3$, $GdBO_3$, $TmBO_3$, and $InBO_3$. Analyses were made on approximately 0.2 g samples, for B_2O_3 only. The results indicated that the samples were deficient in B_2O_3, about 0.5 mol % for $LaBO_3$, $NdBO_3$, and $GdBO_3$; about 0.75 mol % for $TmBO_3$; and about 2 mol % for $InBO_3$. The intermediate com-

pounds would be expected to show similar deviations. As will be noted later, x-ray examination also indicated that some of the heated samples deviated slightly from the equimolar ratio of B_2O_3 to rare-earth oxide.

Apparatus and Method

The temperatures of polymorphic inversions were determined by the well-established quenching technique. Quenched samples were examined mainly by x-ray diffraction powder techniques (Ni-filtered Cu radiation) using a high angle Geiger-counter diffractometer. Where possible, optical data were obtained with the aid of the polarizing microscope. Temperatures were measured with a calibrated platinum versus platinum-rhodium (10%) thermocouple and are given on the International Temperature Scale of 1948. Unless otherwise stated temperature values may be considered accurate to within $\pm 10°$ C. up to about 1300° C., and to within $\pm 15°$ C. at higher temperatures.

Melting points of the compounds were determined in air in a specially designed, inductively heated iridium crucible (Schneider, 1961). Small fragments of material, approximately 1 to 2 mm. in length, were placed in the covered iridium crucible and quickly cooled from various temperatures, by shutting off the power. Temperatures were measured with a calibrated optical pyrometer which was sighted through a hole in the center of the crucible cover. Approximate blackbody conditions prevailed, and the equipment was calibrated against the melting points of Au (1063° C.), Pt (1769° C.) and Rh (1960° C.). Reproducibility of temperature measurements by this method is within $\pm 10°$ C., accuracy better than $\pm 20°$ C.

Results and Discussion

General Relationships

Table 1 lists the significant quenching experiments and includes the temperatures and periods of heat treatments, demonstrations of reversibility, and phases identified by x-ray analysis. The complete data are summarized in Fig. 1, in which the cations are listed along the abscissa, as a function of ionic radius. The dashed lines between adjacent compounds are postulated phase boundaries. The boundaries would probably not be applicable for mixtures of other than adjacent compounds. Melting points of the compounds, as determined with the induction apparatus, are shown by solid squares. Numerical values are given alongside the appropriate cation designations.

The most striking result of this study is that the ABO_3 rare-earth borates possess the same types of structures as calcium carbonate, namely, aragonite, vaterite, and calcite. Of particular interest is the

existence of the vaterite type as a stable phase for ten of the borates. In the $CaCO_3$ system vaterite is apparently only a metastable phase. It may be noted that no one borate compound shows all three polymorphs, as in the case of $CaCO_3$. In fact, only $LuBO_3$ shows two of the polymorphs, *i.e.*, calcite and vaterite. Lanthanum and neodymium borates both show unidentified high-temperature forms.

With decreasing ionic radius, the melting points of the ABO_3 type rare-earth borates decrease from a maximum of $1660 \pm 20°$ C. for $LaBO_3$

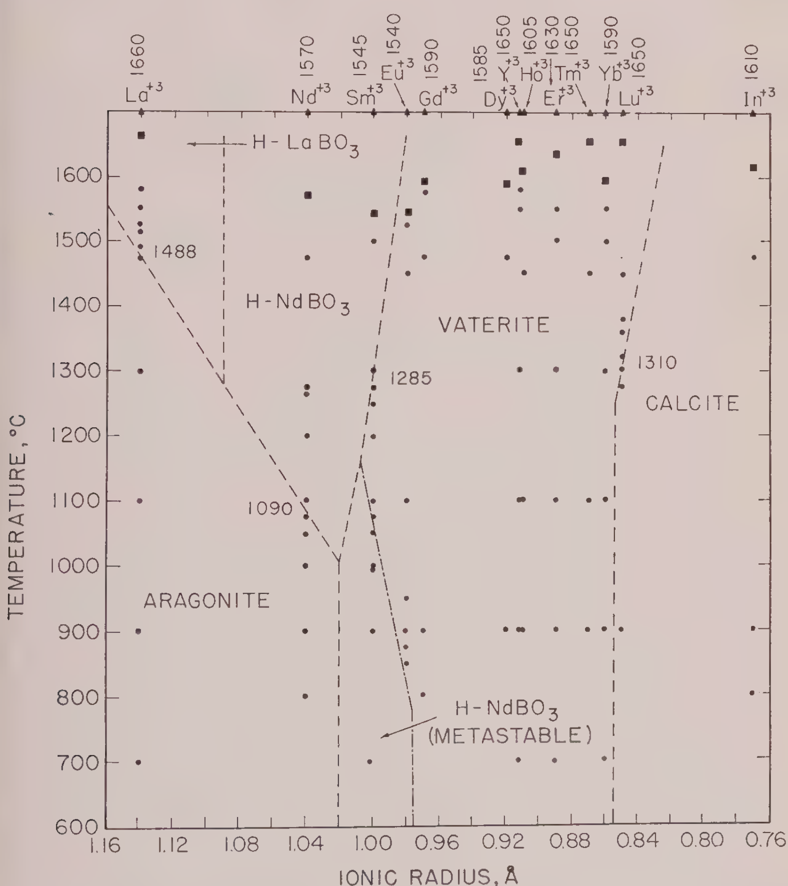

FIG. 1. Stability relationships of the ABO_3-type borates as a function of temperature and ionic radius of the large cation. Temperatures of reversible transitions listed within the diagrams. Dots represent subsolidus experiments. Squares represent liquidus values, given along the top of the figure. Dashed lines indicate boundaries between adjacent ABO_3 compounds. Dash-dot line indicates limit of formation of the metastable high-temperature form in the vaterite field.

to a minimum of 1540 ± 20° C. for $EuBO_3$. The melting points, except for $YbBO_3$ (M. Pt. 1590 ± 20° C.), then increase to a maximum of 1650 ± 20° C. for $LuBO_3$. The non rare-earth borates, YBO_3 and $InBO_3$, melt at 1650 ± 20° C. and 1610 ± 30° C. respectively.

The limitation in accuracy of the melting point determinations is due not so much to the accuracy of temperature measurements but rather to the small variation from compound composition, as revealed by chemical analysis and by some of the *x*-ray diffraction powder patterns. Patterns of the compounds containing the larger ions of La, Nd, Sm, Eu, Gd, and Dy showed a single phase. Vaterite patterns of the borates of Y, Ho, Er, Tm, and Yb showed a few weak extraneous peaks in the 26 to 30° 2θ region. These additional peaks were tentatively ascribed to the compounds of molar ratio 3 R_2O_3 to 1 B_2O_3, as a result of experiments on mixtures of Tm_2O_3 and B_2O_3 (footnote d, Table 1). A compound of the same molar ratio has been found in the La_2O_3-B_2O_3 system (Levin, *et al.*, 1960). Patterns of the compounds of the two smallest ions, Lu and In, showed free Lu_2O_3 and In_2O_3, respectively, indicating that no intermediate compounds form between 1:1 and R_2O_3.

Aragonite Type ABO_3 Rare-Earth Borates

Table 2 gives the indexed *x*-ray diffraction data for $LaBO_3$ and $NdBO_3$, aragonite-type structures, compared with that for $CaCO_3$. The aragonite type structure is orthorhombic, space group Pnam (No. 62), Z = 4. The unit cell dimensions determined for $LaBO_3$ are $a = 5.104$ Å, $b = 8.252$ Å, $c = 5.872$ Å; for $NdBO_3$, $a = 5.037$ Å, $b = 8.076$ Å, $c = 5.729$ Å. The powder patterns for the three compounds are shown diagrammatically in Figure 2. For $CaCO_3$ the a axis and the b axis are smaller than for $NdBO_3$ and $LaBO_3$, whereas the c axis is slightly larger than for $NdBO_3$. These relationships are indicated by the position of the 200, 041, and 002 reflections. The data of Goldschmidt and Hauptmann (1931–32) (Table 2) are in reasonable agreement with the present work. The neodymium ion is the smallest rare earth ion to form an aragonite-type borate. The borates of trivalent praesodymium and cerium, with ionic radii intermediate between lanthanum and neodymium, would be expected also to show an aragonite form.

High-Temperature Polymorphs

Lanthanum borate inverted at 1488 ± 5° C. to a high-temperature form of low symmetry. As may be seen from Table 3, this form has the same powder pattern as that obtained by Keith and Roy (1954) below 1560° C.; however, the optical properties discussed elsewhere (Levin, *et al.*, 1961) do not agree.

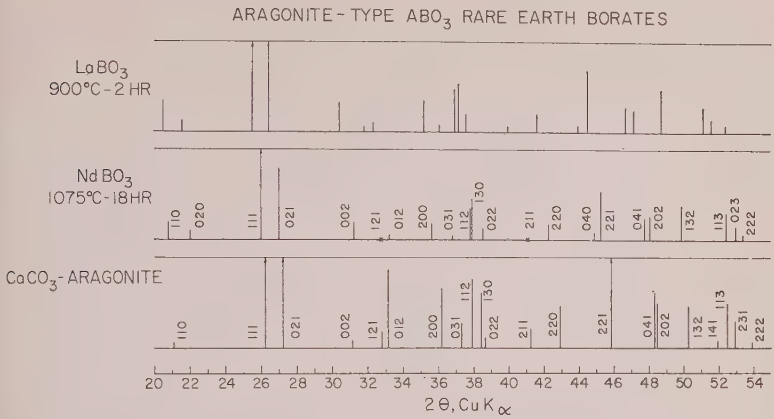

FIG. 2. Diagramatic x-ray diffraction patterns of the aragonite-type ABO_3 borates compared with $CaCO_3$. $CaCO_3$-aragonite after Swanson, Fuyat and Ugrinic (1954).

Neodymium, samarium, and europium borates yielded high temperature forms similar to each other but different from lanthanum borate (Fig. 3). The x-ray powder diffraction data for the high-$NdBO_3$ type polymorph are given in Table 4. Neodymium borate transformed reversibly at 1090° C. to the high form (Fig. 1). Samarium borate showed a reversible transformation above 1285° C. to the high form; below 1050° C. the high form occurred metastably. The high-temperature form of $EuBO_3$ was never obtained as a single major phase but occurred metas-

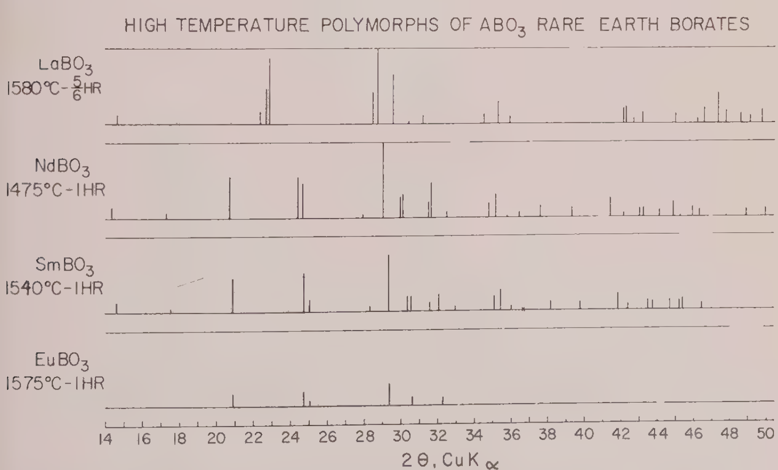

FIG. 3. Diagramatic x-ray diffraction patterns of the unindexed high-temperature polymorphs of ABO_3 borates. $LaBO_3$ differs from $NdBO_3$, $SmBO_3$, and $EuBO_3$.

TABLE 1. PHASES IDENTIFIED IN THE ABO_3 TYPE RARE EARTH BORATES

Compound	Heat Treatment[a] Temp., ° C.	Time, hrs.	*X*-Ray[b]	Notes
$LaBO_3$	700	1.5	Aragonite	
	1475	1	Aragonite	Pattern indexed
	1525/1475[c]	0.67/1	Arag. (l)+H-Form(s)	Shows reversibility
	1490	1	H-Form	
	1580	0.83	H-Form	Pattern measured
$NdBO_3$	800	2	Aragonite	
	1075	18	Aragonite	Pattern indexed
	1100/1075[c]	2/18	Aragonite	Shows reversibility
	1100	2	H-Form	
	1475	1	H-Form	Pattern measured
$SmBO_3$	700	1.5	H-Form	
	1000	65	H-Form	
	1100/1000[c]	15/92	Vaterite	Vaterite not reversible to H-Form at lower temp.
	1050	68.5	H-Form	
	1050	133	H-Form	
	1100/1050[c]	16/64	Vaterite	
	993/1080[c]	16/16	Vaterite (l)+H-Form (m)	
	1100	64	Vaterite	
	1500/1240[c]	1.17/5.5	Vaterite	Shows reversibility at higher temp.
	1275	1	Vaterite	
	1300	2	H-Form	
	1200/1309[c]	24/21	H-Form	
	1540	1	H-Form	Measured pattern
$EuBO_3$	900/850[c]	2/15.5	Vaterite (m)+H-Form (s)	
	900/850/875[c]	2/15.5/15	Vaterite	Metastable H-Form disappeared.
	900	2	Vaterite (l)+H-Form (m)	
	950	15.5	Vaterite	
	1450	1	Vaterite	Pattern indexed
	1540	0.5	Vaterite	
	1575	1	Vaterite (l)+H-Form (m)	Sample melted
$GdBO_3$	800	2	Vaterite	
	1475	1	Vaterite	Pattern indexed
	1575	1	Vaterite	
$DyBO_3$	800	2	Vaterite	
	1475	0.75	Vaterite	Pattern indexed
YBO_3	700	1	Vaterite (l)+Y_2O_3 (s)	
	900	2	Vaterite	
	1100	15	Vaterite	
	1300	2	Vaterite (l)+$3Y_2O_3 \cdot B_2O_3$[d]? (tr).	
	1580	1	Vaterite (l)+$3Y_2O_3 \cdot B_2O_3$[d]? (tr).	Pattern indexed

[a] All heat treatments above 900° C. done in sealed platinum tubes.

[b] When more than one phase is present, the relative amounts are given as: l=large, m=moderate, s=small, tr=trace.

[c] Indicates successive heat treatments of the same sample.

[d] Compositions 95 mol% TM_2O_3, 5 mol% B_2O_3 and 66.67 mol% Tm_2O_3, 33.33 mol% B_2O_3 heated at 1490° C. for 1 hr. showed major peaks corresponding to this unknown phase, indicating a compound intermediate between the pure oxide and the 2 to 1 ratio with B_2O_3.

TABLE 1—(*continued*)

Compound	Heat Treatment[a] Temp. ° C.	Time, hrs.	*X*-Ray[b]	Notes
$HoBO_3$	900	2	Vaterite	
	1100	10	Vaterite	
	1450	1	Vaterite+$3Ho_2O_3 \cdot B_2O_3$[d]? (tr).	Pattern iddexed
$ErBO_3$	700	1.5	Vaterite (l)+Er_2O_3 (m)	
	900	2	Vaterite	
	1100	15	Vaterite (l)+$3Er_2O_3 \cdot B_2O_3$[d]? (s)	
	1300	23	Vaterite (l)+$3Er_2O_3 \cdot B_2O_3$[d]? (s)	Heated in open Pt tube
	1550	1	Vaterite (l)+$3Er_2O_3 \cdot B_2O_3$[d]? (s)	Pattern indexed
$TmBO_3$	900	2	Vaterite	
	1100	19	Vaterite (l)+$3Tm_2O_3 \cdot B_2O_3$[d]? (s)	
	1450	1	Vaterite (l)+$3Tm_2O_3 \cdot B_2O_3$[d]? (m)	
$YbBO_3$	700	1.5	Vaterite (l)+Yb_2O_3 (l)	
	1100	15	Vaterite (l)+Yb_2O_3 (s)	
	1300	2	Vaterite (l)+$3Yb_2O_3 \cdot B_2O_3$[d]? (tr)	
	1550	1	Vaterite (l)+$3Yb_2O_3 \cdot B_2O_3$[d]? (tr)	Pattern indexed
$LuBO_3$	900	2	Calcite (l)+Lu_2O_3 (m)	
	1100	19	Calcite (l)+Lu_2O_3 (m)	
	1275	1	Calcite (l)+Lu_2O_3 (m)	
	1450/1275[c]	1/1	Vaterite (l)+Calcite (l)+Lu_2O_3 (m)	Calcite to vaterite inversion reversible
	1297	17	Calcite (l)+Lu_2O_3 (m)	Pattern indexed
	1320	1	Vaterite (l)+Calcite (m)+Lu_2O_3 (s)	
	1450	1	Vaterite (l)+Lu_2O_3 (m)	Pattern indexed
$InBO_3$	800	2	Calcite (l)+In_2O_3 (l)	
	900	18	Calcite (l)+In_2O_3 (m)	
	1475	0.75	Calcite (l)+In_2O_3 (m)	Pattern indexed
Mn_2O_3:B_2O_3	600	1.25	MnO_2 (1)+Mn_2O_3 (m)	
	800	5	Mn_2O_3	
	900	16	Unidentified	Not a $CaCO_3$ type structure

tably in minor amounts in samples quenched from above the liquidus or as prepared below 900° C.

Vaterite-Type ABO_3 Borates

A brief review of the literature concerning vaterite is given in the appendix.

Table 5 gives the *x*-ray diffraction data for the ten borates found in this study to possess the vaterite-type structure. The diagrammatic comparison of the diffraction patterns (Fig. 4) shows that they agree with the $CaCO_3$-vaterite pattern of DeKeyser and Degueldre (1950). The *c* axis for $CaCO_3$, evident from the position of the 002 reflection, is smaller than for the borates, whereas the *a* axis (see 100 reflection) is larger. In the

TABLE 2. X-RAY DIFFRACTION DATA FOR ARAGONITE-TYPE ABO_3 BORATES ($Cu\ K_{\alpha 1}$ RADIATION)

hkl	$LaBO_3$[a] (1475°/ 1 hr.)		$LaBO_3$[b]		$NdBO_3$[c] (1075°/18 hr.)		$CaCO_3$[d]	
	dÅ	RI%*	dÅ	RI%*	dÅ	RI%*	dÅ	RI%*
110	4.34	12			4.27	21	4.21	2
020	4.12	4			4.04	10		
111	3.49	100	3.48	100	3.43	100	3.396	100
021	3.38	44	3.36	60	3.30	53	3.273	52
002	2.936	24	2.928	40	2.865	20	2.871	4
121	2.820	4			—	—	2.730	9
012	2.765	11			2.696	5	2.700	46
200	2.552	31	2.547	50	2.518	17	2.481	33
031	2.489	4			2.436	5	2.409	14
112	2.431	33			2.377	42	2.372	38
130	2.422	30	2.415	90	—	—	2.341	31
022	2.391	14	2.394	10	2.336	12	2.328	6
211	2.253	3			—	—	2.188	11
220	2.170	12	2.164	20	2.137	16	2.106	23
040	2.062	4			2.018	8		
221	2.036	47	2.034	100	2.003	50	1.977	65
041	1.947	17	1.940	50	1.903	22	1.882	32
202	1.926	27	1.919	50	1.893	23	1.877	25
132	1.868	37	1.863	90	1.828	34	1.814	33
141							1.759	4
113	1.784	21	1.778	90	1.744	25	1.742	25
231							1.728	15
023	1.769	17	1.762	10	1.727	14		
222	1.745	6	1.740	10	1.713	8	1.698	3
042	1.688	4			1.651	5		
310	1.667	3						
240 } 311 }	1.604	11	1.602	60	1.581	11	1.557	4
051/232							1.535	2
150			1.567	2				
241	1.548	11	1.545	50	1.519	11	1.499	4
321							1.475	3
151	1.517	15	1.513	60	1.484	10	1.466	5
223	1.454	8			1.425	15		
014/312			1.446	70			1.411	5

* RI is the intensity of each diffraction peak relative to the strongest peak.

[a] Orthorhombic cell: $a=5.104$, $b=8.252$, $c=5.872$ Å.

[b] Goldschmidt and Hauptmann, p. 67 (1931 32) d values calculated from corrected θ values listed by authors.

[c] Orthorhombic cell: $a=5.037$, $b=8.076$, $c=5.729$ Å.

[d] Swanson, Fuyat and Ugrinic (1954).

TABLE 2—(*continued*)

hkl	$LaBO_3$[a] (1475°/1 hr.)		$LaBO_3$[b]		$NdBO_3$[c] (1075°/18 hr.)		$CaCO_3$[d]	
	*d*Å	RI%*	*d*Å	RI%*	*d*Å	RI%*	*d*Å	RI%*
330	1.447	11					1.404	3
043	1.420	6						
242	1.408	4			1.381	5	1.365	3
114	1.391	8			1.358	5	1.358	3
060							1.328	2
332	1.298	15			1.276	9	1.261	6
400							1.240	7
204	1.272	8						
313	1.269	9			1.247	11		
134	1.255	19			1.227	7	1.224	5
062	1.246	6					1.205 }	6
243	1.2409	7						
153	1.2250	8					1.1892	5
260	1.2109	10					1.1712	6
421	1.1941	6					1.1599	3
402	1.1707	3						
351	1.1619	6						
115	1.1334	5						
025	1.1297	5						
262	1.1195	6						
314	1.1015	9						
244	1.0832	3						
441	1.0673	5						
423	1.0353	5						
225	1.0327	6						
334	1.0305	6						
045	1.0204	5						
442	1.0180	5						
353	1.0137	15						

vaterite-type borates, if the two weak reflections 101 and 103 were missing, the *c* axis would be halved. In $CaCO_3$, however, the 101 reflection is pronounced (see Fig. 4). Decreasing ionic radii of the rare earth ions from $SmBO_3$ to $LuBO_3$ are associated with decreasing interplanar spacings (larger two theta values) for corresponding reflections.

A number of the *x*-ray diffraction peaks, especially for angles larger than 60° 2θ, were broad and diffuse rather than narrow and sharp as is characteristic of well-crystallized material. Furthermore, the $K_{\alpha 1}$ and $K_{\alpha 2}$ doublets were not resolved in any of the vaterite patterns. Attempts to obtain better material by heating in the sealed platinum tubes for

periods of 64 hrs. at 1100° C. ($SmBO_3$, Table 1) and 23 hrs. at 1300° C. $ErBO_3$) were unsuccessful. Likewise, 5-minute heating periods in the induction furnace just above or below the melting points failed to produce sharper patterns. Study of $YbBO_3$ with a high-temperature x-ray spectrometer up to 1000° C. did not reveal any inversions or improvement of the pattern.

Optical examination showed that the vaterite-type borates had a moderately low birefringence, about .007 for $SmBO_3$ and $EuBO_3$, and

Table 3. X-Ray Powder Diffraction Data for the High-Temperature Form of $LaBO_3$ (Cu $K_{\alpha 1}$ Radiation)

Present Investigation (1580°/$\frac{5}{6}$ hr.)		Keith and Roy (1954) (below 1560°)	
dÅ	RI%*	dÅ	RI%*
6.03	10	5.64	7
3.98	20		
3.92	43	3.91	20
3.89	76		
3.13	44		
3.11	100	3.10	100
3.02	73	3.01	90
2.94	11		
2.87	11	2.86	5
2.60	13		
2.54	34	2.54	7
2.50	13		
2.143	26		
2.135	30	2.13	10
2.114	10	2.085	3
2.092	20	2.07	2
2.013	11	2.01	15
1.962	9		
1.948	28	1.946	5
1.919	56	1.916	15
1.902	21		
1.872	19	1.875	3
1.854	14		
1.831	26	1.828	7
1.738	9		
1.700	7		
1.631	10		
1.613	13	1.610	5
1.582	7		
1.556	10		

* RI is the intensity of each diffraction peak relative to the strongest peak.

TABLE 4. *X*-RAY DIFFRACTION DATA FOR $NdBO_3$, $SmBO_3$ AND $EuBO_3$ HIGH-TEMPERATURE POLYMORPHS ($CuK_{\alpha 1}$ RADIATION)

$NdBO_3$ (1475°/1 hr.)		$SmBO_3$ (1550°/1 hr.)		$EuBO_3$[a] (1575°/1 hr.)	
*d*Å	RI%[b]	*d*Å	RI%[b]	*d*Å	RI%[b]
6.17	16	6.07	13		
5.13	8	5.06	11		
4.29	52	4.26	56	4.26	48
3.65	58	3.60	72	3.60	58
3.61	49	3.56	28	3.55	35
3.20	8	3.15	13		
3.076	100	3.044	100	3.04	100
2.983	28	2.944	27		
2.968	33	2.926	29	2.91	42
2.839	26	2.832	20		
2.828	52	2.789	34	2.775	40
2.753	10	2.715	10		
2.577	18	2.556	30		
2.552	27	2.531	43		
2.507	6	2.490	9		
2.462	6				
2.391	13	2.356	15		
2.290	9	2.264	15		
2.177	20	2.158	26		
2.141	5	2.131	8		
2.100	10				
2.090	10	2.070	12		
2.051	9	2.026	20		
2.018	19				
2.000	19	1.997	23		
1.973	10				
1.957	7	1.953	21		
1.901	9	1.873	21		
1.861	10	1.837	20		
1.824	17	1.801	20		
1.801	13	1.779	21		
1.750	14				
1.735	14	1.728	24		
1.728	12	1.697	12		
1.719	8				
1.674	6				
1.654	11				
1.633	8	1.613	17		
1.603	8				

[a] Formed in quenched liquid, Vaterite is major phase present.
[b] RI is the intensity of each diffraction peak relative to the strongest peak.

TABLE 5. *X*-RAY POWDER DIFFRACTION DATA FOR VATERITE-TYPE ABO_3 RARE-EARTH BORATES ($CuK_{\alpha 1}$ RADIATION)

hkl[a]	$SmBO_3$ (1200°/24 hr.)		$EuBO_3$ (1450°/1 hr.)		$GdBO_3$ (1475°/1 hr.)		$DyBO_3$ (1475°/¾ hr.)		YBO_3 (1580°/1 hr.)		Keith & Roy (1954)	
	*d*Å	RI%[b]	*d*Å	RI%[b]	*d*Å	RI%[b]	*d*Å	RI%[b]	*d*Å	RI%[b]	*d*Å	RI%[b]
002	4.48	44	4.47	37	4.45	52	4.42	40	4.41	30	4.375	30
100	3.34	100	3.33	100	3.32	100	3.28	100	3.27	100	3.277	100
101	3.13	9	3.12	10	3.11	10	3.08	8	3.07	16	3.06	10
102	2.68	91	2.67	94	2.66	99	2.64	51	2.63	72	2.62	60
004	2.24	15	2.23	16	2.22	14	2.21	7	2.20	9		
103			2.22	7	2.20	6			2.19	4	2.195	10
110	1.930	48	1.922	46	1.915	42	1.896	25	1.888	87	1.885	35
104	1.861	41	1.856	40	1.848	49	1.834	17	1.826	59	1.82	25
112	1.773	41	1.766	34	1.760	23	1.742	13	1.735	54	1.73	20
200	1.672	19	1.665	16	1.658	13	1.641	9	1.636	10	1.631	7
202	1.566	26	1.561	21	1.554	21	1.539	9	1.533	13	1.532	15
006									1.468	2		
114	1.462	14	1.456	12	1.451	10	1.438	5	1.433	4		
106	1.363	14	1.359	12	1.354	15	1.344	3	1.338	6	1.337	5
204	1.340	13	1.334	14	1.330	15			1.313	6	1.311	2
210	1.263	13	1.258	12	1.253	12	1.242	5	1.236	5	1.328[c]	2
212	1.216	19	1.212	17	1.208	16	1.195	7	1.190	9	1.189	10
116			1.176	9					1.158	2		
008												
206												
300	1.113	10	1.110	11					1.090	4		
214	1.101	12	1.097	11					1.078	5		
302	1.080	8	1.076	9					1.058	3		
108									1.042	2		

hkl	$HoBO_3$ (1100°/19 hr.)		$ErBO_3$ (1550°/1 hr.)		$TmBO_3$ (1450°/1 hr.)		$YbBO_3$ (1551°/1 hr.)		$LuyBO_3$ (1450°/1 hr.)	
	*d*Å	RI%	*d*Å	RI%	*d*Å	RI%	*d*Å	RI%	*d*Å	RI%
002	4.41	61	4.38	32	4.38	43	4.37	34	4.35	54
100	3.27	100	3.25	100	3.25	100	3.23	100	3.23	100
101	3.06	11	3.05	11	3.04	6	3.03	7	3.02	5
102	2.63	89	2.62	76	2.61	74	2.60	71	2.59	78
004	2.20	15	2.20	8	2.19	10	2.18	8	2.18	15
103	2.19	4	2.18	2	2.17				2.16	2
110	1.888	32	1.880	40	1.873	35	1.866	37	1.861	35
104	1.827	35	1.821	28	1.816	27	1.811	25	1.805	32
112	1.735	24	1.729	28	1.723	26	1.717	27	1.713	27
200	1.635	8	1.629	13	1.622	11	1.616	14	1.613	12
202	1.533	12	1.527	17	1.522	14	1.516	16	1.513	14
006	1.465	2	1.462	2	1.461	1	1.456	1	1.453	2
114	1.432	6	1.429	7	1.423	6	1.419	7	1.419	7
106	1.340	7	1.335	6	1.331	6	1.328	5	1.325	7
204	1.313	6	1.309	7	1.304	6	1.300	6	1.298	7
210	1.236	4	1.231	7	1.227	6	1.222	7	1.219	6
212	1.190	8	1.186	11	1.181	9	1.177	10	1.174	9
116	1.160	2	1.155	3	1.153	3	1.149	2	1.146	2
008					1.096	1	1.092	1	1.089	2
206					1.087	3	1.083	3	1.082	3
300	1.090	4	1.086	5	1.082	4	1.078	4	1.076	4
214	1.078	4	1.074	6	1.071	5	1.067	5	1.065	5
302	1.058	3	1.055	4	1.050	4	1.046	4	1.044	3
108	1.043	2	1.041	2	1.038	2	1.035	2	1.032	2

[a] Unit cell dimensions for the hexagonal indices are listed in Table 9.
[b] RI is the intensity of each diffraction peak relative to the strongest peak.
[c] Out of order, possibly 1.238.

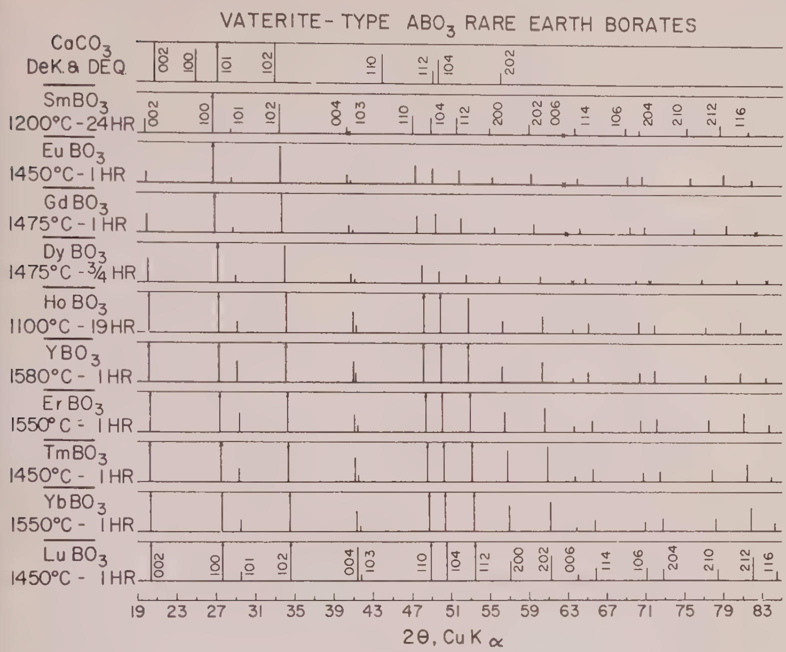

FIG. 4. Diagramatic x-ray diffraction patterns of the vaterite-type ABO_3 borates compared with $CaCO_3$. $CaCO_3$-vaterite after DeKeyser and Degueldre (1950).

about .015 for the others (Table 6). The indices of refraction decreased with decreasing radius of the rare earth cation from Sm^{+3} to Lu^{+3}. With the exception of Y^{+3} (not a rare earth), the indices are grouped by pairs, *e.g.*, $SmBO_3$ and $EuBO_3$, $GdBO_3$ and $DyBO_3$, etc. The positive character of the compounds was easily ascertained on off-centered interference figures. However, as the intersection of the isogyres was never observed, it was not possible to characterize the material as uniaxial, or biaxial with a small optic axial angle. No twinning phenomenon was apparent, although some of the sample showed good anhedral grain growth.

The most logical explanation for the x-ray and optical data is that vaterite-type borates are only pseudo-hexagonal.

An infrared examination made by C. Weir of this Laboratory showed that the pattern of μ-$CaCO_3$ was considerably different from that of the vaterite-type borates. In the three forms of $CaCO_3$, carbon is in a CO_3^{2-} planar group with three-fold oxygen coordination. However, the infrared patterns of the vaterite-type borates can be interpreted as indicating that boron has a tendency toward oxygen coordination greater than 3. A non-planar boron-oxygen configuration may explain the stability of the vaterite-type borates.

TABLE 6. OPTICAL PROPERTIES OF ABO_3 RARE-EARTH BORATES

Compound	Heat Treatment		Indices of Refraction (λ_D, 25° C.)			Sign	2V	Birefringence	Structure Type[b]
	Temp., ° C.	Time, hrs.	alpha	beta	gamma				
Low-$LaBO_3$	1300	$3\frac{1}{4}$	1.800	1.877	1.882	−	~20°	0.084	Aragonite
High-$LaBO_3$	1581	1	1.742	1.856	1.878	−	~50°	0.136	Unknown
Low-$NdBO_3$[a]	1075	18	..	..	..	..			Aragonite
High-$NdBO_3$	1475	1	1.789	..	1.883	−	medium	0.094	Unknown
High-$SmBO_3$	1550	1	1.789	..	1.897	−	medium	0.108	Unknown
			ordinary		extraordinary				
$SmBO_3$	1250	1	1.842		1.849	+[c]		0.007	Vaterite
$EuBO_3$	1525	1	1.841		1.848	+[c]		0.007	Vaterite
$GdBO_3$	1575[d]		1.824		1.840	+[c]		0.016	Vaterite
$DyBO_3$	1525[d]		1.823		1.837	+[c]		0.014	Vaterite
YBO_3	1645[d]		1.788		1.802	+[c]		0.014	Vaterite
$HoBO_3$	1475	1	1.816		1.830	+[c]		0.014	Vaterite
$ErBO_3$	1604[d]		1.815		1.830	+[c]		0.015	Vaterite
$TmBO_3$	1647[d]		1.812		1.828	+[c]		0.016	Vaterite
$YbBO_3$	1550	1	1.809		1.824	+[c]		0.015	Vaterite
High-$LuBO_3$	1647[d]		1.803		1.817	+[c]		0.014	Vaterite
Low-$LuBO_3$[a]	1297	17				−			Calcite
$InBO_3$	1475	1	1.873		1.773	−		0.100	Calcite

[a] Too fine grained to obtain optical data.
[b] From indexed x-ray powder pattern.
[c] From off-centered interference figure.
[d] Held at temperature in induction furnace for about 5 minutes.

The similarity of the x-ray data for vaterite-$CaCO_3$ and many of the borates indicates that the arrangements of the heavy cations are essentially the same. On the other hand, the dissimilarity of the infrared patterns indicates that some differences exist in the anion bonding configuration.

Yttrium Borate

It may be noted from Fig. 1 that YBO_3 lies in the middle of the field of vaterite-type compounds and that no polymorphism is indicated. Various contemporary texts on crystal chemistry list YBO_3 as having the calcite-type structure. The source of this statement is probably the original paper of Goldschmidt and Hauptmann (1931–32). They reported that a sample of YBO_3 quickly cooled from the melt gave a residue ("Reste") of the calcite-type structure. At lower temperatures, a "biaxial-crystal type" was found, which was believed to be related to the vaterite structure. It should be emphasized that the "yttrium" used by Goldschmidt and Hauptmann in the preparation of the yttrium borate was a mixture of yttrium earths of average atomic weight 104.7 (atomic wt. Y = 88.92), obtained from the mineral thalenite.

Keith and Roy (1954) found that only one crystalline form of YBO_3

existed from room temperature to the melting point. They concluded that their YBO_3 compound was not of the vaterite type when compared with the incomplete data of Brooks, Clark and Thurston (1951). However, the x-ray data of Keith and Roy and that obtained in the present study are in good agreement (Table 5). The melting point of YBO_3 (1650 ± 20° C.) determined by the inductively heated iridium crucible method is some 70° C. above that reported by Keith and Roy (1580 ± 20° C.) using a strip furnace.

Calcite-Type ABO_3 Borates

Lutecium borate, formed from the smallest rare-earth ion, and indium borate were the only two calcite-type structures found in this study. Lutecium borate showed a reversible transformation at 1310° C. from the low-temperature calcite form to the high-temperature vaterite form.

The x-ray diffraction data for the calcite-type borates are given in Table 7, together with the data of Goldschmidt and Hauptmann for $InBO_3$. For purposes of comparison the data for calcite are given, and both rhombohedral and hexagonal indexing are shown. A diagrammatic comparison of the powder patterns is shown in Fig. 5. The space group for calcite is $R\,\bar{3}c$, with 6 molecules per unit cell when indexed on a hexagonal basis.

In $InBO_3$, the c axis (from the 006 reflection) is considerably less than in $LuBO_3$, but the a axis (from the 110 reflection) is only slightly smaller. Consequently, for large values of l relative to hk, a number of reversals occur in the order of the position of the reflections, *e.g.*, 108/116 and

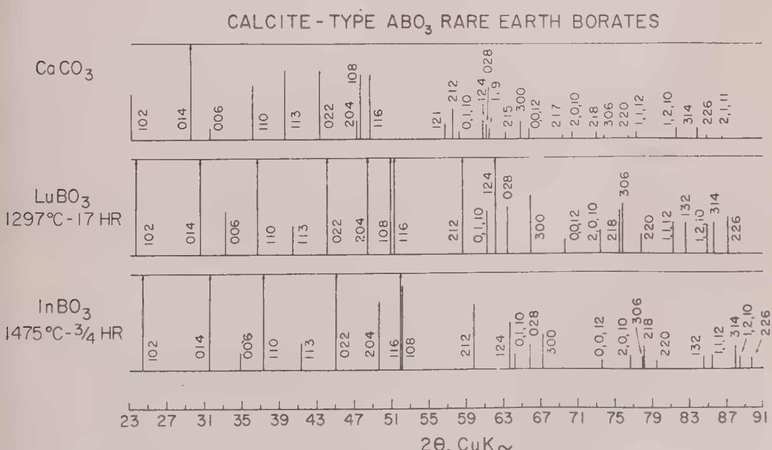

FIG. 5. Diagrammatic x-ray diffraction patterns of the calcite-type ABO_3 borates compared with $CaCO_3$. $CaCO_3$-calcite after Swanson and Fuyat (1953).

TABLE 7. X-RAY POWDER DIFFRACTION DATA FOR CALCITE-TYPE ABO_3 BORATES ($CuK_{\alpha 1}$ RADIATION)

Rhombohedral	Hexagonal	$CaCO_3$[a]		$LuBO_3$		$InBO_3$		$InBO_3$ Gold. & Haupt. (1931–32)	
hkl	*hkl*	*d*Å	RI%[b]	*d*Å	RI%[b]	*d*Å	RI%[b]	*d*Å[c]	RI%[b]
110	102	3.86	12	3.76	96	3.67	100	3.68	50
121	014	3.035	100	2.933	100	2.836	98	2.840	60
222	006	2.845	3	2.699	10	2.574	5	2.583	5
011	110	2.495	14	2.453	53	2.411	36	2.414	40
120	113	2.285	18	2.235	7	2.184	7	2.193	20
020	022	2.095	18	2.057	44	2.016	28	2.016	40
220	204	1.927	5	1.883	26	1.837	20	1.837	30
332	108	1.913	17	1.828	31	1.753*	21	1.756	100
231	116	1.875	17	1.817	54	1.760	36		
$02\bar{1}$	121	1.626	4						
$12\bar{1}$	212	1.604	8	1.577	27	1.547	19	1.546	60
343	0·1·10	1.587	2	1.515	10	1.450*	5	1.457	60
130	124	1.525	5	1.495	23	1.462	14		
242	028	1.518	4	1.468	11	1.418	8	1.418	30
342	119	1.510	3						
230	215	1.473	2						
$11\bar{2}/\bar{1}2\bar{1}$	300	1.440	5	1.418	14	1.392	10	1.390	50
444	0·0·12	1.422	3	1.351	4	1.288	2	1.287	20
241	127	1.356	1						
442	2·0·10	1.339	2	1.290	6	1.242	4	1.243	20
341	218	1.297	2	1.260	10	1.222*	7	1.222	80
141/330	306	1.284	1	1.256	12	1.225	4		
$02\bar{2}$	220	1.247	1	1.228	5	1.206	3	1.206	20
453	1·1·12	1.235	2	1.184	8	1.136*	4	1.136*	40
$03\bar{1}$	132	—	—	1.168	7	1.146	4	1.145	40
352	1·2·10	1.180	3	1.142	7	1.104*	4	1.105	60
231	314	1.154	3	1.133	8	1.110	6		
240	226	1.1425	1	1.118	8	1.092	4	1.091	50
452	2·1·11	1.1244	<1					1.0357	10
464	0·2·14	1.0613	1			0.9761*	1	0.9760*	20
554	1·0·14					1.0673	1	1.0681	20
$22\bar{2}$	402			1.0547	2				
040	044	1.0613	1	1.0290	4	1.0081	3	1.0068	30
251	138	1.0447	4	1.0199	7	.9935	4	.9924	50
$13\bar{2}$	322					.9511	3	.9498	50

* Reversal in order of *hkl* $CaCO_3$-calcite.

[a] Swanson and Fuyat (1953).

[b] RI is the intensity of each peak relative to the strongest peak.

[c] Converted from corrected 2θ to interplanar spacing.

TABLE 7—(*continued*)

Rhombohedral	Hexagonal	$CaCO_3$[a]		$LuBO_3$		$InBO_3$		$InBO_3$ Gold. & Haupt. (1931–32)	
hkl	*hkl*	*d*Å	RI%[b]	*d*Å	RI%[b]	*d*Å	RI%[b]	*d*Å[c]	RI%[b]
363/552	0·3·12					.9455	4	.9445	60
565	0·1·16					.9412	2		
14$\bar{1}$	234					.9304	3		
451	3·1·10					.9268	2	.9278	60
440	408					.9188	2	.9179	20
12$\bar{3}$/1$\overline{32}$	410					.9117	2	.9112	40
563	2·1·14					.9048	2	.9041	20
462	2·2·12					.8803	2	.8800	50
664	2·0·16					—	—	.8781	20
—	—					—	—	.8660	10
150/34$\bar{1}$	146					.8595	4	.8579	100
666	0·0·18					.8587	3		
						.8307	1		
						.8240	2		
						.8144	3		
						.8088	2		
						.8039	2		
						.7993	1		
						.7853	2		

), 1, 10/124 pairs. No reversals in line position occur for the portion of the patterns of $CaCO_3$ and $LuBO_3$ that are shown in Fig. 5.

Scandium borate, reported by Goldschmidt and Hauptmann (1931–32) as having the calcite structure, was not investigated. As Mn_2O_3 has the same structure as Sc_2O_3 a composition of one to one molar ratio of Mn_2O_3 to B_2O_3 was investigated for compound formation. No calcite-type compound was formed (Table 1).

Birefringence of $InBO_3$ was found to be 0.100 (Table 7). According to Hartshorne and Stuart (1952, pg. 148), the greater the oxygen-oxygen separation in a planar group the less the birefringence, because of less inductive effect between the oxygens. The oxygen-oxygen separation in a BO_3^{3-} group was calculated to be about 2.38 Å, from data on $Co_3(BO_3)_2$ and $Mg_3(BO_3)_2$ structures given in Tables of Inter-atomic Distances (1958). This separation is larger than that in the CO_3^{2-} group (2.18 Å) and the NO_3^-group (2.10 Å). Consistent with the principle stated above, with decreasing oxygen separation, the birefringence of the calcite structures increases from 0.100 for $InBO_3$ to 0.172 for $CaCO_3$ to 0.250 for $NaNO_3$.

Factors Affecting Polymorphism

The unit cell parameters for the indexed ABO_3 polymorphs obtained in this study are given in Table 8, together with the larger cation radii, radius ratios (A^{3+}/O^{2-}) and the densities calculated from the *x*-ray powder patterns. Cation radii in parentheses are taken from Roth and Schneider (1960), as determined from a plot of the unit cell dimensions of the C-type rare-earth oxide structures versus the cation radius.

A comparison of the radius ratios for the ABO_3 compounds of the carbonates, borates, and nitrates is instructive. In the carbonates a radius ratio of 0.71 (Ca^{2+}/O^{2-}) appears to be critical. Compounds with radius ratios above 0.71, *e.g.*, $SrCO_3$ and $BaCO_3$, form an aragonite type

TABLE 8. UNIT CELL DIMENSIONS OF ABO_3 RARE-EARTH BORATES

Compound	[a]Radius of A^{3+} Å	[b]Radius ratio	*a*Å	*b*Å	*c*Å	Hex. c/a	[c]Density, Calc. g/cc
Aragonite-Type							
$LaBO_3$	1.14	0.81	5.104	8.252	5.872		5.309
$NdBO_3$	1.04	0.74	5.037	8.076	5.729		5.786
$CaCO_3$	0.99	0.71	4.959	7.968	5.741		2.930
Vaterite Type							
$CaCO_3$	0.99	0.71	4.134		8.47	2.05	2.65
$SmBO_3$	1.00	0.71	3.858		8.96	2.32	6.01
$EuBO_3$	0.98	0.70	3.845		8.94	2.32	6.12
$GdBO_3$	0.97	0.69	3.829		8.89	2.32	6.36
$DyBO_3$	0.92	0.66	3.791		8.84	2.33	6.68
YBO_3	0.92 (.91)	0.66 0.65	3.777		8.81	2.33	4.51
$HoBO_3$	0.91	0.65	3.776		8.80	2.33	6.84
$ErBO_3$	0.89	0.64	3.761		8.79	2.34	6.97
$TmBO_3$	0.87	0.62	3.748		8.76	2.34	7.13
$YbBO_3$	0.86	0.614	3.732		8.74	2.34	7.30
$LuBO_3$	0.85	0.607	3.725		8.71	2.34	7.42
Calcite-Type							
$CaCO_3$[d]	0.99	0.71	4.989		17.062	3.420	2.711
$LuBO_3$[e]	0.85	0.61	4.913		16.214	3.300	6.871
$InBO_3$[f]	0.81 (.77)	0.58 0.55	4.823		15.456	3.204	5.555

[a] Ahren's radii. Values in parenthesis after Roth and Schneider (1960).
[b] Ratio of radii of rare earth cation to oxygen ion.
[c] From lattice parameters, with Z=4 for aragonite, 2 for vaterite, and 6 for calcite.
[d] For rhombohedral cell: $a=6.375$ Å, $\alpha=46.08°$.
[e] For rhombohedral cell: $a=6.104$ Å, $\alpha=47.46°$.
[f] For rhombohedral cell: $a=5.856$ Å, $\alpha=48.64°$.

structure at room temperature and calcite type structure at elevated temperatures. Below a radius ratio of 0.71, *e.g.*, $CdCO_3$, $ZnCO_3$, and $MgCO_3$, calcite-type structures are found. Calcium carbonate at room temperature shows both aragonite and calcite, with the exact stability relationships somewhat in question. This carbonate is the only one which can form a vaterite phase.

The stability relationships of the borate polymorphs are different. Above a radius ratio of 0.71, the aragonite-type borates are stable at room temperature, *e.g.* $NdBO_3$ and $LaBO_3$. Between radius ratios of 0.71 (for $SmBO_3$) and 0.61_4 (for $YbBO_3$), the vaterite-type exists as the only stable phase. At radius ratio 0.60_7 (for $LuBO_3$), the vaterite-type structure is stable above 1310° C.; the calcite-type structure is stable below this temperature. Below a radius ratio of 0.60_7 the calcite-type structure is stable, *e.g.*, $InBO_3$ and $ScBO_3$.

It is interesting to note that $CdCO_3$ among the carbonates and $NaNO_3$ among the nitrates with radius ratios of 0.69 and 0.67, respectively, form calcite-type structures even though the radius ratios fall within the vaterite group when compared with the borates. However, the radius ratio for $NaNO_3$ is 0.54 when based on univalent cation and anion values (Na^+/O^-) (Pauling, 1960). This radius ratio would place it in the calcite group, as the 0.61 borate tolerance ratio would not be greatly lowered when calculated for univalent radii. The next larger alkali ion, K^+, forms aragonite-type KNO_3; thus it is not surprising that a stable vaterite-type structure is not found in the nitrates.

Another significant comparison between the borates and carbonates concerns the densities of the vaterite and calcite-type structures. Whereas the vaterite form of $CaCO_3$ has a slightly lower density than the calcite form at atmospheric pressure, $LuBO_3$-vaterite type has a considerably higher density than the calcite-type polymorph (Table 8). The vaterite-type structure still would be more dense than the calcite-type structure at the temperature of transition, 1310° C., because of the large difference in room-temperature densities of about 0.55 g/cc. Jamieson (1957) did not find a change in *x*-ray pattern when precipitated $CaCO_3$-vaterite containing 10% calcite was pressure cycled up to a maximum of 24,000 bars. Applying LeChatelier's Theorem to the transition of $LuBO_3$ from the low-temperature-calcite type to the high-temperature, denser vaterite form, the effect of increased pressure would be to lower the transition temperature, or at constant temperature to favor the transition.

An increase in pressure would not favor the formation of a calcite-type structure for any of the rare earth borates. Unit cell dimensions and densities of calcite-type structures can be postulated for the rare earth borates, by extrapolation of data from known calcite-type borates. The

postulated calcite-type structures would always be the least dense, as in the case of $LuBO_3$. The fact that the vaterite-type borate has a greater density than the calcite type is consistent with the postulated nonplanar configuration of the BO_3^{3-} group in the vaterite-type structure, which would result in more efficient packing.

Lander (1949) reported that $BaCO_3$ and $SrCO_3$, which have the aragonite structure at room temperature, show a calcite-type structure at elevated temperatures. The calcite-type structure was not quenchable but was observed with high-temperature *x*-ray equipment. The possibility should be considered that $LaBO_3$ and $NdBO_3$, for example, might possess a non-quenchable calcite-type polymorph. High-temperature *x*-ray diffraction patterns showed only the aragonite-type structure up to 1100° C. Therefore, such a transformation seems unlikely.

A consideration of the reported tentative crystal structure of $CaCO_3$-vaterite together with the infrared data of the vaterite-type borates is instructive. Both Hans-Jurgen Meyer (1959) and McConnell (1960) independently arrived at the conclusion that $CaCO_3$-vaterite is one end member of the group bastnaesite ($CeFCO_3$)-parisite ($2CeFCO_3 \cdot CaCO_3$)-roentgenite ($3CeFCO_3 \cdot 2CaCO_3$)-synchisite ($CeFCO_3 \cdot CaCO_3$)-vaterite ($CaCO_3$). However, Donnay and Donnay (1953) conclude that "compositions richer in calcium than synchisite with analogous crystal structures are not to be expected," because with the nearly vertical arrangement of the carbonate groups, the calcium coordination number would be too low. In accordance with this conclusion, $CaCO_3$-vaterite only exists metastably. However, as mentioned previously, the infrared data for the vaterite-type borates indicate that the anion configuration is different from that in $CaCO_3$-vaterite. This difference may account for the greater stability of the vaterite borates.

Summary

(1) Polymorphic relationships as a function of temperature and ionic radius were investigated for thirteen ABO_3-type borates, including all of the normally trivalent rare earth ions as well as La^{+3}, Y^{+3}, In^{+3}, and Mn^{+3}. The chief method of identification was by means of *x*-ray powder diffraction techniques.

(2) The melting points of the ABO_3 compounds determined with an inductively heated iridium crucible were found to be within $\pm 20°$ C. as follows: $LaBO_3$-1660° C.; $NdBO_3$-1570° C.; $SmBO_3$-1545° C.; $EuBO_3$-1540° C.; $GdBO_3$-1590° C.; $DyBO_3$-1585° C.; YBO_3-1650° C.; $HoBO_3$-1605° C.; $ErBO_3$-1630° C.; $TmBO_3$-1650° C.; $YbBO_3$-1590° C.; $LuBO_3$-1650 C., and $InBO_3$-1610° C.

(3) In general, the borate compounds had the same structure types as

the three forms of $CaCO_3$, *i.e.*, aragonite, vaterite, and calcite.

(4) $LaBO_3$ and $NdBO_3$ showed a low-temperature aragonite-type structure. At 1488° C. and 1090° C., respectively, they transformed to high-temperature forms, which were different from each other.

(5) Above 1285° C., $SmBO_3$ showed the same high-temperature polymorph as $NdBO_3$. The stable polymorph below this temperature was vaterite. The behavior of $SmBO_3$ was interesting in that the high form occurred metastably below about 1050° C.

(6) Whereas vaterite only forms metastably in the $CaCO_3$ system, the following borates were found to have a stable vaterite-type phase up to the melting point: $EuBO_3$, $GdBO_3$, $DyBO_3$, YBO_3, $HoBO_3$, $ErBO_3$, $TmBO_3$, and $YbBO_3$.

(7) Lutecium borate, containing the smallest rare earth ion, was found to have a reversible transformation at 1310° C. between the vaterite-type structure at high temperature and the calcite-type structure at low temperature. Indium borate existed only as the calcite form. Yttrium borate did not form a calcite-type structure, as often reported in the literature. Preliminary experiments to form a $MnBO_3$ carbonate-type structure were unsuccessful.

(8) Optical and x-ray examination of the ABO_3 vaterite-type compounds indicated that the unit cell might be only pseudo-hexagonal.

(9) A discussion of radius ratio, density, and pressure, in addition to interpretation of infrared and structure data may explain why the vaterite-type structure is more stable in the borates than in the carbonates.

(10) A comparison of the published powder diffraction data for vaterite is given in an appendix.

References

Brooks, R., Clark, L. M. and Thurston, E. F. (1950–51), Calcium carbonate and its hydrates: *Phil. Trans. Royal Soc.*, **243A**, 145–167.

DeKeyser, W. L. and Degueldre, L. (1950), Contribution à l'étude de la formation de la calcite, aragonite et vatérite: *Bull. Soc. Chim. Belg.* **59**, 40–71.

Donnay, G. and Donnay, J. D. H. (1953), The crystallography of bastnaesite, parisite, roentgenite, and synchisite: *Am. Mineral.*, **38**, 932–963.

Gibson, R. E., Wyckoff, R. W. G. and Merwin, H. (1925), Vaterite and μ calcium carbonate: *Am. J. Sci.*, **10**/5th series/325–333.

Goldschmidt, V. M. and Hauptmann, H. (1931–32), Isomorphie von Boraten und Karbonaten: *Nachr. Ges. Wiss. Gott. Math-Phys. Kl.*, 53–72.

Hartshorne, N. H. and Stuart, A. (1952), Crystals and the Polarising Microscope: Edward Arnold & Co., London.

Heide, F. (1924), Vaterite: *Centralblatt für Mineralogie, Geologie, und Paläontologie*, **21**, 641–651.

Jamieson, J. C. (1957), Introductory studies of high-pressure polymorphism to 24,000 bars by x-ray diffraction with some comments on calcite II: *J. Geol.*, **65**, 334–343.

Keith, M. L. and Roy, R. (1954), Structural relations among double oxides of trivalent elements: *Am. Mineral.*, **39**, 1–23.

LANDER, J. J. (1949), Polymorphism and anion rotational disorder in the alkaline earth carbonates: *J. Chem. Physics*, **17**, 892–901.

LEVIN, E. M., ROBBINS, C. R. AND WARING, J. L. (1961), Immiscibility and the system lanthanum oxide-boric oxide: *Jour. Am. Cer. Soc.*, **44**, 87–91.

MCCONNELL, J. D. C. (1960), Vaterite (μ-$CaCO_3$) from Ballycraigy, Larne, Northern Ireland; Exhibit: *Min. Mag.*, **32**, [249], lxvii. Publication: *Min. Mag.*, **32**, [250], 535–544 (1960).

MEIGEN, E. W. G. (1911), *Verh. Ges. deutsch. Naturfor., Ärzte Königsberg*, **2**, 124.

MEYER, HANS-JURGEN (1959), Über Vaterit und seine Struktur: *Angewandte Chemie, Dtsch.* **71** [21], 678–9.

OLHAUSEN, S. (1925), Strukturuntersuchungen nach die Debye-Scherrer Methode: *Zeit. Krist.*, **61**, 463–514.

PAULING, L. (1960), The Nature of the Chemical Bond: Cornell Univ. Press, Ithaca, N. Y.

PHEMISTER, D. B., ARONSOHN, H. G. AND PEPINSKY, R. (1939), Variations in the cholesterol bile pigment and calcium salts contents of gallstones formed in gall-bladder and in bile ducts with the degree of associated obstruction: *Ann. Surg.*, **109**, 161–186.

PRIEN, E. L. AND FRONDEL, C. (1947), Studies in urolithiasis: I. The composition of urinary calculi: *J. Urology*, **57**/6/949–991.

RINNE, F. (1924), III. Rontgenographische Untersuchungen an feinzerteilten Mineralien, Kunstprodukten und dichten Gesteinen: *Zeit. Krist.*, **60**, 55–69.

ROTH, R. S. AND SCHNEIDER, S. J. (1960), Phase equilibria in systems involving the rare earth oxides: Part I. Polymorphism of the oxides of the trivalent rare earth ions: *J. Research Nat. Bur. Standards*, **64A**, 309–316.

SCHNEIDER, S. J. (1961), *ibid.* Part III. The Eu_2O_3-In_2O_3 System: *J. Research Nat. Bur. Standards*, **65A**, 429–434.

SCHNEIDER, S. J. AND ROTH, R. S. (1960), *ibid.* Part II. Solid State Reactions in Trivalent Rare-Earth Oxide Systems: *J. Research Nat. Bur. Standards*, **64A**, 316–332.

SWANSON, H. E. AND FUYAT, R. K. (1953), Standard x-ray diffraction powder patterns: *Nat. Bur. Standards Circular 539*, Vol. **II**, 52.

SWANSON, H. E., FUYAT, R. K., AND UGRINIC, G. M. (1954), Standard x-ray diffraction powder patterns: *Nat. Bur. Standards Circular 539, Vol.* **III**, 54.

TABLES OF INTERATOMIC DISTANCES AND CONFIGURATION IN MOLECULES AND IONS (1958), The Chemical Society, Burlington House, London.

WYCKOFF, R. W. G. (1931), The Structure of Crystals, 2nd ed.: The Chemical Catalog Co., Inc., New York.

X RAY POWDER DATA FILE (1959), Published by American Soc. for Testing Materials, Phila. 3, Pa.

Manuscript received November 8, 1960.

APPENDIX

Vaterite-Type $CaCO_3$

The literature pertaining to the x-ray data for vaterite is widely scattered and has never been summarized. All published x ray data have been obtained from poorly crystalline artificial preparations. Although vaterite has been recognized as a constituent of gall stones (Phemister, *et al.*, 1939), it has only recently been found as a naturally occurring mineral (McConnell, 1960).

Early confusion in the naming and identification of vaterite was clarified by Gibson, Wyckoff, and Merwin (1925), who were among the first to apply x-ray powder diffraction techniques to the problem. They stated that the name vaterite was first used by Meigen (1911) as an abbreviation for "Vater's Third Modification of Calcium Carbonate."

TABLE 9. REPORTED X-RAY POWDER DIFFRACTION DATA FOR $CaCO_3$-VATERITE

hkl	Rinne (1924)		Heide[a] (1924)		Olhausen[b] (1925)		Gibson *et al.* (1925)		Prien & Frondel[c] (1947)		ASTM[d]		DeKeyser & Degueldre[e,f] (1950)	Brooks *et al.*[f] (1950–51)	McConnell[g] (1960)		Present Work	
	*d*kx	I[h]	*d*kx	I[h]	*d*kx	I[h]	*d*kx	I[h]	*d*kx	RI%[i]	*d*Å	RI%[i]	*d*Å	*d*kx	*d*Å	I[h]	*d*Å	RI%[i]
002			4.30	s	4.29	s					4.26	13	4.278		4.26	m	4.25	25
100	3.5	w	3.59	m	3.58	m	3.59	s	3.59	70	3.58	63	3.568	3.56	3.58	s	3.586	66
101	3.3	m+	3.29	m	3.28	m	3.29	s	3.29	70	3.29	75	3.282	3.278	3.30	s	3.302	100
102	2.7	s+	2.73	s	2.72	s	2.719	s−	2.72	60	2.73	100	2.714	2.714	2.73	s	2.737	89
			2.55	vw	2.55(?)	vw												
j			2.31	m	2.30	m	2.313	vw	2.31	10	2.31	8			2.33, 2.30	wb	2.312	8
103															2.23	w	2.221	7
004															2.127	w	2.119	11
110	2.1	s+	2.08	s	2.07	s	2.058	s+	2.06	100	2.06	63	2.06		2.059	s	2.067	49
112							1.85	w	1.85	20	1.87	15	1.856		1.856	w	1.856	21
104	1.8	s+	1.85	s	1.84	s	1.82	w	1.82	20	1.83	63	1.835		1.825	s	1.823	43
200																	1.792	6
202	1.6	s	1.65	m	1.65	m	1.64	m	1.64	40	1.65	31	1.641	1.635	1.648	wb	1.648	17
105[k]			1.55	w	1.55	w	1.537	w	1.54	20	1.55	8			1.544	vw	1.544	3
114	1.5	w					1.467	vw	1.47	10	1.48	8			1.480	vw	1.479	5
															1.416	vw		
204			1.37	w	1.37	w	1.364	vw	1.36	10	1.37	8			1.369	vw	1.368	5
106			1.31	w	1.31	w					1.32	10			1.316	w	1.312	7
212	1.3	m+	1.29	w	1.28	w	1.283	m	1.28	40	1.29	13			1.288	vw	1.287	8
															1.185	vw		
															1.166	w		
302/214[k]			1.14	vw	1.14	vw	1.14	vw	1.14	10	1.15	8			1.141	w	1.143	6
206			1.11	vw	1.11	vw	1.105	vw	1.11	10	1.11	5			1.112	w	1.107	4
			1.02	vw	1.02	vw												
			0.979	vw	0.977	vw												
			0.946	vw	0.944	vw												

[a] *d* values calculated by present authors from film distances, assuming a 40 mm camera radius.
[b] No radiation wavelength data given. *d* values calculated by present authors from $\theta/2$ observed. Gives *hkl* values.
[c] Also X-ray Powder Data File, Card #4-0844.
[d] X-ray Powder Data File, Card #1-1032. $a=4.120$ Å, $c=8.556$ Å, $c/a=2.073$.
[e] Gives *hkl* values. $a=4.120$ Å, $c=8.556$ Å.
[f] No intensities given.
[g] Pattern originally indexed on unit cell relationship: $a'=a\sqrt{3}$, $c'=c$. Thirteen additional *d* values not listed here.
[h] s—strong, m—medium, w—weak, vw—very weak, b—broad.
[i] RI is the intensity of each diffraction peak relative to the strongest peak.
[j] The corresponding *d* value cannot be indexed on the basis of the hexagonal cell but is believed to be part of the vaterite diffraction pattern.
[k] These *hkl* values do not give a satisfactory fit with either hexagonal cell.

Table 9 lists the x-ray powder diffraction data for vaterite as reported by different investigators. Rinne (1924) and Heide (1924) were the first to report x-ray data. Heide, unfortunately, did not list d values, but they were calculated by the present authors from his stated film distances by assuming a 40 mm. camera radius.

Olhausen (1925) continued Heide's study of vaterite. He did not report radiation wavelength data or d values. The latter were calculated by the present authors, by conversion of his '$\theta/2$ observed' data. Olhausen was the first to show that vaterite crystallizes in the hexagonal system. He indexed the powder pattern on essentially the same unit cell as that used by later investigators: $a=4.110$ kX, $c=8.513$ kX, with 2 molecules per unit cell. However, his reported c/a ratio, 1.036, is exactly half of that calculated from his stated unit cell dimensions. An additional complication arises from the fact that Olhausen used a left-handed coordinate system. For interplanar spacings in the hexagonal system, he used the formula: $Q=p(h_1^2+h_2^2-h_1h_2)+qh_3^2$, which is equivalent, in conventional terminology, to:

$$\frac{1}{d^2}=\frac{h^2+k^2-hk}{a^2}+\frac{l^2}{c^2}.$$

The accepted formula for interplanar spacing, however, is:

$$\frac{1}{d^2}=\frac{h^2+k^2+hk}{a^2}+\frac{l^2}{c^2}.$$

Therefore, in order to convert Olhausen's indices, the value of the expression h^2+k^2-hk, using his indices, must be made equivalent to the sum of h^2+k^2+hk, from which the equivalent indices can be deduced.

Gibson, Wyckoff, and Merwin (1925), pg. 961, showed that the calcium carbonate of spherulitic habit investigated by Rinne, Heide, and several others, was essentially Vater's μ-calcium carbonate (true vaterite); whereas, the form originally designated 'vaterite' was in reality calcite. Gibson, *et al.* and Olhausen apparently were unaware of each other's work. The data of Prien and Frondel (1947), also listed in the X-ray Powder Data File (Card No. 5 0844), is probably that of Gibson, *et al.*, with d values rounded off to 3 figures and intensities given as percentages.

The X-ray Powder Data File contains a second vaterite pattern (Card No. 1 1032), the original source of which is not given. Although indexing is absent, the unit cell dimensions are listed as $a=4.120$ Å, $c=8.556$ Å, apparently obtained from Wyckoff (1931, p. 273).

DeKeyser and Degueldre (1950) and Brooks, Clark and Thurston (1950 51) have reported some of the major interplanar spacings for vaterite found in their studies of the factors governing the formation of calcium carbonate phases from solution. DeKeyser and Degueldre indexed their pattern using the same unit cell dimensions listed by Wykcoff (1931).

The crystal structure of vaterite was reported by Hans-Jurgen Meyer (1959) as a variant of the NiAs type in which the plane of the CO_3 group is parallel to the c axis. He stated that vaterite was probably only pseudo hexagonal, orthorhombic space group Pbnm, $a=4.13$ Å, $b=a\sqrt{3}$, $c=8.48$ Å, $Z=4$. These unit cell dimensions correspond closely to those found in the present work for a specimen of pure vaterite supplied by D. Graf of the Illinois Geological Survey: $a=4.134$ Å, $c=8.47$ Å. McConnell (1960), however, reported $c=8.524$ Å, which value is in closer agreement to that reported by Olhausen (1925). The differences in c dimensions might be related to the methods for precipitation of vaterite.

McConnell (1960) also concluded that the true unit cell of vaterite is hexagonal with a equal to $\sqrt{3}$ times the a value reported by previous investigators. On the basis of the larger cell an attempt was made to index the x-ray diffraction data for the vaterite used in the present study (Table 9). Three interplanar spacings, namely, 2.312 Å, 1.544 Å, and 1.143 Å,

however, could not be satisfactorily indexed on the basis of either cell. These discrepancies lend support to the conclusion made for the vaterite-type borates that the symmetry of vaterite is only pseudohexagonal.

Note Added in Press

Since acceptance of this paper for publication, differential thermal analysis and high-temperature x-ray data have shown that the vaterite-type rare-earth borates have an unquenchable high-temperature polymorph. The x-ray diffraction pattern of the high-temperature form is characterized by a c/a ratio very close to that of $CaCO_3$-vaterite, and the appearance of a new peak indexable as the (200) on the basis of a unit cell with $a = \sqrt{3}$ a' and Z=6. It must be concluded that the high-temperature form is most nearly isostructural with $CaCO_3$-vaterite, whereas the low-temperature form has a slightly different structure of greater density. The high-temperature x-ray patterns never showed improved crystallinity, thus still indicating that both forms are not truly hexagonal. The transition temperatures on heating and cooling, respectively, were found by DTA to be as follows: $SmBO_3$—834°, 530° C.; $EuBO_3$—878°, 561° C.; $GdBO_3$—927°, 578° C.; $DyBO_3$—999°, 627° C.; YBO_3—1024°, 600° C.; $HoBO_3$—1020°, 646° C.; $ErBO_3$—1022°, 632° C.; $TmBO_3$—1040°, 604° C.; $YbBO_3$—1041°, 577° C.; and $LuBO_3$ (metastable inversion)—1037°, 538° C. High-temperature x-ray data for $YbBO_3$ at 1050° C. are as follows: low form—a=6.542A, c=8.771A, c/a=1.341, ρ=7.104 g/cm³; high form—a=6.987A, c=8.336A, c/a=1.193, ρ=6.552 g/cm³. Even though previous thermal history may affect the high↔low vaterite inversion, the very large hysteresis has been found to be relatively independent of the heating rate. For example, no transformation was observed in $SmBO_3$ after holding, in the high-temperature x-ray furnace, either the low-vaterite form at 800° C. for 22 hours or the high-vaterite form at 600° C. for 66 hours.

THE AMERICAN MINERALOGIST, VOL. 46, SEPTEMBER-OCTOBER, 1961

THE DETERMINATION OF IRON IN SPHALERITE BY X-RAY FLUORESCENCE SPECTROMETRY*

B. R. Doe,† A. A. Chodos,‡ A. W. Rose,§ and E. Godijn‡

Abstract

The mutual standards concept of x-ray fluorescence analysis furnishes a rapid, non-destructive method of determining the iron content of sphalerite within 2.5 to 5 per cent of the amount of iron present. Only 0.1 to 20 mg. of sample are needed. A set of independently determined standards is required. For best results, the thicknesses of the standards should be equal to those of the unknowns; samples should be run interspersed with standards; sample holders should be checked for reproducibility; and the amounts of cadmium, copper, and manganese should be analyzed for if their sum is suspected to be greater than 1 or 2 per cent.

Introduction

Temperature and fugacity of sulfur species are two of the variables in the formation of ore deposits. Kullerud (1953, 1959) showed that the iron content of sphalerite in equilibrium with FeS is a function of temperature. Barton and Kullerud (1958) demonstrated that the iron content of sphalerite in equilibrium with pyrite is a function of the fugacity of sulfur in the system as well as of temperature. Thus, under the proper circumstances, the iron content of sphalerite indicates the temperatures of formation of an ore body and or the changes in fugacity of sulfur species during ore deposition. To facilitate such studies, an accurate quantitative measure of the iron content on a few milligrams or less of sample is desirable.

The present paper describes an analytical procedure capable of determining the content of iron to better than ± 5 per cent of the amount of iron present, using as little as a milligram or less of sphalerite. The sample is not destroyed. No internal standardization or binders are required. The analysis takes about 15 minutes per sample. If care is taken, the reproducibility of the iron content may be determined to within about ± 2.5 per cent of the amount present. The method of analysis has been briefly described in an abstract by Chodos, Rose, and Godijn (1957). Certain precautions that are necessary in order to obtain the best results were not stated in the abstract. Thus it seems advisable to describe the procedure at greater length. The method has been employed in the studies of sphalerite by Rose (1958) and Doe (1960).

* Publication of the Division of Geological Sciences, California Institute of Technology, Pasadena, California.

† Geophysical Laboratory, Carnegie Institution of Washington, Washington, D. C.

‡ Division of Geosciences, California Institute of Technology, Pasadena, Calif.

§ Bear Creek Mining Co., Salt Lake City, Utah.

Procedure

General

The method employs the "mutual standards technique" outlined by Coulliette (1943), where it is assumed that the sum of the metallic elements analyzed for equals 100 per cent. For sphalerite, this expression is:

$$X^{zn} + X^{fe} + \Sigma X^{a} = 100 \text{ per cent} \tag{1}$$

where X^{zn} and X^{fe} are the concentrations of ZnS and FeS in weight per cent, and ΣX^{a} is the sum of all the other metallic elements, expressed as sulfides, in the sphalerite. If a sample of sphalerite is bombarded with tungsten *x*-rays, the elements in the specimen will give off their characteristic *x*-rays. The intensity ratio of the Zn to Fe radiation emitted by the sample will be proportional to the ZnS to FeS weight ratio. The relationship between the intensity ratio and weight ratio can be determined from analyzing a set of standards in which the weight ratio is known (Fig. 1). The iron content in weight per cent may be obtained from the weight ratio by rearranging equation 1:

$$X^{fe} = (100 - \Sigma X^{a})/(1 + X^{zn}/X^{fe}) \tag{2}$$

The ΣX^{a} term (mostly manganese, cadmium, and copper) is less than 1 per cent for most specimens of sphalerite. If ΣX^{a} is 1 weight per cent, the assumption that ΣX^{a} is 0 would give an answer for the FeS content only 1 per cent of the FeS content greater than the true value. As most samples of sphalerite contain about 1 to 15 per cent FeS by weight, the error in assuming that the ΣX^{a} term is 0 will be less than 0.1 per cent FeS by weight for most samples. In addition, 0.1 per cent FeS is smaller than the uncertainty in the solvus of the FeS-ZnS system as determined by Kullerud (1953).

In this procedure, 0.1 to 20 mg. of ground sphalerite are weighed into a flat-bottomed circular cavity (1/32-inch deep$\times\frac{1}{4}$-inch diameter) drilled into a lucite holder. The holder is inserted into the spectrometer, which is equipped with a high-purity tungsten *x*-ray tube (Phillips FA-60). The tube is operated at 45 kv and 25 ma. The fluorescent radiation is diffracted from a lithium fluoride crystal in conjunction with a 0.020-inch $\times$3-inch parallel plate collimator. The fluorescent intensity at the iron and zinc peak maxima is measured with a flow proportional counter, using argon-methane gas. The positions of the peak maxima are determined from time to time by counting over the peaks in steps of 0.02° 2θ. The positions of the peaks are quite stable and showed no change over a period of 9 months. For each peak, 25,600 counts are taken to obtain good counting statistics. In addition, 6400 counts for background are taken at about 1.5° 2θ on either side of the peak maxima.

Results of ± 5 per cent of the amount of iron present or better can be

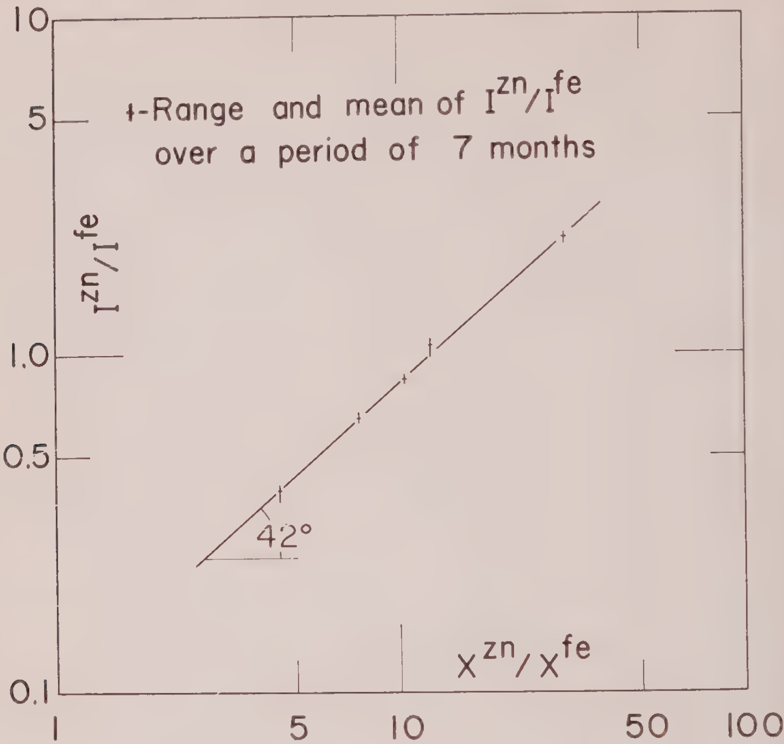

FIG. 1. The Zn to Fe fluorescent intensity ratio (I^{zn}/I^{fe}) versus the ZnS to FeS weight ratio (X^{zn}/X^{fe}) of five chemically determined sphalerites.

obtained provided the following variables are taken into account: the standards, background, sample thickness effect, sample holder effect, and absorption and enhancement effects of metallic elements other than iron or zinc. Short discussions of these topics and of the reproducibility of the method are given below.

Standards

To begin with, synthetic mixtures of ZnS, pyrite, and iron powder were used for standards. The results of samples analyzed chemically by B. Doe at the Missouri School of Mines and by L. Shapiro of the U. S. Geological Survey indicated a small systematic difference between the results of the chemical analyses and the synthetic standards. The reasons for the discrepancy are related to the "matrix" effect (Claisse, 1956). This effect has been found repeatedly in our work and is further illustrated by working curves for the analysis of sulfide nodules from meteorites (Chodos and Nichiporuk, 1958). The present standards consist of

nine specimens of sphalerite calibrated by E. Godijn and A. Rose for iron and zinc content by "wet" chemical procedures. Iron in the standards was determined by reduction in a silver reductor followed by titration with ammonium sulfate. Zinc in the standards was determined by precipitation as zinc ammonium phosphate, ignition at 900° C., and weighing as zinc pyrophosphate. In addition, these specimens were analyzed for Mn and Cd by arc-excitation optical spectrography.

Background

The $\frac{1}{4}$-inch diameter of the sample well used is small compared with the area of the beam from the x-ray tube. Thus the background measured is from the sample holder as well as the sample. The background counting rates are found to be independent of the iron content of the sphalerite. However, some experiments showed background to vary with time, probably due to fluctuations in the electronics. Thus it is necessary to subtract this background from the zinc and iron radiation to achieve the best results.

Sample Thickness Effect

For a sample evenly spread in the well of the sample holder described above, Doe (1960) calculated that a 10-mg. sample of sphalerite should act as an "infinitely" thick sample. In practice, it was found that a sample of 15 mg. or greater acts "infinitely" thick (Fig. 2). If the standards are "infinitely" thick and the unknowns are very thin (for example, a sample size of 1 mg. spread over the $\frac{1}{4}$-inch well), the results for the unknowns may be in error by as much as 20 per cent, or even more (see Fig. 2). This is in accord with the theory of absorption of x-rays. For best results, the standards and unknowns should be measured at the same thicknesses.

Sample Holder Effect

The sample holder and the position of the sample holder in the x-ray beam are found to influence the Zn/Fe intensity ratio from a sample. The position of the holder in the x-ray beam may affect the Zn to Fe intensity ratio by about 4 or 5 per cent. Thus holders should be constructed with the samples located in the same positions in the x-ray beam. Certain lucite holders were found to give consistently different answers, up to 5 per cent of the amount of iron present, from others for the same sample. If more than one sample holder is to be used, the holders should be checked for reproducibility between holders. The reason for the holder effect is not clear but may be related to radiation damage of the lucite holders.

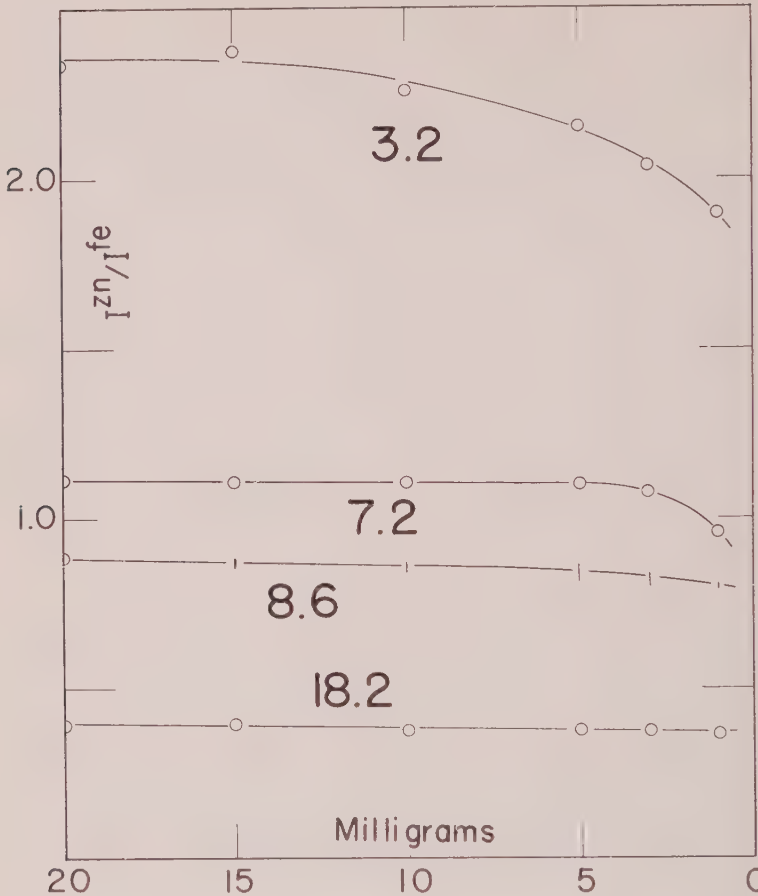

FIG. 2. The effect of sample thickness (in milligram equivalents) on the Zn to Fe fluorescent intensity ratio (I^{zn}/I^{fe}) for sphalerite. (Numbers near curves give the concentration of FeS in weight per cent for the sample represented by the curve. The thickness is represented by the number of milligrams of sample spread over the ¼ inch well of the sample holder.)

Absorption and Enhancement Effects

Sphalerite in nature commonly contains small amounts of Mn and Cu in addition to Fe. The presence of Mn and Cu could influence the Zn/Fe intensity ratio. Manganese may absorb zinc radiation. Fluorescent radiation from any copper present will fluoresce iron. To determine the possible effects of copper and manganese on the intensities of zinc and iron radiation, the following tests were performed. Ten per cent Mn_3O_4 produced a decrease in the Zn/Fe ratio equivalent to about 12 per cent of the amount of iron present. One per cent of Mn_3O_4 mixed with a sample

produced no definite change in the per cent FeS found. Ten per cent CuO produced a slightly smaller change than the equivalent amount of manganese. Most samples of sphalerite analyzed by Rose (1958) and Doe (1960) contained less than 1 per cent manganese and 0.2 per cent copper. Thus, in general, the absorption and enhancement effects are believed to be equivalent to less than 2 per cent of the amount of iron reported.

Reproducibility

A set of five standards was analyzed a total of 18 times over the period of analysis in 1958 (7 months). These data enable an estimate of the reproducibility of the curve for intensity ratio versus concentration ratio. The standards were run interspersed with the unknowns on each day of analysis. The best straight-line curve is fitted through the average values for each standard in Fig. 1. Figure 1 also shows the total range of intensity ratios encountered over the period of analysis, as well as the average values. The range of a ratio over the 7 month period was about ± 5 per cent of the average value.

There is a suggestion that the standardization curve shifts position slightly for different days, as shown on Fig. 3. If the standards as analyzed on 6-12-58 are considered as unknowns and their iron concentrations are determined from the standard curve for 10-7-58, all the standards are indicated to have higher concentrations (by roughly 5 per cent) than the known values. Treatment of the data indicated that the standard deviation of the ZnS/FeS weight ratio is about 1.6 per cent of the ratio, using the curve for Fig. 1. If new working curves are constructed each day, the standard deviation is reduced to about 1.2 per cent.

Results from this procedure agree well with the results obtained from completely independent methods. Splits of five samples of sphalerite from the Balmat No. 2 mine, New York, analyzed at the Missouri School of Mines (Doe, 1956) were reanalyzed by the present method. At the Missouri School of Mines, iron was determined by a permanganate titration and zinc by a potassium ferrocyanide titration using a diphenylamine internal indicator (Kolthoff and Sandell, 1952). The comparison is:

FeS* (wt. %) Volumetric	FeS† (wt. %) Fluorescent
13.2	13.9
7.4	7.0, 7.2, 7.8
8.8	8.8
7.6	7.4
10.6	10.6, 10.8

* Missouri School of Mines (B. R. Doe, analyst).
† California Institute of Technology (B. R. Doe, analyst).

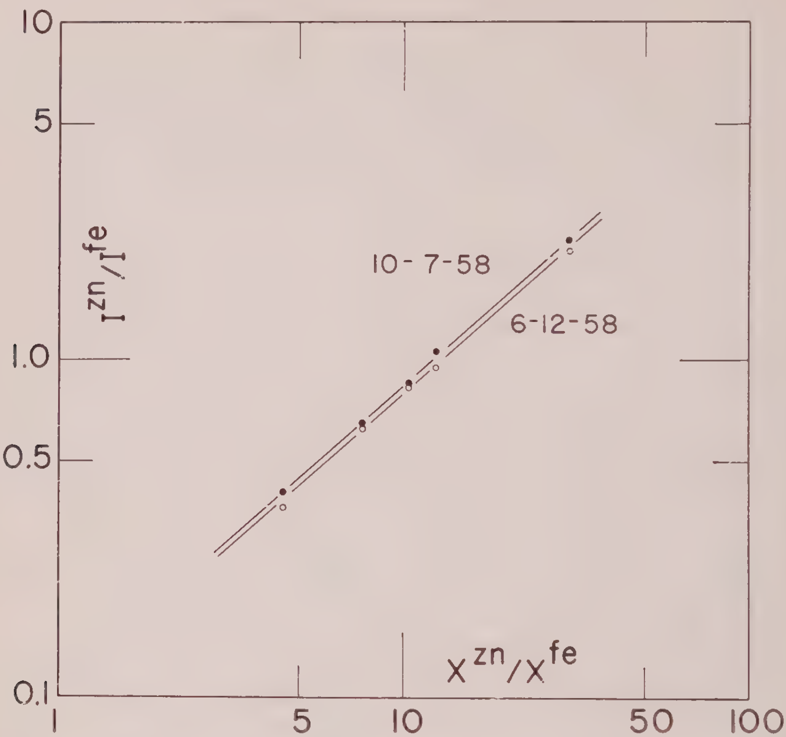

FIG. 3. Shift with time in the position of the standard curve for the Zn to Fe fluorescent intensity ratio (I^{zn}/I^{fe}) versus the ZnS to FeS weight ratio (X^{zn}/X^{fe}) for sphalerite.

Thus, the results obtained by the *x*-ray fluorescence technique are in good agreement with those of standard chemical techniques.

CONCLUSIONS

X-ray fluorescence provides a rapid, nondestructive means of accurately determining the amount of iron in sphalerite. Only a few milligrams or less of sample are needed. The reproducibility of the method is better than 5 per cent of the iron present if standards and unknowns have approximately the same thickness. A set of independently determined standards is required in the procedure. Samples analyzed by this method agree within 5 per cent of the amount present with iron determined by other generally reliable methods.

The amount of iron in sphalerite may be determined to within 2 or 2.5 per cent of the amount present: (1) if sample holders are carefully chosen so that there is no sample holder effect, (2) if the amounts of manganese and copper are small or known, (3) if a set of standards is analyzed inter-

spersed with unknowns on the day of analysis, and (4) if the thicknesses of standards and unknowns are approximately the same.

Acknowledgments

Financial aid for the study was supplied by fellowships from the Kennecott Copper Corporation to Rose (1955–57) and Doe (1957–59) while they were at the California Institute of Technology. Laboratory facilities were provided by the California Institute of Technology. Thanks are also due to Dr. G. Kullerud of the Geophysical Laboratory for helpful suggestions on construction of the manuscript.

References

Barton, P. B., and Kullerud, G. (1958), The Fe-Zn-S system: *Carnegie Inst. Wash. Year Book* **57,** 227–229.

Chodos, A. A., and Nichiporuk, W. (1958), An application of the mutual standards concept to *x*-ray fluorescence spectroscopy: *Seventh Annual Conference on Industrial Applications of X-ray Analysis, Proc., Univ. of Denver*, 247–255.

Chodos, A. A., Rose, A. W., and Godijn, E. (1957), The determination of iron in sphalerite by *x*-ray fluorescence spectrography: Presented before the Pittsburgh Conference on Analytical Chemistry and Applied Spectroscopy, March 1957, Pittsburgh, Pa.

Claisse, F. (1956), Accurate *x*-ray fluorescence analysis without internal standard: *Department of Mines, Province of Quebec, Canada, P. R.* **327**.

Coulliette, J. H. (1943), Spectrographic determination of nickel and chromium in stainless steel: *Ind. Eng. Chem., Anal. Ed.*, **15,** 732.

Doe, B. R. (1956), Geothermometry at the Balmat No. 2 mine, New York, by the FeS-ZnS system: *Missouri School of Mines Thesis Series, M.S.*, 56 p.

Doe, B. R. (1960), The distribution and composition of sulfide minerals at Balmat, New York: *Calif. Inst. of Tech. Thesis Series, Ph.D.*, 151 p.

Kolthoff, I. M., and Sandell, E. B. (1952), Textbook of quantitative inorganic analysis: Macmillan Co., 3rd ed., New York, 759 p.

Kullerud, G. (1953), The FeS-ZnS system: A geological thermometer: *Norsk geol. tidsskrift*, **32,** 61–147.

Kullerud, G. (1959), Sulfide systems as geological thermometers: In *Researches in Geochemistry* (P. H. Abelson, ed.), John Wiley and Sons, New York, 301–335.

Rose, A. W. (1958), Trace elements in sulfide minerals from the Central mining district, New Mexico, and the Bingham mining district, Utah: *Calif. Inst. of Tech. Thesis Series, Ph.D.*, 264 p.

Manuscript received October 17, 1960.

THE AMERICAN MINERALOGIST, VOL. 46, SEPTEMBER-OCTOBER, 1961

PHASE TRANSFORMATIONS IN SILICA-ALUMINA MIXTURES AS EXAMINED BY CONTINUOUS *X*-RAY DIFFRACTION

F. M. WAHL, R. E. GRIM, and R. B. GRAF,* *University of Illinois, Urbana, Illinois.*

ABSTRACT

The formation of mullite from mixtures of different varieties of alumina and silica was studied by high-temperature continuous x-ray diffraction techniques and by diffraction after soaking at high temperatures for various lengths of time. It is shown that the initial form of the alumina and silica has a large influence and that mole per cent variations in mix composition have little effect on mullite development.

The structural stability of component materials largely controls mullite nucleation, and the relationship between the formation of this mineral and preceding transformations in the normal thermal sequence of component alumina and silica materials is emphasized. The addition of mineralizing ions can promote mullitization.

INTRODUCTION

The equilibrium diagram for the system Al_2O_3–SiO_2 has been critically examined and re-evaluated by many persons since it was first determined by Bowen and Greig in 1924. The most recent revision is that of Aramaki and Roy (1960) and is based on data from more than 700 runs. The standard quenching technique has generally been used in studying silicate phase equilibria, and liquidus-solidus relationships at high temperatures have received primary consideration.

The information to be presented herein also deals with high-temperature mineral transformations within the alumina-silica system; however, special consideration is given to the 900°–1500° C. temperature range and to the formation of mullite as it develops from synthetic mixtures of different varieties of alumina and silica. Insley and Ewell in 1935, and more recently West and Gray (1958) in examining reactions in artificial alumina-silica mixtures, suggested the influence which internal structures of materials could have in controlling thermal reactions within this temperature range.

In the present study the development of mullite from various mixtures of alumina-silica materials has been investigated by both continuous heating x-ray diffraction and x-ray diffraction after prolonged heating at elevated temperatures, and it will be shown that temperature and the structural nature of component materials are more important than mole per cent variations in the composition of the mixes in controlling the development of this mineral at elevated temperatures.

* Present Address: General Dynamics Corporation, Fort Worth, Texas.

Samples and Procedure

The following varieties of alumina and silica were selected for firing: diaspore from Missouri; synthetic gibbsite, Merck and Co., Rahway, New Jersey; and corundum from Zoutpansberg District, Transvaal, Africa; also synthetic cristobalite; silicic acid, 100 mesh, A. R. grade, Mallinckrodt Chemical Works; and Ottawa quartz sand from near Ottawa, Illinois.

The effect of mole per cent variations of both alumina and silica on mullite formation was investigated by *x*-raying continuously diaspore-cristobalite mixtures of $Al_2O_3 \cdot 4SiO_2$; $2Al_2O_3 \cdot 3SiO_2$; $3Al_2O_3 \cdot 2SiO_2$; and $4Al_2O_3 \cdot SiO_2$ as they were heated to 1450° C. The combined intensities of the 3.41 Å and 3.38 Å mullite reflections, when present, were measured at regular temperature intervals up to 1450° C.

The role of crystallinity and structure of the alumina-silica components in controlling mullitization was determined by examining, both by continuous heating diffraction and by diffraction after prolonged heating at 1375° C., alumina-silica mixtures of the approximate $3Al_2O_3 \cdot 2SiO_2$ mullite composition. Diffraction intensity measurements of the major mullite reflections as observed from all combinations of these six component materials after firing are plotted, as are the diffraction intensities for cristobalite and corundum.* Both peak height intensity and integrated peak area intensity measurements were recorded and found to be indicative of changes in the diffraction intensity characteristics of these minerals. Thus, the intensity of diffraction data plotted in the following illustrations represent those relative intensity changes that took place as the materials were fired.

Continuous *x*-ray data are based on the heating of the mixtures at a firing rate of 5.6° C. per minute. The prolonged heating data were obtained from the same mixes after they were held at 1375° C. for 24 and 72 hours respectively. All *x*-raying was performed using nickel-filtered copper radiation at 45 kv. and 18 ma.

Experimental Data

Effect of Alumina-Silica Mix Composition on Mullite Formation

Continuous *x*-ray diffraction data from different mole per cents of Al_2O_3 and SiO_2 in mixtures of diaspore-cristobalite while being heated to 1400° C. are shown in Fig. 1. The intensities of the (101) line of corun-

* Three major diffraction lines attributable to the alumina component after firing have *d*-values of 3.48 Å, 2.55 Å, and 2.38 Å and are representative of αAl_2O_3. To avoid confusion with the Al_2O_3 content of prepared mixes before firing, the mineral name for α-Al_2O_3, corundum, will hereafter be used when referring to the alumina component after firing.

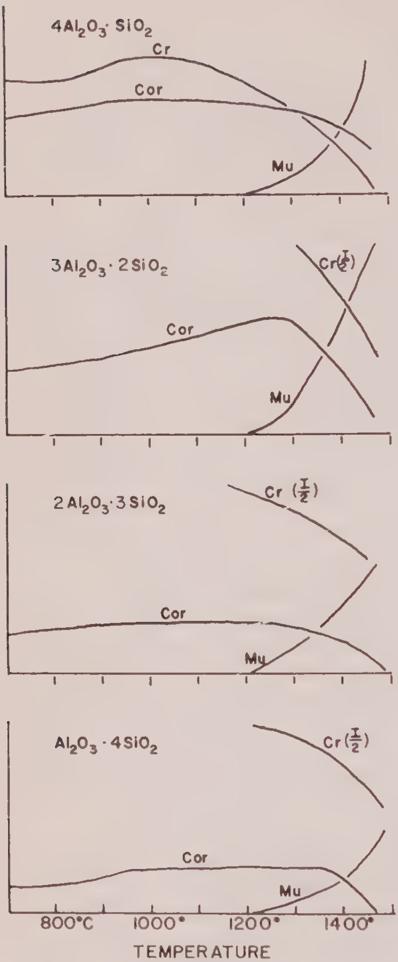

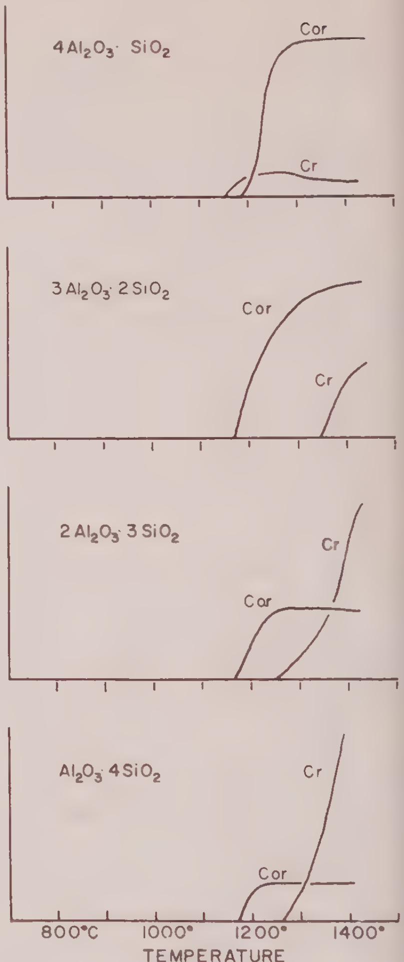

FIG. 1. (*Left*) Intensity of diffraction by high temperature phases in heated alumina-silica mixtures prepared from diaspore cristobalite. Cr Cristobalite; Cor—Corundum; Mu—Mullite.

FIG. 2. (*Right*) Intensity of diffraction by high-temperature phases in heated alumina-silica mixtures prepared from gibbsite-silicic acid.

dum, the (111) line of beta-cristobalite, and the combined intensities of the 3.38 Å and 3.41 Å mullite reflections are plotted against temperature. Mullite diffraction lines first appeared at 1200° C. from all mixes regardless of their alumina to silica ratios. Just prior to the mullite nucleation temperature there was a slight but gradual increase in the intensities of the major corundum and cristobalite peaks in all mixes, but especially in

that with composition $3Al_2O_3 \cdot 2SiO_2$. As the temperature was raised above 1200° C., the intensity of mullite diffraction continually increased with the development of this mineral; also, there was a gradual decrease in the diffraction intensities of corundum and cristobalite. This reduction coincided with, and was inversely proportional to, mullite development.

Gibbsite-silicic acid mixtures of varying composition were also examined while being heated to 1400° C. Corundum and cristobalite de-

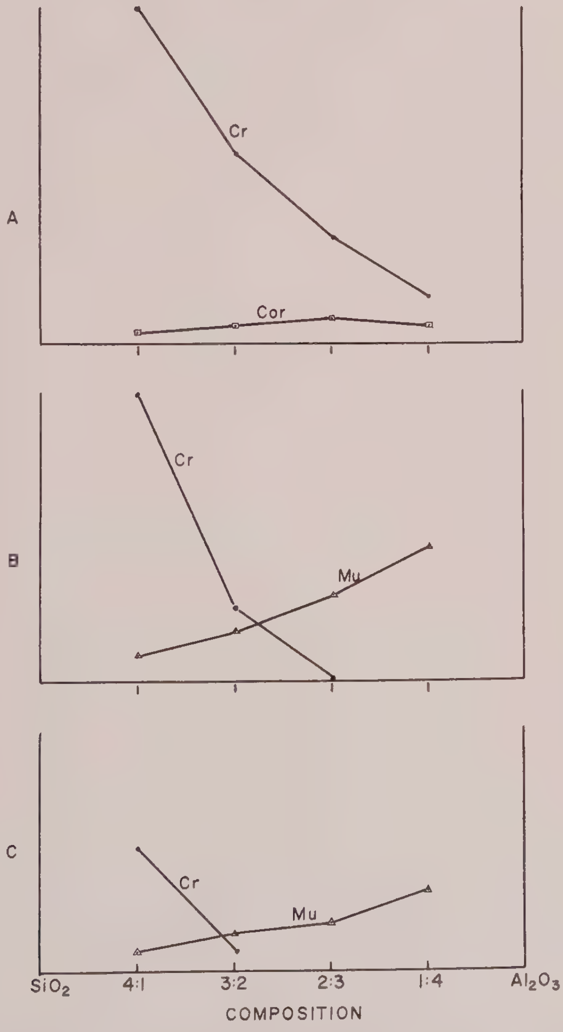

FIG. 3. Intensity of diffraction by high-temperature phases in heated diaspore-cristobalite mixtures after: A) 1 hour at 540° C.; B) 24 hours at 1375° C.; C) 72 hours at 1375° C.

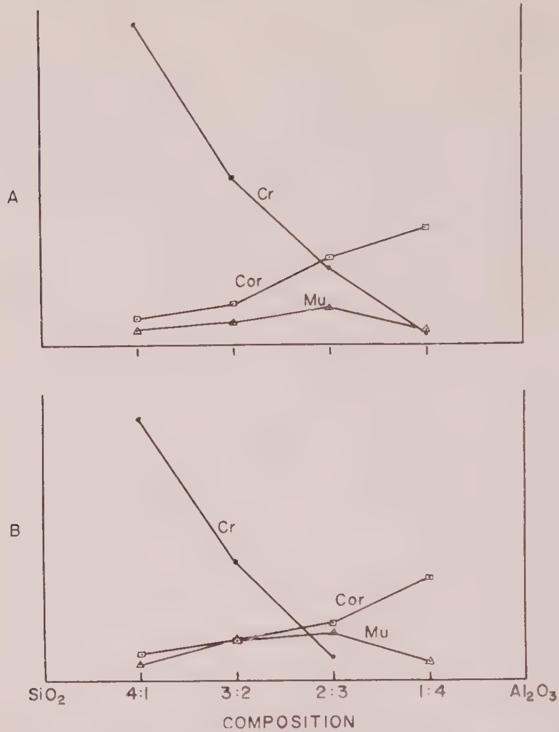

FIG. 4. Intensity of diffraction by high-temperature phases in heated gibbsite-silicic acid mixtures after A) 24 hours at 1375° C.; B) 72 hours at 1375° C.

veloped from each mixture, regardless of mole per cent variations in the mix composition (Fig. 2). In all cases corundum was first observed at 1170° C., but the formation temperature of beta-cristobalite ranged from 1150° to 1350° C. At no time were mullite diffraction lines detected from these components, even when heated to 1425° C.

Figure 3-A shows that the diaspore in heating to 540° C. for one hour changes to corundum, and that under these conditions there is no reaction between the alumina and silica phases. In mixtures of all compositions, corundum diffraction lines were not discernible after heating to 1375° C. (Fig. 3-B). Mullite was present in all diaspore-cristobalite mixes after heating at 1375° C. for 24 hours (Fig. 3-B) and the amount formed was directly proportional to the original alumina content of the mixture. Mixtures rich in silica retained less beta-cristobalite after 72 hours than after 24 hours (Fig. 3-C) indicating more complete mullite development with prolonged heating.

All gibbsite-silicic acid mixtures developed mullite after 24 hours at 1375° C., but maximum mullitization was observed from the $3Al_2O_3$

$2SiO_2$ mix (Fig. 4-A). This same development trend was maintained after 72 hours at 1375° C. (Fig. 4-B). Again, less beta-cristobalite was retained after 72 hours. Corundum development paralleled closely the amount of alumina present in the original mixes and the same was true for cristobalite development and the SiO_2 content.

Influence of Alumina Component on Mullitization

Several mixes equivalent to the mullite composition ($3Al_2O_3 \cdot 2SiO_2$) were fired to determine the role of alumina structure on consequent mullite formation. Continuous diffraction data for diaspore-cristobalite, gibbsite-cristobalite, and corundum-cristobalite mixtures are shown in Fig. 5. Mullite began forming from diaspore-cristobalite at 1200° C. and

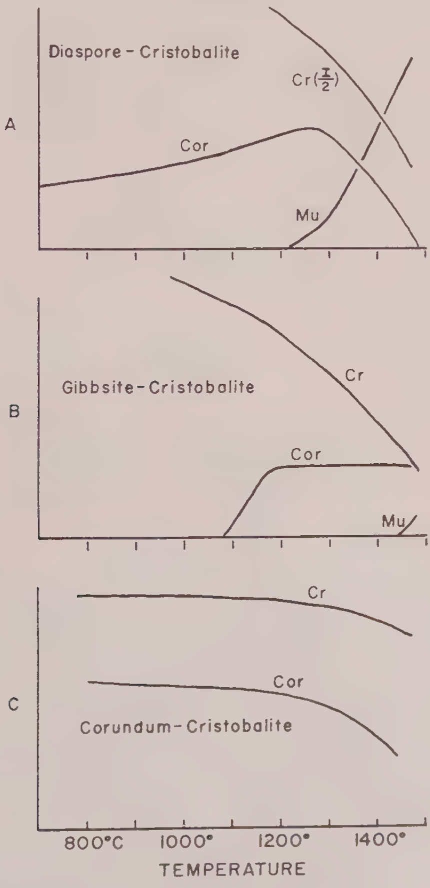

FIG. 5. Intensity of diffraction by high-temperature phases in heated $3Al_2O_3 \cdot 2SiO_2$ mixtures.

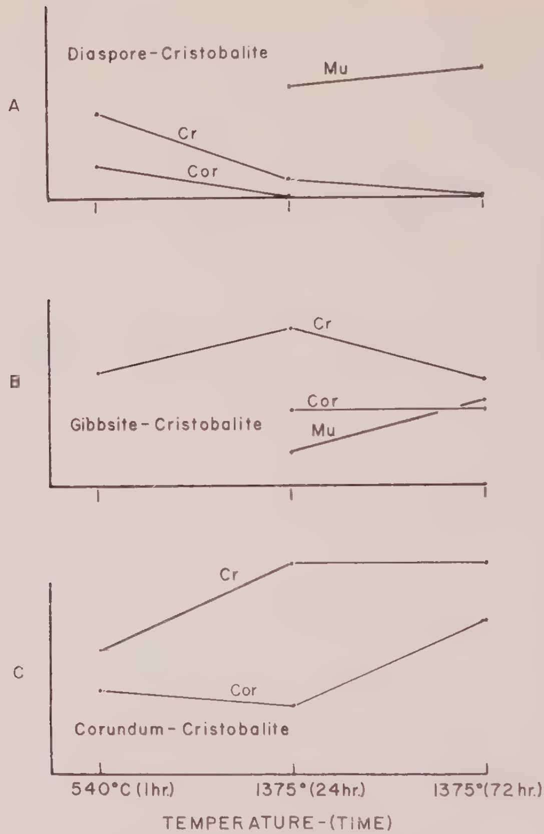

FIG. 6. Intensity of diffraction by high-temperature phases in $3Al_2O_3 \cdot 2SiO_2$ mixtures after prolonged heating.

from gibbsite-cristobalite at 1440° C. but none developed from the corundum-cristobalite mix at this rate of firing up to 1450° C. The intensity decrease of both the cristobalite and corundum peaks (Fig. 5-C) as higher temperatures are attained indicates that a possible structural readjustment to mullite is beginning to take place but is still too slight to be detected.*

X-ray diffraction analyses of these same cristobalite mixtures after prolonged heating at 1375° C. showed the same trend of mullite development (Fig. 6).

* Firing of this same mixture after extensive grinding to an extremely small particle size gave mullite at 1340° C.

Influence of Silica Component on Mullitization

Continuous diffraction data from $3Al_2O_3 \cdot 2SiO_2$ mixtures of diaspore-cristobalite, diaspore-silicic acid, and diaspore-quartz while being fired to 1425° C. are listed in Fig. 7. Cristobalite and silicic acid promote mullite nucleation at 1200° and 1300° C. respectively; whereas, the quartz-diaspore mix developed mullite only after heating to 1320° C. at this rate of firing. The same reactivity trend was observed for these silica components when gibbsite was substituted for diaspore in the mixtures. The batch containing cristobalite was still the first to form mullite (Fig. 5-B), however, none was observed from either the gibbsite-silicic acid mix (Fig. 2) or the gibbsite-quartz mix when heated to 1400° C. at this same firing rate.

All three varieties of silica formed mullite with either diaspore or

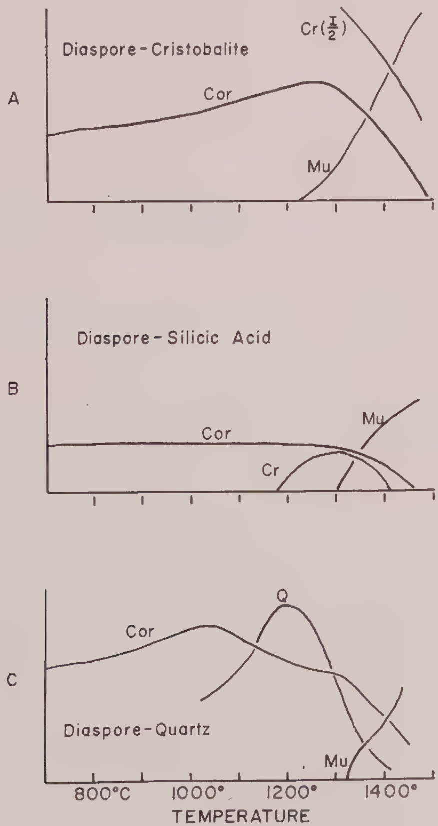

FIG. 7. Intensity of diffraction by high-temperature phases in heated $3Al_2O_3 \cdot 2SiO_2$ mixtures.

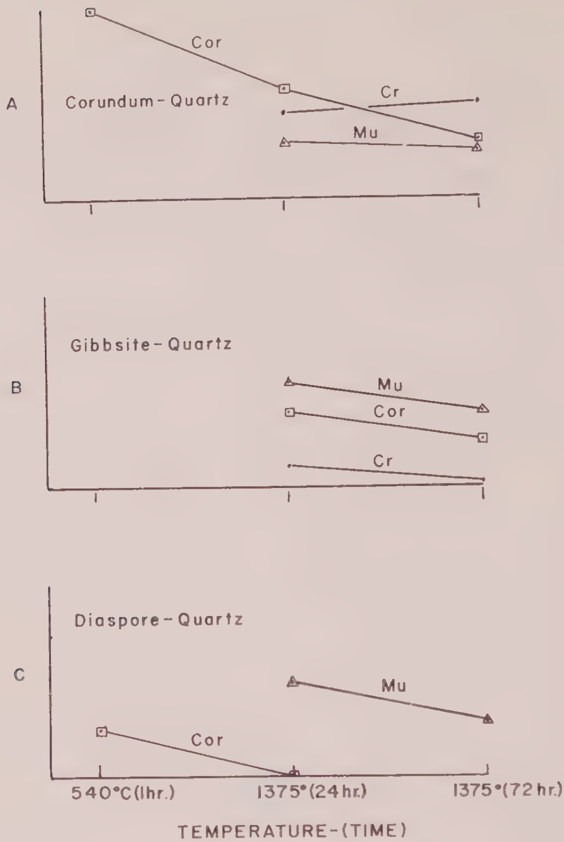

FIG. 8. Intensity of diffraction by high-temperature phases in $3Al_2O_3 \cdot 2SiO_2$ mixtures after prolonged heating.

gibbsite when heated to 1375° C. for 24 hours, Figures 6, 8, and 9; however, after 72 hours at this temperature, mullite diffraction intensity decreased in those batches which contained quartz as the silica component (Fig. 8). The mixtures prepared with cristobalite (Fig. 6) and with silicic acid (Fig. 9) showed the expected normal increase in mullite development after 72 hours.

The effects of chemical additives on mullite nucleation from $3Al_2O_3 \cdot 2SiO_2$ corundum-cristobalite mixes were examined briefly. This particular mixture produced no mullite when fired at 1375° C. for 72 hours; however, the addition of 5% by weight of $CaCl_2$ or $BiCl_3$ promoted mullite nucleation from these components at 1300° and 1400° C. respectively (Fig. 10).

Discussion and Conclusions

The data show that mullitization in synthetic mixtures of various orms of alumina and silica is influenced by the structure of the com-onents used. Limitations imposed by structure may be more important n controlling the formation of this mineral than mole per cent variations n the compositions of the alumina-silica mixes. The temperatures at vhich these materials combine to give mullite are thus an indirect con-equence of this structure stability.

The formation of mullite at 1200° C. from all diaspore-cristobalite nixes, even though they varied in composition from $Al_2O_3 \cdot 4SiO_2$ to $Al_2O_3 \cdot SiO_2$ shows that component materials need not be present in cor-ect molecular ratios before combination and mineral synthesis can oc-

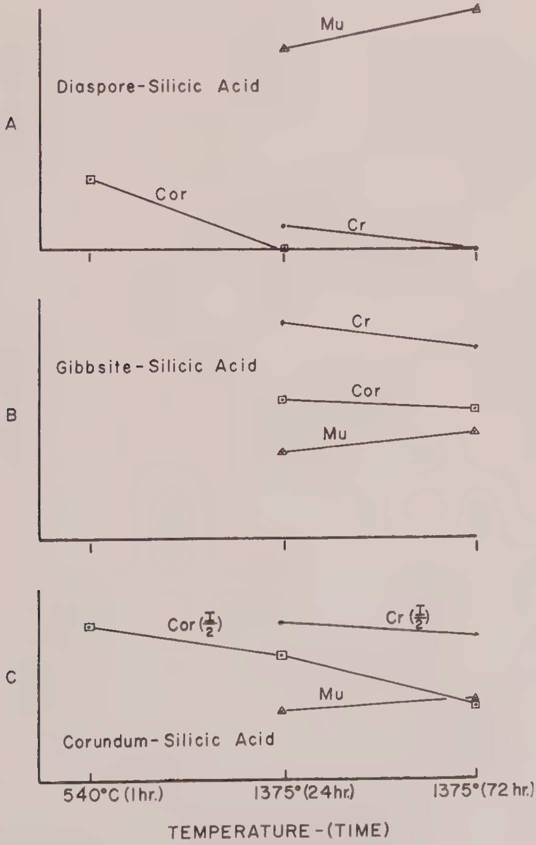

Fig. 9. Intensity of diffraction by high-temperature phases in $3Al_2O_3 \cdot 2SiO_2$ mixtures after prolonged heating.

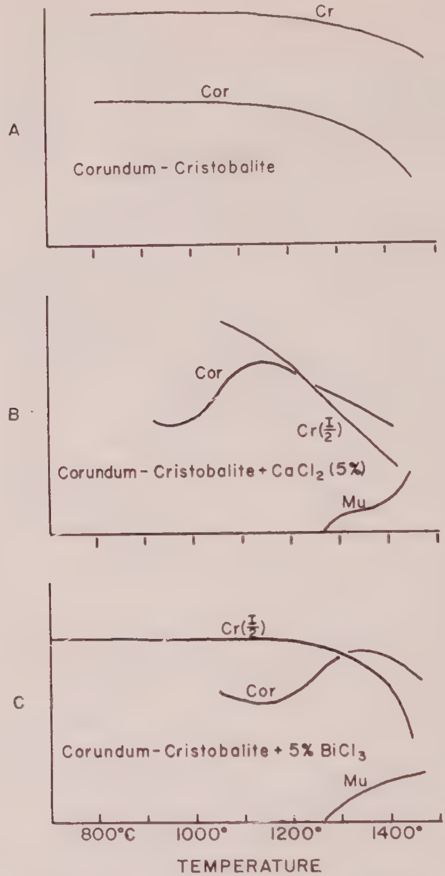

FIG. 10. Intensity of diffraction by high-temperature phases in heated $3Al_2O_3 \cdot 2SiO$ corundum-cristobalite mixtures treated with Ca^{++} and Bi^{+++}.

cur. As long as the proper components are present in the mix, regardles of their relative molecular amounts, they will combine to give mullit when heated to the proper temperature.

Of the varieties of alumina tested, diaspore with the composition c $HAlO_2$ combines more readily with SiO_2 to produce mullite than doe gibbsite which is $Al(OH)_3$. On heating, each of these alumina materia ultimately converts to corundum, the diaspore at a low temperature, an gibbsite nót until about 1100° C. Consequent development of mullit through combination with the silica that is present is related to this pr liminary corundum development. Diaspore forms corundum at a rel tively low temperature (<500° C.), and contributes to mullite develop ment at 1200° C; whereas gibbsite does not convert to corundum unt

1100° C. and does not combine with silica to produce mullite until 1440° C. The reactivity of naturally occurring corundum follows this same pattern of thermal behavior. It does not react with silica to form mullite even when held at 1375° C. for 72 hours. This suggested association between structural stability of the aluminum component and consequent mullite development is in agreement with the findings of West and Gray (1958) who showed that the reactivity in forming mullite from silica-alumina mixtures was dependent on the crystalline modification of alumina that was used.

Analogous to the formation of corundum from alumina components is the transformation of the silica component to beta-cristobalite. Silicic acid, when mixed with diaspore, transforms to beta-cristobalite at 900° C. with consequent mullite nucleation at 1300° C. Quartz, however, does not form beta-cristobalite until 1200° C. and, when mixed with diaspore, does not form mullite until 1325° C. The development of mullite at 1200° C. from mixes prepared with synthetic cristobalite is as expected. The beta-cristobalite used had been prepared at approximately 900° C. from silicic acid. Above this temperature the material apparently becomes relatively unstable, more reactive, and can readily combine with the alumina component to give mullite.

Because the actual temperature of mullite nucleation as determined from a heated alumina-silica mix is related to the development temperatures of corundum and beta-cristobalite, it follows that the original structures of the alumina-silica component materials, which in turn control the transformations to corundum and beta-cristobalite, are fundamental factors in limiting the ultimate development of mullite.

Because mullitization generally precedes the formation of beta-cristobalite when natural alumino-silicate minerals such as kaolinite are heated, and follows beta-cristobalite development from synthetic alumina-silica oxide mixtures, it is emphasized that any material, on heating, will first tend to follow its normal transformation sequence which is determined by the structure of that material. Only after this has occurred is there a reaction to form mullite. The firing of alumina-silica components to form mullite can often be enhanced by the addition of mineralizing ions as when either Bi^{+++} or Ca^{++} were added to corundum-cristobalite mixtures. These same ions also promoted mullitization in kaolinite (Wahl, 1958).

Acknowledgments

This work forms part of a series of high-temperature *x*-ray diffraction studies made possible through a research grant from the National Science Foundation.

References

ARAMAKI, S., AND ROY, R., Revised equilibrium diagram for the system Al_2O_3-SiO_2: *Nature*, **184**, 631–632 (1959).

BOWEN, N. L., AND GREIG, J. W., The System Al_2O_3-SiO_2: *J. Amer. Cer. Soc.*, **7**, 238–54 (1924).

INSLEY, H., AND EWELL, R. H., Thermal behavior of the kaolin minerals: *J. Res. Natl. Bur. Standards*, **14**, [5], 615–627 (1935).

WEST, R. R., AND GRAY, T. J., Reactions in silica-alumina mixtures: *J. Amer. Ceram. Soc.*, **41**, [4], 132–136 (1958).

WAHL, F. M., Reactions in kaolinite-type minerals at elevated temperatures as investigated by continuous x-ray diffraction: Ph.D. dissertation, University of Illinois, Urbana, Ill., 87 pp. (1958).

Manuscript received October 19, 1960.

THE AMERICAN MINERALOGIST, VOL. 46, SEPTEMBER-OCTOBER, 1961

THE CRYSTAL STRUCTURE OF CAHNITE,* $Ca_2BAsO_4(OH)_4$

CHARLES T. PREWITT AND M. J. BUERGER, *Crystallographic Laboratory, Massachusetts Institute of Technology, Cambridge, Massachusetts.*

ABSTRACT

Cahnite is one of the few crystals assigned to crystal class $\bar{4}$. A precession study showed that its diffraction symbol is $4/mI$-/-, which contains space groups $I4$, $I\bar{4}$, and $I4/m$. Because of the known $\bar{4}$ morphology, it must be assigned to space group $I\bar{4}$. The unit cell, whose dimensions are $a=7.11$ Å, $c=6.20$ Å, contains $2Ca_2BAsO_4(OH)_4$. The structure was studied with the aid of intensity measurements made with a single-crystal diffractometer. Patterson syntheses were made for projections along the c, a, and [110] directions. The atomic numbers of the atoms are in the ratio As:Ca:O:B:H=33:20:8:5:1, so that the Patterson peaks are dominated by the atom pairs containing As as one member of the pair. Since there are only two As in a body-centered cell, one As can be arbitrarily assigned to the origin. Then the major peaks of the Patterson syntheses are at locations of atoms in the structure. The structure, determined approximately in this manner, was refined by least-squares and by two-dimensional difference maps.

The structure consists of As tetrahedrally surrounded by O_1 at a distance of 1.68 Å, and B tetrahedrally surrounded by O_2 at a distance of 1.47 Å. Ca_1 is surrounded by four O_1 at a distance of 2.44 Å, and by four O_2 at 2.55 Å, while Ca_2 is surrounded by four O_1 at 2.38 Å and four O_2 at 2.54 Å. The structure of cahnite is somewhat similar to that of zircon and its numerous isomorphs, but more specifically, it is a derivative structure based upon KH_2AsO_4, so that its formula can be written $CaH_2B_{\frac{1}{2}}As_{\frac{1}{2}}O_4$.

INTRODUCTION

Cahnite, $Ca_2BAsO_4(OH)_4$, is a rare mineral found originally in the mines at Franklin, New Jersey. This paper contains the results of an investigation of its crystal structure, using single-crystal x-ray diffraction methods.

Cahnite was first mentioned in the literature by Palache (1921) in a paper read by title only at a meeting of the Mineralogical Society of America. Subsequently, Palache and Bauer (1927) published a paper describing the occurrence, morphology, chemistry, and physical properties of Franklin cahnite. Palache (1941) gave additional morphological information. Bügge (1952) reported an occurrence of cahnite in the Klodeborg mine, Arendal, Norway.

PREVIOUS WORK

Palache and Bauer (1927) published three analyses of cahnite. These are given in Table 1 along with the composition calculated from the

* Presented at the Fifth Congress of the International Union of Crystallography, Cambridge, England, August 17, 1960, and at the 41st Meeting of the Mineralogical Society of America, Denver, Colorado, October 31, 1960.

TABLE 1. CHEMICAL ANALYSES OF CAHNITE, AFTER PALACHE AND BAUER (1927)

	1	2	3 very pure material	4 calculated
CaO	38.27	37.13	37.62	37.64
B_2O_3	10.14	11.64	11.86	11.74
As_2O_5	36.79	37.47	38.05	38.54
H_2O	11.75	11.78	12.42	12.08
PbO	1.15	trace	—	
MgO	0.24	—	—	
ZnO	trace	1.58	—	
CO_2	trace	—	—	

formula $Ca_2BAsO_4(OH)_4$. According to these authors, analysis 3 in Table 1 came from a very pure sample. From these figures it is evident that there is little likelihood that much substitution exists in cahnite, nor is there any doubt that the formula is correct. According to Palache and Bauer, the density of cahnite is 3.156 and the hardness is 3; cahnite is uniaxial positive with $n_O=1.662$ and $n_E=1.663$.

Palache (1941) assigned cahnite to the crystal class $\bar{4}$ on the basis of the development of the form {311}. Cahnite is one of the few minerals in this class.

Space Group and Unit Cell

X-ray photographs were taken with the Weissenberg and precession cameras using CuKα and MoKα radiations. Precession photographs lead to a tetragonal unit cell with

$$a = 7.11 \text{ Å},$$
$$c = 6.20 \text{ Å}.$$

The diffraction symbol, $4/mI$-\-, contains space groups $I4$, $I\bar{4}$, and $I4/m$. Because of the morphological symmetry, it must be assigned to the space group $I\bar{4}$.

There are two formula weights per body-centered cell. Palache and Bauer's (1927) c/a ratio corresponds to the face-centered cell. If the diffraction results are referred to a face-centered cell, the axial ratio is

$$c/a = 6.20/(7.11 \times 1.414) = 0.616$$

as compared to the morphological value of 0.615. This relation must be considered when aligning cahnite crystals for x-ray analysis using Palache's indexing.

It is interesting to note that, to our knowledge, no other terrestrial minerals have been reported in space group $I\bar{4}$. The only minerals assigned to this space group by Donnay and Nowacki (1954) are the meteoric phosphides of the schreibersite (Fe_3P) type.

Collection of Intensities

Collection of three-dimensional diffraction intensities was carried out using an equi-inclination single-crystal diffractometer with a Geiger counter as a detector. Several small splinters were cleaved from the original crystals and checked for twinning with the polarizing microscope and by Weissenberg photographs. The crystal chosen was untwinned and had the following dimensions: $0.061 \times 0.064 \times 0.3$ mm., with the longest dimension in the direction of the c axis.

All intensities were collected using CuKα radiation. An absorption correction was made by assuming that the crystal approximated a cylinder after the method of Buerger and Niizeki (1958).

Patterson Projections

Patterson syntheses were computed for the projections along c, a and [110]. The projection along c, given in Fig. 1, turned out to be the most useful because its plane group, $p4$, is the same as that of the electron-density projection along c. Because of the relatively small number of Fourier coefficients available for each computation, the Patterson maps show large series-termination effects. Any attempt to interpret the Patterson, or, for that matter, the electron-density maps, must take these effects into account when determining atom locations.

The atomic numbers of the atoms in cahnite are in the ratio As:Ca:O:

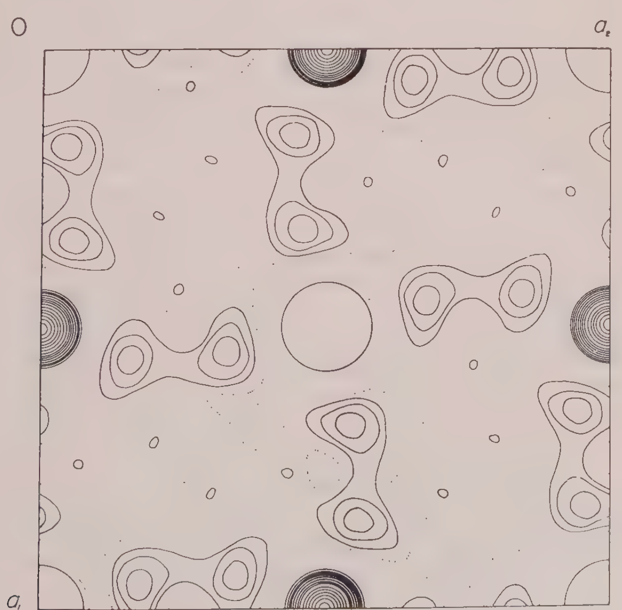

Fig. 1. Patterson projection of cahnite along c.

B:H=33:20:8:5:1 so that the Patterson peaks are dominated by atom pairs containing As as one member of the pair. Since the body-centered unit cell contains 2 $Ca_2BAsO_4(OH)_4$, there are 2 As, 2 B, 4 Ca, and 16 O to be distributed among the equivalent positions of the space group. Table 2 gives the equipoints for space group $I\bar{4}$. It is obvious that As must be assigned to position *2a*, *2b*, *2c* or *2d*, which are indistinguishable. If As is arbitrarily assigned to the origin, equipoint *2a*, the major peaks of the

Table 2. Assignment of Atoms in Cahnite to Equivalent Positions of $I\bar{4}$

Equipoint	Point Symmetry	Equivalent Positions $(000, \frac{1}{2}\frac{1}{2}\frac{1}{2})+$	Atom Assignment
2a	$\bar{4}$	000	As
2b	$\bar{4}$	$00\frac{1}{2}$	Ca_1
2c	$\bar{4}$	$0\frac{1}{2}\frac{1}{4}$	B
2d	$\bar{4}$	$0\frac{1}{2}\frac{3}{4}$	Ca_2
4e	2	$00z$, $00\bar{z}$	—
4f	2	$0\frac{1}{2}z$, $\frac{1}{2}0z$	—
8g	1	xyz, $\bar{x}\bar{y}z$, $y\bar{x}\bar{z}$, $\bar{y}x\bar{z}$	O_1, O_2

Patterson projections can be expected to lie at locations of atoms in the structure.

With As assigned to position *2a*, then 2 B and 4 Ca must occupy either two or three of the positions *2b* through *4f*. Examination of Fig. 1 shows that the strongest peaks occur at the origin and at $0\frac{1}{2}$. These peaks represent the usual origin peak plus peaks due to the atoms in special positions. Since the projection along *a* and [110] showed only peaks which could be due to atoms in equipoints *2b*, *2c* and *2d*, equipoints *4e* and *4f* were eliminated as possible Ca locations.

Two additional sets of peaks in Fig. 1 are in fourfold coordination around the origin and $0\frac{1}{2}$. From the formula of cahnite and from the results of other structure analyses, it is reasonable to assume that As and B are tetrahedrally surrounded by oxygen. If this is true in cahnite, each of the two additional peaks represents superposed images of oxygen as seen from As and Ca. The peaks, therefore, determine the approximate oxygen locations. The distribution of oxygen atoms, as well as B and Ca, is then as given in the right-hand column of Table 2 It does not matter whether B is assigned to equipoint *2c* or *2d* until the signs of the *z* coordinates of the oxygens are established.

If the positions of the four cations are fixed, the relative positions of the the oxygens can be obtained by taking the *x* and *y* coordinates from Fig. 1 and assuming regular tetrahedral coordination around the As and B. The orientation of each tetrahedron with respect to two positions which differ

from each other by a 90° rotation around the 4 axis cannot be determined from the Patterson projections. Calculation of the closest O_1-O_2* distance for each of the four possible combinations of orientations gives 1.95 Å, 1.21 Å, 2.77 Å, and 1.97 Å. The only acceptable O_1-O_2 distance is 2.77 Å which uniquely determines the oxygen locations.

Refinement

The structure, established as described in the preceding section, was refined by least-squares and two-dimensional difference maps. The parameters varied during least-squares refinement were the scale factor, the coordinates of O_1 and O_2, and individual isotropic temperature factors. Computations were carried out on the IBM 704 digital computer using a two-dimensional Fourier program and the crystallographic least-squares program written by Busing and Levy (1959).

The oxygen parameters converged in three cycles to the values given in stage 4 of Table 3. However, the temperature factors of As and Ca refined to negative values. Further cycles were run in which different conditions were imposed on the refinement to try to determine the cause of the negative temperature factors. When reflections with sin $\theta<0.2$ were not included and the cation temperature factors were set to 0.4, the results in stage 5 of Table 3 were obtained. When the temperature factors were refined they again became negative. The coordinates in stage 6 resulted from a cycle of refinement in which a separate scale factor was assigned to each level. An interesting result of this was that, when the temperature factors were allowed to vary, all of them refined to positive quantities. This suggests that the data for the separate levels differed in some way not taken into account. Since the temperature factors obtained are thus not considered to be reliable they have not been included in Table 3. It can be seen from the table, however, that changes in temperature factors and number of reflections used in refinement, as well as changes in scale factors, have very little effect on the oxygen coordinates.

In order to test the refinement results, and at the same time to detect any possible anomaly due to hydrogen, two-dimensional difference maps were computed for the projection along *c*. These confirmed the least-squares results. The hydrogen locations are discussed in the next section.

Final Structure

The final structure is shown in Fig. 2. The cahnite structure is similar to that of zircon and its numerous isomorphs (Durif-Varambon, 1959), the main difference being that cahnite contains hydrogen. The Ca atoms in cahnite are in the same position as Zr, and the B and As are in the same

* O_1 is the oxygen neighbor of As, and O_2 is the neighbor of B.

TABLE 3. RESULTS OF LEAST-SQUARES REFINEMENT

Atom	Parameter	Stage of Refinement 1	2	3	4	5	6
O_1	x	.169	.174	.179	.178	.178	.178
	y	.031	.043	.054	.053	.054	.055
	z	.137	.154	.165	.167	.167	.167
O_2	x	.160	.159	.159	.159	.159	.160
	y	.454	.448	.444	.445	.444	.444
	z	.114	.110	.112	.113	.112	.113
$R=\dfrac{\Sigma\lvert\lvert F_o\rvert-\lvert F_c\rvert\rvert}{\Sigma\lvert F_o\rvert}$		—	.127	.105	.076	.075	.059

Stage
1 Original coordinates from Patterson maps.
2 End of 1st cycle.
3 End of 2nd cycle.
4 End of 3rd cycle (including all reflections except 002 which was greatly affected by extinction). Temperature factors of As and Ca_2 set to .01; other temperature factors allowed to vary.
5 Reflection with $\sin\theta<0.2$ removed. Temperature factors of cations set to 0.4.
6 Separate scale factors assigned to each level. Other conditions same as stage 5.

position as Si in zircon. But the structure of cahnite is more closely related to that of KH_2AsO_4, and can be regarded as a derivative of it in which half the arsenic is replaced by boron, and neutrality is maintained by substituting Ca for K. From this point of view the formula of cahnite can be written $CaH_2B_{\frac{1}{2}}As_{\frac{1}{2}}O_4$. Accordingly, cahnite may be expected to act as a piezoelectric, and, possibly, as a ferroelectric at low temperatures.

On the basis of least-squares refinement and difference maps, the oxygen coordinates, $O_1=.178$, .054, .167, and $O_2=.160$, .444, .114, were regarded as the best set. Interatomic distances computed using these coordinates are given in Table 4. As is surrounded by 4 O_1 at a distance of 1.68 Å in a tetrahedron elongated along the c axis. B is surrounded by 4 O_2 at a distance of 1.47 Å in a nearly regular tetrahedron. The O_1-O_1 distance is 2.56 Å along the two horizontal edges of the AsO_4 tetrahedron and 2.79 Å along the other two edges. The edges of the BO_4 tetrahedra are all about 2.40 Å. Ca_1 is surrounded by 4 O_1 at a distance of 2.44 Å and by 4 O_2 at 2.55 Å. Ca_2 is surrounded by 4 O_1 at a distance of 2.38 Å and 4 O_2 at a distance of 2.54 Å.

The most probable location for the hydrogen bond is between the two oxygens connected with dotted line A in Fig. 2. This O_1-O_2 distance is

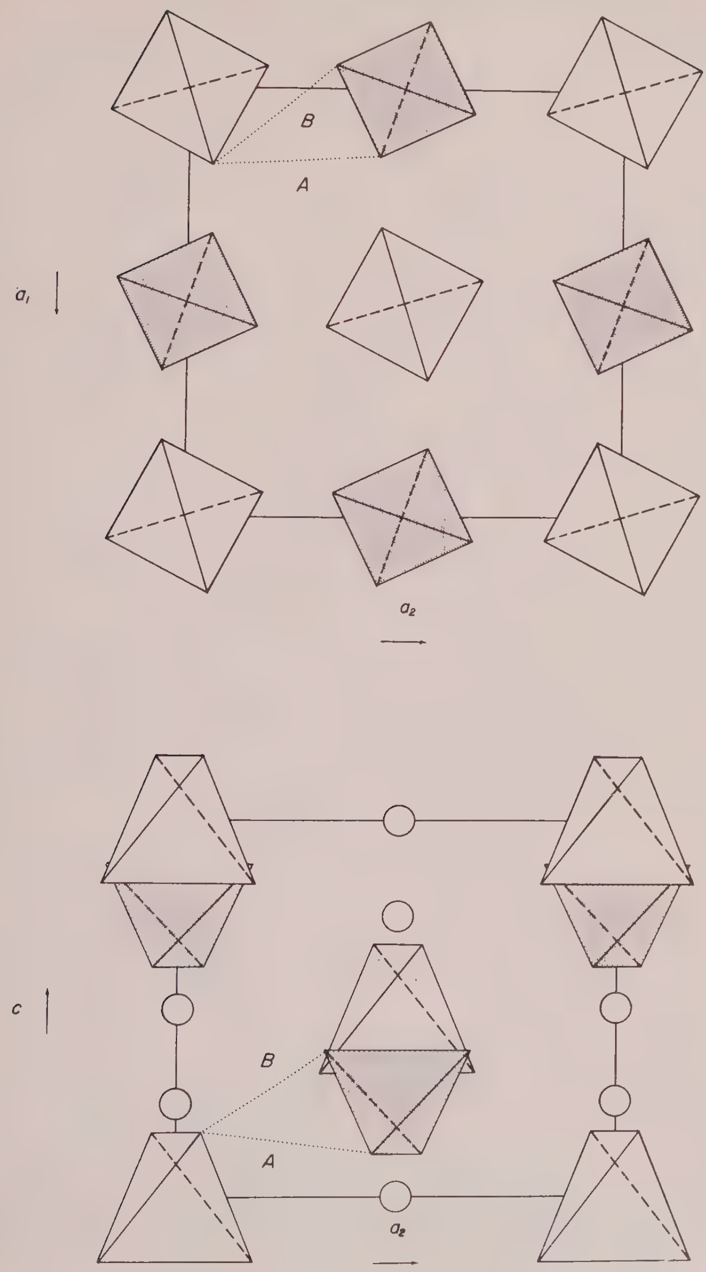

FIG. 2. Projections of the model of the cahnite structure along c (top) and along a (bottom). The unshaded tetrahedra are AsO_4 and the shaded ones are BO_4. Ca is shown by circles. Dotted lines A and B indicate possible hydrogen bonds.

TABLE 4. INTERATOMIC DISTANCES IN CAHNITE

Atom	Coordinate	Neighbor	Coordinate	Distance (Å)	Number of Neighbors
As	000	O_1	xyz	1.68	4
B	$0\frac{1}{2}\frac{1}{4}$	O_2	xyz	1.47	4
Ca_1	$00\frac{1}{2}$	O_1	xyz	2.44	4
		O_2	xyz	2.55	4
Ca_2	$0\frac{1}{2}\frac{3}{4}$	O_1	xyz	2.38	4
		O_2	xyz	2.54	4
O_1	xyz	O_1	$\bar{x}\bar{y}z$	2.56	1
			$y\bar{x}\bar{z}$	2.79	2
		O_2	xyz	2.80	1
			$y-\frac{1}{2}, \frac{1}{2}-x, \frac{1}{2}-z$	2.96	1
			$\frac{1}{2}-x, \frac{1}{2}-y, z-\frac{1}{2}$	2.98	1
			$y\bar{x}\bar{z}$	3.65	1
O_2	xyz	O_2	$\bar{x}\bar{y}z$	2.40	1
			$y\bar{x}\bar{z}$	2.40	2

2.80 Å, the closest approach of O_1 to O_2. The two-dimensional difference maps, however, show a peak between the oxygens connected by dotted line *B* in Fig. 2. This latter distance is 2.96 Å. It is felt that nothing furthur can be said about the location of the hydrogen without further intensity data.

ACKNOWLEDGMENTS

This work was supported by a grant from the National Science Foundation. The computations were carried out at the M.I.T. Computation Center. The writers are indebted to Professor Clifford Frondel for supplying some of the type specimens of cahnite from the collection at Harvard University.

ADDITIONAL NOTE

P. Embrey (1960) has kindly sent to us the proof sheets of a forthcoming paper concerning a new occurrence of cahnite and his suggestions for a structure based on a comparison of the powder x-ray photographs of cahnite and xenotime. The occurrence is at Capo di Bove, near Rome, Italy. Embrey determined cell dimensions from a modified Nelson-Riley extrapolation of powder data and found

$$a = 7.0952 \pm 0.0015 \text{ Å}$$
$$c = 6.1904 \pm 0.003 \text{ Å}$$

These values are probably more accurate than ours. We are in agreement as to the similarity of the cahnite structure to that of xenotime and zircon.

REFERENCES

BUERGER, M. J. AND NIIZEKI, N. (1958), Correction for absorption for rod-shaped single crystals. *Am. Mineral.* **43,** 726–731.

BÜGGE, JENS A. W. (1952), Minerals from the skarn iron ore deposits at Arendal, Norway. I. Cahnite from the Klodeberg mine. *K. Norske Vidensk. Selskab. Förh.* **24** (for 1951), 79–81.

BUSING, WILLIAM R. AND LEVY, HENRI A. (1959), A crystallographic least-square refinement program for the IBM 704. Oak Ridge National Laboratory Central Files No. 59-4-37. Oak Ridge, Tenn. 1–139.

DONNAY, J. D. H. AND NOWACKI, WERNER (1954), Crystal Data. Memoir 60, Geological Society of America, 40.

DURIF-VARAMBON, A. (1959), Etude de la substitution du silicum dans quelques types d'orthosilicates. *Bull. Soc. Franç. Minér. Crist.* **82,** 285–314.

EMBREY, PETER (1960), Cahnite from Capo di Bove, Rome. *Min. Mag.* **32,** 666–668.

PALACHE, CHARLES (1921), Holdenite and cahnite, two new minerals from Franklin Furnace, N. J. (title only). *Am. Mineral.* **6,** 39.

PALACHE, CHARLES (1941), Crystallographic notes: cahnite, stolzite, zincite, ultrabasite. *Am. Mineral.* **26,** 429–436.

PALCHE, CHARLES AND BAUER, L. H. (1927), Cahnite, a new boro-arsenate of calcium from Franklin, New Jersey. *Am. Mineral.* **12,** 149–153.

Manuscript received December 3, 1960.

THE AMERICAN MINERALOGIST, VOL. 46, SEPTEMBER-OCTOBER, 1961

OBSERVATIONS ON THE THERMAL BEHAVIOR OF BRANNERITE

HANS H. ADLER, *U. S. Atomic Energy Commission, Washington, D. C.*

AND

JOSEPH A. PUIG, *Grumman Aircraft Engineering Corp., Bethpage, L. I., N. Y.*

ABSTRACT

Five specimens of brannerite were examined by differential thermal analysis. The thermal curves indicate loss of water at relatively low temperatures and recrystallization above 550° C., accompanied by two exothermic reactions. Experiments involving preheating of brannerite from Cordoba, Spain, suggest that initial recrystallization is a three-stage process involving both loss and gain of energy. Thermal curves of brannerite are sufficiently different to distinguish material from various localities.

INTRODUCTION

Certain radioactive minerals presumably undergo changes in structure due to internal alpha bombardment, resulting in lattice disorder. The amorphous condition arising from this transformation is commonly referred to as the metamict state. Although metamict characteristics are not peculiar to all radioactive minerals, the condition is generally prevalent in uraniferous and thoriferous multiple oxides of titanium, columbium, and tantalum, as well as in certain other minerals such as allanite and zircon which contain minor amounts of uranium and thorium as vicarious constituents.

The metamict state is characterized by optical isotropism, hence *x*-ray diffraction and optical characteristics are not an aid in identification of the natural mineral. The metamict nature of the mineral may, however, be detected by *x*-ray study. Although recrystallization of metamict minerals is frequently brought about by the application of heat, it has been suggested that, in some cases, the original crystal structure may not be reconstituted. Several investigators have, therefore, resorted to differential thermal analysis to facilitate identification of these minerals.

The differential thermal method of analysis has been employed with particular success in the differentiation and identification of clay minerals and has been generally applied to the study of a large number of individual minerals and mineral groups which yield thermic reactions. Kerr and Holland (1951) have applied the differential thermal technique to metamict minerals in their study of davidite and other multiple oxides; Orcel and Levy (1953) have applied it to betafite; and Kulp, Volchok, and Holland (1952) have shown its usefulness in determining the ages of metamict minerals.

This paper describes briefly some observations on the thermal behavior f brannerite, a metamict multiple oxide of uranium and titanium which ormally contains minor amounts of calcium, rare earths, thorium, and on.

Application and Technique

DTA reactions usually involve oxidation, the loss of adsorbed and ttice water, inversion, recrystallization, melting, and sublimation, and ccur in many instances at different temperatures and rates for various inerals owing to diverse compositions and chemical bond strengths. Iany minerals undergo more than one transformation in the course of eating. The peaks that have been observed for metamict minerals are elated as a rule to two principal reactions: the loss of water and the ransition from the metamict to the crystalline state. The latter involves xothermic reactions accompanied by loss of energy which has accumuted in the lattice as a result of atomic displacements caused by alpha radiation.

Thermic reactions are usually represented graphically by plotting the agnitude and rate of evolution or absorption of heat energy as a funcon of temperature. Characteristic reaction peaks often suffice for the dentification of a mineral, the amplitude and shape of the thermal peak eflecting the rate of the reaction, and the area under the thermal peak pproximating proportionality to the energy exchange involved in the action. Thermal peaks due to the recrystallization of metamict minrals contain areas that are assumed to be proportional to lattice disrganization caused by bond breakage.

The apparatus used in this study is a modification of the portable ifferential thermal analyzer originally described by Hendricks, Goldrich, nd Nelson (1946). The thermocouples are chromel-alumel and the rucibles are iron-nickel alloy. Energy differences were measured on a alvanometer, and crucible temperature was recorded from a pyrometer. rimary voltage fluctuations were stabilized by a constant voltage transormer, while the rate of heating was maintained at approximately 10 to 3 degrees Centigrade per minute by means of a manually adjustable ariable transformer. The instrument is provided with a sensitivity elector which permits relative sensitivity factors of 1, 3, and 9. The hermal curves shown were obtained at highest sensitivity. When derable, the variable transformer could be regulated to heat sample marial at a fairly constant temperature over prolonged periods of time. he pyrometer was calibrated after the method of Barshad (1952) by sing inversion and melting-point temperatures of several inorganic alts, and reference points were established at 160° C. and 212° C. with

silver nitrate and at 314° C. with sodium nitrate. The inversion temperature of quartz (573° C.) and reaction temperatures of kaolinite (600° C. and 980° C.) proved useful in establishing additional reference points.

The samples were prepared for analysis by grinding to pass a 100-mesh sieve. Thermal analyses were made in air at atmospheric pressure. Alumina (90 mesh) was used as the inert standard. Material for thermal analysis was carefully selected under binocular and petrographic microscopes to exclude obvious impurities. *X*-ray determinations using copper radiation were obtained on all samples before and after heating, and identification was made by comparison with diffraction patterns obtained from type material available at the U. S. Geological Survey's *x*-ray laboratory in Washington, D. C.

Parker, Hathaway, and Blackmon (1956) discuss the disadvantages inherent in the routine use of portable equipment similar to that employed in this study. Although the curves obtained during this investigation may not be strictly comparable with those obtained using standard differential thermal analysis equipment, the use of controlled heating rate and temperature reference points should minimize any differences and avoid the principal disadvantages cited by Parker *et al.* The thermal curves may be considered valid inasmuch as reproducible experimental conditions were maintained. The utilization of this instrument under controlled conditions enhances its application to more rigid studies of the nature of thermal reactions.

Specimen Description

Prior to 1950 brannerite was, for all practical purposes, a mineralogical curiosity. It had been reported (George, 1949) in a pegmatite deposit near Fuenteovejuna, Cordoba, Spain, as more or less distinct crystals and in a placer gravel in Kelley Gulch, Custer County, Idaho. It was first discovered in significant quantity at Crockers Well, South Australia, and in the Blind River district, Canada, where it constitutes an important fraction of the uranium ores.

The specimens used for this study originated near the following localities:

(1) Fuenteovejuna, Corboda, Spain
(2) Crockers Well, South Australia
(3) Bou Ázzer, French Morocco
(4) Florence, Montana
(5) Elk City, Idaho

All five specimens in the unheated state are metamict as determined by *x*-ray powder patterns.

Brannerite from a pegmatite at Fuenteovejuna, Cordoba, Spain, was originally considered to be uraninite pseudomorphous after beryl; however, identification as brannerite was subsequently established by chemical analysis. Chemical determinations reported by George (1949) show a uranium content of about 51 per cent and indicate that the mineral is primarily an oxide of titanium and uranium. The unheated material is massive, jet black, with vitreous luster, and shows conchoidal fracture. Surfaces of several fragments examined are partially coated with thin layers of light-brown alteration products, and small flakes of muscovite occur superficially; however, no other extraneous substances were observed.

In transmitted sodium light the index of refraction of the Cordoba brannerite is 2.21 ± 0.03. The specific gravity is approximately 5.17. Fragments of the unheated mineral are optically isotropic. On heating to 960° C. the refractive index is increased to 2.39 ± 0.03, due to loss of water as well as recrystallization from the amorphous state.

Brannerite from Crockers Well, South Australia, occurs as irregular masses and scattered crystals in fracture zones in syenitic rock. The mineral appears olive green to red brown and is coated with yellow to red-brown alteration products. Fresh mineral surfaces show a greasy or resinous luster and irregular to semiconchoidal fracture.

In transmitted light thin splinters of the mineral are pale yellow to brown and isotropic, whereas larger fragments seem opaque. The index of refraction in sodium light is close to 1.95, and the specific gravity is 4.13. After heating to 960° C. refractive indices of 2.2 to 2.3 in sodium light were obtained for various fragments. Alteration may account for the relatively low index and specific gravity of the unheated material. The low index is, furthermore, consistent with high water content indicated by the large endothermic peak between 100° and 300° C. (Fig. 1). The area under the dehydration curve, as determined by trapezoidal integration, is 3.9 times greater than the area of the corresponding peak of the Cordoba mineral, suggesting an increment in water content of this magnitude. This agrees well with the ratio of 4.2 shown by chemical analyses of samples of the Crockers Well (9.95% H_2O by weight) and Cordoba (2.35% H_2O) minerals in Table 2.

A polished surface of the Crockers Well material shows very minor included matter which is seemingly inert, or the amount is insufficient to produce a detectable thermal reaction. The *x*-ray diffraction pattern obtained on unheated brannerite fragments contains a few lines that are not characteristic of heated brannerite but agree most closely with lines produced by thorite and rutile.

Brannerite at Bou Azzer, French Morocco, is disseminated in metallic

sulfide veins. It appears black with a vitreous luster and fractures conchoidally. In transmitted light the fragments are opaque to transparent brown and are isotropic at the thin edges. In sodium light the index of refraction is 2.22±0.03.

At Florence, Montana, brannerite is found as small, subrounded detrital grains in heavy sands consisting largely of rutile, ilmenite, and garnet. The brannerite is green to red brown. A few of the brannerite grains are subhedral crystals. The fragments appear opaque in transmitted light but have transparent isotropic edges. The index of refraction in sodium light is 2.26±0.03.

Table 1. Variation in Indices of Refraction of Brannerite

	S. Australia	Spain	Fr. Morocco	Montana	Idaho
Unheated	1.95±0.03	2.21±0.03	2.22±0.03	2.26±0.03	2.26±0.03
Heated to 350° C.	2.06±0.03	2.28±0.03	2.23±0.03	2.30±0.03	2.30±0.03
Heated to 960° C.	2.2 to 2.3	2.39±0.03	2.39±0.03	2.39±0.03	2.39±0.03

Brannerite occurs as rounded black pebbles in a placer deposit near Elk City, Idaho, together with ilmenite, rutile, garnet, and magnetite. Davidite, betafite, and euxenite were also identified in the gravel. The brannerite pebbles show no crystal faces. In sodium light the refractive index of the unheated brannerite is 2.26±0.03.

Refractive indices of the five brannerite specimens obtained on unheated fragments as well as material heated to 350° and 960° C. are included in Table 1. The index of refraction increases slightly with loss of water (350° C.), and a further increase takes place after heating to 960° C. presumably as a result of recrystallization of the mineral.

Discussion of Thermal Curves

All five brannerite specimens failed to yield *x*-ray diffraction powder patterns before heating; however, all produced similar characteristic lines after heating to high temperatures. The detectable energy changes produced are shown by the thermal curves in Fig. 1, which are characteristic of each specimen but show marked dissimilarities. Although each curve contains two exothermic peaks, there are major differences in peak position, shape, area and amplitude which can not reasonably be attributed to variations in particle size, but may reflect varying degrees of lattice disorganization as well as compositional variance.

The endothermic peak between 100° and 300° C. is due to release of water, and the area under the dehydration peak should be roughly indica-

tive of the amount of low-temperature water which these specimens contain. The Idaho material may have lost much of its water below 100° C. Both the South Australia and Montana brannerite have a relatively high water content, which may be due to alteration and may account for the resinous appearance and green to red-brown color of the specimens.

The thermal curve of the Cordoba brannerite shows two exothermal

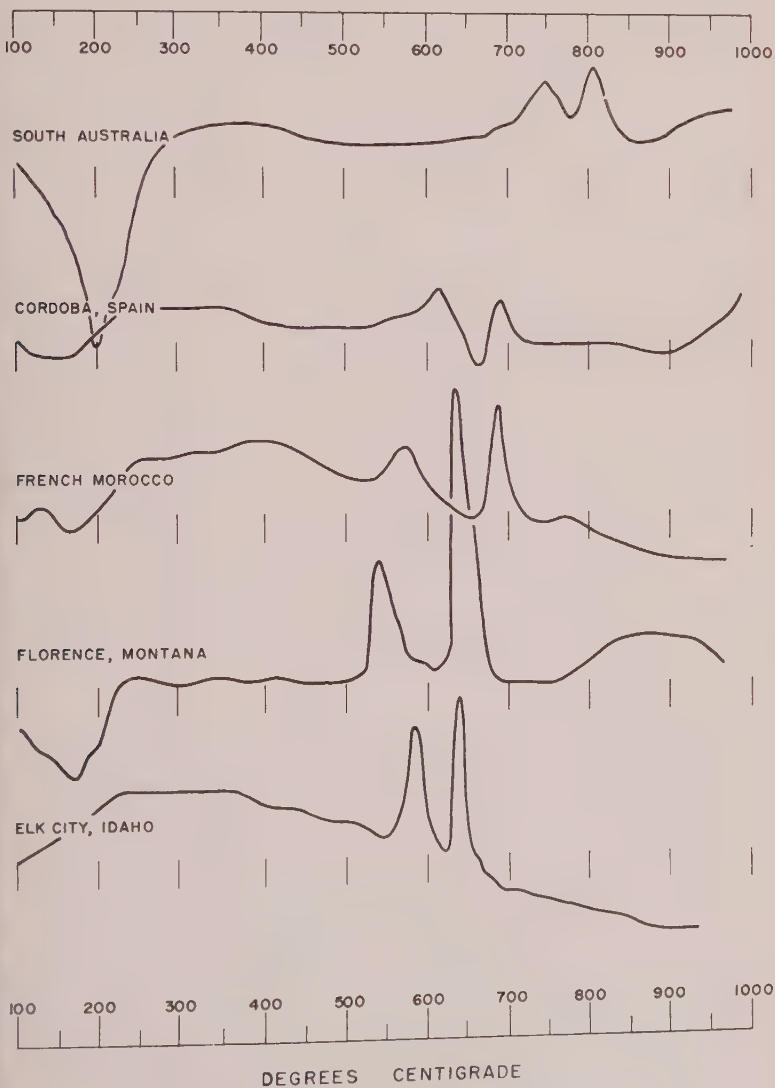

FIG. 1. Thermal curves of brannerite.

peaks, the significance of which has been established to some extent. After heating the sample to 660° C. no x-ray lines are obtained, indicating the persistence of an essentially random structure. On heating to 740° C. broad and somewhat diffuse lines are obtained, suggestive of initial reorientation. The x-ray pattern, however, is not typical of heated brannerite although several lines coincide. The resultant material, referred to as Phase I, has not been identified. Further heating to 980° C. is accompanied by a marked change in the x-ray pattern and a concomitant increase in the sharpness of the lines, which are typical of recrystallized brannerite. Preheating the Cordoba material at 550° C. for 9 hours produces no pattern, but subsequent heating to about 900° C. produces an x-ray pattern which is identified as Phase I; however, the lines appear sharper than in the pattern obtained after heating directly to 740° C., indicating less random orientation. Although substantial exothermic reactions accompany the changes in atomic reorientation yielding Phase I, the only reflection of modification to the brannerite structure is the sharp exothermic rise in the thermal curve above 900° C. This transition requires further investigation. The existence of several crystalline phases emphasizes, of course, the importance of controlled heating before x-ray analysis, as either structure could possibly result from heating this brannerite in the Bunsen flame.

Brannerite from South Australia heated to 840° C. yields an x-ray pattern which is identical to that obtained from the Cordoba material heated to 980° C. Brannerite specimens from Idaho, Montana, and French Morocco heated to above 900° C. also yield similar x-ray patterns. The thermal curves, on the other hand, show characteristic variances which uniquely identify the specimens from each locality. In all cases the exothermal doublet is related to energy liberated during recrystallization.

Further study of the thermal behavior of Cordoba brannerite has revealed an interesting phenomenon that is evidently associated with the transformation to Phase I. Curves 1, 2, 3, and 4 in Fig. 2 show the effects of preheating the mineral at 550° C. for about 3, 5, 7, and 9 hours, respectively. The Cordoba curve in Fig. 1 shows an initial exothermic peak at about 610° C., the amplitude of which exceeds that of the high-temperature peak at 690° C. On preheating for prolonged periods, the amplitude of the peak at 610° C. diminishes with a corresponding increase in the amplitude of the peak at 690° C. Also, the combined area under both peaks of the curve in Fig. 1 is smaller than the area under curve 4 in Fig. 2, suggesting that the lattice has gained energy as recrystallization proceeds. There is a suggestion of energy absorption in the endothermic peak at 665° C. which is not apparent in the South Australia, Montana or

Idaho brannerite curves, but does appear in the curve obtained on the French Morocco mineral. Most of this energy increment is presumably gained from furnace heat inasmuch as the energy loss of the first reaction (610° C.) is considerably less than the energy gain reflected in the second exothermic peak (690° C.). The reaction at 610° C. is ascribed to initial reorientation of atomic groups within the lattice, which results ap-

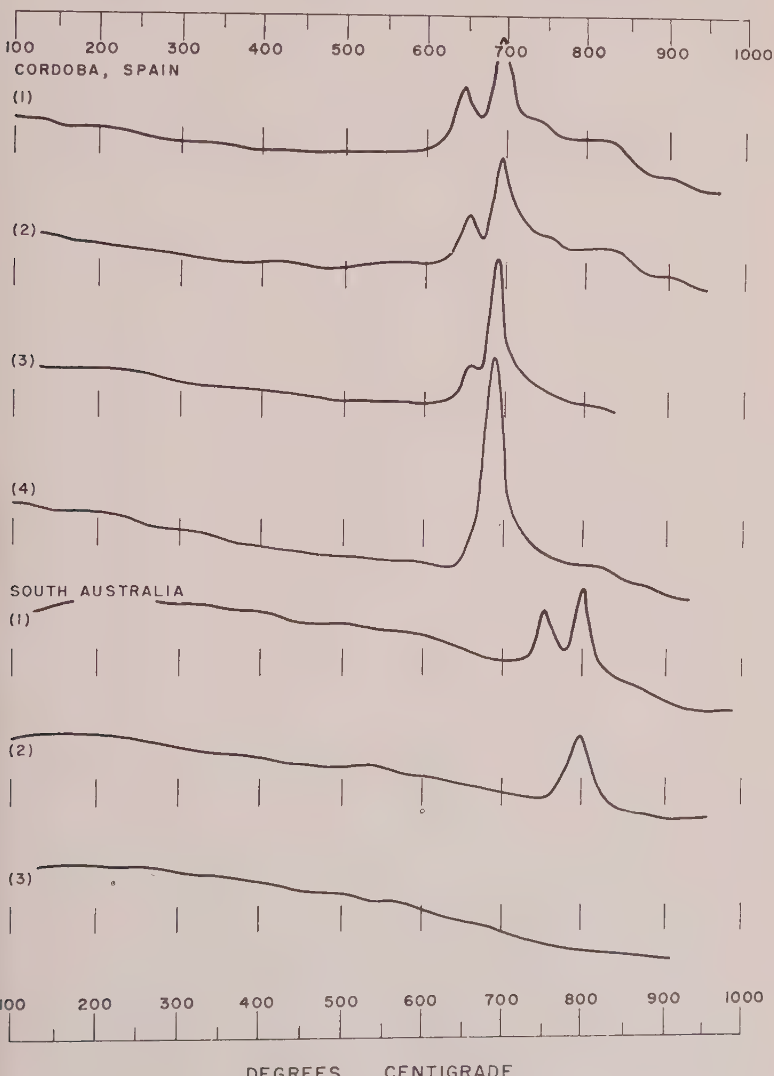

FIG. 2. Progressive heating curves of brannerite.

parently in no detectable lattice order. The accompanying energy changes evidently enable recrystallization to proceed to a more stable and ordered state at 690° C. Hence, recrystallization of the Cordoba mineral to Phase I is seemingly a three-stage process involving both loss and gain of energy, although evolution of heat is largely reflected in the thermal curve (Fig. 1).

Similar effects were not observed after preheating brannerite from South Australia. The writers believe, however, that the temperature and

TABLE 2. CHEMICAL ANALYSES OF BRANNERITE, IN WEIGHT PER CENT (after Frondel, 1958)

	1	2
CaO	2.74	—
PbO	2.34	2.79
FeO	3.11	—
UO_2	—	—
UO_3	—	31.83
U_3O_8	51.76	—
ThO_2	1.20	12.81
Ce_2O_3	1.10	1.43
$(Y, Er)_2O_3$		3.71
TiO_2	32.45	35.13
H_2O	2.35	9.95
Rem*	~.16	1.69
Total	97.21	99.34

1. Cordoba, Spain.
2. Crockers Well, Australia.
* Additional minor constituents are reported in the reference cited.

time variants used may not have been sufficient to obtain ample resolution and intermediate results. Curves 1, 2, and 3 in Fig. 2 were obtained respectively on material preheated at 685° C. for 1 hour, at 705° C. for 3 hours, and at 770° C. for 6 hours. It is also conceivable that the state of lattice disorder may differ for the Cordoba and South Australia specimens inasmuch as they are compositionally different (see Table 2). This may account for the difference in thermal behavior, *i.e.*, the higher exothermic reaction temperatures of the South Australia brannerite and the results obtained during preheating experiments.

The results of the present study also suggest that differences in amplitude of thermal peaks obtained on specimens of a single species of metamict multiple oxide may be due partially to a natural exchange of energy at temperatures too low to produce recrystallization. The reactions may

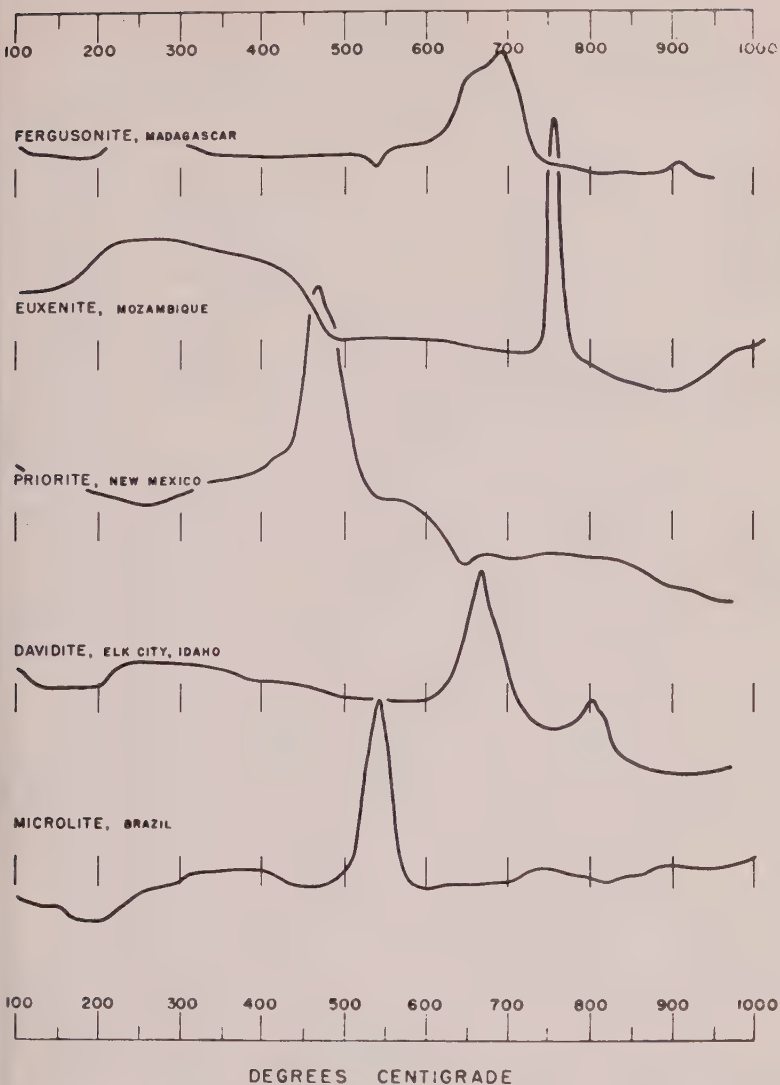

FIG. 3. Thermal curves of various multiple oxides of columbium, tantalum, and titanium.

have been effected by heat of disintegration of radioactive elements contained in the mineral and, in certain cases, by renewed igneous or hydrothermal activity.

Attempts to relate differences in the thermal curves to compositional variations in brannerite have been unsuccessful owing to the lack of adequate analytical data. Published analyses (Pabst, 1954; Frondel, 1958)

of Crockers Well and Cordoba brannerite shown in Table 2 do not distinguish between UO_2 and UO_3 content. The distinction may be important inasmuch as disruption of the lattice structure, and subsequent reorganization, may be partially related to oxidation-induced changes in the size and valence of the uranium ion.

Thermal curves of several other multiple oxides of uranium and thorium are shown in Fig. 3. These compare favorably with curves obtained by Kerr and Holland (1951) and Kulp, Volchok, and Holland (1952).

References

Barshad, I. (1952), Temperature and heat of reaction calibration of the differential thermal analysis apparatus: *Am. Mineral.*, **37,** 667–694.

Frondel, C. (1958), Systematic mineralogy of uranium and thorium: *U. S. Geol. Survey Bull.* **1064,** p. 333.

George, D. (1949), Mineralogy of uranium and thorium bearing minerals: *U. S. Atomic Energy Comm. RMO*-**563,** p. 78.

Hendricks, S. B., Goldrich, S. S., and Nelson, R. A. (1946), A portable differential thermal analysis unit for bauxite exploration: *Econ. Geol.*, **41,** 64–76.

Kerr, P. F., and Holland, H. D. (1951), Differential thermal analyses of davidite: *Am. Mineral.*, **36,** 563–572.

Kulp, J. L., Volchok, H. L., and Holland, H. S. (1952), Age from metamict minerals: *Am. Mineral.*, **37,** 709–718.

Orcel, J., and Levy, C. (1953), Analyse thermique de la betafite, mineral métamicte: *France, Acad. Sci., Comptes Rendus*, **236,** 1, 1177–1179.

Pabst, A. (1954), Brannerite from California: *Am. Mineral.*, **39,** 109–117.

Parker, C. J., Hathaway, J. C., and Blackmon, P. D. (1956), Some curves from a portable differential thermal analysis unit: *U. S. Geol. Survey Bull.* **1021-G,** 237–251.

Manuscript received December 1, 1960.

THE AMERICAN MINERALOGIST, VOL. 46, SEPTEMBER-OCTOBER, 1961

POLYSYNTHETIC TWINNING IN PLAGIOCLASE

JOSEPH A. VANCE, *Geology Department, University of Washington, Seattle, Washington.*

ABSTRACT

Primary polysynthetic twinning in plagioclase, though much less common than secondary twinning, can be demonstrated by the relations between crystal morphology and primary twin lamellae in euhedrally zoned plagioclase. In twinned plagioclase grains cut normal to the *a*-axis and showing the (001) and (010) cleavages, both the zones and cleavages—(001) in albite twinning, (010) in pericline twinning—make a zigzag of about 8° as they cross the composition planes. The relations of truncated twin lamellae to crystal morphology in such *a*-normal sections indicates that the twinning is primary. The parallelism of zones and clevages further establishes that the plagioclases studied grew in essentially their present triclinic form and cannot have inverted from a hypothetical plagioclase of markedly higher symmetry. The twinning of these plagioclases therefore cannot be transformation twinning.

Contrary to a widely held view, it is not so much plagioclase composition and structure, but environmental conditions during crystal growth which largely determine whether or not primary twinning develops and the frequency of primary twin lamellae. Formation of primary twins is favored by euhedral growth and by rapid crystallization. Slow crystallization and anhedral growth tend to inhibit development of primary lamellae. Primary twinning on the albite and pericline laws is quite common in igneous plagioclase, but is uncommon in metamorphic plagioclase.

Glide lamellae in plagioclase are typically of uniform thickness and characteristically found in genetic relation to bending or other deformation of the crystal. They differ markedly from primary lamellae, usually permitting easy distinction. Texture is an important factor in determining abundance of glide lamellae in the plagioclase of deformed rocks. In both igneous and metamorphic plagioclase, glide twinning on the albite law is exceedingly common and is usually associated with somewhat less abundant glide twinning on the pericline law.

INTRODUCTION

It has long been recognized that some polysynthetic twinning in plagioclase is of secondary origin. Glide twinning was first clearly demonstrated by van Werveke in 1883, and in 1931 was produced experimentally by Mügge and Heide. Since van Werveke's early observations many petrographers have confirmed his evidence, so that today the existence of secondary twinning is generally accepted. More recently, however, several workers have taken the extreme position that most and perhaps all polysynthetic twinning in plagioclase is secondary. These include Baier (1930, p. 494), Köhler and Raaz (1947, p. 169), Köhler (1949, p. 598), Emmons and Gates (1943, p. 288), and Emmons and Mann (1953, p. 41). Representative of this view is the statement of Köhler and Raaz,—"dass polysynthetische Zwillinge—das gilt nicht nur für die Plagioklase-niemals primär gewachsen sind, sondern das Ergebniss sekundärer Prozesse sind."

Other petrographers either endorse the opposing view that some and perhaps most polysynthetic twinning is primary or imply such without specifically noting the problem. Along with these investigators, the writer had assumed that most polysynthetic twinning in plagioclase was a growth phenomenon and thus primary. Surprisingly, a search of the literature failed to reveal any really cogent evidence for a primary origin. Is the theory of primary origin a mistaken one which has been uncritically accepted, or can it be demonstrated by direct petrographic evidence? The problem has considerable significance in petrogenesis. Gorai (1951), on the tacit assumption that twinning in plagioclase is primary, has statistically compared the twinning habit of plagioclases in a large number of igneous and metamorphic rocks. If all or some of this twinning is secondary and only accidentally superimposed on the plagioclase independent of its crystallization, his conclusions may justly be questioned. Starting with the assumption that polysynthetic twinning is secondary, Emmons and Mann (1953) arrive at other petrogenetic interpretations which are open to similar criticism. Over the years a number of useful articles have appeared dealing with the frequency of the different twin laws in various plagioclases. In these, the origin of the plagioclase (plutonic, volcanic, metamorphic, etc) has been considered, but the equally critical problem of the origin of the twinning has again been generally ignored. If both primary and secondary twinning do occur, criteria must be established by which they may be distinguished. By detailed study of individual rocks it may become possible to frame valid, if more limited, generalizations as to the petrogenetic significance of polysynthetic twinning. Failure to consider the origin of plagioclase twinning, whether primary or secondary, and the conditions responsible for its formation is clearly to ignore a major problem of plagioclase genesis.

This paper is submitted as a review and criticism of some aspects of the problem of twinning genesis, with emphasis on the criteria for distinguishing between primary and secondary twinning and the genetic factors which determine the twinning. In particular, it presents a new line of evidence in support of primary polysynthetic twinning. Other significant new contributions are the role of growth habit as a factor in primary twinning, and the importance of textural controls in glide twinning. The evidence adduced here is largely petrographic. No exhaustive review of the problem as found in a diffuse and voluminous literature is intended. Of the ideas expressed here, some are frankly speculative while others are at variance with the generally accepted views on twinning. The writer is aware of the breadth of the problem and the limitations of the data presented. Consequently some of the conclusions reached are tentative and all deserve scrutiny in the light of more

detailed investigation. This study will have been successful if it does nothing more than bring awareness of the problems of plagioclase twinning and indicate some of the points to be considered in their final evaluation.

Primary Polysynthetic Twinning

General statement

Primary twinning (the growth twinning of Buerger, 1945, p. 473) develops as the result of addition of individual atoms or small groups of atoms to a growing crystal. Primary twinning is contrasted to secondary twinning in which an already formed or partially formed crystal develops twins through processes other than simple growth. The literature offers little discussion of primary polysynthetic twinning in plagioclase. Only a few petrographers—*e.g.* Barber (1936, p. 257) and Turner (1951, p. 587)—consider specific evidence for primary origin, and most of this is far from conclusive. Barber believes that the occurrence of vicinal composition faces demonstrates primary twinning, but this seems less than compelling in view of our present meagre understanding of vicinal phenomena and of the genesis of primary twinning itself. Certainly many secondary glide lamellae—*e.g.* pericline lamellae as well as long, slender, regularly tapering albite lamellae which are obviously related to the bending of a crystal—also have composition faces diverging slightly from rational crystallographic directions.

Evidence for primary twinning

Criteria for primary twinning can be developed from considerations of crystal morphology. Baier (1930, p. 483) appreciates this when he notes that "sie (primary twinning) steht meist in deutlicher Beziehung zu einem einspringenden Winkel der äusseren Umgrenzung." Thus, there should be, in euhedral crystals with primary twinning, a regular relation between the distribution of twin lamellae and external morphological form, and especially an occurrence of re-entrant angles at twin boundaries. This is true, of course, for primary twinning, but it is also true for secondary glide twins, as visualization of the well known experiment of artificial twinning of calcite will show. In itself, then, this relation proves neither primary nor secondary origin of the lamellae. It does, however, become significant when considered with other details of both external and internal crystal morphology.

The relations between twinning and zoning are of particular significance. In this paper, as traditionally, euhedral zoning is considered to be a primary feature and to mark the various stages in crystal growth. Powerful evidence supports this view. Euhedral zones are just as logically

growth features as are the external crystal faces which they parallel. Further, the variable width and composition of different zones are much better understood as the result of a changing physical and chemical environment around a growing crystal than as superimposed secondary features. The very differences in the degree of development of the various "crystal faces" in one zone as compared to corresponding "faces" in adjacent zones rule out any hypothetical inward migration of secondary zones parallel to the crystal faces. Finally, it is difficult even to imagine a secondary process which could impress euhedral oscillatory zoning on earlier crystals. Irregular zones in igneous plagioclase which truncate earlier zones and are logically interpreted as due to resorption become inexplicable if referred to processes postdating crystal growth. The continuity of individual zones of distinct composition around doubly or multiple cored aggregates of plagioclase grains is readily understood as the result of coalescent growth (Vance, 1957, p. 1849), but is incomprehensible if zoning is secondary.

Zoning can thus be expected to show the same relation to twinning as does the external morphology, but with the advantage that it reveals the relations between twinning and crystal form during crystal growth (internal morphology). There is also the practical advantage that euhedrally zoned crystals are much more common than crystals with euhedral outer form.

A systematic relation between twinning and zoning was revealed during routine determination of the composition of euhedrally zoned plagioclase in a large group of igneous rocks, principally Tertiary quartz diorites, granodiorites, basalts, andesites, and dacites from western Washington. In each thin section plagioclase crystals cut normal to the *a*-crystallographic axis were located for extinction angle measurement. These (*a*-normal) sections are easily recognized in that they are perpendicular to both the (001) and (010) cleavages (Fig. 1 A–D). In *a*-normal crystals which show albite twin lamellae the (001) cleavage zigzags abruptly at each twin boundary and deviates about 8° from a straight line (Fig. 1 A, C, D). In *a*-normal sections with pericline twinning, (no attempt has been made to separate pericline and acline twins in this paper), the (010) cleavage switches its position from twin to twin in a similar way (Fig. 1 B, C). In every case where these oriented sections show sharply marked euhedral zoning, it was found that zones parallel to (001) and (010) rigidly follow their respective cleavages in making the zigzag shift in trend across twin boundaries (Fig. 1 A–D). Similar relations were found in plagioclase crystals with euhedral outer form; here, however, not only the zones but also the (001) and (010) crystal faces (in albite and pericline twinning respectively) change position from one

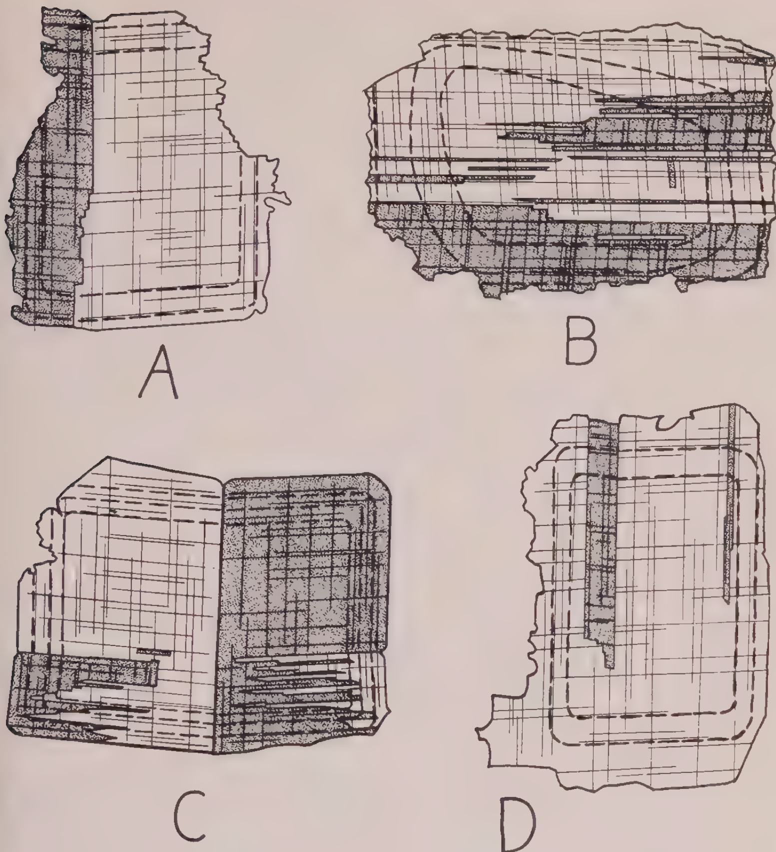

FIG. 1. Relations of euhedral zoning and primary twinning in *a*-normal sections of lagioclase. (010) is oriented near vertical, (001) is oriented near horizontal. Note the arallelism of the cleavage and zoning (generalized by dashed lines). All the plagioclases re igneous and show oscillatory zoning with a normal trend.

A. Simple albite twinning in andesine (An_{49}-An_{27}) from Tertiary quartz diorite, Monte Cristo, Washington. Width of grain 1.7 mm.

B. Pericline twinning in andesine-oligoclase (An_{41}-An_{17}) from the Tertiary Squire Creek quartz diorite Darrington, Washington. Width of grain 2.5 mm.

C. Albite and pericline twinning in andesine (An_{45}-An_{34}) from a vitrophyric hypersthene andesite dike north of Glacier Peak, Washington. Width of grain 1.4 mm.

D. Albite twinning in andesine-oligoclase (An_{40}-An_{16}) from the Squire Creek quartz diorite, Darrington, Washington. Width of grain 0.4 mm.

win lamella to the next (Fig. 1 C). When these relations had become pparent, approximately 200 additional thin sections showing plagioclase ith euhedral oscillatory zoning were checked. Normal calc-alkaline neous rocks were used exclusively and the relations were found to be

consistent for both volcanic plagioclase (An_{30}-An_{60}) and plutonic plagioclase (An_{20}-An_{55}). A large number of thin sections was necessary because only about one out of five showed crystals suitably combining the polysynthetic twinning, proper orientation, lack of alteration, and sufficiently sharp zoning necessary to conclusively establish the relations between twinning and zoning. However, every crystal which did fulfill these conditions revealed the same rigid parallelism between zones parallel to (001) and (010) and the respective cleavages. Altogether some 50 clear-cut examples were found.

This close and consistent relation between polysynthetic twinning and zoning is compatible with either primary (growth) twinning or secondary glide twinning. In almost half the crystals showing this twin-zone relation, however, some of the lamellae concerned do not traverse the entire crystal but pinch out step-like in a blunt irregular manner, within the crystal. In the *a*-normal sections studied this tendency to terminate within the grain is especially marked in the pericline lamellae, but is also seen in the albite lamellae, though to a lesser degree. These terminated lamellae are not thin and regular or gently tapering, as characterizes most secondary glide lamellae, nor are they associated with bending, twisting, or fracturing of the crystal as is so general with secondary lamellae. (See Table 1 for a comparison of the characteristics of primary lamellae and glide lamellae.) Where several lamellae terminate within a crystal, they do so independently of one another, unlike glide lamellae which almost universally show a systematic distribution within the crystal and a regular sense to the direction of pinch-out. The crystals studied, even near the terminated lamellae, reveal no indication of the bending and strain so characteristically associated with glide lamellae. Since these lamellae terminate without strain, the crystal being undisturbed along their projected continuation, the twinning is considered to be primary. Additional evidence of primary origin is revealed by an examination of either the gross outer form of the crystal or of the zonal outline in crystals with terminated lamellae. A re-entrant angle is associated with each of the terminated lamellae in Fig. 1 B–D. This is readily understood if the lamellae are primary, while a mysterious diminution in volume of part of the crystal—an exceedingly unlikely occurrence—must be invoked if the lamellae are considered to be secondary. Finally, it is to be stressed that, if the twinning in these crystals were glide twinning, both the crystals themselves and adjacent crystals in the fabric would show cataclastic effects where the new lamellae had made room for themselves. Such strain features are lacking in the rocks studied, except insofar as entirely later glide twinning and deformation may have developed in some specimens. (Generally at least a few extremely narrow,

TABLE 1. COMPARISON OF PRIMARY LAMELLAE AND GLIDE LAMELLAE IN PLAGIOCLASE

Primary Lamellae	Glide Lamellae
Twinning is simple, or, if multiple, lamellae are few.	Twinning is multiple and lamellae are usually numerous.
Lamellae in individual grains vary widely in thickness.	Lamellar thickness is essentially uniform within each set of lamellae or for all lamellae in individual grains.
Lamellae are usually rather broad and coarse. They often change width or terminate within the crystal abruptly and irregularly.	Lamellae are slender and may be extremely fine. They are usually very regular and may traverse the entire grain with uniform thickness.
Lamellae thicken and thin independently of each other. The changes in width are step-like and abrupt and unrelated to later bending.	Lamellae thicken and thin gradually and regularly, in unison, and in the same direction, often in conjunction with bending of the crystal.
Individual lamellae terminate independently of each other and without relation to later bending or fracture.	Lamellae terminate regularly as long tapering points which are often localized in areas of bending and may be bent themselves. Termination and changes in thickness are common across fractures.

regular glide lamellae, presumably due to stresses set up during contraction with cooling or inversion, were also present in the igneous plagioclases studied, and broader, more abundant glide lamellae were found in all rocks showing stronger deformation. Such glide twinning may completely obscure an earlier generation of primary lamellae. This later twinning, however, does not bear on the origin of the primary features discussed here.)

For these reasons it is believed that the albite and pericline lamellae studied are primary and thus, that these crystals grew twinned. Strictly this conclusion applies only to the specific *a*-normal crystals described, but it is reasonable to conclude that twinning is also primary in other plagioclase crystals in the same rocks, at least in so far as the twinning characteristics are comparable and evidence of secondary twinning is lacking. These relations between twinning and zoning provide a quick and simple petrographic method by which primary polysynthetic twinning in plagioclase may be established in euhedrally zoned material. These relations are by no means anomalous or unexpected, but are demanded by the triclinic symmetry requirements of the albite and pericline laws. Implications of these twin-zone relations with regard to trans-

formation twinning are considered below. It is to be hoped that eventually some line of evidence, other than the negative evidence of the absence of definite indications of secondary lamellae, can be developed to establish primary twinning in plagioclases which lack euhedral zoning and euhedral outer form.

In the material studied, primary albite and pericline (including acline) lamellae appear to be about equally common. The frequency with which primary polysynthetic twinning was encountered in the rocks studied indicates that it is quite common in igneous plagioclase.

The origin of primary twinning

The causes of primary polysynthetic twinning must be sought in terms of environmental conditions and in the process of crystal growth itself, rather than in secondary factors such as inversion or exposure of the finished crystal to mechanical stress. Buerger (1945, p. 473), has given a convincing theoretical explanation of primary twinning in which the rate of growth is considered the principal controlling factor. According to this theory, formation of primary twinning is favored by rapid growth and minimized by slow growth. Minimum energy requirements are fulfilled when atoms are added to a growing crystal in parallel position so as to continue the initial pattern. There are, however, other positions—twin positions—in which atoms can be added in coordination with those atoms already present without continuing the earlier pattern. Atoms added in this way do not quite meet the lowest energy condition and thus tend to be dislodged and replaced by more favorably oriented ones. If, however, an already coordinated group of atoms joins the growing crystal in the position of near minimum energy, it may remain in place, being more stable than a single atom. This twin will grow if joined by other atoms in the same orientation. Other conditions being equal, the probability that newly arrived atoms or groups of atoms will persist in twin position is the greater the more rapid is the addition of atoms and thus, the more rapid the growth. Buerger further states that since crystal growth is rapid in the earliest stages when nuclei first develop under conditions of supersaturation, twins may then be initiated which persist and continue to grow in the following period of slower growth. The simple albite twins in Fig. 1 C in which the composition plane passes through the center of the crystal may be of this sort. This situation, however, is not typical and recurrent supersaturation, leading to rhythmic growth, may be more general than appreciated by Buerger, (see Padurow, 1949, p. 212), so that lamellae may be initiated as a result of rapid growth at various stages of crystallization. Oscillatory zoning, as recognized by Harloff (1927), Phemister (1934), and Hills (1936), strongly suggests such rhythmic supersaturation for igneous plagioclase.

Buerger's theory clarifies many features of primary polysynthetic twinning (See Table 1), which would otherwise be puzzling. Variable rates of crystallization could account for differences in twinning habit of compositionally similar plagioclases in rocks of the same composition. Both the characteristic variation in width and the blunt termination and abrupt change in thickness of primary lamellae are explained by this theory. Primary lamellae of unequal width are obviously to be expected where variations in the rate of growth are more or less random causing initiation of twins irregularly through time. Uneven lamellae will also generally develop even where variations in the rate of growth are regular and periodic, for the tendency is always to satisfy the minimum energy condition and for growth to continue the untwinned configuration. It is therefore improbable that primary lamellae will always be initiated on both sides of the crystal simultaneously. The possibility of even lamellar thickness is, in fact, so foreign to primary twinning that regular, uniform lamellae are an almost conclusive indication of secondary origin. Abrupt change in thickness and blunt termination of lamellae result where, during lamellar growth, the twin orientation is maintained in only one direction and is lost in the other to the original untwinned configuration by irregular transgressive growth of the twin composition surface. Primary lamellae change thickness quite independently of each other, unlike glide lamellae which thicken and thin in unison. Sharply parallel continuous lamellae might be favored by rapid growth which initiates the twins, followed by slower growth which causes them to develop regularly throughout the remainder of crystallization. Episodic growth resulting from recurrent supersaturation—and this appears to be the most usual case in igneous plagioclase—would tend to produce a relatively few twin lamellae of unequal width, many of which terminate within the crystal or abruptly change thickness.

Buerger's theory of variation in the rate of growth accounts very adequately for many characteristics of primary twinning in crystals with euhedral growth habit. In anhedrally grown plagioclase, however, growth habit, the form of the crystal during its growth, appears chiefly responsible for the general absence or scarcity of primary lamellae. Anhedral growth is reflected in irregular grain boundaries during crystallization. On an atomic scale this implies relative irregularity in the surficial layer of atoms—such that many indentations and unoccupied positions are present. These anhedral surfaces cut across the directions of the potentially most stable surfaces in the crystal, those of possible crystal faces. Clearly such anhedral surfaces have a higher surface energy than euhedral faces. Since a still higher energy condition will necessarily result from the addition of atoms in twin position, it is apparent that initiation of twins should be less frequent on growing anhedral faces than on

euhedral ones. This is only a tendency, of course, and, in addition to the irregularity of surface, factors such as rate of growth will influence the number of lamellae initiated and, indeed, whether or not twinning is developed at all. Surface irregularities would have other effects as well. Small gaps in the surface where one or several atoms are missing are unlikely to be filled with atoms in twin position due to the difficulty of lateral coordination with the adjacent atoms. Even if added in this manner, the twin could not be extended in all directions laterally by growth, since some of the adjacent positions are already occupied by atoms in the original untwinned configuration. Irregular surfaces are also less likely to have a form conducive to the addition of groups of already coordinated atoms whether this be in parallel or in twin position. Anhedral growth, while it cannot, perhaps, entirely exclude the formation of primary twinning, clearly discourages development of numerous lamellae.

These theoretical considerations find abundant empirical confirmation, for primary twinning appears to be almost entirely restricted to plagioclase which, as demonstrated by the zoning, grew euhedrally. Primary twin lamellae are typical not only of the usual euhedrally zoned igneous plagioclases, but of the few euhedrally zoned metamorphic plagioclases examined. The much more common anhedrally zoned metamorphic plagioclase showed few or no primary twin lamellae. The dependence of the frequency of primary twin lamellae on growth habit may well amount to a rigid control. Examination of over 150 thin sections of metamorphic plagioclase with anhedral zoning (chiefly schists, amphibolites, and gneisses from the Northern Cascades of Washington revealed that, after excluding specimens in which polysynthetic twinning was clearly secondary, few of the remaining sections showed much, if any, twinning. Even if all the remaining twinning in these plagioclases is considered to be primary, it is apparent that primary lamellae are conspicuously subordinate in the plagioclase which grew anhedrally. Other workers -Köhler (1948, p. 62) and Turner (1951, p. 581) have also noted the tendency for many metamorphic plagioclases to be little twinned or untwinned.

Although zoning has been useful in relating polysynthetic twinning to growth habit, it must be emphasized that growth habit, not the zoning itself, controls the twinning. This is apparent in both the igneous and metamorphic plagioclases studied, for the type of zoning (normal, reverse, or oscillatory), the degree of compositional difference in the zoned crystals, and the number and thickness of the zones proved to be essentially independent of the frequency of the lamellae. Euhedrally zoned crystals of igneous plagioclase with a wide compositional range in zoning did not appear to differ systematically in frequency of lamellae from

other euhedrally zoned crystals with an almost imperceptible compositional range. This suggests that the degree of zonal compositional difference is unrelated to the number of lamellae developed and that even unzoned plagioclase which grew euhedrally would have similar twinning. In the same way, anhedrally grown metamorphic plagioclase which ranges in different rocks from sodic oligoclase to medium labradorite and which is partly zoned and partly unzoned proved in general to be scantily twinned or to lack primary lamellae entirely. Since zonal form appears to be the only feature of zoning to which the frequency of primary lamellae can be systematically related, growth habit must be considered the decisive factor.

The dependence of primary twinning on growth habit may well amount to a general control applying to other minerals besides plagioclase. Hornblende with euhedral growth habit, as is typical of most igneous hornblende, appears to be twinned more often than metamorphic hornblende which more commonly has an anhedral growth habit. It likewise appears significant that epidote, kyanite, and staurolite, metamorphic minerals which commonly are idioblastic and have grown euhedrally, are often twinned.

Secondary Polysynthetic Twinning

General statement

Several types of secondary twinning are theoretically possible in plagioclase. To discover which types actually occur, each specific type must be considered in the light of the available evidence. Buerger (1945, p. 477) recognizes two types of secondary twins, gliding twins and transformation twins; these latter develop when rearrangement of atoms during inversion of a high to a low form leads to configurations which are in twin relationship. It may be noted here that some investigators (Baier, 1930, p. 483; Eitel, 1958, p. 119) fail to clearly differentiate between transformation twinning and glide twinning, two entirely different genetic classes of secondary twinning. A third and much less widely appreciated genetic type of secondary twins includes those formed by the drifting together and joining of crystals in a magma according to a twin law. These *synneusis twins*, the "combination twins" of Ross (1957, p. 650), are not considered here, however, as they do not typically lead to polysynthetic groupings in the usual meaning of the term. The abundance of Carlsbad twins in igneous plagioclase and their contrasted infrequency in metamorphic plagioclase can only be due to their frequent origin by synneusis, a process operative only in a fluid medium where free movement of crystals is possible. Some examples of chessboard albite with which I am acquainted appear to be the result of incipient recrystal-

lization of plagioclase in which small patches within earlier lamellae have recrystalized in twin orientation. Although, in a sense, the twinning of such chessboard albite may be regarded as in part secondary, this constitutes a separate problem which will not be considered here.

Glide twinning

Van Werveke's (1883) early demonstration of polysynthetic glide twinning in plagioclase has since been supported by a large body of data including work by Judd (1887), Fedorow (1899, p. 365), Colomba (1908) Baier (1930, p. 480), Chudoba (1931, p. 488), Harker (1932, p. 164), Emmons and Gates (1943, p. 290), Turner (1951, p. 583), and many others. As a final confirmation, Mügge and Heide (1931) have artificially produced both albite and pericline glide lamellae in natural plagioclase.

Secondary glide lamellae usually show distinctive characteristics permitting easy recognition in thin section. These lamellae often terminate at cracks within the crystal and fail to match in either number, width, or relative distribution across these cracks (Fig. 2, A, B). These cracks permitted a different mechanical response to deformation in the separated parts of the crystal and are clearly older than the twinning. Even more commonly secondary lamellae are genetically related to an evident bending or twisting of the crystal such that the lamellae are localized and most broadly developed in the areas of greatest strain (Fig. 2 B–F) while they pinch out or are only scantily developed in the unstrained or more weakly deformed parts of the crystal. The distribution of these lamellae is inseparably linked to the deformation of the crystal, and finds no conceivable explanation in terms of any mechanism of development of the twins during crystal growth. These glide lamellae usually taper to very long, fine points which commonly are bent and transect the direction of the usual composition plane—(010) in albite twinning, the rhombic section in pericline twinning—at a slight angle. In groups of such narrow secondary lamellae, the individuals either thicken, thin, or wedge out in a concerted fashion, most often in areas of obvious bending. This behavior is entirely different from that of primary lamellae which terminate independently of one another—more often somewhat bluntly and irregularly than as regular slender wedges—and which, if bent, show no relation between changes in thickness and any bending which is present. A final characteristic of secondary polysynthetic twinning, as noted by Baier (1930, p. 480) and others, is the tendency of the lamellae to be slender and of rather uniform and regular thickness. This regularity reflects relatively homogeneous release of stress in the deforming plagioclase and is incompatible with a primary origin of the lamellae. Primary

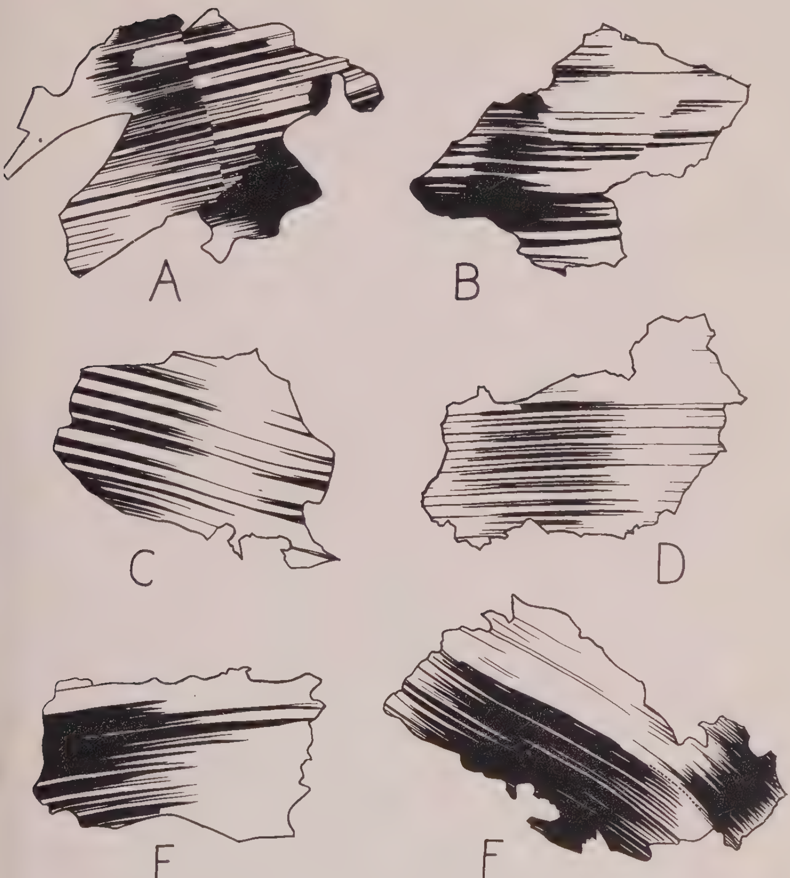

FIG. 2. Representative examples of glide twinning in plagioclase. Twinning postdates rack in A and B (right-hand side). Twinning in B-F shows clear genetic relationship to ending. A–D albite twinning. E pericline twinning. F combined Carlsbad-albite twinning.

A. Andesine (An_{41}) from garnet-bearing quartz dioritic gneiss, Whitechuck River, Washington. On lower right is separate small grain. Width of grain 2.5 mm.

B. Andesine from same specimen as A. Width of grain 2.6 mm.

C. Andesine (An_{33}) from quartz diorite near Entiat, Washington. Width of grain 0.7 mm.

D. Andesine (An_{37}) from quartz dioritic gneiss, Whitechuck River, Washington. Width of grain 1.9 mm.

E. Andesine (An_{39}) from same specimen as A. Width of grain 1.1 mm.

F. Andesine, oscillatory zoning with one recurrence (An_{38}-An_{46}). Same specimen as A. Width of grain 2.7 mm.

lamellae, as the result of the temporally more or less sporadic and random twin initiation (and termination) characteristic of growth twinning, typically vary widely among themselves both in width and continuity within a single crystal. Curiously, when both sets of glide lamellae are about equally developed it usually cannot be determined which set represents the original and which the twin orientation.

There is an interesting feature of some glide twinning which is not discussed in the literature, although occasionally figured there (*e.g.* the *a*-normal section shown in Emmons and Gates, 1943, p. 300, Pl. 1, Fig. 3). This is the development of so many secondary glide lamellae on one end of a plagioclase crystal that they essentially merge into one broad lamella, and the entire end of the crystal goes over into the new "twin" position. Figure 2 E of the present paper shows incipient development of this condition. With continued deformation such crystals may actually become "untwinned" in the sense that an earlier twinning is lost. These crystals, initially undeformed, become strained with simultaneous bending and development of glide lamellae. With further deformation the lamellae coalesce involving more and more of the crystal which finally becomes unstrained as the bending and secondary lamellae are eliminated and the twin orientation is assumed by the entire crystal. Characteristically associated with this process, as with glide twinning in general, are marked cataclastic and strain effects on adjacent crystals produced as room is made to accommodate the crystal in its new position. The general characteristics of primary and secondary lamellae, as determined from observation of a large number of twinned crystals, are compared in Table 1.

When the features described are abundant in a thin section and the twinning shows a general uniformity from crystal to crystal, it may be presumed that much, and perhaps most, of the plagioclase has undergone glide twinning. It is evident, of course, that not every random slice of a plagioclase crystal with glide twinning will show positive evidence for its origin. On the other hand, if secondary twinning in a rock is at all prominent, many other crystals will be diagnostic. Without strong evidence, it cannot be assumed that every crystal in such a section has undergone secondary twinning or that all the lamellae are secondary. The possible presence of an earlier generation of primary lamellae, or even of earlier secondary lamellae, should not be overlooked. Diligent examination will sometimes permit distinction of these two. It is anticipated that detailed analysis of the mechanism of twin gliding in plagioclase, a problem now largely untouched, will greatly extend the usefulness of the petrofabric field for the petrographer.

As judged by the criteria developed, glide twinning is much more common than primary polysynthetic twinning, and albite glide lamellae

are considerably more abundant than pericline glide lamellae. Primary lamellae are rarely developed except in euhedrally grown crystals which largely restricts them to igneous plagioclases, and even here later superimposed glide twinning is generally present and may obscure or eliminate all traces of the primary twinning. Glide twinning, by contrast, is very widespread in both igneous and metamorphic plagioclase.

Origin of glide twinning

In rocks which have otherwise experienced the same degree of deformation, the texture of the rock is believed to be a significant control of glide twinning. This became apparent from study of anhedrally zoned and unzoned metamorphic plagioclase from the Northern Cascades of Washington. Over 200 specimens of isochemical and metasomatic rocks were investigated. These rocks occur closely interlayered in a migmatitic terrane and clearly have both participated equally in post-crystalline deformation. The relatively coarse, irregularly bounded, interlocking plagioclase grains of the inequigranular feldspathized schists and metasomatic gneisses examined were found to exhibit abundant secondary glide lamellae. However, the finer-grained, more equant plagioclase in the isochemical schists and amphibolites studied showed distinctly fewer secondary lamellae and in many of these rocks was largely untwinned.

The differing textures of these contrasting rock types are thought to be responsible for the variable susceptibility to secondary twinning. Stress in the finer-grained isochemical rocks is taken up in rotation of the more or less round, equant plagioclase grains, while the large interlocking plagioclase grains which dominate the fabric of the metasomatic gneisses cannot escape strain in the form of crystal bending and concomitant twin gliding. The mechanical properties of the other minerals present appear to have played an important modifying role in determining the extent of twin gliding in the plagioclase. Minerals such as quartz and biotite when present in considerable amount tend to take up most of the strain leaving the tougher plagioclase relatively undeformed. Gorai, (1951, p. 891), notes that the frequency of twinned plagioclase varies directly with the grain size in the metamorphic rocks that he has studied. It is quite possible that his twinning is largely secondary and that the abundance of lamellae depends not so much on grain size but on the related factor of the degree to which the feldspar crystals are interlocking. Similar relationships may apply in the Adirondack paragneiss studied by Engel and Engel (1960, p. 14). In the finer-grained, relatively equigranular phases of this paragneiss the plagioclase shows only minor polysynthetic twinning, while it is abundantly twinned in the coarser-grained, more inequigranular varieties richer in plagioclase.

Many processes have been invoked to account for the stresses producing glide twinning. Deformation of the plagioclase by forces external to the rock as a whole is most often cited and clearly the most significant single process. Other suggested processes, some of rather dubious merit, may be mentioned briefly with no attempt at evaluation. These include differential contraction upon cooling of phenocrysts or interlocking grains (Alling, 1936, p. 157), stresses set up within crystals upon either heating or cooling (Baier, 1930, p. 480), stresses caused by mutual interference of grains during crystal growth (Taylor, Darbyshire, and Strunz, 1934, p. 494; Chapman, 1936, p. 42), and stresses set up by vesiculation of lava or by the flow of viscous magma or small crystals against phenocrysts (Emmons and Gates, 1943, p. 293 and p. 295). Volume increase of phenocrysts upon sudden decrease of confining pressure on a magma could also possibly lead to glide twinning. Finally, glide lamellae may probably form due to differential stresses set up by contraction during high-low inversion. These lamellae are the result of deformation of the crystal (by volume decrease) and involve mechanical displacement of the crystal within one set of lamellae. Such lamellae must not be confused with transformation twins which develop through small-scale atomic rearrangement. In consequence of its larger decrease in volume such inverted plagioclase should show a stronger development of glide lamellae due to contraction than either quenched plagioclase or plagioclase which has grown below its inversion.

Transformation twinning

The view that polysynthetic twinning in plagioclase may form through transformation, that is, inversion of the high-temperature to a low-temperature form, has wide currency. The mechanism of this twinning, however, is seldom clearly stated. Adhering to Buerger's definition (1945) of transformation twinning the twin configuration must arise through small-scale rearrangement of atoms during inversion. Glide twins, even though caused by stresses set up by inversion, do not meet this definition. Köhler and Raaz (1947, p. 169) envision twin formation through the inversion of a monoclinic or nearly monoclinic plagioclase to its present triclinic form. Buerger (1948, p. 120) notes that albite and anorthite have a common high-temperature form which may well be monoclinic and that both albite and pericline twinning may be related to inversion. Tuttle and Bowen (1950, p. 583) remark that the nature of the twinning should certainly be different when the crystals have grown below their inversion, as compared with that developed when they are inverted from the high-temperature modification. According to Buerger (1945, p. 481) the transformation from the monoclinic orthoclase struc-

ture to the triclinic albite structure requires only slight structural displacements in the order of magnitude of heat motion. If the postulated inversion involves, instead, the transformation of a more nearly monoclinic plagioclase to a plagioclase of lower symmetry, then the required structural displacements presumably would be still smaller.

It appears significant that none of the writers cited presents any evidence for transformation twinning in natural plagioclase. Muir (1955, p. 563) and other workers have produced extremely fine, secondary albite and pericline lamellae by heat-treatment of low- and intermediate-temperature plagioclase. This secondary twinning, however, is almost certainly glide twinning caused by stresses set up in the low-high inversion, and cannot be true transformation twinning which must develop on inversion of the high to the low form. Polysynthetic twinning does occur in synthetic plagioclase (Tuttle and Bowen, 1950, p. 574; Laves and Chaisson, 1950, p. 585), but it is by no means certain that this is not glide twinning.

It is especially significant that, although inversion of low-temperature plagioclase to the high-temperature form has been produced artifically in albite by heating above 700° C. (Tuttle and Bowen, 1950), attempts to produce the high-low transformation, much less to synthesize low-temperature albite, have been singularly unsuccessful. It remains problematical how far generalizations based on x-ray-determined structural changes produced on the heating of plagioclase can be carried over to presumed structural changes in the cooling of natural plagioclase, changes which are not reproducible in the laboratory. Thus, the question of whether plagioclase shows transformation twinning is closely tied to the larger question of whether inversion itself can be demonstrated to have occurred in the cooling of natural plagioclase, and, if so, what is the extent of the structural changes involved. The cleavage-zone relations described in the section on primary twinning have a direct bearing on this problem.

The best evidence for transformation twinning lies in the fact that inverted plagioclase should, in its morphology, preserve some "memory" of high-temperature origin (*c.f.* Tuttle and Bowen, 1950, p. 583). Since inversion presumably involves only slight structural displacement of atoms, the original "monoclinic" or "more nearly monoclinic" form should be preserved both by the zones and in the external morphology, just as the high-temperature symmetry is preserved in euhedral crystals of inverted high quartz. In inverted crystals these elements of original high-temperature symmetry will be contrasted with the present low-temperature structure and lower symmetry. These younger elements may be discovered by x-ray studies and more simply by cleavage which is

determined by the present structure. Thus, a-normal sections of zoned plagioclase which have undergone inversion should show a lack of parallelism of the (001) and (010) cleavages which represent the present structure, with regard to their respective zones and crystal faces which reflect the primary structure. Similarly, in a-normal sections with transformation twinning, euhedral zoning, the primary element, should pass undeflected across the twin lamellae. If natural high-low inversion of plagioclase and transformation twinning are to be demonstrated, the evidence must lie in relations of this kind.

Study of a large number of thin sections of normal volcanic and plutonic igneous rocks revealed more than 50 zoned plagioclase crystals which clearly cannot have undergone inversion in anything like the sense generally visualized. It will be recalled that a-normal sections of zoned crystals showed a sharp parallelism between both (001) and (010) cleavages and their respective zones (as well as crystal faces when such were present), even across albite and pericline lamellae (Fig. 1 A–D). These zones and faces are primary features and demonstrate that the crystal was triclinic when it grew. The cleavage, which expresses the internal structure of the crystal (after any presumed inversion), is equally triclinic. Since the zones and cleavages are sensibly parallel optically, the inference is clear that neither crystal symmetry nor structure have changed appreciably, but that instead the plagioclase crystallized initially in the same or very nearly the same triclinic form it now exhibits. The plagioclase either has not inverted at all, or the structural changes measured in terms of crystal morphology have been so slight as to be negligible. It is certainly clear that these plagioclases were never monoclinic. Since these crystals show no evidence of significant inversion, there is no reason to suppose that other plagioclase crystals in the same rocks have experienced any profound inversion either, and there is every reason to suspect they have not. However, quite apart from the problematical question of inversion and the magnitude of the structural changes involved, it is obvious that the described twin lamellae across which the zones are deflected cannot have formed by small-scale atomic rearrangement upon inversion and thus cannot be transformation twins.

The evidence against any marked structural change in inversion of the plagioclases studied appears significant, for the many igneous rocks examined comprise ordinary dacites, andesites, basalts, granodiorites, and quartz diorites and can in no way be considered abnormal. On the basis of occurrence, both high-temperature plagioclase (An_{30}–An_{60}) and low-temperature plagioclase (An_{15}–An_{55}), (Köhler, 1941), may be represented. If these plagioclases have not markedly inverted, one may wonder what

the general order of magnitude of structural change is in the inversion of natural plagioclase. In any case, we may reserve some skepticism for unsupported statements about transformation twinning and inversion in natural plagioclase.

It is necessary also to consder the unlikely proposition that inversion in plagioclase entails not merely slight structural displacement, but the large-scale rearrangement of a reconstructive transformation. Such a process could conceivably account for the relations observed between cleavage and crystal and zonal form. However, the volume of material displaced in producing twinning and altering the crystal symmetry in such a transformation would greatly exceed that associated with glide twinning and would, in fact, be so great as to amount to complete recrystallization. Primary zoning in the crystal could scarcely survive this redistribution, if anything, the plagioclase should tend to become homogeneous. In the crystals studied, however, the delicate zonal features are sharp and intact. As already discussed, many characteristics of the zoning are such as to preclude a secondary origin, and, in any case, secondary molecular redistribution would tend to eliminate, not create, zoning. For structural reasons, discussed by Goldsmith (1952, p. 289), diffusion within plagioclase on the scale required here is highly unlikely even where magmatic temperatures are long maintained. The slight importance of diffusion in plagioclase is empirically supported by the general presence of delicate oscillatory zoning in igneous plagioclase—commonly even in plutonic rocks where crystallization and cooling from high temperature are presumed to be slow. This indicates that reaction between melt and crystal by diffusion as visualized in Bowen's scheme (1913, p. 597) is seldom, if ever, more than imperfectly realized. (These same considerations militate against any mechanism of elimination zoning in alternate twin lamellae as has been reported by Emmons and Mann (1953). In the examination of many thousands of zoned, polysynthetically twinned plagioclases cut normal to the composition plane I have always found perfectly uniform zonal development in both sets of lamellae.) Finally, such inversion would often occur with the plagioclase embedded in a solid crystal medium, as in glomeroprophyritic aggregates or groups of coalescent plagioclase grains. The change in outer crystal form attendant to this kind of inversion should produce cataclastic and strain effects on adjacent crystals at least as extensive as those developed in glide twinning. Such features are not developed in the rocks studied.

Plagioclase Structure and Twinning

A discussion of the origin of polysynthetic twinning would be incomplete without considering the theory that the abundance of twin lamellae

varies as a function of plagioclase composition and thus is structurally controlled. The leading proponent of this idea is Donnay (1940 and 1943) who correlates the frequency of lamellae with crystallographic "obliquity" which varies with the degree of triclinicity, itself a function of plagioclase structure and composition. More recently Gay (1956) and Smith (1958) have extended Donnay's theory to include structural differences between the high- and low-temperature plagioclase series and to include metamorphic plagioclase. While these workers do consider some environmental factors in twinning, a dominant role is ascribed to internal, structural controls. In support of the structural control theory the generalizations of a number of petrographers are cited as to the variation of lamellar width with plagioclase composition. These generalizations are believed to conform to the predictions of the theory.

The evidence for the structural control theory fails in many ways to be compelling. No physicochemical basis has been given to explain why "obliquity" should be the major control of lamellar width. My own experience has not revealed the systematic regularity in lamellar width with composition which the other investigators have apparently seen. Exceptions to their generalizations are, in fact, so common as to bring the theory strongly in question. In addition, the generalizations are in many ways vague and say nothing on such critical matters as the relation of lamellar width to grain size without which lamellar frequency has little meaning. Most important of all, however, the structural control theory has entirely ignored the genesis of the twinning. To the present writer it appears that the major features of both primary twinning and glide twinning can be explained largely or entirely in terms of the genetic factors already discussed without appealing to structure.

In plagioclase with primary twinning, for instance, not only lamellar width, but lamellar form, and the very presence or absence of twinning appear adequately explained in terms of environmental factors alone. Primary twinning in the material studied failed to disclose any systematic variations in lamellar frequency which could conceivably be related to a compositional-structural control. In the igneous plagioclase studied, the width of the primary lamellae tends always to be large relative to grain size, without regard for composition. Far from reflecting uniform structure for all these plagioclases, this simply indicates that conditions of igneous crystallization do not generally favor development of numerous lamellae. This relation throws considerable doubt on the structural control theory with regard to the formation of primary lamellae. Because these conclusions are based on limited data, they must remain tentative and will require further investigation. It is significant, however, that a structural control finds no support in the primary twinning studied.

The structural control theory appears to rest on equally weak foundations as related to glide twinning. This is significant since glide twinning is by far the commonest type of twinning in plagioclase, and most of the twinning cited in support of the structural control theory is presumably of this origin. It is clear that any plagioclase regardless of composition, structure, or the presence or absence of earlier twinning, will develop glide lamellae if sufficiently stressed. In such material the width of the lamellae developed must depend largely upon the intensity of the stress applied and the distribution of this stress in the crystal, not upon plagioclase structure. The fact that metamorphic plagioclases which differ little among themselves structurally vary greatly in frequency of twinning and lamellar width (see above) serves to emphasize the importance of rock texture and deformation and to minimize the role of plagioclase structure as controls of glide twinning. Structural factors are, of course, indirectly involved in the formation of glide lamellae through contraction during cooling or inversion, inasmuch as they determine the magnitude of the stresses set up. The structural control here, however, is an entirely different thing than Donnay's "obliquity" factor.

The status of the structural control theory must remain uncertain until all factors, both structural and environmental, which bear on the origin of the twinning and on lamellar width can be evaluated for the data cited in support of the theory. It will also be necessary to conclusively establish the structure of the plagioclase at the time of twinning, a task which is certain to involve formidable problems. Eventually it may be possible to divorce the structural effects postulated by Donnay and his followers from the many other factors which determine lamellar width and to determine the relative importance of these controls. To date, however, this has not been done, nor can it be done with the incomplete and fragmentary data available.

Acknowledgments

The research for this paper was done largely under a National Science Foundation post-doctoral grant, and the writing under a summer grant of the Graduate School of the University of Washington. The illustrations were drafted by Phyllis Wood to whom the writer is greatly indebted. Thanks are extended to faculty members and graduate students of the University of Washington, Department of Geology, for generous permission to examine material from their petrographic collections. In particular the writer thanks G. E. Goodspeed, H. A. Coombs, P. Misch, and J. Hoover Mackin for critical reading and discussion of the manuscript and for many valuable suggestions. Finally, I must express my indebtedness to R. C. Emmons and to the late A. Köhler whose stimulating

work on the plagioclases, more than anything else, led to the writing of this article.

References

Alling, H. L., 1936, Interpretative petrology of the igneous rocks: McGraw-Hill Book Co., New York and London, 353 p.

Baier, E., 1930, Lamellenbau und Entmischungsstruktur der Feldspate: *Zeits. Krist.*, **73**, 465–560.

Barber, C. T., 1936, The Tertiary igneous rocks of the Pakokku district, Burma, with special reference to determination of feldspars by the Federow method: *Geol. Survey India Mem.* **68**, pt. 2, esp. p. 221–281.

Bowen, N. L., 1913, Melting phenomena in the plagioclase feldspars: *Am. Jour. Sci.*, **35**, 577–599.

Buerger, M. J., 1945, The genesis of twin crystals: *Am. Mineral.*, **30**, 469–482.

———, 1948, The role of temperature in mineralogy: *Am. Mineral.*, **33**, 101–121.

Chapman, W. M., 1936, Feldspar twinning in a differentiated sill: *Am. Mineral.*, **21**, 33–47.

Chudoba, K., 1931, Über die Feldspate der Sanidinite aus dem Laacher Seegebeit: *Neues Jahrb., Beilage-Bd.* **64**, *Abt. A.*, p. 443–475.

Colomba, L., 1908, Sulla supposta esistenza di lamelle secondarie di geminazione nei feldispate plagioclasici: *Boll. Soc. Geol. Italia*, **27**, 540–546.

Donnay, J. H. D., 1940, Width of albite-twinning lamellae: *Am. Mineral.*, **25**, 578–586.

———, 1943, Plagioclase twinning: *Geol. Soc. America Bull.*, **54**, 1645–1651.

Eitel, W., 1958, Structural conversions in crystalline systems: *Geol. Soc. America Special Paper* **66**, 183 p.

Emmons, R. C. and Gates, R. M., 1943, Plagioclase twinning: *Geol. Soc. America Bull.*, **54**, 287–304.

——— and Mann, V., 1953, A twin-zone relationship in plagioclase feldspar: *Geol. Soc. America Mem.* **52**, 41–54.

Engel, A. E. J., and Engel, C. G., 1960, Progressive metamorphism and granitization of the major paragneiss, northwest Adirondack Mountains, New York, Part II, Mineralogy: *Geol. Soc. America Bull.* **71**, 1–57.

Fedorow, E., 1899, Biegungsaxe der Feldspathe: *Min. Pet. Mitt.*, **18**, 360–366.

Gay, P., 1956, A note on albite twinning in plagioclase feldspars: *Min. Mag.*, **31**, 301–304.

Goldsmith, J. R., 1952, Diffusion in plagioclase feldspars: *Jour. Geology*, **60**, 288–291.

Gorai, M., 1951, Petrological studies of plagioclase twins: *Am. Mineral.* **36**, 884–901.

Harker, A., 1939, Metamorphism: 2nd edition, Methuen, London, 362 p.

Harloff, C., 1927, Zonal structure in plagioclases: *Leidsche Geol. Medeleel.*, **2**, 100–113.

Hills, E. S., 1936, Reverse and oscillatory zoning in plagioclase feldspars: *Geol. Mag.*, **73**, 49–56.

Judd, J. W., 1887, The theory of schillerization, etc.: *Min. Mag.*, **7**, 81–92.

Köhler, A., Die Abhängigkeit der Plagioklasoptik vom vorangegangenen Wärmeverhalten: *Min. Pet. Mitt.*, **53**, 24–29.

———, 1948, Erscheinungen an Feldspaten in ihrer Bedeutung für die Klärung der Gesteinsgenesis: *Min. Pet. Mitt.*, **1**, 51–67.

———, 1949, Recent results of investigations of the feldspars: *Jour. Geol.*, **57**, 592–599.

——— , and Raaz, F., 1947, Gedänken über die Bildung von Feldspatzwillingen in Gesteinen: *Geol. Bundesanstalt Verh.*, 163–171.

Laves, F., and Chaisson, U., 1950, An X-ray investigation of the high-low albite relations: *Jour. Geol.*, **58**, 584–592.

MÜGGE, O., AND HEIDE, F., 1931, Einfache Schiebung am Anorthit: *Neues Jahrb., Beilage-Bd.* **64,** *Abt. A.*, 161–170.

MUIR, I. D., 1955, Transitional optics of andesine and labradorite: *Min. Mag.*, **30,** 145–168.

PADUROW, N. W., 1949, Vizinalen und Vizinaloiden: *Neues Jahrb., Bd.* **80,** *Abt. A.*, 209–262.

PHEMISTER, J., 1934, Zoning in plagioclase feldspar: *Min. Mag.*, **23,** p. 541–555.

ROSS, J. V., 1957, Combination twinning in plagioclase feldspars: *Am. Jour. Sci.*, **255,** 650–655.

SMITH, J. V., 1958, The effect of temperature, structural state and composition on albite, pericline and acline-A twins of plagioclase feldspars: *Am. Mineral.*, **43,** 546–551.

TAYLOR, W. H., DARBYSHIRE, J. A., AND STRUNZ, H., 1934, An X-ray examination of the feldspars: *Zeit. Krist.*, **87,** 464–498.

TURNER, F. J., 1951, Observations on twinning of plagioclase in metamorphic rocks: *Am. Mineral.*, **36,** 581–589.

TUTTLE, O. F., AND BOWEN, N. L., 1950, High temperature albite and contiguous feldspars: *Jour. Geol.*, **58,** 572–583.

VANCE, J. A., 1957, Coalescent growth of plagioclase grains in igneous rocks: (Abs.) *Geol. Soc. America Bull.*, **68,** 1849.

VAN WERVEKE, L., 1883, Eigenthümliche Zwilligsbildung an Feldspat und Diallag: *Neues Jahrb., Bd.* **2,** 97–101.

Manuscript received November 30, 1960.

CATION SIEVE PROPERTIES OF THE OPEN ZEOLITES CHABAZITE, MORDENITE, ERIONITE AND CLINOPTILOLITE

L. L. Ames, Jr., *General Electric Company, Richland, Washington.*

Abstract

The partial cation sieve properties of the "open" zeolites chabazite, mordenite, erionite and clinoptilolite were studied in an effort to determine the mechanism responsible for the type and intensity of the observed cation replacement series. It was found that neither the hydration state of the cations before entering the zeolite structure nor relative loading rates had any significant effect on the type or intensity of alkali metal or alkaline earth metal cation replacement series. Molten salt experiments with Cs_{137}-containing zeolites demonstrated that at higher temperatures the normal hydrated type replacement series could be reversed to a coulombic replacement series without destruction of the alumino-silicate framework. The above results were interpreted as being caused by the presence or absence of structural water. Additional stereochemical studies are necessary to determine the details of the mechanism.

Introduction

There are at least three mechanisms responsible for the cation sieve properties exhibited by natural zeolites. One such mechanism is the positive exclusion of certain cations due to the inability of these larger cations to enter the zeolite lattice in significant amounts. The sieve effect shown by analcite for Cs^+ is an example of such an exclusion based on cation size (Barrer, 1950).

A second mechanism for a cation sieve effect is the inability of the negative charge distribution on the zeolite structure to accommodate a given cation. An example of this mechanism is given in the difficulty of obtaining calcium or barium-rich analcites (Barrer, 1950) or sodium-rich heulandites (Mumpton, 1960) by cation exchange. Determination of a third mechanism constitutes the object of this paper. Only the so-called "open" zeolites, or those zeolites that can accept any of the alkali metal or alkaline earth metal cations, will concern us here. Examples of such zeolites are chabazite, mordenite, erionite and clinoptilolite. Knowledge of the mechanism that causes the cation sieve effects shown by these open zeolites may also assist in understanding the extreme cation selectivity of clinoptilolite.

To ascertain the cause or causes of the partial cation sieve action, the exchange kinetics of chabazite, mordenite and erionite were investigated. The cation sieve effects shown by clinoptilolite were reported previously (Ames, 1960).

Previous Work

Barrer has done the bulk of the research on cation exchange properties of zeolites. General references concerning the cation exchange properties

of chabazite and mordenite include Barrer (1948, 1950), Barrer and Gammon (1955), and Barrer and Brook (1953). Dent and Smith (1958) reported on the crystal structure of chabazite. Barrer (1950) discussed the hydration factor in cation exchange in relation to ease of entry of the cation into the zeolite crystal, and mentioned that replacement order was the same from melts and aqueous solutions. Barrer (1958) also pointed out the unsolved problem of cation selectivity shown by the "open" zeolites that theoretically can accept all cations of the alkali metal and alkaline earth metal series. This same reference also reported the replacement series $Ba^{+2} > Sr^{+2} > Ca^{+2} > Mg^{+2}$ for near sodium-based faujasite. Barrer and Raitt (1954) reported the replacement series $Li^{+} > Na^{+} > K^{+} > Rb^{+} > Cs^{+}$ and $Mg^{+2} > Ca^{+2} > Ba^{+2}$ for silver-based ultramarine. Barrer and Falconer (1956) reported the replacement series $Na^{+} > K^{+} > Rb^{+} > Cs^{+}$ for silver-based cancrinite. Milligan and Weiser (1937) reported the dehydration characteristics of chabazite and several other zeolites.

Methods of Investigation

The exchange kinetics of chabazite, mordenite and erionite were investigated using methods previously described (Ames, 1960). Figure 1 is a diagram of the experimental apparatus used to determine cesium diffusion rates in sodium-based clinoptilolite and erionite particles and the effect of sodium on their cesium loading rates.

A half-gram sample of zeolite was placed into a coarse fritted glass

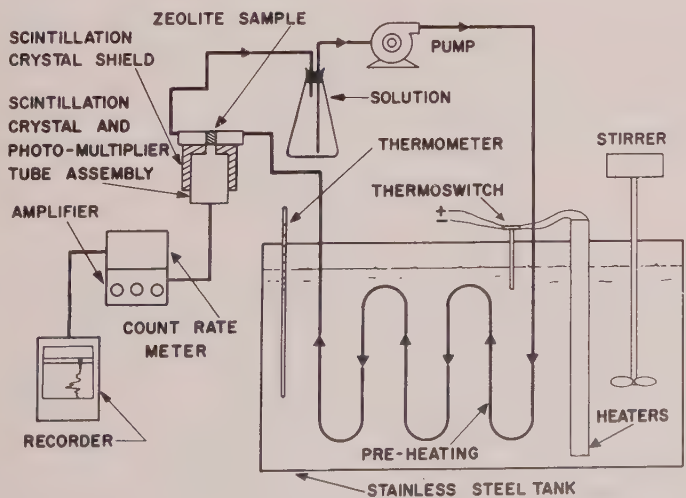

FIG. 1. Experimental apparatus used to obtain zeolite loading curves.

filter tube and held in position with Pyrex wool. This tube was then clamped in position over the top of the opening in the lead-lined crystal shield, connected onto the influent and effluent lines, and the pump started to circulate the solution through the zeolite sample at 7000 ml per hour. In addition to being 0.2 *M* CsCl, this influent solution contained sufficient Cs^{137} to allow full cesium loading of the one-half gram zeolite sample while removing less than two per cent of the Cs^{137} from solution. This solution was allowed to circulate through the zeolite overnight to obtain an equilibrium cesium capacity. Since these zeolites reached greater than 90 per cent capacity in 15 to 20 minutes, the assumption that equilibrium was reached in 10 to 15 hours is a valid one.

The count rate meter was adjusted to assure that equilibrium was reached for the highest capacity zeolite while the recorder remained on-scale The apparatus was checked frequently with a standard Cs^{137} source to insure that the recorder returned to the same relative position between experiments. Knowing the amount of CsCl corresponding to a given Cs^{137} count, the loading curves per half gram of zeolite could be compared.

To study the diffusion of a cation pair within the zeolite particle or grain, three conditions are assumed to prevail: (1) that within the limits of experimental error (plus or minus two per cent), the concentration of the radioactivity in the influent equals that in the effluent, and that this condition does not change with increases in flow rate or concentration of exchanging cation, (2) that the zeolite particles are spherical and of known radius or surface area, and (3) that the specific diffusion rates of each cation of the pair are the same, a condition that is strictly valid only in the case of the exchange of one isotope for that of another isotope of the same element (Helfferich and Plesset, 1958). Boyd, *et al.* (1947) showed that the following expression should hold, given the above conditions,

$$F = \frac{Q_t}{Q_\infty} = 1 - \frac{6}{\pi^2} \sum_{n=1}^{\infty} \frac{e^{-n^2 Bt}}{n^2}$$

where

F = the fractional approach to equilibrium loading,

$B = \dfrac{\pi^2 D_i}{r^2}$ = a specific reaction rate,

where

D_i = effective diffusion coefficient,

Q_t = particle loading at time t,

Q_∞ = particle loading at time infinity, and

r = particle radius.

Reichenberg (1953) published values of Bt for corresponding F values. Plotting Bt vs. t yields a straight line of slope B. From B, the effective diffusion coefficient D_i may be computed. Given values of B at two different temperatures, the Arrhenius activation energy Ea, can be calculated from the modified Arrhenius equation,

$$\ln \frac{k_2}{k_1} = \frac{Ea(T_2 - T_1)}{RT_2T_1} \quad \text{(Daniels and Alberty, 1955),}$$

where

k_1 = a specific reaction rate at T_1,
k_2 = a specific reaction rate at T_2 and
R = the gas constant.

The effect of higher temperatures on the Cs^{137} distribution between zeolites and anhydrous melts was studied utilizing $LiNO_3$ and KNO_3.

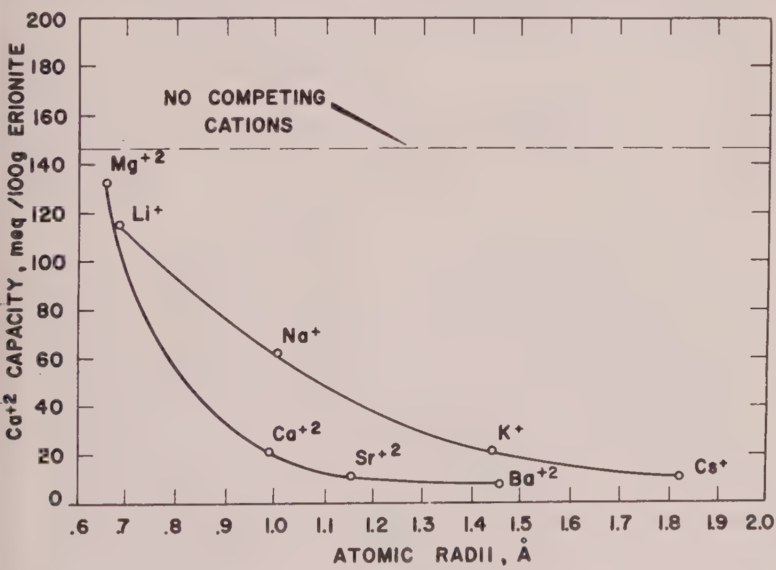

FIG. 2. The effect of competing cations on the calcium capacity of erionite. The point for calcium was obtained by adding sufficient Ca^{+2} to the original $0.01N$ Ca^{+2} to total $0.06N$ Ca^{+2} and computing the final 50 per cent breakthrough capacity on the basis of $0.01N$ Ca^{+2}. A similar procedure was followed when Cs^{137} rather than Ca^{45} was used as the tracing radioisotope.

Common influent solution	$0.05N$ competing cations as indicated, $0.01N$ Ca^{+2}, 10,000 Ca^{45} d/m/ml.
Common temperature	25° C.
Common influent pH	7.0
Common flow rate	473 ml./cm.²/hr.
Common column	25 g., 0.25 to 1.0 mm., sodium-based erionite

Initially, ten grams of the zeolite (1.0 mm. diameter grain size) were saturated with 0.01 M CsCl plus 5.0×10^{-8} M Cs^{137}, washed thoroughly with several volumes of distilled water, and dried at 105° C. One gram of this material was then placed in a platinum crucible with four grams of $LiNO_3$ or KNO_3 respectively. These crucibles were placed in a furnace for at least 24 hours at within plus or minus five degrees of the desired temperature. Upon termination of the experiment, a small portion of the molten salt was separated from the 1.0 mm. zeolite by decantation onto a cold, clean surface. This salt bead was then immediately weighed, dis-

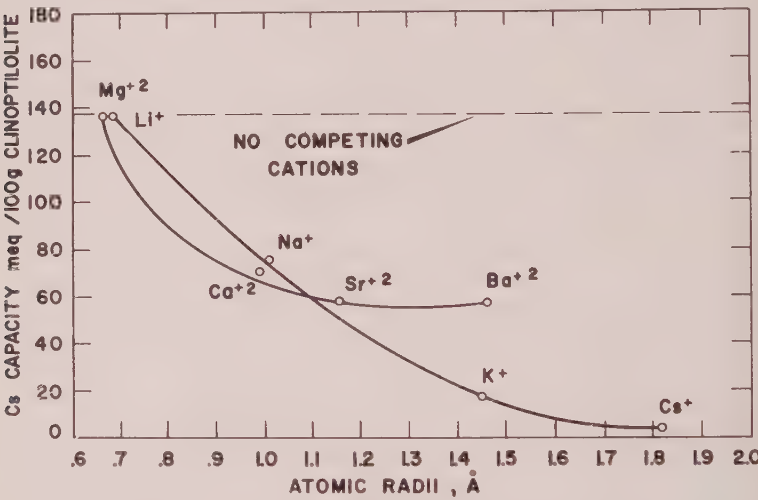

FIG. 3. The effect of competing cations on the cesium capacity of clinoptilolite.

Common influent solution	1.0N competing cations as indicated, 0.01N Cs^+, $1.74\times10^{-8}N$ Cs^{137}
Common temperature	25° C.
Common influent pH	5.0
Common flow rate	294 ml./cm.^{2}/hr.
Common column	50 g., 0.25 to 1.0 mm., sodium-based clinoptilolite.

solved in a known volume of water and counted for Cs^{137} on a gamma spectrometer. These results were reported as Cs^{137} per gram of $LiNO_3$ or KNO_3 after correction for salt volatility at that temperature and length of heating time. The procedure followed in studies with Na^{22} was similar to that for Cs^{137} except the zeolites were saturated with 0.01 M $NaNO_3$ plus 12.0×10^{-8} M Na^{22} after initial rinse with 3.0 M $CaCl_2$ solution. The zeolite samples were then washed from the remaining salt in the platinum crucible and an x-ray diffraction pattern obtained to be certain that the zeolite had remained structurally intact.

The clinoptilolite used in this study was obtained from the National Lead Company's Hector, California, deposits. The erionite was from Nevada, and the chabazite and mordenite were obtained from Ward's Natural Science Establishment. Both the mordenite and chabazite were originally from Nova Scotia. The purity of the erionite and clinoptilolite, as closely as could be ascertained, varied from 85 to 90 per cent. The chabazite and mordenite were hand-picked to greater than 95 per cent purity.

Results

Figures 2, 3, 4 and 5 show the cesium capacities of erionite, clinoptilolite, mordenite and chabazite respectively, plotted vs. the atomic radii of

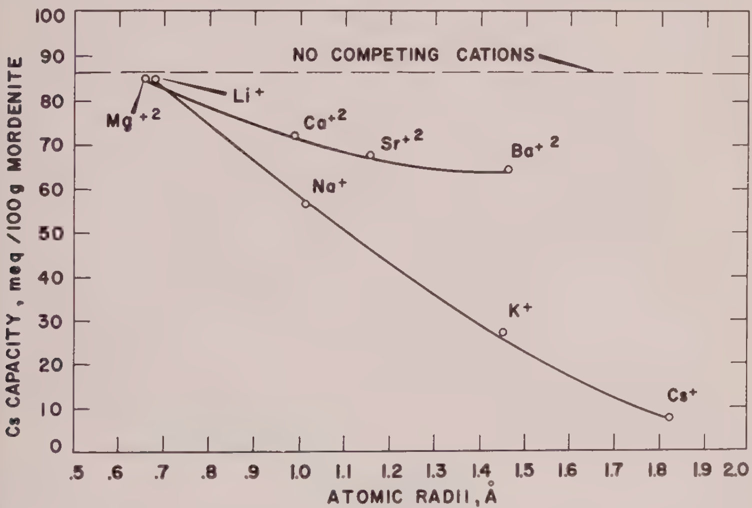

Fig. 4. The effect of competing cations on the cesium capacity of mordenite.

Common influent solution	0 01N competing cations as indicated, 0.01N Cs^+, 1.74×10^{-8}N Cs^{137}
Common temperature	25° C.
Common influent pH	7.0
Common flow rate	473 ml./cm.^{2}/hr.
Common column	50 g., 0.25 to 1.0 mm., sodium-based mordenite.

competing cations according to Green (1959). Two aspects of these data are noteworthy; first, the replacement series of all these open zeolites are quite similar, and second, the cation selectivities of these zeolites are highlighted by varying the amounts of competing cations from one to one hundred times the concentration of cesium.

Cesium loading curves were obtained both with and without the addi-

tion of competing sodium, utilizing the apparatus shown in Fig. 1. Figure 6 gives cesium loading curves for clinoptilolite with sodium concentrations of 0, 5, and 10 times that of cesium. Figure 7 represents comparable information for erionite. The curves of Figs. 6 and 7 cannot be used to compute specific reaction rates because the fractions of loading are not indicated. Figures 6 and 7 are useful, however, in showing that clino-

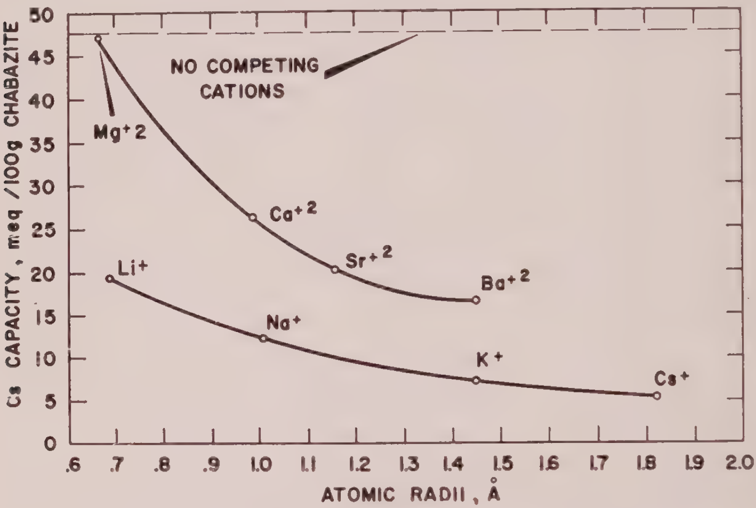

FIG. 5. The effect of competing cations on the cesium capacity of chabazite.

Common influent solution	0.01N competing cations as indicated, 0.01N Cs^+, $1.74\times10^{-8}N$ Cs^{137}
Common temperature	25° C.
Common influent pH	7.0
Common flow rate	473 ml./cm.²/hr.
Common column	50 g., 0.25 to 1.0 mm., sodium-based chabazite.

ptilolite tends to maintain a given cesium distribution between zeolite and solution despite an increasing sodium concentration.

Curves indicating fraction of loading may be used to compute specific reaction rates and diffusion coefficients for the cation exchange $Na^+ \rightleftharpoons Cs^+$. The specific reaction rates are determined from loading fraction values by plotting corresponding Bt values vs. t. The diffusion coefficients computed from the specific reaction rates are given in Table I. Differences in the cation selectivities between erionite and clinoptilolite are not caused by differences in diffusion coefficients.

For comparative purposes, most organic cation exchange resins yield D_i values of about 1×10^{-5} cm.²/sec., essentially aqueous diffusion (Boyd, Adamson and Myers, 1947). Diffusion through a solid would yield a

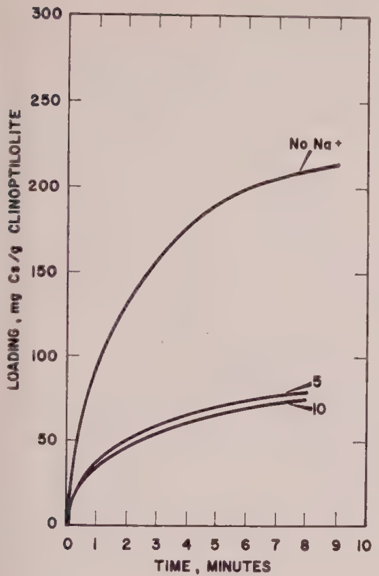

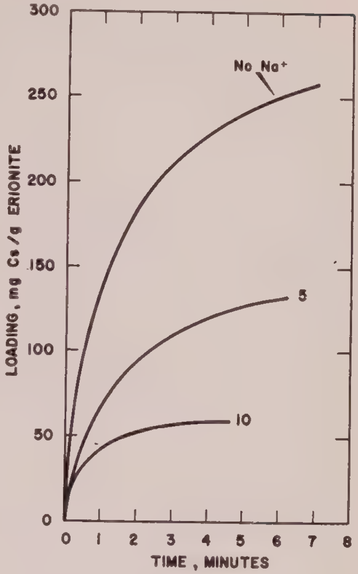

FIG. 6 (left). Cesium loading curves for clinoptilolite.

Common influent solution	$0.2N$ Cs^+, sodium to cesium concentration ratios as indicated $5.0\times10^{-8}N$ Cs^{137}.
Common temperature	25° C.
Common flow rate	7000 ml./cm.²/hr.
Common influent pH	7.0
Common column	0.5 g., 0.0134 cm. avg. diam., sodium-based clinoptilolite.

FIG. 7 (right). Cesium loading curves for erionite.

Common influent solution	$0.2N$ Cs^+, sodium to cesium concentration ratios as indicated, $5.0\times10^{-8}N$ Cs^{137}
Common temperature	25° C.
Common flow rate	7000 ml./cm.²/hr.
Common influent pH	7.0
Common column	0.5 g., 0.0134 cm. avg. diam., sodium-based erionite.

TABLE I. KINETICS OF THE EXCHANGE SYSTEM $Na^+ \rightleftharpoons Cs^+$ IN CLINOPTILOLITE AND ERIONITE

Zeolite	Temperature ° C.	B, sec.$^{-1}$	D_i, cm.²/sec.	Ea Kcal/mole
Erionite	25	3.3×10^{-2}	1.55×10^{-7}	
Erionite	50	4.4×10^{-2}	2.06×10^{-7}	2.2
Clinoptilolite	25	3.5×10^{-2}	1.66×10^{-7}	
Clinoptilolite	50	6.6×10^{-2}	3.07×10^{-7}	4.7

D_i of 1×10^{-11} or less (Barrer, 1958). Barrer (1958) also reported very small ΔH values for the open zeolite chabazite.

The cation exchange characteristics of the open zeolites in fused salt solutions were studied. Table II gives a portion of the results of the molten salt experiments.

It is quite likely that equilibrium was not attained in any of the examples given in Table II because ionic migration is relatively slow through fused salts. However, there was apparently little difference in the total amount of Cs^{137} displaced in one day or five days of contact time.

TABLE II. THE EFFECT OF TEMPERATURE ON CESIUM AND SODIUM DISTRIBUTIONS IN MORDENITE, ERIONITE AND CLINOPTILOLITE

Zeolite	Salt	Temperature ° C.	Counts/min/g salt	Distribution ratio, $\frac{LiNO_3}{KNO_3}$	Contact time hours
			Cs^{137}		
Mordenite	$LiNO_3$	350	7,377		40
Mordenite	KNO_3	350	10,540	0.70	40
Mordenite	$LiNO_3$	460	16,723		25
Mordenite	KNO_3	460	8,928	1.87	25
Erionite	$LiNO_3$	360	37,678		24
Erionite	KNO_3	360	81,029	0.47	24
Erionite	$LiNO_3$	460	108,232		24
Erionite	KNO_3	460	81,174	1.33	24
Clinoptilolite	$LiNO_3$	340	31,165		130
Clinoptilolite	KNO_3	340	30,488	1.02	130
Clinoptilolite	$LiNO_3$	360	42,689		65
Clinoptilolite	KNO_3	360	33,449	1.28	65
			Na^{22}		
Erionite	$LiNO_3$	345	9,320		24
Erionite	KNO_3	345	13,994	0.67	24
Erionite	$LiNO_3$	420	11,125		24
Erionite	KNO_3	420	7,539	1.48	24
Clinoptilolite	$LiNO_3$	345	4,815		24
Clinoptilolite	KNO_3	345	4,383	1.10	24
Clinoptilolite	$LiNO_3$	420	6,213		24
Clinoptilolite	KNO_3	420	3,588	1.73	24

Note the reversal of the cesium replacement series with rising temperature by lithium and potassium respectively. The melting point of 334° C. for KNO_3 prevented experiments at temperatures lower than 340° C., since results on the Cs^{137} displaced by Li^+ alone would be meaningless.

Conclusions

The replacement series $Cs^+ > K^+ > Na^+ > Li^+$ and $Ba^{+2} > Sr^{+2} > Ca^{+2} > Mg^{+2}$ of Figures 2, 3, 4 and 5 are typical of hydrated series where the affinity of a given cation for a polar molecule such as water is directly proportional to its field strength (Grimm, 1953). It is unlikely, however, that Li^+ is entering the zeolite while surrounded with 10 to 15 molecules of water. The dimensions of most of the openings for chabazite, erionite and mordenite are known with some degree of accuracy (Barrer and Kerr, 1959), and would not permit the entry of such a 10 angstrom hydrated cation as Li^+. The structure of clinoptilolite is largely unknown so that no statement can be made concerning its channel dimensions except to say that they are greater than the diameter of Cs^+.

If cation hydration state before entering the zeolite resulted in a hydrated type replacement series, then cation exchange from an anhydrous molten salt should yield a normal coulombic replacement series under all circumstances. The results of Table II show that, except for clinoptilolite, it was still possible to obtain a hydrated type of replacement series at 340° C. Further evidence that the hydration state of the entering cation does not significantly affect the type of replacement series is seen in the reported replacement series for anhydrous feldspathoids (Barrer and Raitt, 1954, and Barrer and Falconer, 1956). Normal coulombic replacement series prevailed at low temperatures with the feldspathoids.

Thus cationic hydration state before entry into the zeolite was not a significant causal factor, but the hydrated type replacement series at low temperatures remained to be explained. The data of Table II at the higher temperatures suggested that the hydrated series was a function of the structural water rather than external water. At higher temperatures the molten salt-zeolite experiments yielded a coulombic type replacement series, suggesting that the partial cation sieve properties of open zeolites are a result of interactions between the presence or absence of structural water and cations of the alkali metal and alkaline earth replacement series (Taylor, 1934). The enhanced cation selectivity of clinoptilolite is probably due to unusually favorable steric factors involving the exchanging cations, the exchange sites and structural water. The results of the molten salt-clinoptilolite experiments shown in Table II, and the D.T.A. pattern of clinoptilolite given by Mumpton (1960),

suggest that the structural water of clinoptilolite is not as firmly bonded to the aluminosilicate framework as is water to the other, less cation-selective, open zeolites. At least part of the structural water of clinoptilolite is relatively loosely held and free to exert a more intense sieving effect on the cations entering the aluminosilicate framework.

A high field strength cation such as Li^+ would tend to block its own diffusion path to an exchange site and to approach exchange sites less closely in clinoptilolite than the same cation in an open zeolite in which the structural waters are more firmly bonded to the aluminosilicate framework. A low field strength cation such as Cs^+ is relatively free to migrate and becomes fixed on an exchange site more readily under the same circumstances. Removal of most of the structural water would, of course, tend to favor the high field strength cation. Thus a situation normally present in these open zeolites is intensified in the case of clinoptilolite.

Understanding of the details of the mechanism awaits determination of steric relationships between structural water and exchangeable cations in clinoptilolite, along with more detailed structural work on the other open zeolites. Such an understanding could lead to the synthesis of zeolites with even more intense cation selectivities.

Acknowledgments

The author wishes to acknowledge the able assistance and helpful suggestions of Mrs. Olevia C. Sterner in the laboratory work. The samples of erionite were collected by Dr. Richard H. Olson of the Nevada State Bureau of Mines at Reno, Nevada.

References

Ames, Jr., L. L. (1960), Cation sieve properties of clinoptilolite. *Am. Mineral.*, **45**, 689-700.

Barrer, R. M. (1958), Crystalline ion exchangers. *Jour. Chem. Soc. London*, 99–112.

Barrer, R. M. (1950), Ion-exchange and ion-sieve processes in crystalline zeolites. *Jour. Chem. Soc. London*, 2342–2350.

Barrer, R. M. (1948), Syntheses and reactions of mordenite. *Jour. Chem. Soc. London*, 2158–2163.

Barrer, R. M. and Brook, D. W. (1953), Molecular diffusion in chabazite, mordenite and levynite. *Trans. Farad. Soc.*, **49**, 1049–1059.

Barrer, R. M. and Falconer, J. D. (1956), Ion exchange in feldspathoids as a solid state reaction. *Proc. Royal Soc.*, **A236**, 227–249.

Barrer, R. M. and Kerr, I. S. (1959), Intracrystalline channels in levynite and some related zeolites. *Trans. Farad. Soc.*, **55**, 1915–1923.

Barrer, R. M. and Raitt, J. S. (1954), Ion exchange in ultramarine. *Jour. Chem. Soc. London*, 4641–4651.

Barrer, R. M. and Sammon, D. C. (1955), Exchange equilibria in crystals of chabazite. *Jour. Chem. Soc. London*, 2838–2849.

BOYD, G. E., ADAMSON, A. W. AND MYERS, L. S., JR. (1947), The exchange adsorption of ions from aqueous solutions by organic zeolites. II. Kinetics. *Jour. Am. Chem. Soc.*, **69,** 2836–2848.

DANIELS, F. AND ALBERTY, R. A. (1955), Physical Chemistry. J. Wiley and Sons, *2nd. Edition*, 315–320.

DENT, L. S. AND SMITH, J. V. (1958), Crystal structure of chabazite, a molecular sieve. *Nature*, **181,** 1794–1796.

GLASSTONE, S. (1946), Textbook of physical chemistry. D. Van Nostrand and Co., *2nd. Edition*, 828–830.

GREEN, J. (1959), Geochemical table of the elements for 1959. *Geol. Soc. Am. Bull.*, **70,** 1127–1183.

GRIM, R. E. (1953), Clay mineralogy. McGraw-Hill Book Co.. N. Y., 146–149.

HELFFERICH, F. AND PLESSET, M. S. (1958), Ion exchange kinetics. A non-linear diffusion problem. *Jour. Chem. Phys.*, **28,** 418–424.

KRESSMAN, T. R. E. AND KITCHENER, J. A. (1949), Cation exchange with a synthetic phenolsulphonate resin. *Farad. Soc. Discussions*, **7,** 90–114.

MILLIGAN, W. O. AND WEISER, H. B. (1937), The mechanism of the dehydration of zeolites. *Jour. Phys. Chem.*, **41,** 1029–1040.

MUMPTON, F. A. (1960), Clinoptilolite redefined. *Am. Mineral.*, **45,** 351–361.

REICHENBERG, D. (1953), Properties of ion-exchange resins in relation to their stıucture. III. Kinetics of exchange. *Jour. Am. Chem. Soc.*, **75,** 589–597.

TAYLOR, W. H. (1934), The nature and properties of aluminosilicate framework structures. *Proc. Royal Soc.*, **A145,** 80–103.

Manuscript received January 26, 1961.

THE AMERICAN MINERALOGIST, VOL. 46, SEPTEMBER-OCTOBER, 1961

ISOTOPIC ANALYSES OF SINGLE GALENA CRYSTALS: A CLUE TO HISTORY OF DEPOSITION

CARL F. AUSTIN, *New Mexico Bureau of Mines and Mineral Resources,*

AND

WILLIAM F. SLAWSON, *Geophysics Laboratory, University of Toronto.*

ABSTRACT

A detailed study of lead isotopes has been undertaken in order to evaluate variations in the isotopic composition of lead with respect to the geologic environment of a single lead deposit.

INTRODUCTION

For the purpose of this investigation a lead deposit was desired in which the number of geologic variables would be at a minimum, and which would be well exposed by mine-development workings. The Blanchard Property mine, located in the Hansonburg mining district of Socorro County, New Mexico, was selected for study. Numerous development adits have been driven into the galena-fluorite-barite ore body of the Blanchard Property mine. These adits are nearly at right angles to a number of subparallel, steeply dipping, mineralized fractures. The Number 1 entry was selected for the first detailed studies. Figure 1 presents a section of the Number 1 entry.

The mineral deposit chosen for this study is typical of the Hansonburg mining district and consists of galena, fluorite, and barite, with minor pyrite, chalcopyrite, and light yellow brown sphalerite. The principal gangue mineral is quartz. Not only is the limestone host rock intensely silicified adjacent to the deposit but quartz crustification is present in the open spaces.

The ore controls of the deposit studied have not been established in detail, but in a general sense consist of a favorable bed, the Council Spring limestone (Pennsylvanian), a capping shale, and steeply dipping

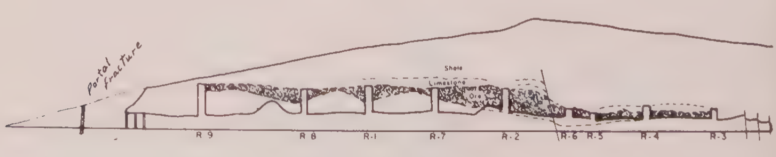

FIG. 1. Section of the No. 1 entry in which the galena samples were collected.

nineralized fractures that intersect the favorable bed. Much of the so-alled bedded ore appears in the field to be the result of solution-cavity nd/or breccia zone filling. Openings lined with coarse, museum-quality rystals of the ore minerals are plentiful both in the bedded ores and in ne brecciated fracture zones. The deposit, in common with others in ne Hansonburg district, exhibits a great uniformity of deposition with espect to mineralogy.

Sample collecting within the lead deposit was done initially to de-rmine the gross variations in lead isotopes across a number of parallel actures. To this end composite samples were taken at the portal frac-ure and at raises R-1 and R-2. These sample sites are illustrated in Fig. Grab samples composed of a number of galena crystals and crystal agments were taken. As an interesting local isotopic variation became parent, a single crystal from each of the above three sites was singled ut for detailed analyses.

Single Crystal Analyses

A large galena crystal from the portal fracture had the form of a cube t in half along a diagonal plane. The diagonal surface of the crystal as attached to a large breccia fragment of silicified limestone. The ystal was sampled by cutting it into small cubes with a diamond saw. corner sample (111), two samples (222 and 333), along a diagonal and edge sample (211) were analyzed. The positions of these samples are dicated in Fig. 2. The isotopic compositions of the samples are listed Table II. The corner sample (111) was found to be less radiogenic an the other two samples (222 and 333). The edge sample (211) was eaved into three portions, as shown in Fig. 2. The crystal's outer sur-ce or "skin" was found to be much less radiogenic than the inner por-ons (see Table II and Fig. 3).

Single galena crystals were selected also from raises R-1 and R-2. hese crystals were sampled by cleaving. The portions taken are illus-ated in Fig. 2 and comprise three samples from each crystal: an outer in, the portion of the crystal immediately under the outer skin, and e core of the crystal. The isotopic compositions of these samples are ted in Table II, as are the results of the composite grab-sample alyses from the three sample locations.

The initial sample preparation was carried out at the New Mexico ureau of Mines. This comprised separation of galena from the gangue d associated ore minerals and the sawing and cleaving of the single ystal samples. Following this initial preparation, the samples were sent Toronto for analysis. They were dissolved in hydrochloric acid, and e lead precipitated as lead iodide. A Grignard reaction of lead iodide

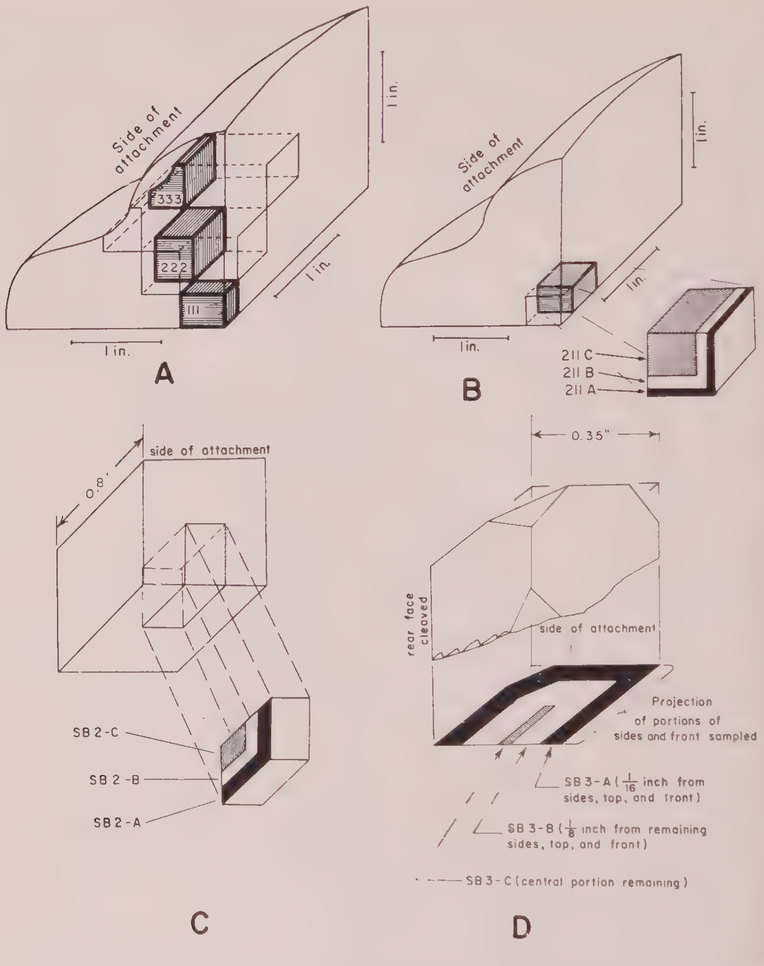

FIG. 2. Sample locations within single galena crystals. A, portal crystal, diagonal sampling; B, portal crystal, edge sampling; C, R-1 crystal; D, R-2 crystal.

and methyl magnesium bromide (CH_3-Mg-Br) at room temperature was used to produce lead tetramethyl. The lead tetramethyl was mass analyzed in the Nier-type 180-degree mass spectrometer operated by the Geophysics Laboratory of the University of Toronto. The analytical precision is shown in Table I.

The samples from the Number 1 entry show a linear relationship when plotted as Pb^{207}/Pb^{204} versus Pb^{206}/Pb^{204}. This is illustrated in Fig. 3, which includes the plots of 22 samples taken from lead deposits in the surrounding 5,000 square miles (Slawson and Austin, 1960). Figure 3 also presents a detailed plot of the single crystal analyses.

TABLE I. PRECISION OF DATA

Replica Analysis of Sample #1040

Date of run	Pb^{204}	Pb^{206}	Pb^{207}	Pb^{208}
July 20, 1959	1.255%	27.85%	20.05%	50.84%
	1.000	22.19	15.98	40.51
Nov. 11, 1959	1.248%	27.83%	20.08%	50.85%
	1.000	22.30	16.09	40.75
Jan. 28, 1960	1.253%	27.85%	20.06%	50.83%
	1.000	22.23	16.01	40.57
Feb. 22, 1960	1.250%	27.83%	20.14%	50.78%
	1.000	22.26	16.11	40.62
June 20, 1960	1.251%	27.83%	20.04%	50.88%
	1.000	22.25	16.02	40.67
July 21, 1960	1.250%	27.87%	20.03%	50.85%
	1.000	22.30	16.03	40.68
Sept. 1, 1960	1.253%	27.87%	20.08%	50.80%
	1.000	22.24	16.02	40.54
Sept. 13, 1960	1.248%	27.83%	20.05%	50.87%
	1.000	22.30	16.06	40.76
Sept. 13, 1960	1.256%	27.83%	20.05%	50.86%
	1.000	22.17	15.97	40.51
Oct. 12, 1960	1.248%	27.79%	20.03%	50.93%
	1.000	22.26	16.05	40.80
Mean *	1.251 ± 0.003	27.84 ± 0.03	20.06 ± 0.03	50.85 ± 0.04
	1.000	22.25 ± 0.04	16.03 ± 0.04	40.64 ± 0.11

Upper row for each run is percent, lower row for each run is ratio with respect to Pb^{204}.

* Sample variation: $S = \left[\frac{\Sigma(x-\bar{x})^2}{n-1}\right]^{\frac{1}{2}}$

INTERPRETATION

Since a linear isotopic relationship is obtained for all leads in both the eposit studied in detail and the surrounding deposits, a common history f origin is indicated for all the isotopic variations encountered. This pparent common history of origin lends much strength to relative age eterminations based on local isotopic variations within the deposit, as indicates that ore fluids with random discrete isotopic compositions ave not been active in the region studied.

From the foregoing data (Table II) it appears that the lead isotope mposition of the ore fluids definitely underwent measurable changes ith time. The mineralizing solutions contained somewhat less radio-nic lead as time progressed, thus causing a decrease in the radiogenic ntent of the lead deposited.

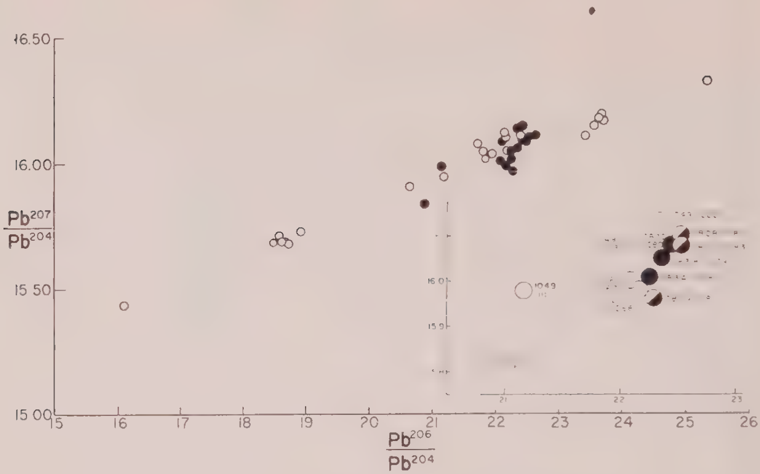

FIG. 3. Regional and detailed lead isotope data. Samples from No. 1 entry show as black circles on large graph.

Detailed Insert: Open circles are from the portal fracture,
Half-filled circles are from the R-1 raise,
Filled circles are from the R-2 raise.

Two theories currently in vogue attempt to explain changes in the isotopic composition of lead ores with continuing deposition. Russell and Farquhar (1960) have emphasized the suggestion that radiogenic lead probably was collected as a contaminant by isotopically homogeneous ore fluids when the fluids passed through whatever country rock intervened between the site of fluid generation and the site of ore deposition. Thus the early fluids that travel through a given fracture or similar permeable zone should extract relatively large quantities of radiogenic lead. Later fluids passing through the same conduits should encounter a decreasing amount of extractable radiogenic material adjacent to the fracture and thus will show corresponding decreases in their radiogenic content as time progresses.

The second theory (Eckelmann, *et al.*) advanced by the geochemists of the Lamont Geological Observatory, is based upon the assumption of an isotopically nonhomogeneous source for the mineralizing solutions. Thus when the ore solutions leave the source area, the readily mobilized radiogenic lead components leave the source in the early solutions, and the radiogénic content of the ore solutions should again decrease with increasing time. (Radiogenic lead, being interstitial and not in rock mineral structures, is believed to be more mobile than that lead tied into mineral structures during the formation of the rocks comprising the fluid source area and/or the wall rocks of the fluid conduits.)

TABLE II. DATA COLLECTED

	Location	Toronto number	Data *			
			Pb^{204}	Pb^{206}	Pb^{207}	Pb^{208}
Raise R-2	SB3-A	1078	1.255% 1.000	27.94% 22.26	20.09% 16.01	50.71% 40.41
	SB3-B	1079	1.252% 1.000	27.98% 22.34	20.09% 16.04	50.68% 40.47
	SB3-C	1080	1.249% 1.000	28.02% 22.43	20.07% 16.07	50.66% 40.55
Raise R-1	SB2-A	1081	1.254% 1.000	27.95% 22.29	20.01% 15.96	50.79% 40.50
	SB2-B	1082	1.244% 1.000	28.02% 22.52	20.04% 16.10	50.70% 40.75
	SB2-C	1083	1.245% 1.000	28.04% 22.51	20.03% 16.08	50.68% 40.69
	211-A	1066	1.291% 1.000	26.96% 20.88	20.50% 15.88	51.24% 39.69
	211-B	1067	1.256% 1.000	27.75% 22.09	20.10% 16.00	50.90% 40.53
	211-C	1068	1.252% 1.000	27.74% 22.16	20.01% 15.98	51.00% 40.73
	111	1049	1.282% 1.000	27.13% 21.16	20.49% 15.98	51.10% 39.86
	222	1049	1.244% 1.000	27.80% 22.35	20.07% 16.13	50.88% 40.90%
	333	1049	1.254% 1.000	27.72% 22.11	20.16% 16.08	50.87% 40.57

*pper row for each sample is percent, lower row for each sample is ratio with respect o Pb^{204}.

The favorable bed (Council Spring limestone) presumably received the fluids through the steeply dipping, highly permeable fracture zones t cut this bed. In dealing, however, with interpretations concerning loci of deposition in a given favorable bed, the actual means of fluid y into the favorable area is not significant. Probably the entire rable bed was never fully permeated by ore-bearing fluids. Some s may have been protected, as the result of sealing by early silica osition. Other areas may well have received only early solutions and have remained stagnant for long periods, receiving fresh ore solu-s only intermittently as early deposition would change the permea-

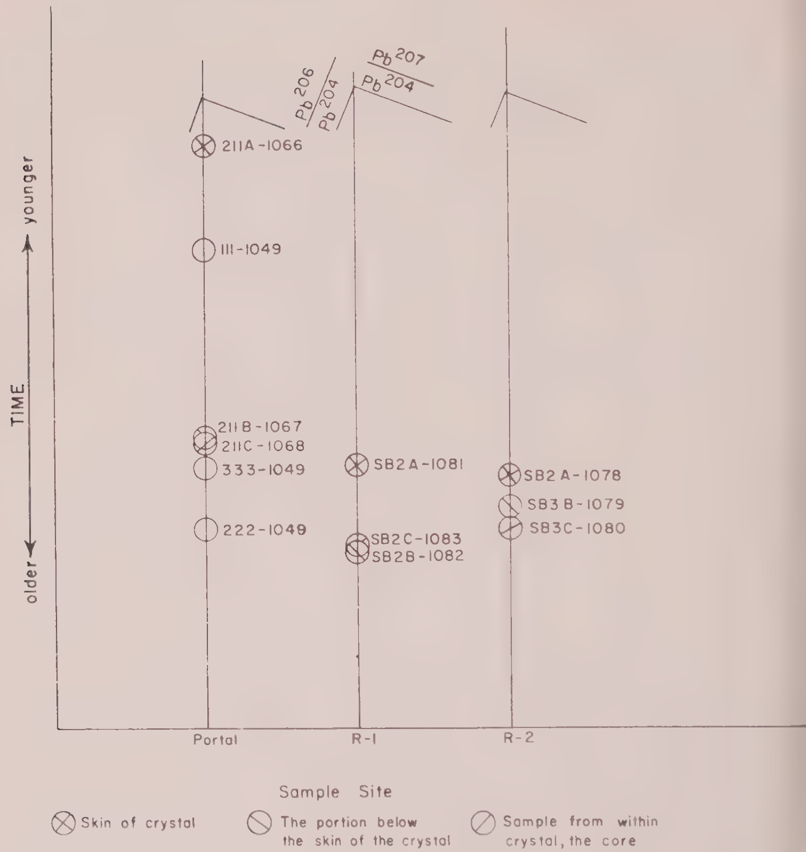

FIG. 4. Time correlation chart for various portions of three galena crystals collected in the No. 1 entry.

bility of surrounding areas. Thus local variations in physicochemic conditions created scattered depositional sites, the location of whic shifted with time.

The first lead sulfide that was deposited in the area studied in det had an isotopic composition about equal to that of sample 1082. raise R-1 the single crystal studied grew fast enough to retain hom geneity between its core (1083) and the portion immediately below t skin (1082). At raise R-2, however, the rate of crystal growth appears have been somewhat slower, for the core (1080), the portion below t skin (1079), and the "skin" or outer surface (1078) of the crystal studi show a gradual and fairly uniform change in isotopic composition. T final deposition at sites R-1 and R-2 must have occurred at the sar time, as is indicated by the similarity of the composition of the out

most "skins" of crystals from both areas (1081 and 1078). The most reasonable implication is that physicochemical conditions were varying locally in such a fashion as to cause a temporary cessation of deposition at site R-1 after a brief, initial rapid deposition, whereas deposition continued rather steadily at site R-2.

The deposition of galena along the portal fracture appears to have started at about the same time as R-1 and R-2. The isotopic constitution of sample 1049–333 is not as radiogenic as that found at other places in the inside of the crystal. Owing, however, to the manner of sampling, 333 is not necessarily representative of the true, early core of the crystal. Deposition at the portal fracture site must have been very slow, or else very intermittent, as the outer portion of the crystal sampled even less radiogenic than the "skins" from crystals at sites R-1 and R-2, thus indicating deposition at a later time. The "skin" of the galena crystal sampled at the portal fracture zone is much less radiogenic than any sample yet analyzed from the Hansonburg district. Thus, it must have been one of the last sites of deposition in the district. Figure 4 is a correlation chart for the three sample sites.

Regardless of the theory of origin adopted, one should keep in mind the ever-present possibility of renewed structural activity that either formed new, unleached fluid conduits or released new fluids into existing conduits, thus causing a resurgence of higher radiogenic lead content in the lead ores deposited later. The lack of cyclic radiogenic variations in the Hansonburg district indicates a stable structural environment following formation of the initial fluid conduits. The entire region appears to have been structurally stable with respect to fluid conduits throughout the time of ore deposition.

The data at hand are equally applicable to the concept of wandering skipping loci of galena deposition within a fluid-saturated favorable bed, to the concept of partial fluid saturation of the favorable bed; that is, the wandering of deposition reflects the lack of complete fluid saturation the favorable bed. In the case of the samples from the portal fracture, the low-radiogenic skin or overgrowth is very definitely younger than the rest of the crystal. There is no evidence to support skeletal growth of such a delicate nature at any site examined in the district. In addition, the crystals from all sites are sufficiently fresh to preclude selective isotope removal through weathering and the sharpness of the crystal edges and corners indicates that leaching by hypogene fluids is unlikely. We can conclude that relative isotopic variations of single crystals within this district yield relative ages of deposition, and thus permit the wanderings of loci of deposition to be traced about the district with respect time.

In view of the interesting possibilities of using isotopic data as a rela-

tive age determinant in the interpretation of the depositional history of a lead deposit, the authors are continuing their isotopic investigations in the Hansonburg district and surrounding vicinity.

Acknowledgment

Support for this project was provided by the New Mexico Bureau of Mines and Mineral Resources and the Geophysics Laboratory of the University of Toronto.

References

Eckelmann, F. D., Kulp, J. L., Ault, W. U. and Miller, D. S. Lead and sulfur isotopes and the history of mineralization in Southeast Missouri. *Bull. Geol. Soc. Amer.* (in press).

Russell, R. D. and Farquhar, R. M. (1960), Lead isotopes in Geology, Chapter 5, Interscience Publ., New York.

Slawson, W. F. and Austin, C. F. (1960), Anomalous leads from a selected geological environment in West-Central New Mexico. *Nature*, **187**, 400.

Manuscript received November 26, 1960.

THE AMERICAN MINERALOGIST, VOL. 46, SEPTEMBER-OCTOBER, 1961

MAGNETIC SUSCEPTIBILITY AS A MEASURE OF TOTAL IRON PLUS MANGANESE IN SOME FERROMAGNESIAN SILICATE MINERALS

R. H. VERNON,* *Mineragraphic Investigations, Commonwealth Scientific and Industrial Research Organization, University of Melbourne, Parkville, Victoria, Australia.*

ABSTRACT

Specific magnetic susceptibilities of biotites, amphiboles and pyroxenes, are directly related to total Fe (as FeO)+MnO content. For common varieties of these minerals, in which MnO is low, magnetic susceptibility effectively indicates total iron content. Measurements on biotites and amphiboles made with a calibrated Frantz isodynamic separator are sufficiently accurate to make specific susceptibility useful in petrological studies.

INTRODUCTION

The magnetic susceptibilities of some ferromagnesian silicate minerals have been measured in recent years by a number of workers with a magnetic balance—an instrument not readily available in most petrological laboratories. However, the method devised by McAndrew (1957) for the simple measurement of specific susceptibility with the Frantz isodynamic separator has brought such measurements within the scope of the many laboratories equipped with this instrument. The present study, therefore, was directed towards the measurement of the susceptibilities of some biotites and amphiboles with the Frantz separator. In addition, correlations between specific susceptibility and total iron plus manganese content are presented for these biotites and amphiboles, and for previously published data on amphiboles, clinopyroxenes and orthopyroxenes. Such correlations permit estimation of iron-manganese content, for which optical methods may be unreliable, e.g. in biotites and amphiboles.

PREVIOUS MEASUREMENTS

Olivines

Nagata, Yukutake and Uyeda (1957) measured with a magnetic balance the magnetic susceptibility of six olivines, five of which varied in composition from Fa_{04} to $Fa_{ca.35}$, the other being a knebelite. They also showed how the magnetic susceptibility may be calculated from the concentrations and magnetic moments of the paramagnetic ions. The compositions of some of the olivines were estimated from refractive indices. Apart from the knebelite, the only olivine for which a published analysis is available is a common magnesian olivine containing 10.26 per

* Present address: Geology Dept., University of Sydney, Sydney, N.S.W., Australia.

cent FeO and 0.09 per cent MnO (Ross, Foster and Myers 1954, p. 707). Its specific susceptibility range calculated by the writer from these figures is 16.9 to 18.7 ($\times 10^{-6}$ e.m.u./gm.), which is in excellent agreement with the measured value (18×10^{-6}) given by Nagata, Yukutake and Uyeda (1957, p. 52).

Clinopyroxenes

Chevallier and Mathieu (1958) measured with a magnetic balance the specific susceptibility of thirteen clinopyroxenes from the Skaergaard intrusion, east Greenland, obtaining good agreement between measured values and susceptibilities calculated by adding the contributions of the magnetic moments of the main paramagnetic ions present.

Orthopyroxenes

Akimoto, Hôrai and Boku (1958) measured with a magnetic balance the specific susceptibility of eight orthopyroxenes varying in composition from Of_{65} to Of_{88} mol. per cent, and showed that the molecular susceptibility at room temperature increased with increasing ferrosilite content. The discrepancies between the measured susceptibilities and those calculated by the writer from the analyses given by Akimoto *et al.*, are larger than for the clinopyroxenes of Chevallier and Mathieu (1958) and for the biotites and amphiboles investigated in the present study.

Biotites and amphiboles

Syono (1960) measured with a magnetic balance the specific susceptibility of five analyzed biotites and six amphiboles. For the biotites and three of the amphiboles, the measured susceptibility is much higher than the calculated susceptibility. These discrepancies are attributed by Syono (1960, p. 91) to the presence of combined water, but no similar discrepancies were found in the present study, as shown later.

Cordierites

Syono (1960) showed that the specific susceptibility, measured with a magnetic balance, of four cordierites increased with increasing iron content. Fair agreement between measured and calculated susceptibilities was obtained.

Garnets

Syono (1960) measured the specific susceptibility of four analyzed garnets with a magnetic balance, finding good agreement between measured and calculated values. Frost (1960) measured the specific susceptibility of 23 garnets with a calibrated Frantz isodynamic separator and deduced the susceptibilities of the theoretical garnet end-members.

Calculation of Specific Susceptibility

As a check on measurements it is desirable to calculate approximate susceptibilities from the chemical analyses. It has long been known that the magnetic susceptibility of paramagnetic compounds is determined by the magnetic moments and concentrations of the constituent paramagnetic ions. In the ferromagnesian silicates, which are paramagnetic, the main paramagnetic ion is usually Fe^{2+}, but commonly there are smaller amounts of Fe^{3+} and Mn^{2+}, and Ti^{3+}, Cr^{3+} and Ni^{2+} may also be present. Chevallier and Mathieu (1958) considered Fe^{2+}, Fe^{3+} and Mn^{2+} to be the effective paramagnetic ions in clinopyroxene, and derived expressions by which the specific susceptibility at 20° C. may be calculated from the concentrations and magnetic moments of these ions. The expressions, which may also be applied to other ferromagnesian minerals, are:

$$\chi_1 = 423.6 \times 10^{-6}[27.6x + 34.6(y + z)]$$
$$\chi_2 = 423.6 \times 10^{-6}[30.6x + 34.6(y + z)]$$

where χ_1 and χ_2 are the calculated specific susceptibilities (e.m.u./gm.), and x, y, z are the ionic concentrations (gm.ions/gm.) of Fe^{2+}, Fe^{3+}, and Mn^{2+}, respectively. Chevallier and Mathieu (1958) used the magnetic moments shown in Table 1, as did Syono (1960), and the writer has followed this usage to facilitate comparisons. The values χ_1 and χ_2 correspond to the ends of the range taken for the magnetic moment of Fe^{2+} (Table 1), so that ideally, the measured susceptibility (designated χ_m in this paper) should fall between χ_1 and χ_2. However, the calculated susceptibility is best regarded only as an approximate guide.

Relative Effects of the Paramagnetic Ions

Table 1, in conjunction with chemical composition, shows that the magnetic susceptibility of ferromagnesian silicates is due mainly to iron

Table 1. Magnetic Moments Used for Paramagnetic Ions, to which Reference is Made (after Stoner 1934, p. 312)

Ion	Magnetic Moment
Ti^{3+}	ca. 1.7*
Cr^{3+}	3.86
Mn^{2+}	5.88
Fe^{3+}	5.88
Fe^{2+}	5.25–5.53
Ni^{2+}	3.23–3.43

* Deduced from the value of 1.74 given for V^{4+}.

and manganese. Fe^{3+} and Mn^{2+} have slightly higher magnetic moments than Fe^{2+} and must therefore be granted the same degree of importance as Fe^{2+}, both for the calculation of susceptibilities and for plotting susceptibility against composition. However, if FeO is high, small amounts of Fe_2O_3 and MnO have only small effects on the susceptibility compared with the effect of the FeO. In this paper, both Fe^{3+} and Mn^{2+} have been taken into consideration, even where present in small concentrations, principally because these ions are invariably bracketed with Fe^{2+} in calculations involving the degree of substitution of Fe for Mg in common ferromagnesian minerals. In some garnets Mn is so high that its effect overshadows that of Fe; e.g., Frost (1960) deduced that the susceptibility of pure spessartite is higher than that of pure almandine.

Except for some uncommon varieties, ferromagnesian minerals generally contain only small amounts of titanium, although common biotites may contain as much as 5 per cent TiO_2 by weight. Though Ti^{4+} is diamagnetic, Ti^{3+}, containing one unpaired electron, is paramagnetic, with a magnetic moment of about 1.7 (Table 1). The colours of titaniferous pyroxenes, amphiboles and biotites indicate that small amounts of Ti^{3+} are present, but Ti^{3+} is probably subordinate to Ti^{4+}, since the reverse situation can be expected only when almost all the iron is present as Fe^{2+} (Goldschmidt 1954, p. 412). This probability, together with the small magnetic moment of Ti^{3+}, indicates that the effect of titanium is negligible compared with that of iron and manganese. This has been confirmed in practice by measurement of a titanian amphibole (kaersutite) containing 5.64 per cent TiO_2, the measured susceptibility being in good agreement with the susceptibility calculated on the basis of iron and manganese only (Table 5, No. 2).

Chromium is generally a very minor or trace constituent of common ferromagnesian minerals, excepting pyroxenes from certain ultramafic rock types. Thus Ross, Foster and Myers (1954) reported up to 2.43 per cent Cr_2O_3 in chromian diopside and up to 0.94 per cent Cr_2O_3 in enstatite. The relatively high magnetic moment of Cr^{3+} (Table 1), together with the low concentrations of Fe and Mn in these minerals would make it necessary to take the effect of Cr into consideration.

Small amounts of nickel occur in some magnesian olivines, the largest quantity of NiO reported by Ross, Foster and Myers (1954) being 0.50 per cent. However, Ni^{2+} has such a low magnetic moment (Table 1) and NiO is so subordinate to FeO, that the effect of the nickel should be insignificant. Thus, the analyzed magnesian olivine of Nagata, Yukutake and Uyeda (1957), referred to earlier, shows good agreement between the measured susceptibility and that calculated on the basis of iron and manganese only, despite its NiO content of 0.41 per cent.

New Measurements on Biotites and Amphiboles

The specific magnetic susceptibilities of some Australian biotites and amphiboles have been measured at room temperature with a Frantz isodynamic separator using the method and calibration of McAndrew (1957). The critical currents—the currents at which equal flow down each channel of the chute takes place at a particular transverse slope—were obtained by graphing weight against current. Weighing is preferable to visual estimation and enables the use of smaller samples; about 0.5 gm. was found to be satisfactory. The measurements were made at a corrected transverse slope of 20°, the currents required being less than 0.90 amp.

Compressed air was used for cleaning the chute and hopper between runs on different samples, since the correction to the transverse slope reading may change when the chute is removed.

Ferromagnetic impurities were removed as thoroughly as possible from the samples to be measured, by a hand magnet and by a pass through the Frantz separator at low current. The samples were sized fractions of $-52+100$ mesh (B.S.S.), except for biotite No. 11 and amphibole No. 2, of which the $-52+200$ fractions were used. The $-52+100$ fraction was favoured because the instrument was calibrated with material of this size range (McAndrew 1957, p. 64).

Biotites

The eleven biotites measured are from Precambrian metamorphic rocks of the Broken Hill district, New South Wales, which have been studied in recent years by the Mineragraphic Investigations section of the C.S.I.R.O., Melbourne. Five of these were separated by the late Dr. A. B. Edwards and analyzed in 1954. The other six were separated by the writer during a study of the banded albite-rich rocks of the district (Vernon 1961). The large range in iron content shown by these biotites makes them especially suitable for the present study.

The chemical composition and optical properties of the biotites are shown in Table 2, and the structural formulae calculated on the basis of 12 (O, OH, F) atoms are shown in Table 3. The analyzed concentrates were at least 99.5 per cent pure, quartz being the most common impurity, although chlorite is present in No. 6 and garnet in No. 11. Biotite No. 11 contains 1.93 per cent CaO, which cannot be ascribed to impurities of apatite, since P_2O_5 is only 0.01 per cent, or of garnet, since grain-counts of the concentrate revealed only 0.4 per cent by weight of a garnet containing about 3 per cent CaO. The calcium therefore appears to be accommodated in the X group of the biotite structure (Table 3).

The measured specific susceptibilities are given in Table 4, together

TABLE 2. CHEMICAL COMPOSITION OF ELEVEN BIOTITES FROM THE BROKEN HILL DISTRICT, N.S.W.

	1	2	3	4	5	6	7	8	9	10	11
SiO_2	39.51	39.94	38.76	38.28	35.89	35.84	39.00	38.26	35.53	35.16	33.21
Al_2O_3	19.66	18.10	19.07	19.69	17.72	15.47	21.80	16.73	15.79	17.50	17.26
Fe_2O_3	1.66	3.86	3.74	4.21	6.05	3.45	1.60	3.59	7.77	1.86	3.59
FeO	5.71	4.81	9.46	12.10	11.25	15.25	15.94	19.00	16.57	23.95	26.60
MgO	20.74	18.20	17.02	13.64	12.31	12.12	6.08	7.00	7.52	5.07	3.24
CaO	0.09	0.07	0.07	0.12	0.73	0.36	0.18	0.39	0.49	0.43	1.93
Na_2O	0.90	0.18	0.66	0.34	0.50	0.26	0.24	0.42	0.30	0.14	0.10
K_2O	8.20	9.46	8.36	9.48	8.26	8.74	7.20	7.62	8.74	8.66	7.20
H_2O^+	1.37	2.38	1.92	1.37	3.97	2.38	4.04	3.37	2.10	2.43	3.21
H_2O^-	0.20	0.12	0.05	0.05	0.45	0.07	0.22	0.19	0.10	0.00	0.10
CO_2	0.00	0.00	0.00	0.00	0.00	0.00	0.00	0.00	0.00	0.00	0.00
TiO_2	0.73	1.39	0.91	0.56	1.59	4.80	3.06	2.70	4.80	3.27	2.86
P_2O_5	0.03	0.08	0.02	0.04	tr.	0.96	0.26	0.37	0.16	0.70	0.01
MnO	tr.	0.08	tr.	tr.	0.11	0.12	0.12	0.19	0.18	0.37	0.39
Li_2O	0.00	0.00	0.00	0.00	0.00	—	—	—	0.00	—	0.04
F	2.24	2.00	0.80	1.02	1.79	—	—	—	—	—	0.00
Total	101.04	100.67	100.84	100.90	100.62	99.82	99.74	99.83	100.05	99.54	99.74
Less 0 for F	0.94	0.84	0.34	0.43	0.75						
Corrected Total	100.10	99.83	100.50	100.47	99.87						
$\gamma(\pm 0.003)$	1.596	1.603	1.610	1.620	1.631	1.638	1.650	1.659	1.659	1.665	1.671
X	Very pale fawn (almost colourless)	Very pale fawn (almost colourless)	Pale greenish fawn	Pale greenish fawn	Straw	Greyish straw	Straw	Straw	Straw	Straw	Straw
Y = Z	Light orange brown	Light fox brown	Olive green	Olive green	Dark brown	Dark greyish brown	Rich red-brown	Very deep brown (almost opaque)	Very deep brown (almost opaque	Very deep brown (almost opaque)	Very deep red-brown (almost opaque)

1. From biotite seam in albite-rich rock, adit of Big Hill Mine, Thackaringa area. Analyst, P. J. Sinnott.
2. From albite-rock, Pyrite Hill, east limb of Stirling Vale Syncline. Analyst, P. J. Sinnott.
3. From biotite seam in albite-rich rock, northern part of main body of albite-rich rock, Thackaringa area. Analyst, P. J. Sinnott.
4. From biotite seam, same locality as 3. Analyst, P. J. Sinnott.
5. From biotite mass about 1 mile north-west of Big Hill, Thackaringa area. Analyst, P. J. Sinnott.
6. From biotite mass enclosed in Augen Gneiss, 3,200 ft. north east of entrance gate to Aerodrome, Broken Hill. Analyst, G. C. Carlos.
7. From biotite-sillimanite garnet schist, dump of Centennial Mine, about 5 miles north west of Broken Hill Analyst, G. C. Carlos.
8. From Augen Gneiss (Alma Gneiss), north side of Ansett A.N.A. hangar, Broken Hill Aerodrome. Analyst, G. C. Carlos.
9. From quartz-oligoclase-rock, Pyrite Hill, east limb of Stirling Vale Syncline. Analyst, P J. Sinnott
10. From Hanging Wall Gneiss, D.D.H. 834, 494 ft. 496 ft., Cosgrove section, north of De Bavay Fault, North Broken Hill Mine, Analyst, G. C. Carlos.
11. From Potosi Gneiss (Footwall Gneiss), D.D.H 510, 835 ft. 837 ft., 48 section, North Broken Hill Mine. Analyst, P. J. Sinnott.

TABLE 3. STRUCTURAL FORMULAE OF ELEVEN BROKEN HILL BIOTITES*

		1	2	3	4	5	6	7	8	9	10	11
(Z)	Si	2.83	2.87	2.84	2.88	2.65	2.78	2.86	2.92	2.78	2.79	2.66
	Al	1.17	1.13	1.16	1.12	1.35	1.22	1.14	1.08	1.22	1.21	1.34
(Y)	Al	0.49	0.41	0.49	0.62	0.19	0.19	0.74	0.43	0.23	0.43	0.29
	Ti	0.05	0.08	0.06	0.03	0.09	0.28	0.17	0.16	0.28	0.24	0.17
	Fe'''	0.09	0.21	0.21	0.24	0.34	0.20	0.09	0.21	0.46	0.11	0.22
	Fe''	0.34	0.29	0.58	0.76	0.69	0.99	0.98	1.21	1.08	1.59	1.78
	Mg	2.21	1.95	1.86	1.53	1.35	1.40	0.66	0.80	0.88	0.60	0.39
	Mn	-	0.01	—	—	0.01	0.01	0.01	0.01	0.01	0.03	0.03
(X)	Ca†	0.01	—	—	0.01	0.06	—	—	—	0.02	—	0.16
	Na	0.12	0.03	0.09	0.05	0.07	0.04	0.03	0.06	0.06	0.02	0.02
	K	0.75	0.87	0.78	0.91	0.78	0.86	0.67	0.74	0.87	0.88	0.73
	OH	0.65	1.14	0.94	0.69	1.95	1.23	1.98	1.72	1.10	1.29	1.71
	F	0.51	0.46	0.19	0.24	0.42		—	—		—	—
Z		4.00	4.00	4.00	4.00	4.00	4.00	4.00	4.00	4.00	4.00	4.00
Y		3.18	2.95	3.20	3.18	2.67	3.07	2.65	2.82	2.94	3.00	2.88
X		0.88	0.90	0.87	0.97	0.91	0.90	0.70	0.80	0.95	0.90	0.91
(OH, F)		1.16	1.60	1.13	0.93	2.37	1.23	1.98	1.72	1.10	1.29	1.71

* Ideal formula $XY_3Z_4O_{10}(OH, F)_2$. Nos. 1–11 as for Table 2.

† P_2O_5 and equivalent CaO to make apatite, subtracted from analysis.

with susceptibilities calculated from the concentrations of paramagnetic ions, showing there is general agreement between measured and calculated values.

Amphiboles

The measured and calculated specific susceptibilities of seven amphiboles from various Australian localities are given in Table 5 (Nos. 1–7), together with partial compositions and ionic concentrations of paramagnetic ions. Full compositions are not given, because they are, or shortly will be, incorporated in readily obtainable publications. For six of the amphiboles, χ_m falls either between χ_1 and χ_2 or very close to one of these values. In addition, a tremolite from Mount Fitton, South Australia was found to have a very low susceptibility (1.2×10^{-6} e.m.u./gm.), as expected.

Additional data have been obtained from a paper by Rosenzweig and Watson (1954), who measured the currents at which equal separation occurred on a Frantz separator at a transverse slope of 30°, for eight

TABLE 4. COMPOSITION AND MAGNETIC SUSCEPTIBILITY OF ELEVEN BIOTITES

Specimen Number*	Iron and manganese content (weight per cent)				Concentration of magnetic ions (gm. ions/gm. of biotite)			Calculated specific susceptibility (e.m.u./gm.)		Measured specific susceptibility (e.m.u./gm.)
	FeO	Fe_2O_3	MnO	Total Fe (as FeO) +MnO	10^4x (for Fe^{2+})	10^4y (for Fe^{3+})	10^4z (for Mn^{2+})	$10^6\chi_1$	$10^6\chi_2$	$10^6\chi_m$
1	5.71	1.66	trace	7.20	7.93	2.08	—	12.3	13.3	12.0
2	4.81	3.86	0.08	8.36	6.68	4.83	0.11	15.1	15.9	12.0
3	9.46	3.74	trace	12.83	13.14	4.68	—	22.2	23.9	21.7
4	12.10	4.21	trace	15.89	16.81	5.26	—	27.4	29.5	27.4
5	11.25	6.05	0.11	16.81	15.63	7.56	0.15	29.6	31.6	28.5
6	15.25	3.45	0.12	18.48	21.18	4.31	0.17	31.3	34.0	34.0
7	15.94	1.60	0.12	17.50	22.14	2.00	0.17	29.1	31.9	35.6
8	19.00	3.59	0.19	22.42	26.39	4.49	0.27	37.8	41.2	43.2
9	16.57	7.77	0.18	23.74	23.01	9.71	0.25	41.5	44.4	39.1
10	23.95	1.86	0.37	25.99	33.26	2.33	0.52	43.1	47.3	48.0
11	26.60	3.59	0.39	30.22	36.94	4.49	0.55	50.6	55.3	50.7

* Nos. 1–11 as for Table 2.

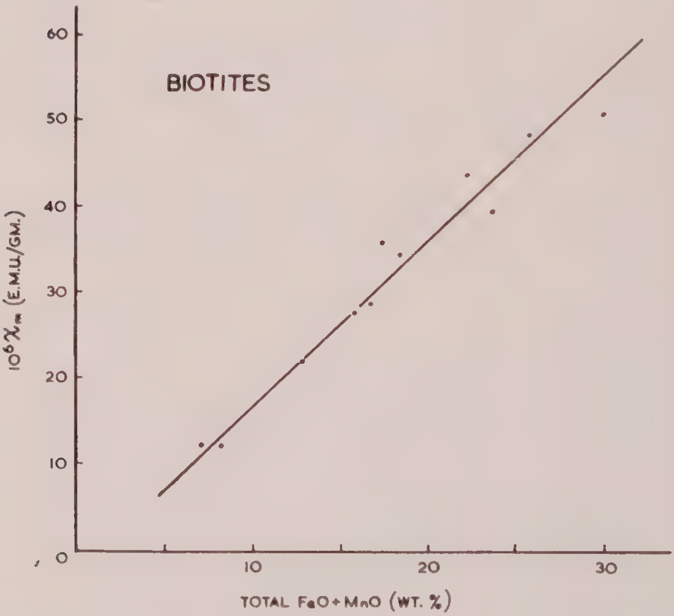

FIG. 1. Relation between χ_m and total Fe (as FeO)+MnO for the biotites of Table which may be expressed: $C=1.15+0.53\times 10^6\chi_m$, where C is weight per cent total I (as FeO)+MnO. The correlation coefficient (corrected for the small number of cases) +0.979, and the residual variance is 4.21 per cent.

TABLE 5. COMPOSITION AND MAGNETIC SUSCEPTIBILITY OF FIFTEEN AMPHIBOLES

Specimen Number*	Iron and manganese content (weight per cent)				Concentration of magnetic ions (gm. ions/gm. of amphibole)			Calculated specific susceptibility (e.m.u./gm.)		Measured specific susceptibility (e.m.u./gm.)
	FeO	Fe_2O_3	MnO	Total Fe (as FeO) +MnO	10^4x (for Fe^{2+})	10^4y (for Fe^{3+})	10^4z (for Mn^{2+})	$10^6\chi_1$	$10^6\chi_2$	$10\ \chi_m$
1	6.82	0.30	0.57	7.66	9.47	0.38	0.80	12.8	14.0	13.4
2	10.92	1.75	0.09	12.59	15.17	2.19	0.13	21.1	23.1	22.6
3	10.24	2.35	0.36	12.72	14.22	2.94	0.51	21.7	23.5	24.3
4	14.41	1.47	0.23	15.96	20.01	1.84	0.32	26.6	29.1	29.8
5	14.32	0.92	0.24	15.39	19.89	1.15	0.34	25.4	28.0	31.1
6	16.84	1.89	0.84	19.38	23.39	2.36	1.18	32.5	35.5	35.6
7	19.92	9.10	0.63	28.74	27.67	11.38	0.89	50.3	53.9	53.7
8	8.89	1.11	0.13	10.02	12.35	1.39	0.18	16.7	18.3	17.1
9	9.12	2.33	0.23	11.45	12.67	2.91	0.23	19.5	21.2	18.5
10	10.14	3.90	0.24	13.89	14.08	4.88	0.34	24.1	25.9	22.8
11	11.07	2.87	0.40	14.05	15.38	3.59	0.56	24.1	26.0	25.0
12	10.50	4.42	0.28	14.76	14.58	5.53	0.39	25.7	27.6	23.5
13	12.61	2.87	0.22	15.41	17.51	3.59	0.31	26.2	28.4	25.8
14	12.58	5.04	0.30	17.42	17.47	6.30	0.42	30.3	32.5	29.6
15	14.69	5.33	0.43	19.92	20.40	6.66	0.61	34.5	37.1	33.0

* 1. Pale brown hornblende (pargasite) from hornblende-pyroxene-granulite, Peak Hill, Broken Hill district, New South Wales (Edwards 1958, p. 7).

2. Titaniferous amphibole (kaersutite) from alkali olivine-basalt, near Spring Mountain, W. of Glen Innes, northern N.S.W.

3. Green hornblende from amphibolite, 8000 ft. N.E. of Duchess railway station, northwestern Queensland. Analyst: P. J. Sinnott.

4. Brown hornblende from hornblende gabbro, 2 miles W. of Beaconsfield, northern Tasmania (Baker 1959, p. 27).

5. Green hornblende (contaminated with several per cent of blue-green and brown hornblende) from amphibolite, Broken Hill Basin, N.S.W (Edwards 1958, p. 7).

6. Cummingtonite from same rock as No. 3. Analyst: P. J. Sinnott.

7. Deep green hornblende, from area of massive hornblende, W. of Silver Rock Tank, Broken Hill district, N.S.W. (Edwards 1958, p. 7).

8–15. Amphiboles from Pennsylvania and Delaware investigated by Rosenzweig and Watson (1954). The host-rocks are: metagabbro (8, 9), hornblende gneiss (10), metagabbro (11), hornblende-biotite schist (12), norite (13), pegmatoid schlieren in gneiss (14), hornblende gneiss (15).

amphiboles from hornblende gneisses and gabbroic rocks occurring in Pennsylvania and Delaware. The writer has calculated χ_m, χ_1, and χ_2 (Table 5, Nos. 8–15) from the Frantz settings and analyses of these amphiboles, using the calibration of McAndrew (1957). The discrepancies are larger than for Nos. 1–7, χ_m generally being lower than χ_1. This consistent discrepancy undoubtedly arises from the writer's use of the calibration of another instrument, along with the fact that the transverse slope as read on the Frantz separator scale is not necessarily the actual slope of the chute (McAndrew 1957, p. 64).

Relation Between Specific Susceptibility and Iron-Manganese Content

The variation of χ_m with weight per cent total Fe (as FeO)+MnO for the biotites of Table 4, the amphiboles of Table 5, the clinopyroxenes of Chevallier and Mathieu (1958), and the orthopyroxenes of Akimoto, Hôrai and Boku (1958) are shown in Figs. 1, 2, 3, and 4, respectively. Conventionally, composition is shown as the abscissa in determinative charts of this kind. However, since the object of such charts is to permit

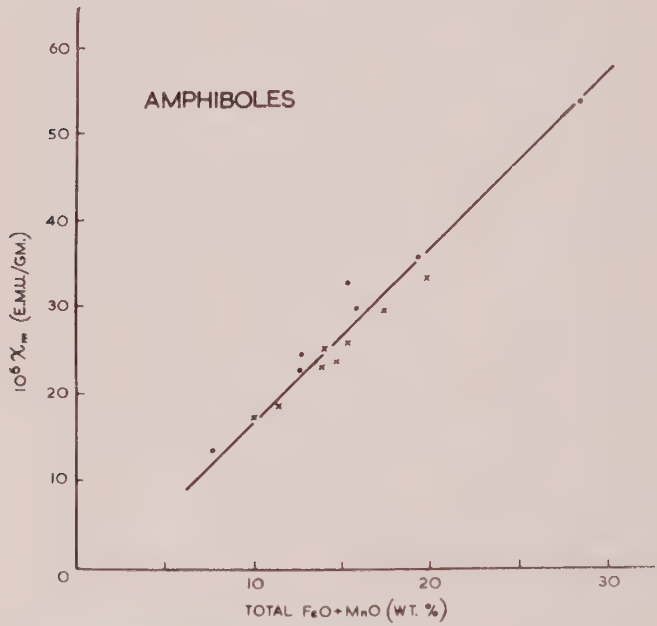

Fig. 2. Relation between χ_m and total Fe (as FeO)+MnO for the amphiboles of Table 5. Dots represent amphiboles 1–7; crosses represent amphiboles 8–15. The linear relationship is: $C = 1.63 + 0.50 \times 10^6 \chi_m$, where C is total Fe (as FeO)+MnO. The residual variance is 5.06 per cent, and r (corrected) is +0.974.

estimation of composition from the physical property, χ_m has been made the independent variable, and the calculated lines of regression are those of composition on χ_m. The biotites, amphiboles and clinopyroxenes show high degrees of positive linear correlation, but the relationship for the orthopyroxenes is more variable. This may be related to the much larger discrepancies between measured and calculated susceptibilities shown by these orthopyroxenes.

The olivines of Nagata, Yukutake and Uyeda (1957) have not been

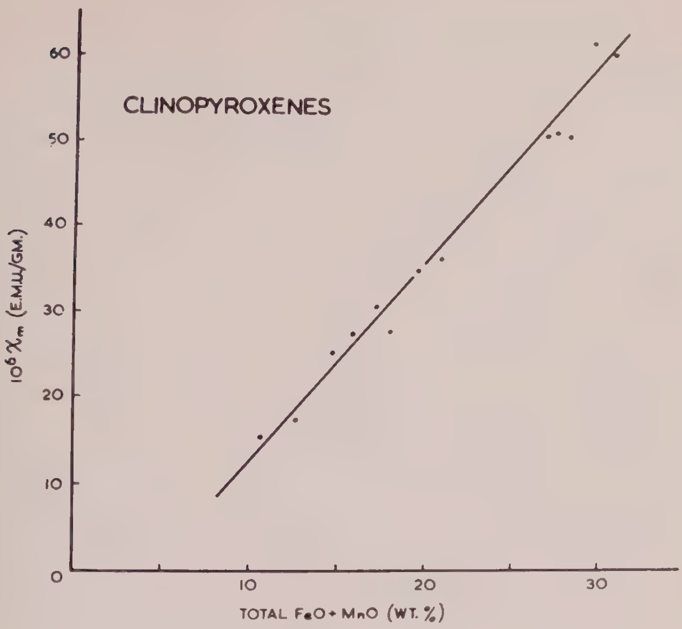

FIG. 3. Relation between χ_m and total Fe (as FeO)+MnO for the clinopyroxenes of Chevallier and Mathieu (1958), which may be expressed: $C=4.43+0.44\times10^6\chi_m$, where C is total Fe (as FeO)+MnO. The residual variance is 2.04 per cent, and r (corrected) is +0.990.

plotted in this way, since more chemical data are required. Nagata, Yukutake and Uyeda (1957) plotted molecular susceptibility at room temperature against mol. per cent Fa. However, their most iron-rich olivine (knebelite) is rich in manganese, which is not taken into account in their chart. Removal of this point would make a better linear fit for the other, more common varieties.

Conclusions

Specific magnetic susceptibilities given in this and previously published papers give a good measure of total iron plus manganese content for the biotites, amphiboles and clinopyroxenes. For common varieties of these minerals, in which MnO is low, specific susceptibility effectively indicates total iron. The published results for orthopyroxenes and olivines also strongly suggest a direct relationship between susceptibility and iron-manganese content. However, the relationship for the orthopyroxenes is as yet not well defined, and more chemically analyzed samples will need to be measured before the exact relationship for olivines is known.

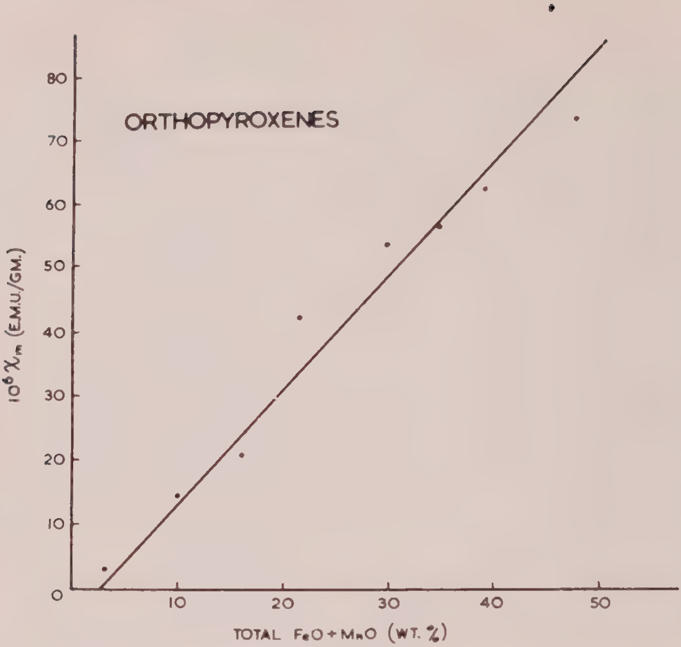

FIG. 4. Relation between χ_m and total Fe (as FeO) + MnO for the orthopyroxenes of Akimoto, Hôrai and Boku (1958), which may be expressed: $C = 2.53 + 0.57 \times 10^6 \chi_m$, where C is total Fe (as FeO) + MnO. The linear regression accounts for only slightly more than half the total variance of C, so the chart has little determinative value, though it does indicate a general increase of χ_m with increasing total Fe (as FeO) + MnO.

Estimation of iron content from magnetic susceptibility is not complicated by the presence of titanium, unlike estimation from refractive indices, e.g. in biotites (Hall 1941).

Measurements made with the Frantz isodynamic separator appear to be satisfactory, showing that specific susceptibility can be added to the properties of ferromagnesian minerals commonly employed in petrological studies.

ACKNOWLEDGMENTS

I wish to thank Professor J. F. G. Wilkinson of the Department of Geology, University of New England, N.S.W., for kindly providing a specimen of kaersutite (Table 4, No. 2), and Dr. G. Baker and Dr. J McAndrew for helpful criticism of the manuscript. I also wish to record my gratitude to the late Dr. A. B. Edwards, who suggested the study and gave me the benefit of his advice.

REFERENCES

AKIMOTO, S., HÔRAI, K., AND BOKU, T. (1958), Magnetic susceptibility of orthopyroxenes *J. Geomagn. Geoelect.*, **10**, 7–11.

BAKER, G. (1959), Rodingite in nickeliferous serpentinite, near Beaconsfield, northern Tasmania: *J. Geol. Soc. Aust.*, **6**, 21–36.

CHEVALLIER, R., AND MATHIEU, S. (1958), Susceptibilité magnétique spécifique de pyroxènes monocliniques: *Bull. Soc. chim. Fr.*, no. **5**, 726–729.

EDWARDS, A. B. (1958), Amphibolites from the Broken Hill district: *J. geol. Soc. Aust.*, **5**, 1–32.

FROST, M. J. (1960), Magnetic susceptibility of garnet: *Miner. Mag.*, **32**, 573–576.

GOLDSCHMIDT, V. M. (*Ed.* MUIR, A.) (1954), Geochemistry: Clarendon Press, Oxford.

HALL, A. J. (1941), The relation between chemical composition and refractive index in the biotites: *Am. Mineral.*, **26**, 34–41.

MCANDREW, J. (1957), Calibration of a Frantz isodynamic separator and its application to mineral separation: *Proc. Aust. Inst. Min. Metallurg.*, no. **181**, 59–73.

NAGATA, T., YUKUTAKE, T. AND UYEDA, S. (1957), On magnetic susceptibility of olivines: *J. Geomagn. Geoelect.*, **9**, 51–56.

ROSENZWEIG, A., AND WATSON, E. H. (1954), Some hornblendes from southeastern Pennsylvania and Delaware: *Am. Mineral.*, **39**, 581–599.

ROSS, C. S., FOSTER, M. D., AND MYERS, A. T. (1954), Origin of dunites and of olivine-rich inclusions in basaltic rocks: *Am. Mineral.*, **39**, 693–737.

STONER, E. C. (1934), Magnetism and Matter: Methuen and Co. Ltd., London.

SYONO, Y. (1960), Magnetic susceptibility of some rock forming silicate minerals such as amphiboles, biotites, cordierites and garnets: *J. Geomagn. Geoelect.*, **11**, 85–93.

VERNON, R. H. (1961), Banded albite-rich rocks of the Broken Hill district, New South Wales: *C.S.I.R.O. Aust. Mineragr. Invest. Tech. Pap.*, no. **3**.

Manuscript received December 12, 1960.

THE AMERICAN MINERALOGIST, VOL. 46, SEPTEMBER-OCTOBER, 1961

SILLIMANITE AND CORDIERITE FROM VOLCANIC XENOLITHS

SHIGEO ARAMAKI, *Geological Institute, University of Tokyo, Tokyo, Japan.*

ABSTRACT

Basement sedimentary rocks containing various minerals formed during pyrometamorphism have been ejected from the Asama Volcano. The physical properties of sillimanite and cordierite reflect the unusual conditions of their formation at higher temperatures and lower pressures.

INTRODUCTION

Asama Volcano is a composite stratovolcano with an active crater at the top. It is situated about 140 km. northwest of Tokyo, Japan, and is about 2500 m. above sea level. The volcano has been active throughout historic time, the largest known eruption being that in 1783. After this eruption, violent "Vulcanian" eruptions have occurred repeatedly from the top crater. Among the ejected blocks of such eruptions there are many kinds of sedimentary rocks which constitute the basement of the volcano. These sedimentary rocks contain sillimanite, andalusite, corundum, cordierite, osumilite, hypersthene, diopside, wollastonite, feldspars, iron oxides, etc., which were formed during the pyrometamorphism by the magma. Sillimanite and cordierite crystals were separated from the host rock and their chemical composition and physical properties were determined. The physical properties of both the sillimanite and cordierite were found to reflect the unusual conditons of their formation, *i.e.* the higher temperatures and lower pressures.

P-t conditons of pyrometamorphism

The andesite occurring as bombs of the recent eruptions and representing the host rock of the sedimentary xenoliths contains phenocrysts of augite, hypersthene, plagioclase, magnetite, and small amounts of olivine and is calc-alkali andesite in composition (Aramaki, 1956, 1957). T. Minakami of the Earthquake Research Institute measured the temperature of the lava pool at the bottom of the open crater-pit directly by a thermocouple and obtained a value of about 1000° C. (Minakami, personal communication). Hydrothermal experiments (Aramaki and Roy, in press)* showed that the glass formed by the partial fusion of the

* Hydrothermal experiments on this glass were made as a part of the study on the system Al_2O_3–SiO_2–H_2O at the Department of Geochemistry, Pennsylvania State University. The glass was separated by a heavy liquid. The concentrate contained some cordierite and sillimanite crystals embedded in the glass. In the presence of excess water

sediments becomes fluid at a temperature range between 945 and 1005° C. and water pressure of about 200 bars. The metamorphosed sediments appear to have been derived from shale, calcareous rocks, tuff, and other volcanic rocks. Such rocks occur among the Miocene to Pliocene formations which are exposed around the volcano and supposedly continue beneath it at a depth of about 1 to 3 km. from the crater. From these observations it is inferred that the metamorphism took place at a temperature between 945 and 1005° C. and under a solid pressure of 200–800 bars.

Sillimanite

The sillimanite occurs as needles up to 0.1×0.02 mm. in a transparent, colorless glass ($n=1.487$) which was formed by partial melting of clastic(?) sediment rich in Al_2O_3 and SiO_2. The glass occupies up to half the volume of the original rock and the remaining crystalline part contains cordierite, detrital quartz, magnetite, andalusite and corundum in a general order of decreasing amount.

Practically all the needles of sillimanite are confined in the glass and therefore crystallized directly from the liquid during the pyrometamorphism.

---

the following results were obtained.

Run	Temperature	Pressure	Length of run	Result
A	680° C.	300 bars	773 hours	No crystallization. Glass did not become fluid.
B	945	200	280	No crystallization. Glass did not become fluid.
C	1005	200	2	No crystallization. Glass became fluid.
D	1070	300	50	No crystallization (?). Glass became fluid.

That the glass became fluid after heating was detected by observing that the original angular glass fragments were completely changed to a compact mass of glass cast into the shape of the platinum container. This happened in runs C and D whereas in runs A and B the powder remained incoherent and the shape of the original angular grains of glass remained unchanged.

The refractive index of the glass ($n=1.487 \pm 0.002$, including the heterogeneity of the glass) remained practically unchanged after the heating. In no case could any new product of crystallization of the glass during the treatment be detected except for possible formation of sillimanite or mullite as fine fibres with mottled extinction in run D.

Andalusite occurs with sillimanite in most of the rock specimens examined. In the specimen No. AS2X10 from which the sillimanite was separated, idiomorphic andalusite crystals (up to 1×0.2 mm.) are found under the microscope. They occur sporadically in the portion where the glass formed by pyrometamorphism is apparently absent. In another specimen small andalusite prisms (up to 0.5×0.1 mm.) occur more abundantly in the glass. In this case the crystals are honeycombed, suggesting resorption. Parallel growth or a replacement relation between andalusite and sillimanite is never observed.

The rock powder was treated with cold HF for a week to ensure the decomposition of minerals other than sillimanite. The residue was washed with a concentrated mixture of $1HCl \cdot 3HNO_3$, then with a dilute mixture of the same. Sillimanite was then concentrated by Clerici solution and the proportion of the three minerals was carefully measured with an integration table (Table 1).

TABLE 1. CHEMICAL COMPOSITION OF SILLIMANITE FROM ASAMA VOLCANO: SAMPLE NO. AS2X10
Chemical analysis by H. Haramura

	No. 1	No. 2
SiO_2	32.72	31.6
Al_2O_3	64.69	65.6
TiO_2	0.12	—
Fe_2O_3	0.86	—
FeO	0.71	—
MnO	0.02	—
MgO	0.00	—
CaO	0.00	—
$H_2O(+)$	0.18	—
$H_2O(-)$	0.05	—
Total	99.81	
Amount of sample analyzed	1.2g	0.13g
Mineral composition of sample analyzed (wt%)		
sillimanite	93.7	92.6
andalusite	2.6	3.1
corundum	3.7	3.8
unidentified impurity	0.0	0.5
	100.0	100.0
Molecular ratio of SiO_2 and Al_2O_3 in sillimanite (corrected for andalusite and corundum)		
SiO_2	47.6	46.4
Al_2O_3	52.4	53.6

The chemical composition of the mixture of the three minerals is given in Table 1 (No. 1). When corrected for the andalusite and corundum, the $Al_2O_3:SiO_2$ ratio is 52.4:47.6. This is appreciably higher than the ideal ratio 1:1 for sillimanite. TiO_2, Fe_2O_3, and FeO may be considered to substitute for Al^{3+} in the octahedral position in the sillimanite structure rather than Si^{4+} in the tetrahedral position. Therefore, even if all three oxides reported in the analysis are taken into account as essential constituents in the sillimanite structure, they will not decrease the ratio $R_{octahedral}:R_{tetrahedral}$ as represented by the ratio $Al_2O_3:SiO_2$ but will increase it.

In order to check the above result, another batch of sillimanite concentrate was prepared. Partial analysis (No. 2, Table 1) again indicates the excess of alumina over silica. According to H. Haramura who undertook the analysis, the error in the analysis is probably less than $\pm 0.5\%$ by weight. Therefore the amount of excess alumina over silica is far greater than the analytical error.

There are still other possibilities for getting an incorrect $Al_2O_3:SiO_2$ ratio. They are: 1) incorrect estimation of the amount of the corundum, 2) possible persistence of amorphous alumina as decomposition product in the residue of the HF-treated sample and 3) differential leaching of SiO_2 from the sillimanite during the treatment.

The first possibility is rather unlikely, for in order to reduce the ratio to 50:50 it would be necessary to have about 12% corundum by weight in the batch instead of about 4% as actually measured. A glance under the microscope reveals that even the total amount of the impurities is far less than 10%. For the same reason it is difficult to conceive that there was present about 10% amorphous alumina in the concentrate. The possibility of leaching SiO_2 from the sillimanite during a week's treatment might be admitted, for the action of HF on sillimanite is not well known. However, the following evidences appear to be against the leaching hypothesis: 1) under the microscope, the sillimanite shows no abnormal appearance indicative of leaching or decomposition—the sillimanite prisms are clear throughout without any marring of their sharp outlines, 2) the refractive indices show no appreciable variation in different fractions, and 3) the *x*-ray powder pattern shows sharp peaks giving well-defined spacings.

From these considerations, it was concluded that the sillimanite has a composition intermediate between ideal sillimanite and ideal mullite.

It has been almost established (Agrell and Smith, 1960, Aramaki and Roy, in press) that a continuous solid solution exists between mullites of compositions $3Al_2O_3 \cdot 2SiO_2$ and $2Al_2O_3 \cdot SiO_2$. As is shown by Agrell and Smith (1960) for the mullite solid solution, it is possible for the sillimanite

structure to substitute Al for an equal amount of Si with a corresponding falling off of oxygen from the structure (one oxygen per two Si-Al replacements). As the structure of mullite is essentially the same as that of sillimanite—Al-O octahedral chains cross-linked by tetrahedral Si and Al—there is good reason to believe there exists a continuous solid solution between sillimanite and $3Al_2O_3 \cdot 2SiO_2$ mullite.

Almost all the reliable analyses of sillimanites in the literature show the ratio $Al_2O_3:SiO_2$ as close to 1:1, but these are from rocks formed by low temperature metamorphism. The Asama sillimanite may owe its abnormal composition to the unusually high temperature and low pressure of its formation.

Kennedy (1960) reported the synthesis of a part of the solid solution between sillimanite and mullite by breaking down kaolinite at high temperature and pressure, although he did not state how these phases were identified.

Accurate measurement of the unit cell dimensions of the sillimanite was carried out by means of the North American Philips Geiger-counter diffractometer (Table 2), using silicon as the internal standard. The method of measurement is described by Aramaki and Roy (in press). According to Agrell and Smith, mullites and sillimanites fall into two separate groups in the plottings *a*–*c*, *b*–*c*, and volume-*c* of the unit cell (Agrell and Smith, 1960), thus making the identification quite unequivocal. The unit cell volume-*c* plotting is reproduced schematically in Fig. 1. They also found that four specimens of natural sillimanites have very similar unit cell dimensions, the total range being $a = 7.4876$–7.4839 Å, $b = 7.6758$–7.6718 Å, $c = 5.7728$–5.7692 Å, and volume $= 331.24$–331.62 Å^3.

A fibrolite from an eastern Pennsylvania metamorphic rock and a xenocrystic sillimanite in granite porphyry from Japan also fall close to this range (see Fig. 1 and the analysis and *x*-ray data by Aramaki and Roy, in press). In the plottings *a*–*c* and *b*–*c*, the Asama sillimanite falls on the points reasonable for the sillimanite group and not for mullite, although the *b*-spacing of the Asama mineral is closer to mullite than to sillimanite. In the plotting unit cell volume-*c* (Fig. 1), the Asama sillimanite falls on a point rather apart from either the field of six sillimanites mentioned above or that of mullite without Fe^{3+} and Ti.

According to Agrell and Smith, the entrance of Fe^{3+} and Ti into the structure of mullite increases the *c*-edge considerably while the change in *a*- and *b*-edges is less conspicuous. They showed that while pure mullite irrespective of $Al_2O_3:SiO_2$ ratios has a *c*-edge of about 2.885 Å, TiO_2(0.55wt%) and Fe_2O_3(5.93wt%) increase the *c*-edge of a natural mullite to 2.8952 Å. The presence of Ti and Fe in the Asama sillimanite may reasonably explain the difference in *c*-spacings between the Asama

TABLE 2. X-RAY POWDER DATA OF SILLIMANITE FROM ASAMA VOLCANO: SAMPLE No. AS2X10
CuK_α Radiation

I	*hkl*	$2\theta_{obs}$	$2\theta_{calc}$
(3	andalusite	15.97)	
32	110	16.51	16.52
(2	andalusite	19.45)	
9	200	23.71	23.73
(3	{andalusite, corundum}	25.63)	
100	120	26.04	26.06
96	210	26.43	26.44
5	002	30.96	30.95
(2	andalusite	32.20)	
43	220	33.39	33.38
17	112	35.25	35.26
13	130	37.07	37.07
3	202	39.38	39.35
22	122	40.88	40.87
19	230	42.72	42.72
(4	corundum	43.2)	
5	400	48.53	48.52
2	312	49.67	49.63
3	330	51.00	51.02
(2	corundum	52.51)	
7	240	53.54	53.57
8	420	54.39	54.41
9	042	57.57	57.59
2	402	58.64	58.66
13	332	60.86	60.87
2	422	63.92	63.92
2	004	64.47	64.47
3	250	65.60	65.61
2	014	65.78	65.75
3	520	66.95	66.92
3	440	70.11	70.09
5	152	70.49	70.49
4	252	74.31	74.29
3	224	74.55	74.57
3	522	75.56	75.54
2	600	76.12	76.09
1	161	77.33	77.32

$a = 7.498 \pm 0.003$ Å
$b = 7.690 \pm 0.003$
$c = 5.797 \pm 0.003$

Table 3. Optical Properties of Sillimanite and Cordierite from Asama Volcano

Sillimanite (AS2X10)	Cordierite (AS297)
$\alpha=1.659\pm0.003$	$\alpha=1.537\pm0.002$
$\beta=1.664\pm0.003$	$\beta=1.542\pm0.002$
$\gamma=1.681\pm0.001$	$\gamma=1.546\pm0.002$
$\gamma-\alpha=0.022$	$\gamma-\alpha=0.009$
	$2V(+)=83, 82, 82, 80°$

and other sillimanites, the latter supposedly very low in Ti and Fe contents, while the abnormal increase in unit cell volume may be ascribed to the increase in $Al_2O_3:SiO_2$ ratio.

The refractive indices of the Asama sillimanite (Table 3), after having been corrected for the amount of Fe^{3+} and Ti according to the curves given by Bowen, Greig, and Zies (1924), fall very close to a point representing an imaginary sillimanite free from impurities.

Only a preliminary discussion will be given in the following on the for

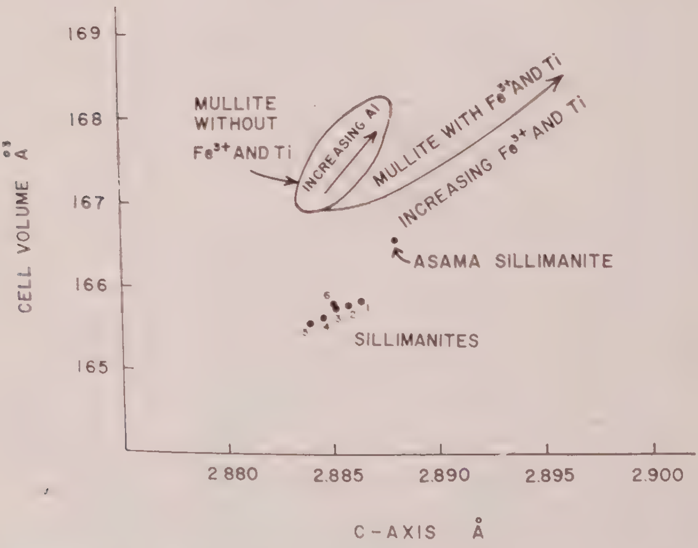

Fig. 1. Variation of cell volume with the cell edge c for mullite and sillimanite (afte Agrell and Smith, 1960; Aramaki and Roy, in press). Sillimanites are: Nos. 1, 2, 3, and from Agrell and Smith, No. 5 fibrolite from eastern Pennsylvania, No. 6 xenocrystic si limanite in granite porphyry, central Japan. Oval area represents the mullite solid solutio of the composition from $3Al_2O_3\cdot2SiO_2$ to $2Al_2O_3\cdot SiO_2$.

mation and stability relations of sillimanites, leaving the full arguments to the paper by Aramaki and Roy on the Al_2O_3-SiO_2-H_2O system.

The Asama sillimanite may be considered as a variety stable at high-temperatures, *i.e.* at 1000° C., and low pressures. If this holds true and the well-known occurrence of mullites in the Hebridian province (Agrell and Langley, 1958; Agrell and Smith, 1960) also represents stable conditions, the sillimanite$\rightleftharpoons$mullite+silica mineral boundary goes beyond a temperature a little above 1000° C., probably not far above 1200° C., at a relatively low pressure. It follows then that the boundary curve sillimanite$\rightleftharpoons$mullite+silica mineral given tentatively by Clark, Robertson, and Birch (Fig. 3, p. 638, 1957) should be shifted towards the high-temperature side and cross the temperature axis at 1000° C. or a little higher. The fact that andalusite occurs with the sillimanite in Asama might indicate that the sillimanite$\rightleftharpoons$andalusite boundary curve is steeper with respect to pressure in the phase diagram than that given by Clark, *et al.*, and crosses the temperature axis at a higher temperature. The known occurrences of volcanic sillimanite and mullite appear to be consistent with the postulated temperatures for the sillimanite$\rightleftharpoons$mullite+silica mineral boundary. The mullites which have been distinguished from sillimanites with certainty are all products of pyrometamorphism found in basalt and dolerite including picritic varieties, whereas sillimanites are found in andesite and trachyte.

It is possible, however, that the Asama sillimanite has been crystallized metastably from the liquid produced by the partial fusion of the xenoliths. The fact that sillimanite is easily synthesized by a simple squeezer in the *p-t* range well within the supposed stability field of kyanite (Kennedy, 1959, and Aramaki and Roy, in press) might indicate its ready formation in a metastable state.

Cordierite

The high-temperature polymorph of cordierite was first proposed by Miyashiro, Iiyama, Yamasaki, and Miyashiro (1955). The basis of distinction between high- and low-temperature forms of cordierite was the difference in refractive indices for the same $Fe^{2+}+Mn/Mg+Fe^{2+}+Mn$ ratio, the high-temperature form having lower refractive indices than the low-temperature form. Later Miyashiro (1957) found all gradations of structural ordering from hexagonal indialite through "subdistortional cordierite" to "perdistortional cordierite." Systematic measurements of optical properties and unit cell dimensions were made on the cordierite and indialite series by Iiyama (1956). Cordierite from Asama was identified as a typical high-temperature (and perdistortional) cordierite in all of the papers mentioned above where its various properties, except its chemical composition, were already described.

An ejected block of silicic tuff(?) of the basement rock now pyrometamorphosed into a compact porcelain-like mass (which has been called by previous Japanese petrologists "ceramicite"; Koto, 1916) contains quartz, cordierite, and sillimanite, in order of decreasing amounts, with very small amounts of acid plagioclase, K-feldspar and glass. As is described in detail by Hussak (1883) the cordierite crystals occur in aggregates a few millimeters across which can be seen as purple spots in a hand specimen.

About 30 kg. of the rock were crushed, the cordierite was separated by heavy liquid and magnetic separators, and about 1.2 grams of comparatively pure material were finally obtained. The impurity is estimated as less than 0.2% by volume. Its chemical composition is given in Table 4. The structural formula is fairly well satisfied for cations with remarkably low contents of Na, K, and H_2O. A very high content of TiO_2 may also be noticed.

TABLE 4. CHEMICAL COMPOSITION OF CORDIERITE FROM ASAMA VOLCANO: SAMPLE NO. AS297
Chemical analysis by H. Haramura

SiO_2	47.67	O (excluding O in H_2O)	18.00	
Al_2O_3	31.12	Si	4.93	6.00
TiO_2	2.05	Al	1.07	
Fe_2O_3	1.18			
FeO	11.53	Al	2.72	
MnO	0.41	Ti	0.16	
MgO	6.14	Fe^{3+}	0.09	
CaO	trace	Fe^{2+}	1.00	4.97
Na_2O	0.12	Mn	0.04	
K_2O	0.03	Mg	0.95	
$H_2O(+)$	0.05	Na	0.01	
$H_2O(-)$	0.05	K	0.00	
Total	100.35			
$\frac{Fe^{2+}+Mn}{Mg+Fe^{2+}+Mn} = 0.52$		$H_2O(+)$	0.02	
		$H_2O(-)$	0.02	

Iiyama (1958) has shown that the difference between the so-called high- and low-temperature cordierites is due to the difference in the H_2O content. According to his hydrothermal experiments a natural cordierite with refractive indices of the "low-temperature" variety was found to decrease its refractive indices when heated above a certain temperature. This change is reversible and the transition temperature is strongly pressure-dependent, varying from 600° C.* at very low water pressure to 800° C.* at 600 bars. Iiyama concludes that this change is due to the

* Values corrected by the original author.

hydration-dehydration of cordierite and the so-called high-temperature polymorph has a lower content of H_2O than the so-called low-temperature polymorph.

It is of interest that the Asama cordierite contains a lower amount of H_2O than any of the analyzed natural cordierites reported by Miyashiro, Iiyama, Yamasaki, and Miyashiro (1955), Miyashiro (1957) and Iiyama (1956). The *p-t* conditions of the formation of the Asama cordierite fall within the stability field of the high-temperature form of Iiyama's diagram, and its low water content is therefore in accord with the general scheme.

However, it is noted that although the difference between the so-called high- and low-temperature polymorphs of cordierite exactly corresponds to the difference in H_2O content, such a pair of varieties of cordierite cannot be called a polymorphic pair because of the necessary difference in the chemical composition.

TABLE 5. X-RAY POWDER DATA OF CORDIERITE FROM ASAMA VOLCANO: SAMPLE NO. AS297
CuK_α radiation

I	*hkl*	$2\theta_{obs}$	$2\theta_{calc}$*
77	200	10.34	10.30
76	110	10.43	10.42
11	310	17.95	17.95
11	002	19.02	19.05
73	112	21.76	21.76
100	312	26.31	26.27
73	022	26.44	26.42
53	511	29.18	29.14
50	421	29.27	29.27
37	131	29.49	29.49
27	422	33.75	33.77
9	620	36.34	36.33
7	040	36.77	36.77
21	004	38.66	38.63
9	?	39.35	
11	622	41.31	41.33
11	242	43.08	43.09
11	?	48.0	
5	350	49.20	49.23
9	334	50.74	50.72
11	10.00	53.25	53.26
24	624	54.05	54.07

$a = 17.18_6$ Å*
$b = 9.76_9$
$c = 9.31_5$

* Calculated by T. Iiyama (1956, Table 8).

X-ray powder diffraction data are given in Table 5 together with calculated 2θ values for another sample of cordierite from Asama given by Iiyama (1956, Table 8). Iiyama's calculated 2θ values fit very closely the observed 2θ of the analyzed cordierite and therefore the same unit cell dimensions may be assigned to Iiyama's and the chemically analysed cordierites. Coincidence in refractive indices of the two cordierites also suggests the close similarity in chemical composition.

The ratio $Fe^{2+}+Mn/Mg+Fe^{2+}+Mn$ of the Asama cordierite is 0.52 (Table 4). If this value is plotted in Iiyama's diagrams (Figs. 1, 2, and 5 1956) it is apparent that the Asama cordierite has anomalous a-spacing and refractive indices compared to those of artificially heated and dehydrated cordierites of various ratios of $Fe^{2+}+Mn/Mg+Fe^{2+}+Mn$. This tendency has been already noted by Iiyama, though he had no exact value of the ratio $Fe^{2+}+Mn/Mg+Fe^{2+}+Mn$ at the time his paper was written. It appears possible, as Iiyama pointed out, that natural volcanic cordierites belong to a polymorph different from that to which artificially dehydrated cordierites would belong.

Acknowledgments

The writer is indebted to the following persons in various ways: Professors T. Minakami, H. Kuno, A. Miyashiro, T. Iiyama, R. Roy, and J. V. Smith. The chemical analyses were made possible through the kind arrangements of Prof. I. Iwasaki, Dr. Katsura, and Mr. H. Haramura.

References

Agrell, S. O., and Langley, J. M. (1958), The dolerite plug at Tievebulliagh, nea Cushendall, Co. Antrim: *Proc. Roy. Irish Acad.*, **59**, 93–127.

Agrell, S. O. and Smith, J. V. (1960), Cell dimensions, solid solution, polymorphism, ar identification of mullite and sillimanite: *Jour. Amre. Ceram. Soc.*, **43**, 69–76.

Aramaki, S. (1956 57), The 1783 activity of Asama Volcano: *Jap. Jour. Geol. Geogr.*, **2** 189–229, **28**, 11–33.

Aramaki, S. and Roy, R. (in press).

Bowen, N. L., Greig, J. W., and Zies, E. G. (1924), Mullite, a silicate of alumina: *Jou. Wash. Acad. Sci.*, **14**, 183–191.

Clark, S. P., Jr., Robertson, E. C., and Birch, F. (1957), Experimental determinatio of kyanite sillimanite equilibrium relations at high temperatures and pressures: *Am. Jour. Sci.*, **255**, 628–640.

Hussak, v. E. (1883), Über den Cordierit in vulkanischen Auswürflingen: *Sitzungsber. d. Akad. d. Wissensch. in Wien*, **87**, 332–360.

Iiyama, T. (1956), Optical properties and unit cell dimensions of cordierite and indiali *Mineral. Jour.*, **1**, 372–394.

Iiyama, T. (1958), Transformation des formes haute temperature, bases temperature de cordierite: *Compt. rendus d. l'Acad. des Sci.*, **246**, 795–798.

Kennedy, G. C. (1959), Phase relations in the system Al_2O_3-H_2O at high temperatu and pressures: *Amer. Jour. Sci.*, **257**, 563–573.

Kennedy, G. C. (1960), Phase relations of some rocks and minerals at high temperatures and high pressures: *Trans. Amer. Geophys. Union*, **41**, 283–286.
Koto, B. (1916), The great eruption of Sakura-jima in 1914: *Jour. Coll. Sci., Imper. Univ. Tokyo*, **38**, art. 3, 1–237.
Miyashiro, A. (1957), Cordierite-indialite relations: *Amer. Jour. Sci.*, **255**, 43–62.
Miyashiro, A., Iiyama, T., Yamasaki, M., and Miyashiro, T. (1955), The polymorphism of cordierite and indialite: *Amer. Jour. Sci.*, **253**, 185–208.

Manuscript received December 17, 1960.

THE AMERICAN MINERALOGIST, VOL. 46, SEPTEMBER-OCTOBER, 1961

PHASE RELATIONS IN CORDIERITE-GARNET-BEARING KINSMAN QUARTZ MONZONITE AND THE ENCLOSING SCHIST, LOVEWELL MOUNTAIN QUADRANGLE, NEW HAMPSHIRE*

By Fred Barker, *U. S. Geological Survey, Washington, D. C.*

Abstract

The assemblage biotite-cordierite-garnet microcline plagioclase-quartz is found in portions of the large Cardigan pluton of metamorphosed Kinsman quartz monozonite in the east central part of the Lovewell Mountain quadrangle and in the southeastern part of the Sunapee quadrangle, New Hamsphire. Adjacent pelitic schists of the Littleton formation consist largely of the assemblages biotite-garnet-oligoclase-quartz sillimanite and biotite-garnet oligoclase-quartz-sillimanite-orthoclase. A graphical phase analysis of these rocks has been made, following the methods of Korzhinskii and Thompson, and using Heald's analyses of biotite, cordierite, and garnet. Mineral assemblages of the kinsman pluton are related to those of the Littleton rocks by the divariant relation:

cordierite + garnet + potassic feldspar = biotite + sillimanite, with quartz and plagioclase present in excess. Thus the pluton and its pelitic wallrocks, though metamorphosed together, are of different metamorphic facies probably because the pluton was hotter than the wallrock and/or because the chemical potential of water was less in the pluton than in the schist.

Introduction

The mineral pair cordierite-garnet has been found in pelitic rocks of high metamorphic rank in many localities. Heald (1950, p. 58–60) has described an interesting occurrence of this pair in a portion of the large Cardigan pluton of Kinsman quartz monzonite, here metamorphosed, in the Lovewell Mountain quadrangle, southwestern New Hampshire. Heald (1950, p. 65–67) also gave chemical analyses of coexisting biotite, cordierite, and garnet from this rock. A phase analysis is made in the present paper of the cordierite-garnet-bearing plutonic rock and of its wallrock, the adjacent schist of the Littleton formation, following the methods of Korzhinskii (1959) and Thompson (1957). Mineral assemblages of these two rock masses are represented graphically in Thompson-type ternary plots and in projections of tetrahedral diagrams. These diagrams show that assemblages of rocks of the Kinsman and Littleton formations are mutually incompatible, and may be represented by a divarient reaction.

The geologic map of Fig. 1 shows the southern half of the Cardigan pluton and the enclosing Littleton formation.

Petrography of the Plutonic Rocks

The Cardigan pluton is exposed for almost 60 miles in a direction slightly east of north, and has a breadth of about 4 to 14 miles (Billings,

* Publication authorized by the Director, U. S. Geological Survey.

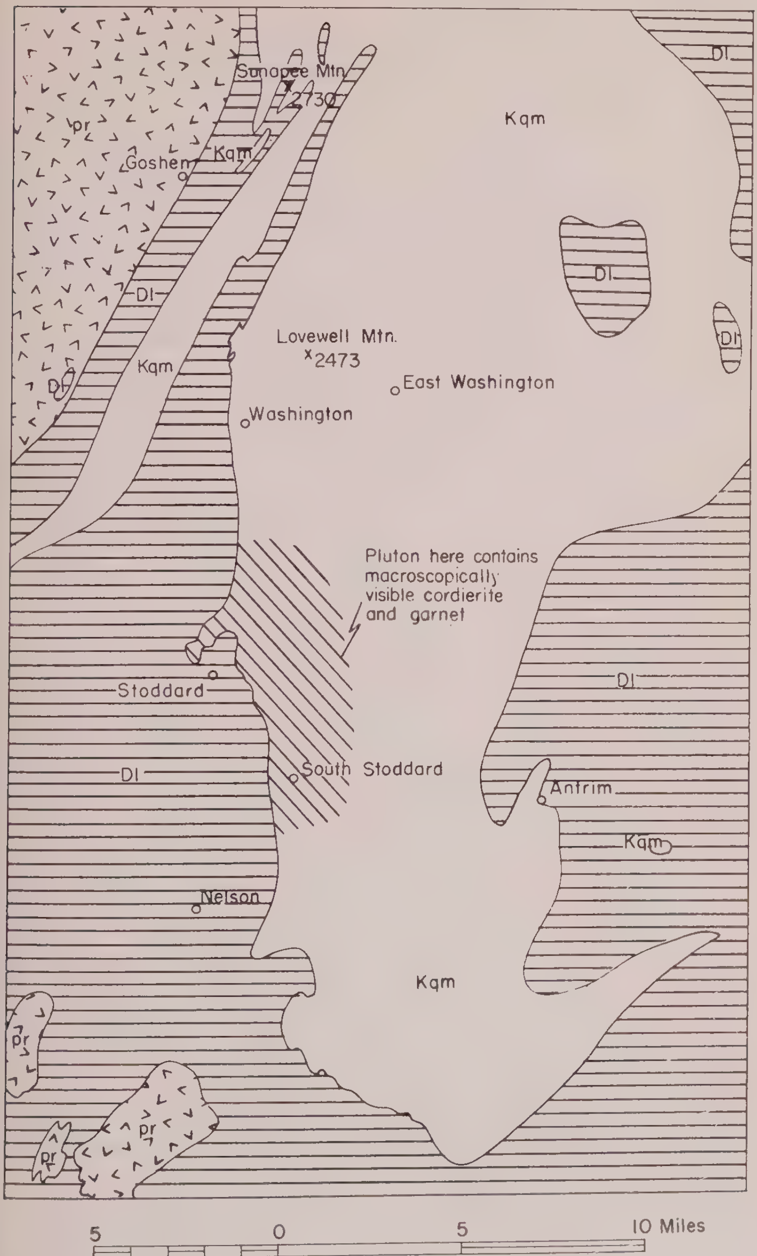

FIG. 1. Generalized geologic map of a part of south-western New Hampshire (after Billings, 1955), showing the southern half of the Cardigan pluton of Kinsman quartz monzonite (Kqm), the Devonian Littleton formation (Dl, horizontally ruled), and other plutonic rocks (pr, checked pattern.).

1955). Excellent, detailed descriptions of this rock in the Lovewell Mountain quadrangle and northward Sunapee quadrangle have been given by Heald (1950, p. 58–61) and Chapman (1952, p. 394–397). The pluton in this area is mostly light gray porphyritic granodiorite with tabular megacrysts of perthitic microcline 3 to 12 cm. long. Grains of plagioclase as large as 5 cm. are abundant in much of the rock. The matrix is coarse-grained, subhedral to anhedral, and consists largely of oligoclase or andesine, quartz, and biotite. Small amounts of myrmekite, and retrograde muscovite and chlorite are present. Tiny needles of sillimanite are scattered through the quartz. Magnetite, ilmenite, apatite, zircon, and graphite are accessory. The composition of the Kinsman body in this area ranges from quartz monzonite to quartz diorite, but granodiorite is most abundant. An average of fourteen volumetric modes is given in percentages by Heald (1950, p. 59): oligoclase-andesine 47, quartz 29, microcline microperthite 11, biotite 10, and garnet 2; and an average of nine by Chapman (1952, p. 397): oligoclase-andesine 49, quartz 28, biotite 11, and microcline perthite 7. The variations in bulk composition, however, have little affect on the fabric of the pluton and its mineral assemblages.

Most of the Kinsman quartz monzonite in the Lovewell Mountain quadrangle contains garnet. Cordierite is also a macroscopically visible constituent of the granodiorite in the town of Stoddard and in nearby Antrim and Nelson (Heald, 1950, p. 60), as shown in Fig. 1. Excellent exposures of the porphyritic cordierite-garnet granodiorite may be seen in the road cut on Route 9 from 200 to 300 yards east of Morse Brook. Cordierite forms 3 to 5 per cent of most of the granodiorite, and garnet is present in roughly equal amount but is more widespread in occurrence. The cordierite is partly anhedral, partly subhedral, roughly equant to elongate in outline, 1 to 16 mm. in size, and slightly to wholly altered to muscovite and chlorite. Polysynthetic and sectorial twins and pleochroic haloes about zircons are rare in the cordierite. Garnet is mostly anhedral, equant, 2 to 15 mm. in diameter, and usually slightly altered along fractures to chlorite and biotite. Biotite embays garnet in many instances. Garnet is commonly partly sheathed in biotite.

Small quantities of garnet and cordierite are also present in the Kinsman quartz monzonite in the Sunapee quadrangle (Chapman, 1952, p. 395–396).

The long, sheet-like extension of the pluton that lies southwestward from the east flank of Sunapee Mountain contains only a little garnet and no cordierite (Heald, 1950, p. 61), and is less metamorphosed than the main body of the pluton to the east.

Assemblages in the porphyritic granodiorite, in its inclusions, and in

the adjacent Littleton formation were studied in 19 thin sections. Biotite, microcline perthite, plagioclase, and quartz form the usual assemblage in the granodiorite. Cordierite and garnet lie in contact with all of these minerals; however, contacts of these two mafic minerals with microcline perthite are rare because they are partially rimmed with biotite. Thin films of secondary sericite have formed along many of the interfaces between the potassic feldspar and both cordierite and garnet. Thus the assemblage is: biotite-cordierite-garnet-microcline-plagioclase-quartz. Sillimanite needles in quartz and in feldspar are separate from the mafic minerals and thus are not part of the above assemblage. They form a subassemblage microcline-plagioclase-sillimanite.

A small, dark inclusion in the porphyritic granodiorite, collected on Route 9 about 200 yards north of the junction with Route 123, consists of about 4 per cent garnet megacrysts set in a partially muscovitized, massive mosaic of $\frac{1}{4}$ to $\frac{1}{2}$ mm. equant grains of microcline, plagioclase, and cordierite, and chunky tablets of biotite. Sharp contacts of microcline with cordierite and garnet are plentiful in unaltered parts of this rock. The mineral assemblage of this inclusion is identical to that of the enclosing cordierite-garnet granodiorite.

Sillimanite is abundant in some of the inclusions (Heald, 1950, p. 59–60) in the pluton. One inclusion from Route 123, 300 feet east of the Antrim-Nelson town line, consists partly of massive quartz, microcline, plagioclase, garnet, biotite, and cordierite, and partly of irregular lenses of biotite-garnet-sillimanite-quartz schist with pseudomorphs of muscovite and sillimanite after cordierite. Many of the garnets in these lenses are embayed by biotite and sillimanite. These textural relations and the fact that the number of phases if greater than the phase rule allows indicate that this rock is not in equilibrium. This inclusion probably was an assemblage biotite-cordierite-garnet-microcline-plagioclase-quartz, in equilibrium with the granodiorite, that suffered a later, retrogressive alteration in which cordierite, garnet, and microcline partly reacted to biotite, muscovite and sillimanite.

Heald (1950, p. 83–84) has pointed out that the presence of garnet in the Kinsman quartz monzonite is probably due to metamorphism, rather than to assimilation of more mafic rocks. The bulk composition of the garnet-cordierite-bearing granodiorite is essentially the same as that of the garnet-cordierite-free variety, so assimilation may be ruled out. The garnet and cordierite are found only in the central, more intensely metamorphosed portion of the pluton.

The pluton of Kinsman quartz monzonite in the Keene-Brattleboro area, southwesternmost New Hampshire, is only slightly metamorphosed; it contains about 5 to 10 per cent muscovite, only traces of

garnet, and no cordierite (Moore, 1949, p. 1642). The components that formed muscovite in the Kinsman pluton near Keene may have entered the minerals cordierite, garnet, and microcline in the Cardigan pluton in the Lovewell Mountain area, according to a reaction such as:

muscovite+biotite=cordierite+garnet+microcline (with quartz in excess). Or, following Heald (1950, p. 84), there may have been a reaction between muscovite and biotite to produce a more magnesian biotite, garnet, and microcline. A balanced reaction between a hypothetical, strictly igneous Kinsman quartz monzonite and its actual metamorphic equivalent, as now found near South Stoddard and vicinity, would probably involve both of the above reactions, but would be more complex.

Assemblages in the Littleton Formation

The Littleton formation immediately west of the Cardigan pluton is formed of pelitic rocks which have been highly metamorphosed. Potassi feldspar is stable in these rocks. The common assemblages of these rock are: biotite-garnet-oligoclase-quartz-sillimanite and biotite-garnet-oligo clase-quartz-sillimanite-orthoclase (Heald, 1950, p. 54-55). Biotite an sillimanite are intergrown in these rocks; this mineral pair is not found i the cordierite-garnet granodiorite. Heald found cordierite in only tw specimens of this rock (1950, p. 52 and 54); the ratio of FeO:MgO i usually so high that garnet forms, rather than cordierite.

Muscovite occurs in the Kinsman and Littleton assemblages only as retrograde mineral. It is not known if this mineral is stable under the con ditions of the main metamorphism. The pair sillimanite+sodic micro cline (or orthoclase) is stable, and the related pair muscovite+plagio clase is not. Below its breakdown muscovite may be stable with bot sillimanite and microcline (or orthoclase) that is more sodic than th muscovite (Dr. James B. Thompson, Jr., oral communication, 1960 The pair, sillimanite+sodic microcline (or orthoclase), may separate, i a compositional sense, the assemblages muscovite-sodic microcline (c orthoclase)-sillimanite and soda-saturated microcline (or orthoclase sodic plagioclase-sillimanite. The rocks described here contain the latt assemblage, and the possibility remains that muscovite would be stabl under these same external conditions in rocks of generally similar con position except with higher ratios of K_2O:Na_2O.

Graphical Representation of Assemblages

These assemblages of the Kinsman quartz monzonite and the Littleto formation may be represented graphically. The rocks are considered sy tems of eight essential components: Al_2O_3, CaO, FeO, H_2O, K_2O, Mg(Na_2O, and SiO_2. With the condition that quartz be present in excess, tl

component SiO_2 is also present in excess, and need not be directly represented in compositional plots of the system. This method has been developed by Korzhinskii (1959, p. 66–71) and Thompson (1957).

Most of the CaO of these rocks is found in the ubiquitous plagioclase. The garnet contains only 1.13 weight per cent of CaO (Heald, 1950, p. 64), and so the effect of this component is neglected. Similarly, much of the Na_2O is present in plagioclase. However, appreciable amounts of soda are present in the microcline of the Kinsman quartz monzonite and in the orthoclase of the Littleton formation: two representative analyses by Heald (1950, p. 63) showed 14 mole per cent of albite in the former and 21 mole per cent in the latter. In this analysis microcline and orthoclase are plotted as $KAlSi_3O_8$ for convenience, but it should be kept in mind that these feldspars actually are sodic and of compositions stable with oligoclase-andesine.

The small molar ratios of Fe_2O_3:FeO in these rocks (Heald, 1950, p. 77, 84; Chapman, 1952, p. 389) give only trace amounts of magnetite; and so the effects of Fe_2O_3 in the system are also neglected. The temperature, pressure, and chemical potential of H_2O are assumed to have had nearly constant values during formation of the assemblages. Thus each of these rock units may be represented by the components Al_2O_3, FeO, K_2O, and MgO, with the phases quartz and oligoclase-andesine present in excess, and at given conditions of nearly constant temperature, pressure, and chemical potential of H_2O. The temperature and chemical potential of H_2O in the schist apparently were different from those in the granodiorite; this point is discussed below.

In the terminology of Korzhinskii (1959, p. 71) Al_2O_3, FeO, K_2O and MgO are inert components, and H_2O is a perfectly mobile component. SiO_2 is an excess component. The Na_2O and CaO may be considered together as a single excess component in the ratio that they are found in the plagioclase, if one neglects their entrance into the potassic feldspar and garnet.

Four variables may be plotted in a tetrahedron, or one of the variables may be held constant and the remaining three plotted in a two-dimensional projection similar to that given by Thompson (1957). Both a direct perspective view of the tetrahedron and the method of Thompson will be given here.

Probable mineral assemblages of muscovite-bearing schists of the sillimanite zone have been graphically represented by Thompson (1957, p. 856). Starting with temperature, pressure, and chemical potential of H_2O given, and with quartz present in excess, he made a projection in the tetrahedron Al_2O_3-FeO-K_2O-MgO from the muscovite point to the plane Al_2O_3-FeO-MgO. Thus a diagram of phases stable with both muscovite

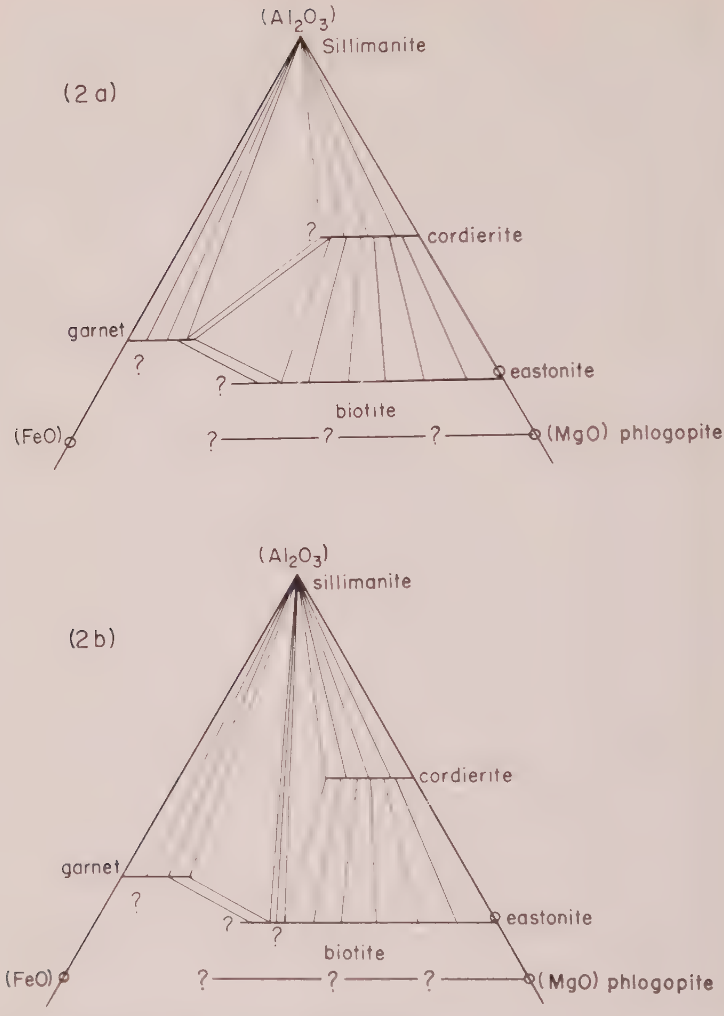

FIG. 2. Minerals stable with quartz, oligoclase-andesine, and potassic feldspar at con stant temperature, pressure, and chemical potential of H_2O in: (*a*) cordierite-garnet bearing Kinsman quartz monzonite, and (*b*) Littleton formation east of the orthoclase iso grad. Extent of biotite field and relations near FeO corner not known. The lines in biotite cordierite field are schematic.

and quartz was made. A similar projection, from the point for potassic feldspar, may be made for the muscovite-free rocks described above. The two diagrams of Fig. 2 are obtained; that for the cordierite-garnet-bearing granodiorite is determined from the assemblage biotite-cordierite-garnet-microcline (-quartz-plagioclase), using Heald's analyses (1950, p. 64–67)

of the three mafic silicates; and that for the Littleton formation by the two biotite-sillimanite-bearing assemblages given above.

Figure 2*b* does not show the potentially important potash feldspar-free assemblage biotite-cordierite-garnet-sillimanite (plagioclase-quartz) which would be expected in rocks with less K_2O than the schists of the Littleton formation. This assemblage occurs at Sturbridge, Massachusetts, and is being studied by the author. To show this assemblage and its relation to those of Fig. 2*a*, two perspectives of the tetrahedron Al_2O_3-FeO-K_2O-MgO are given in Fig. 3. The region bounded by the five compositions sillimanite, sodic microcline or orthoclase, ferrous cordierite, magnesian almandine, and biotite contains five possible four-phase regions. Two are shown in Fig. 3*a*.

cordierite-garnet-potassic feldspar-sillimanite,
and cordierite-garnet-potassic feldspar-biotite;

and they are separated by the three-phase region:

cordierite-garnet-potassic feldspar.

The remaining three assemblages are shown in Fig. 3b:

biotite-cordierite-potassic feldspar-sillimanite,
biotite-garnet-potassic feldspar-sillimanite,
and biotite-cordierite-garnet-sillimanite;

and are separated by the three-phase fields:

biotite-potassic feldspar-sillimanite,
biotite-cordierite-sillimanite,
and biotite-garnet-sillimanite.

Compositions of minerals in the three-phase fields are related by tie planes, which are analogous to tie lines of two-dimensional diagrams. These five regions intersect in a small volume, where a general divariant reaction, approximating the transition from Figs. 2*a* and 3*a* to Figs. 2*b* and 3*b*, takes place:

cordierite + garnet + potassic feldspar = biotite + sillimanite (with quartz in excess and the chemical potential of H_2O externally determined). This abrupt type of reaction has been called a discontinuity in facies by Thompson (1957, p. 856).

The conclusion is drawn that the Cardigan pluton was not in facies equilibrium with the immediately enclosing schists of the Littleton formation, and that these rock masses are related by the equation of the previous paragraph. The pattern of regional metamorphism suggests that the assemblage of the Kinsman quartz monzonite is of higher metamorphic grade than that of the adjacent schist. It is probable that the

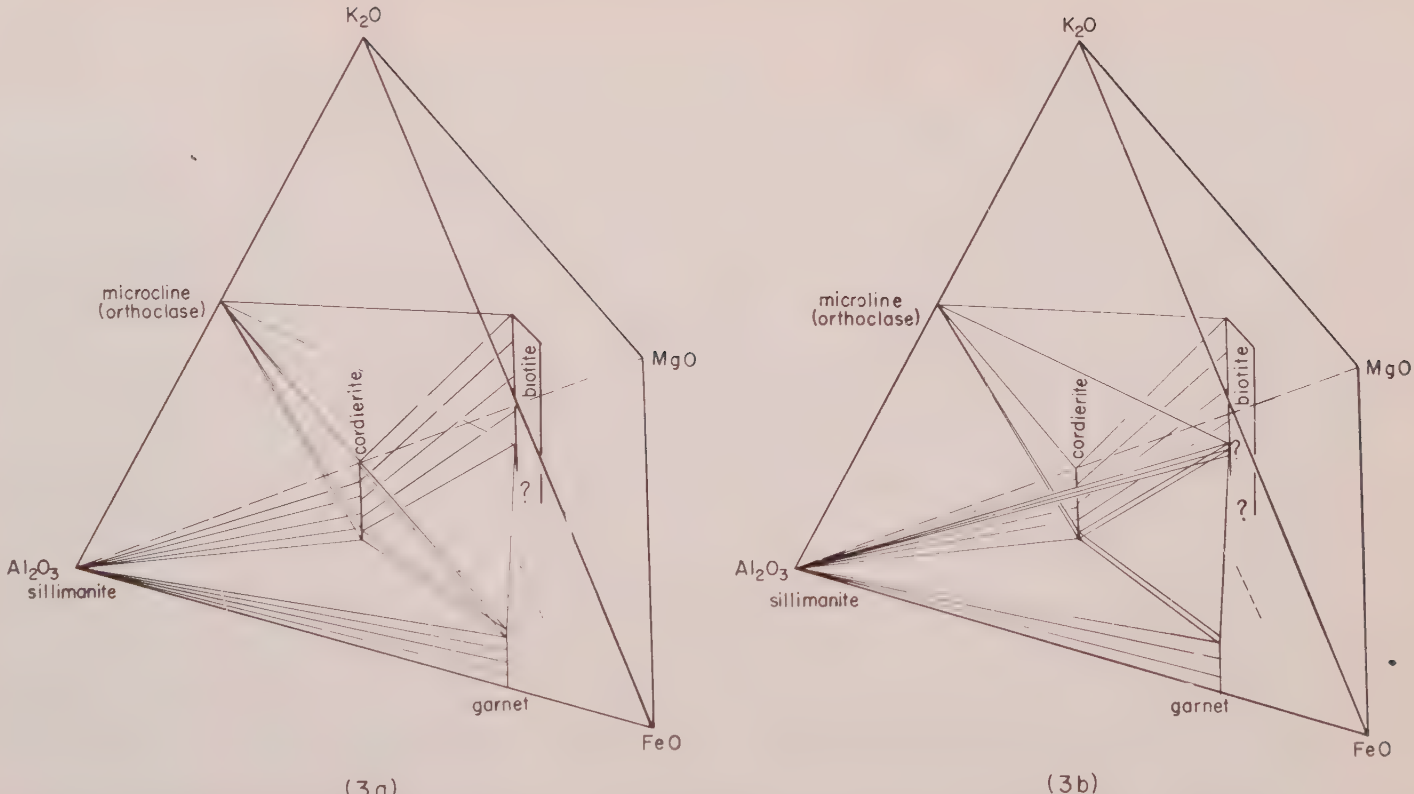

FIG. 3. Phase relations in part of the system Al_2O_3-FeO-K_2O-MgO, with quartz and oligoclase-andesine in excess, and at constant temperature, pressure, and chemical potential of H_2O. (*a*) (left) Cordierite-garnet-bearing Kinsman quartz monozonite. (*b*) (right) Littleton formation east of the orthoclase

plutonic rock was hotter than the schist, or that its chemical potential of H_2O was lower than that of the schist, or both, and that these gradients of temperature and/or chemical potential of H_2O were existent during the peak of metamorphism. In other words the more restricted range of biotite in the granodiorite, as compared with its range in the schist, is a reflection of conditions that favor formation of anhydrous phases. If the granodiorite had been metamorphosed at still higher temperatures or lower chemical potentials of H_2O one might expect the biotite to have been altered to hypersthene and potassic feldspar.

Similar Occurrences

Assemblages similar to those described above were found by Korzhinskii (1936) in metasedimentary rocks of the Southern Baikalia region, southeastern Siberia. His analysis is similar to the writer's, as would be expected; unfortunately his work was not known to the writer until the above paper was completed. Korzhinskii (1936, p. 279) found four stages of equilibrium with assemblages:

I	II
alm-bio-fay-hyp	alm-bio-fay-hyp
alm-or -bio-hyp	alm-bio-cdt-hyp
alm-or -cdt-hyp	bio-or -cdt-hyp
alm-or -cdt-sil	alm-bio-or -cdt
	alm-or -cdt-sil

III	IV
alm-bio-fay-hyp	alm-bio-gr?-hyp
alm-bio-cdt-hyp	alm-bio-cdt-hyp
alm-bio-cdt-sil	alm-bio-cdt-sil, and
alm-bio-or -sil	alm-bio-or -sil, and
bio-cdt-or -sil	

(Abbreviations are: alm—almandine, and—andalusite, bio—biotite, cdt—cordierite, fay—fayalite, gr—grunerite, hyp—hypersthene, or—orthoclase, sil—sillimanite).

Each assemblage is stable with quartz, magnetite, apatite, zircon, pyrrhotite, and graphite. Plagioclase and rutile are stable with all assemblages except those containing fayalite. Stage I is stable at the highest temperature, II and III at intermediate temperatures, and IV at the lowest temperature. Korzhinskii gives a number of the reactions that take place between one stage and another, including the one given by the author. Assemblages of the Kinsman quartz monzonite are in Korzhinskii's stage II, and those of the Littleton formation in stage III, with the important difference that anthophyllite would be stable for highly mafic compositions in the New Hampshire area, rather than hypersthene.

A metamorphic reaction similar to that given has been postulated for rocks in southwestern Finland. Pehrman (1936) suggested that biotite-cordierite-garnet-microcline-oligoclase-quartz gneiss at Åbo has been transformed to cordierite-garnet-bearing granite by the reaction:

biotite + sillimanite + quartz = cordierite + potassic + feldspar + water.

Analyses of biotite from the gneiss and of cordierite and garnet from the granite are given (1936, p. 16–19); the ratios of FeO:(Fe+MgO) are 0.37 for biotite, 0.16 for cordierite, and 0.70 for garnet (neglecting 1 mole per cent of grossularite end member). In Pehrman's reaction the biotite and cordierite should have the same ratio of FeO:(FeO+MgO); the fact that they are different necessitates the presence of another mafic mineral in the reaction, which probably is garnet.

Acknowledgments

The author is grateful to Drs. James B. Thompson, Jr., Harvard University, Andrew Griscom and E-an Zen, U. S. Geological Survey, for helpful suggestions in the preparation of this paper.

References

Billings, M. P. (1955), Geologic map of New Hampshire, scale 1 250,000: U. S. Geol. Survey.

Chapman, C. A. (1952), Structure and petrology of the Sunapee quadrangle, New Hampshire: *Geol. Soc. Amer. Bull.* **63,** 381–425.

Heald, M. T. (1950), Structure and petrology of the Lovewell Mountain quadrangle, New Hampshire: *Geol. Soc. Amer. Bull.* **61,** 43–89.

Korzhinskii, D. S. (1936), Paragenetic analysis of quartz-bearing calcium-poor schists of the Archean complex of Southern Pribaikal'e: *Zap. Vses. min. Obshch.*, no. 2, 247–280 ; (1959), Physiochemical basis of the analysis of the paragenesis of minerals. Translated from Russian. New York, Consultants Bureau, Inc., 142 p.

Moore, G. E. (1949), Structure and metamorphism of the Keene Brattleboro area, New Hampshire-Vermont: *Geol. Soc. Amer. Bull.* **60,** 1613–1669.

Pehrman, G. (1936), Über cordierit führende gesteine aus dem migmatitgebiet von Åbo (S. W. Finland): *Medd. från. Åbo Akad. Geol. Min. Inst.*, no. **20,** 1–26.

Thompson, J. B. (1957), The graphical analysis of mineral assemblages in pelitic schists *Am. Mineral.* **42,** 842–858.

Manuscript received Jan. 4, 1961.

THE AMERICAN MINERALOGIST, VOL. 46, SEPTEMBER-OCTOBER, 1961

MICROSPECTROCHEMICAL ANALYSIS OF MINERALS*

CLAUDE L. WARING AND HELEN W. WORTHING,
with accompanying mineralogical note by ALICE D. WEEKS,
U. S. Geological Survey, Washington, D. C.

ABSTRACT

A rapid microspectrochemical method is presented for the estimation of 68 elements from a single arcing of 1 mg. or less of sample.

The results are obtained through visual estimates of line intensities based on synthetic powder standards and reported in percentage brackets of 10 to 3, 3 to 1, 1 to 0.3, etc. No attempt is made to attain any high degree of detectability because a knowledge of the trace element content is not necessary for mineral identification.

A spectrographic emulsion with high speed in the red part of the spectrum and low speed in the ultraviolet part was adapted to these procedures by installing an extra slide in the plateholder. This slide permitted limited exposure of the high wavelengths while the alkalies were in the arc vapor and at the same time the ultraviolet part was exposed during the total arcing period.

INTRODUCTION

Microspectrochemical analysis is used commonly in the Geological Survey laboratory in conjunction with x-ray diffraction methods for the identification of unknown minerals and as an aid in selecting chemical procedures when a limited amount of sample is available.

In the past, the spectrographic procedures described by Stich (1953) were used to aid the mineral identifications. The techniques applied to the I-L (Eastman) type of spectrographic plates which responded equally well to the ultraviolet and red portions of the spectrum (2000 to 10,000 Å). It is necessary to cover the range of the spectrum in one arcing of the limited sample. This makes it possible to estimate the percentage of all significant elements present. The discontinuance of the I-L plates by the manufacturer created a problem with reference to continuing the spectrochemical analyses of small mineral samples.

The manufacturer has recommended the I-N (Eastman) type of spectrographic emulsion to replace the I-L series. Tests with the I-N plates have shown this type to be out of balance, when the conditions Stich used were applied to identifying small mineral samples, because of the great speed in the red part of the spectrum and diminished response in the ultraviolet. For example, a set of spectrographic conditions that gave enough intensity for the identification of B, Si, Be, and other elements in the ultraviolet would completely overexpose K, Na, Li, Rb, and Cs in the red part of the spectrum. In order to find a suitable method for the 1-N plates, many unsuccessful tests with filters were made. By in-

* Publication authorized by the Director, U. S. Geological Survey.

stalling a special slide in the plateholder, permitting the principle of photographic dodging to be applied, a better balance was obtained.

The results by the techniques described are especially useful in distinguishing between similar minerals such as autunite, torbernite, saléeite, and to aid in the identification of metamict specimens. The information provided has a high degree of reliability because no compounds are added to the samples prior to arcing, and it is possible to correlate x-ray and spectrographic data on the same material.

Apparatus

Spectrograph, medium quartz, dispersion varying from 4.6 Å/mm. at 2500 Å to 11.5 Å/mm. at 7000 Å. Special opaque slide installed in plateholder in addition to the regular slide.

Excitation source, full wave mercury vapor rectifier, 220 volts, 15 amperes maximum, inductance for smooth operation of arc, rheostat for controlling the current, connected in series with the arc. The rheostat has three fixed positions of 74, 38, and 19 ohms, producing 2, 4, and 9 amperes.

Neutral filters

Viewing box; magnifier or comparator.

Developing equipment, rocking development tank, plate washer and drier.

Electrodes, lower $\frac{1}{4}$ in. pure spectroscopic graphite rod $1\frac{1}{2}$ in. long.

Crater, outside diameter	0.223 in.
Crater, inside diameter	0.193 in.
Crater, depth	0.180 in.
Outside shoulder below crater rim	0.44 in.

Electrode, upper, $\frac{1}{4}$ in. pure graphite rod, cut to 0.06 in. hemispherical radius.

Precision balance

Iron rod, $\frac{1}{4}$ in. pure as obtainable for reference spectra.

Aluminum alloy, used as reference, and standard if composition is known.

Standards

The method of preparing standards was first suggested by Murata (in Fleischer, Murata, Fletcher, and Narten, 1952) and later by Bastron and others (1960). These standards are known as the pegmatite type, and the base consists of 60 parts of purified quartz, 40 parts of microcline, and 1 part of Fe_2O_3.

The elements to be sought are added to the matrix as pure oxides and thoroughly ground in agate or boron carbide mortars. For example, the elements Cu, Ni, Co, Ti, Mn, and Zr, which have similar burning characteristics and often occur together in nature, are added to pegmatite base to make one stock standard. For the micro work covering 69 elements, 20 stock standards were prepared and their groupings are shown in Table 1. The element groupings were diluted with pegmatite base to produce concentrations of 10, 5.6, 1.8, 0.56, 0.18, 0.056 and 0.018 per cent

TABLE 1. ELEMENT GROUPINGS USED IN THE PREPARATION OF MICROSPECTROCHEMICAL STANDARDS

Standard No.	Element groupings	Standard No.	Element groupings
1	W, Tl, Ru, Os, Ir	11	Rb, Cs, K, Li
2	Sc, Ge, B, Pb	12	Th
3	Sn, Mo, Be, Re, Cr, V	13	U
4	Hf, Mg, Sr, Ca, Ba	14	Pt, Pd, Rh, Au, Ag
5	Ga, Al	15	In, Zn, Sb, Bi, Cd
6	Tm, Tb, Lu, Ho, Eu	16	Te, P, Hg, As
7	Si	17	Na, Li, Cs, Rb
8	Sm, Pr, Nd, La, Ce	18	Zr, Cu, Mn, Ni, Ti, Co
9	Yb, Er, Gd, Dy, Y	19	Fe
10	Ta, Nb	20	F

of each element. These element percentages are the approximate midpoints of the brackets 10 to 3, 3 to 1, etc.

The elements Si, K, Al, and Fe require special standards because they are present in the matrix material. The Si standard matrix consisted of 8.8 parts Al_2O_3, 1 part Na_2CO_3, and 0.2 part Fe_2O_3. The K standard matrix components were: quartz, 8.1 parts; Al_2O_3, 0.88 part; Na_2CO_3, 1 part; and Fe_2O_3, 0.1 part. The Al matrix consisted of quartz, 25 parts; Na_2CO_3, 3 parts; $CaCO_3$, 1.7 parts, and Fe_2O_3, 0.3 part. The Fe matrix ingredients were quartz, 9.1 parts; Al_2O_3, 0.88 part; and Co_3O_4, 0.1 part. The matrix composition of the standards for these elements has been found satisfactory for the identification work on the basis of previous tests.

Each element grouping is used to prepare a standard plate. The electrodes are loaded with 1 mg. of the standard mixture containing 10, 5.6, 1.8, 0.56, 0.18, 0.056, and 0.018 per cent of each element. These electrodes are arced to completion at 8–9 amperes and 220 volts. Iron and aluminum alloy are also arced on each plate for reference spectra.

The following source and plate processing conditions are used:

Resistance	19 ohms
Amperes	8–9
Spectrograph	medium quartz
Slit	10μ
Optics	arc focused on collimating lens
Emulsion	I-N (Eastman)
Development	4 min. at 18° C. $\pm\frac{1}{2}$° C., D-19
Gap	5–6 mm.
Transmission	40% (neutral filters)

TABLE 2. SPECTRAL LINES USED IN THE MICRO-SPECTROCHEMICAL METHOD
Wave lengths in Å

Ag	3280.7, 3382.9, 5465.5
Al	2568.0, 2575.1, 2652.5, 2660.4, 3059.9, 3082.2, 3092.7
As	2288.1, 2349.8, 2860.5, 2780.2, 2898.7, 2492.9
Au	2675.9, 2427.9, 3122.8, 2748.3, 2700.9, 2641.5, 2352.7
B	2496.7, 2497.8
Ba	4934.1, 6141.7, 5853.7, 3071.6, 2634.8, 5535.5, 4554.0, 2335.3
Be	3131.1, 3130.4, 2348.6, 3321.3, 2350.7
Bi	3067.7, 2938.3, 2897.9, 3024.6, 2989.0, 2780.5, 2627.9
Ca	4226.7, 3179.3, 3158.9, 8542.1, 8662.1, 8498.0, 4456.6
Cd	3261.1, 2980.6, 2288.0, 2265.0, 4799.9, 2981.3, 2836.9, 3466.2, 2763.9
Ce	4222.6, 3272.3, 3056.8, 3055.2, 2651.0, 4186.6, 4040.7, 4012.4
Co	3453.5, 3412.6, 3412.3, 3044.0, 2521.4, 2663.5, 2649.9, 2519.8, 3465.8, 3449.2, 3283.5, 3243.8
Cr	4289.7, 4274.8, 4254.3, 2843.3, 2835.6, 2860.9, 2855.7, 2769.9, 2731.9
Cs	8521.1, 4593.0, 4555.5, 3347.4, 3247.5
Cu	3274.0, 3247.5, 2618.4, 2492.1, 2766.4, 2441.6, 2824.4, 2293.9
Dy	3407.8, 3393.6, 3385.0, 3280.1, 3251.3, 3645.4, 3454.3
Er	3264.8, 3230.6, 2964.5, 4419.6, 3499.1, 3372.8
Eu	2813.9, 2906.7, 2727.8, 2665.6, 2678.3, 2814.0, 2816.2, 4435.6
F	CaF_2 Band Heads 5291.0, 6036.9, 6064.4
Fe	3020.6, 2599.4, 2739.5, 2598.4, 3100.3, 3099.9, 3099.8, 2598.4
Ga	2943.6, 2944.2, 2874.2, 2719.6, 2500.2
Gd	3100.5, 3034.1, 3032.8, 3027.6, 2840.2, 2809.7, 3671.2, 3646.2, 3358.6, 3082.0
Ge	3039.1, 2651.6, 2651.2, 3269.5, 2691.3, 2740.4, 2589.2, 2533.3
Hf	3134.7, 3072.9, 3012.9, 2861.7, 2861.0, 2683.4, 2531.2, 2820.2, 2773.4
Hg	2536.5, 3131.8, 3131.5, 3125.7, 4358.3, 3650.2
Ho	3456.0, 3453.1, 3416.5, 3398.9, 4254.4
In	3256.1, 3039.4, 3258.6, 2753.9, 2710.3, 4511.3
Ir	3220.8, 2639.7, 2543.9, 2534.5, 2533.1, 2664.8, 2849.7, 2924.8
K	7698.9, 7664.9, 4047.2, 4044.1, 3447.7, 3446.4
La	3337.5, 3344.6, 3303.1, 3265.7, 2808.4, 2610.3, 3380.9, 4333.8, 4429.9
Li	6707.8, 6103.6, 3232.6, 2741.3
Lu	3077.6, 2615.4, 2619.3, 2613.4, 2685.1, 2392.2, 2911.4, 3198.1
Mg	2852.1, 2802.7, 2795.5, 2782.9, 2779.8, 2776.7, 4351.9
Mn	2576.1, 2605.7, 2593.7, 2939.3, 2933.1, 3044.6, 2584.3, 2798.3
Mo	3193.9, 3170.3, 2816.2, 3208.8, 3158.2, 2784.9, 2763.6, 4251.9
Na	5895.9, 5889.9, 3302.9, 3302.3
Nb	3225.5, 3094.2, 2931.5, 2876.9, 2875.4, 2746.1, 2745.7, 3358.4
Nd	4303.6, 4247.4, 3328.3, 3275.2, 4325.8
Ni	3050.8, 3002.5, 2992.6, 2943.9, 2907.5, 2798.7, 3492.9, 3433.6, 3414.8, 2320.1

TABLE 2—(*continued*)

Os	**Rb**	2552.4	**Ta**	2941.9	**W**
3058.7	7947.6	2555.8	2685.1	2619.9	2946.9
2909.1	7800.2	2545.2	2635.9	2605.2	2444.4
3301.6	4297.7	2822.1	2714.7	3372.8	2947.4
2838.6	3436.7	3019.3	2675.9	3224.2	2589.2
	3428.3	3369.0	2902.0	3088.0	4302.1
P	2810.6	3907.5	2891.8		4294.6
2553.3	2810.0	3911.8	4574.3	**Tl**	3049.7
2535.7		4246.8	3642.1	2767.9	
2554.9	**Re**		3317.9	5350.5	**Y**
2534.0	3464.7	**Si**	3311.2	2918.3	3242.3
	3460.5	2881.6	3012.5	3775.7	3216.7
Pb	2715.5	2516.1		3529.4	3200.3
2833.1	2674.3	2987.6	**Tb**	3519.2	3195.6
2802.0		2435.2	4278.5	2767.9	2984.3
2614.2	**Rh**	2532.4	3324.4	2379.6	2422.2
2873.3	3434.9	2438.8	3219.9		3086.9
2823.2	3396.9	2528.5	3218.9	**Tm**	3055.2
2663.2	3283.6	2524.1	3293.1	3133.9	3327.9
2393.8	3280.6		4318.9	3131.3	
	3271.6	**Sm**		4242.2	**Yb**
Pd	3263.1	3273.5	**Te**	3462.2	3289.4
3421.2	4374.8	3272.8	2385.8	3362.6	2970.6
3242.7		3254.4	2383.3	3151.3	3031.1
3251.6	**Ru**	3254.3		3362.6	2653.8
2763.1	2874.9	3253.9	**Th**		3107.9
3002.7	2735.7	4256.4	2837.3	**U**	2891.4
2922.0	2678.8	4424.4	2832.3	4244.4	3988.0
3114.0	2886.5		2870.4	4241.7	
3634.7	2734.3	**Sn**	2842.8	2882.7	**Zn**
	2810.0	3034.1	2703.9	4287.9	3345.0
Pr	2810.6	2839.9	2565.6	3566.6	3302.6
4241.0	3428.3	3009.1	4391.1	2837.3	3282.3
4225.3	3436.7	2863.3	4619.5	2837.2	2800.9
5322.8	4297.7	2850.6	4019.1		4810.5
5259.7		2661.2	3108.3	**V**	2770.9
4206.7	**Sb**	2571.6	2752.2	3185.4	2770.8
	2598.1	3262.3		3183.9	4680.1
Pt	2877.9	3175.0	**Ti**	3183.4	
3064.7	2769.9		3241.9	3202.4	**Zr**
2997.9	2718.9	**Sr**	3239.0	3198.0	3438.2
2659.5	2670.6	4607.3	3236.6	3214.7	3391.9
2650.8	3267.5	3464.5	3234.5	3212.4	2758.8
2646.9	2528.5	4305.4	3088.0	4379.2	2752.2
2803.2	2311.5	3380.7	3078.6	3276.1	2889.4
2639.4		3351.3	3072.9	3267.7	2888.0
4242.6	**Sc**	2569.5	3072.1	3184.0	3556.6
3042.6	2560.2		2956.1		3273.0

PROCEDURE FOR SAMPLES

A 1 mg. or less sample is weighed and placed in a prepared electrode with the aid of a stainless steel funnel. The sample is subjected to a direct current arc of 8–9 amperes for a period of 80 seconds. Iron and an aluminum alloy are also arced under similar conditions to produce reference spectra. The special shutter on the plateholder is opened at 22 seconds

TABLE 3. APPROXIMATE VISUAL DETECTION LIMITS FOR THE ELEMENTS DETERMINED BY THE MICROSPECTROCHEMICAL METHOD, BASED ON 1 MG. OF SAMPLE

Element	%	Element	%	Element	%
Ag	0.018	Hf	1.8	Re	0.18
Al	0.056	Hg	0.56	Rh	0.18
As	0.56	Ho	0.056	Ru	0.56
Au	0.018	In	0.018	Sb	0.56
B	0.056	Ir	0.56	Sc	0.018
Ba	0.056	K	0.018	Si	0.056
Be	0.018	La	0.056	Sm	0.56
Bi	0.018	Li	0.018	Su	0.056
Ca	0.056	Lu	0.056	Sr	0.056
Cd	0.18	Mg	0.018	Ta	0.56
Ce	0.18	Mn	0.018	Tb	0.18
Co	0.018	Mo	0.018	Te	10
Cr	0.018	Na	0.018	Th	0.56
Cs	0.56	Nb	0.18	Ti	0.018
Cu	0.018	Nd	0.18	Tl	0.56
Dy	0.18	Ni	0.056	Tm	0.018
Er	0.18	Os	0.56	U	0.56
Eu	0.18	P	0.56	V	0.018
F	0.56*	Pb	0.056	W	0.56
Fe	0.018	Pd	0.018	Y	0.018
Ga	0.018	Pr	0.56	Yb	0.018
Gd	0.18	Pt	0.018	Zn	0.18
Ge	0.056	Rb	0.056	Zr	0.18

* A second exposure is required for the fluorine determination.

and closed at 62 seconds, exposing the alkali portion of the spectrum on half of the total arcing time. Some refractory elements, such as Nb, Ta and Zr, require a second burn of the same sample.

When the sample is very limited, the x-ray spindle is weighed and previously determined blank is subtracted. The spindle, frequently con taining as little as 0.01 mg. of sample, is placed in the electrode cup an arced.

After the plates are processed, the quantities of unknown element are estimated by visual comparison of certain lines of the elements i question with those on previously prepared standard plates. Two meth ods are available to the operator for viewing the lines. The hand len with a millimeter scale and an enlargement of approximately ten times preferred by some operators. Also, the standard plates and the unknow plates may be placed in a comparator in juxtaposition with an enlarge ment of approximately twenty times.

The results are reported in the following brackets: 10 to 3, 3 to 1, 0.3 t

TABLE 4.—COMPARISON OF CHEMICAL[1] AND MICROSPECTROCHEMICAL ANALYSES OF MINERALS[2]

Element	Kimzeyite		Valleriite		Corvusite-like mineral		Sherwoodite	
	Chemical[2]	Spectrochemical	Chemical[2]	Spectrochemical	Chemical[2]	Spectrochemical	Chemical[2]	Spectrochemical
Si	4.5	3	0.84	1	0.3	0.3		
Al	5.5	3	4.3	1			1.3	1
Fe	9.9	>10	21.2	>10	1.6	3	.5	.3
Mg	< .03	.01	9.8	>10			.3	.3
Ca	21.4	>10	1.2	1	1.7	3	9.3	>10
Mn	< .08	.03	< .04	.01				
Ti	3.3	3						
Zr	22.2	>10						
Nb	.7	1						
Cu			17.6	>10				
V					44.1	>10	31.8	>10

Element	Metaheinrichite		New calcium vanadyl vanadate		Abernathyite	
	Chemical[2]	Spectrochemical	Chemical[2]	Spectrochemical	Chemical[2]	Spectrochemical
Fe	1.03	1	<0.07	0.03		
Ca	.07	.03	6.0	3		
K					3.6	3
Ba	11.9	>10				
U	43.6	>10			49.2	>10
As	9.5	>10			21.8	>10
Pb	.7	.3				
V			38.8	>10		
Sr			.85	1		

[1] Chemical analyses by Robert Meyrowitz and Blanche L. Ingram; results as oxides converted to elements.

[2] These minerals have been studied by x-ray diffraction patterns by Daphne R. Ross.

0.1, etc. When less than 1 mg. of unknown is arced, the results are adjusted by the appropriate factors.

The estimation of fluorine, the 69th element on our list, requires a separate exposure. An excess of calcium (0.2 mg.) is added to the electrode containing the unknown to produce the calcium fluoride molecular band which is recorded by the photographic emulsion.

Spectral Lines

The lines used for the estimations were selected from the M. I. T. Wavelength Tables (Harrison, 1939), and are listed as follows in Table 2, in order of decreasing usefulness. The percentage range for each line is not included because the wide variety of materials usually tested, and the interferences encountered, affect the sensitivities of the lines. Many different wavelengths are included to help the operator cross-check his results and also to allow for interferences.

The detectabilities of all elements are shown in Table 3. The percentages shown represent the lowest concentration detectable in the standard. Some combinations of elements affect the detectabilities; therefore approximate values are given. In unusually favorable materials, concentrations somewhat lower than the values given may be detected. In unfavorable materials the given detectabilities may not be attained for some of the elements.

Comparative Results

A comparison of chemical and microspectrochemical analyses of seven minerals is shown in Table 4.

The results provided by these techniques are visual estimates and should be given only a relative quantitative interpretation. Even under ideal conditions the brackets (10 to 3, 3 to 1, etc.) would overlap. Experience has shown that the judgment of the operator is important and his accuracy improves considerably with experience. When identifying a mineral, the information provided by these spectrographic techniques should be added to the *x*-ray diffraction data and (or) other chemical data before any final identification is made.

Acknowledgments

The authors wish to express their appreciation to Robert Meyrowitz and Blanche L. Ingram for the chemical analyses, Daphne R. Ross for completing the *x*-ray studies, Katherine V. Hazel for making a few of the earlier plates, and Joseph F. Abell and Edward C. Curtis for altering the plateholder.

References

Bastron, H., Barnett, P., and Murata, K. J., 1960. Method for the quantitative spectrochemical analysis of rocks, minerals, ores, and other materials by a powder d-arc technique: *U. S. Geological Survey Bull.*, **1084-G**, 165–182.

Fleischer, M., Murata, K. J., Fletcher, J., and Narten, P. F., 1952. Geochemical association of niobium and tantalum and its geological and economic significance: *U. S. Geol. Survey Circ.* **225**.

HARRISON, GEORGE P., 1939. Massachusetts Institute of Technology wavelength tables: John Wiley and Sons, New York.

STICH, J. N., 1953. The spectrographic identification of mineral grains: *U. S. Geol. Survey Circ.* **234,** 16 p.

Manuscript received January 6, 1961.

MINERALOGICAL NOTE

ALICE D. WEEKS

The method of spectrographic analyses of very small samples (1 mg. or less) described in the preceding article by C. L. Waring and H. W. Worthing has been extremely useful in many mineralogical problems. The method has been used effectively in the study of uranium, thorium, rare earth and vanadium minerals, but is equally applicable to other mineralogical or chemical studies. The spectrographic analyses are especially helpful in the identification of minerals which are difficult or unsatisfactory to determine by optical properties or which do not give unique *x*-ray diffraction powder patterns; they are very useful for very small mineral samples or if there is a question in sampling to make sure that the *x*-ray pattern and the chemical constituents are determined on the same material. A few examples follow.

1) Distinguishing minerals that have similar *x*-ray powder patterns or checking minerals in which one element commonly substitutes for another. Metatorbernite $Cu(UO_2)_2(PO_4)_2 \cdot 8H_2O$ and metazeunerite $Cu(UO_2)_2(AsO_4)_2 \cdot 8H_2O$ give similar *x*-ray patterns but the relative abundance of the phosphorus or arsenic anion can be checked spectrographically to give a satisfactory identification on a very small sample. An analysis also will check the presence of a significant amount of Ca, Ba, or various other elements that commonly substitute for the cation in the autunite and torbernite group of minerals. As with many hydration-sensitive minerals, the optical properties of the autunite-torbernite minerals vary with the hydration and commonly overlap from one species to another, resulting in inconclusive optical identification. The uranyl vanadates in some samples are difficult to distinguish with certainty from one another by optical properties either because of very fine grain size, hydration changes, or reaction with high index liquids. The distinctive cation can be checked spectrographically if necessary, on the *x*-ray spindle. This is particularly useful for the Ca and Ba in the metatyuyamunite ($Ca(UO_2)_2V_2O_8 \cdot 3\text{-}5H_2O$)-francevilleite ($Ba(UO_2)_2V_2O_8 \cdot 3\text{-}5H_2O$) pair which give very similar powder patterns.
2) Identification of small amounts of metamict minerals. This is often difficult because optical and *x*-ray determinations may be inconclusive. The spectrographic analysis may give the necessary additional data to complete the identification.
3) Very small samples or closely associated minerals which are difficult to distinguish and therefore present sampling problems. The sandstone-type uranium and vanadium deposits contain many fine-grained and closely associated minerals. It may not be possible to handpick enough pure mineral for many different tests or to tell by binocular examination whether thin coatings scattered on diflerent parts of an ore sample are the same mineral. In the study of the Colorado Plateau samples in

the early 1950's the problem of sampling was critical as we were trying to accumulate data on new minerals and to untangle conflicting data on poorly defined or incorrectly described species. Abernathyite ($KUO_2AsO_4 \cdot 3H_2O$) is an example of a mineral that was recognized very quickly as a new mineral on the basis of a 1 mg. spectrographic analysis showing the presence of K, U, and As. Without the spectrographic check it would have been placed simply in the meta-autunite group.

4) Checking samples for x-ray powder pattern standard films. This is another use of the spectrographic analysis (if chemically analyzed material is not available) and it helped to build up a large set of reference x-ray films of minerals in our laboratory as quickly as possible.
5) Aid in microchemical analyses of small mineral samples. Spectrographic analyses of 1 mg. or less material have provided useful checks in testing residues or various steps in the chemical procedure when the sample was not large enough to make all the tests of a complete chemical analysis

In the past ten years the method of spectrochemical analysis of very small samples has served as a very effective exploratory technique before making time-consuming mineral separations and complete chemical analyses, as a check on other methods of identification, and as a source of useful semiquantitative data on composition.

THE AMERICAN MINERALOGIST, VOL. 46, SEPTEMBER-OCTOBER, 1961

THE REACTION SERIES, GIBBSITE→CHI ALUMINA →KAPPA ALUMINA→CORUNDUM. II*

G. W. BRINDLEY, *Department of Ceramic Technology, The Pennsylvania State University, University Park, Pennsylvania.*

Since the experiments described in Part I (Brindley and Choe, 1961) were submitted for publication, an extensive study of the dehydration of gibbsite and of the crystallography of the transition aluminas has been published by Saalfeld (1960). Since the results of the two investigations agree in some respects and disagree in others, it will be worth while to make a brief comparison to see what general conclusions can be drawn.

In the first place, it should be emphasised that these studies are the first attempts to apply single crystal methods to obtain a better understanding of the reaction series, gibbsite→χ→κ→α-corundum. Saalfeld employed relatively large crystals of gibbsite which, under hydrothermal conditions, yielded the boehmite→γ→θ→α reaction series, and under atmospheric heating gave additionally the χ→κ→α series. In order to study the latter reaction series independently of the former, Brindley and Choe used <1 micron sized single crystals and electron diffraction technique.

Whether the crystal size of the gibbsite modifies the precise course of the χ→κ→α reactions is a question to be considered. The possible role of impurities, particularly alkali ions, has been mentioned by Saalfeld. The gibbsite sample used by Brindley and Choe contained Na_2O of the order of 0.3%.

FORMATION AND STRUCTURE OF χ-ALUMINA

The two investigations agree that χ-alumina is formed at about 270° C., that it is stable to about 850° C., that initially it contains considerable 'water' which is gradually lost at the higher temperatures, and that the structure is hexagonal with $a_H=5.56$ (S) or 5.57 (B & C).†

There is difference of opinion regarding the c parameter, given as 13.44 Å (S) and 8.64 Å(B & C). If the structures are composed of close-packed oxygen layers, then these cells contain respectively 6 and 4 such layers, of the same thickness as that of the octahedrally coordinated layers in gibbsite, as the following data show:

$$13.44/6 = 2.24 \text{ Å}$$
$$8.64/4 = 2.16 \text{ Å}$$

Thickness of Al-OH layer in gibbsite = 2.12 Å.

* Contribution No. 61-20 from the College of Mineral Industries, The Pennsylvania State University, University Park, Pa.

† Here, and elsewhere, (S) signifies Saalfeld, (B & C) Brindley and Choe.

The reflections for χ-alumina listed by Brindley and Choe with one exception have *even l* indices and therefore could be indexed equally well with the larger cell given by Saalfeld; $l=2$ becomes $l=3$, $l=4$ becomes $l=6$, and so on. The exceptional reflection, (003), is a weak x-ray powder line which does not fit the larger cell. Saalfeld comments on the disorderly packing of the oxygen layers in χ-alumina which produces considerable diffuse scattering parallel to c^* and possibly gives rise to non-integral maxima. It is conceivable that different layer sequences can be obtained by using different starting materials and/or heat-treatments.

The pseudo-cubic character of χ-alumina is more readily interpreted by Saalfeld's cell. The question can be asked, however, whether Saalfeld's use of relatively large crystals of gibbsite predisposed his material to transform to a state nearer to the cubic γ-form. Although the x-ray powder data for χ-alumina given by different investigators are sparse and mainly ill-defined, there appear to be divergencies which perhaps can be attributed to differences in the stacking sequences of the various χ-aluminas.

Formation and Structure of κ-Alumina

The two investigations agree that this form is stable in the range 800–1200° C. (S) or about 900–1200° C. (B & C), and that the structure is hexagonal. It is agreed also that more than one structural form exists in this temperature range. Saalfeld records no data for forms other than the one he labels κ, while Brindley and Choe record the hexagonal a-parameters for four different cells, of which one agrees with that given by Saalfeld. In this respect the electron diffraction data have provided more information than the x-ray data.

For material heated to temperatures between 900 and 1200° C. Brindley and Choe found the following:

7 patterns of χ-alumina, with $a_H = 5.53$ Å
54 patterns of κ_1-alumina, with $a_H = 16.78$ Å
4 patterns of κ_2-alumina, with $a_H = 9.70$ Å
4 patterns of ν-alumina, with $a_H = 5.54$ Å
2 patterns of ξ'-alumina, with $a_H = 5.37$ Å.

The designations κ_1 and κ_2 are used here for the first time. Saalfeld record an hexagonal parameter $a_H = 9.71$ Å which agrees with the relatively rare κ_2 found by Brindley and Choe. There is no ambiguity nor uncertainty in the electron diffraction data as regards the κ_1 and κ_2 forms; the κ_1 type with the large a_H parameter is much the more common. Figure shows that the κ_1 and κ_2 basal reciprocal nets are related in a simple way and that $hk0$ reflections of κ_2 can be indexed on the larger κ_1 cell; the converse is obviously not true. The indexing of the powder diagrams given by Saalfeld could be based equally well on the larger cell. The write

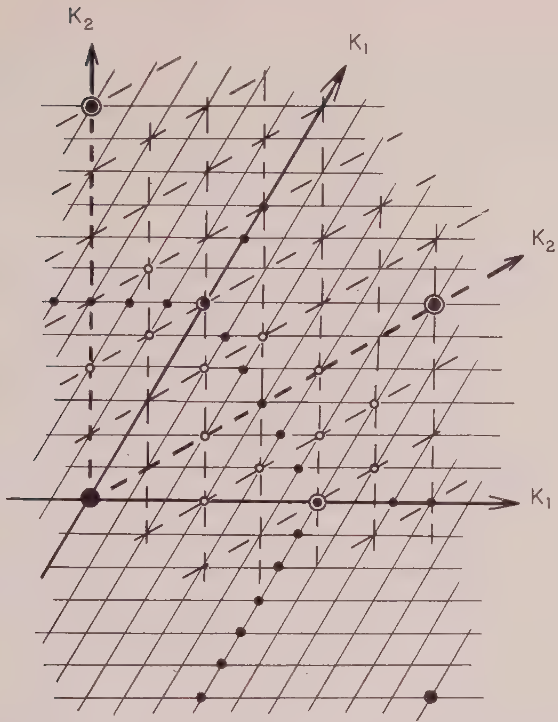

FIG. 1. Superposed single crystal, electron diffraction diagrams for $\kappa_1-Al_2O_3$ (hexagonal parameter $a_H=16.78$ Å) and $\kappa_2-Al_2O_3$ (hexagonal parameter $a_H=9.70$ Å). Solid circles show reflections from $\kappa_1-Al_2O_3$ and open circles from $\kappa_2-Al_2O_3$; continuous lines apply to κ_1 and dashed lines to κ_2. Observe that the κ_2 reflections can be indexed on the κ_1 axes, but the reverse is not valid.

does not question the correctness of the unit cell given by Saalfeld *for his material*, but at the same time it must be affirmed that the gibbsite studied by Brindley and Choe yielded predominantly a different unit cell for the same temperature of heat-treatment.

Saalfeld recognized that different structural forms occur in the temperature range 800–1200° C. and he named these "κ-like" structures. In the light of the two investigations, it can now be stated that several κ-type structures exist, and that, according to particular circumstances, *one or other of these may be dominant, but not always the same structure.*

CONCLUSIONS

It appears that the crystallography of the transition aluminas χ- and κ- can vary according to precise experimental conditions. χ-alumina is essentially hexagonal with $a_H=5.56$ Å, with disorderly stacking in the c-

direction and a variable c-parameter corresponding to 6 or 4 layers. A number of κ-type forms are recognized and at least two hexagonal cells are recognized with a_H respectively 16.78 and 9.71 Å. These are now called κ_1 and κ_2. The forms ν- and ξ'-alumina, previously noted by Cowley (1953), have also been observed in the same temperature range in which the κ-aluminas are found.

Acknowledgment

This work forms part of the program on high-temperature reactions, supported by the National Science Foundation, Grant No. G-5799.

References

Brindley, G. W., and Choe, J. O. (1961), *Am. Mineral.*, **46**, 771–785.

Cowley, J. M. (1953), Structure analysis of single crystals by electron diffraction. III. Modifications of alumina, *Acta Cryst.*, **6**, 846–853.

Saalfeld, H. (1960), Strukturen des Hydrargillits und der Zwischenstufen beim Entwässern, *N. Jb. Miner., Abh.*, **95**, 1–87.

THE AMERICAN MINERALOGIST, VOL. 46, SEPTEMBER-OCTOBER, 1961

NOTES AND NEWS

A PRELIMINARY NOTE ON THE RELATIVE STABILITY OF ANDALUSITE, KYANITE, AND SILLIMANITE

DANIEL F. WEILL AND WILLIAM S. FYFE, *Department of Geology, University of California, Berkeley, California.*

INTRODUCTION

In recent years there has been considerable interest in the stability relations of the polymorphic modifications of Al_2SiO_5 and their high-temperature breakdown products, mullite+silica. Clark, Robertson, and Birch (1957) synthesized sillimanite from kyanite at $1{,}340 \pm 30°$ C. and $18{,}600 \pm 100$ bars in $7\frac{3}{4}$ hours. They converted sillimanite to kyanite in $2\frac{3}{4}$ hours at $1{,}220 \pm 50°$ C. and $23{,}000 \pm 200$ bars. From syntheses based on various other starting materials the same authors established a phase boundary between the two polymorphs in the range 900–1,300° C. and 18,000–24,000 bars. This boundary was extrapolated back to lower temperatures and pressures within the metamorphic range. The only certain deduction that can be drawn from a synthesis is that the products have a lower chemical potential than the reactants. It is obvious that if the kinetics of reversibility of a polymorphic transition are highly unfavorable, a synthesis from other phases having much higher free energy than either polymorph can lead to a misleading version of the equilibrium phase diagram. The reversibility between kyanite and sillimanite established by Clark, Robertson, and Birch, *ibid.*, in relatively short runs indicates that their equilibrium curve is well founded in the high temperature and pressure range. Extrapolation back to metamorphic conditions may be less reliable for it is based largely on results of syntheses at conditions where the polymorphic transitions were too slow to observe. Moreover there are no reliable experimental data on the stability relations between sillimanite, andalusite, and mullite+silica.

In an attempt to provide further data at lower temperatures and pressures, the writers made more than a dozen runs starting with various mixtures of andalusite, kyanite, sillimanite, and water as a solvent, in the range 700–900° C. and 700–2,000 bars. It was hoped that the most stable phase would be augmented at the expense of the less stable phases, thus overcoming the difficulty of nucleation which must certainly be significant in the kinetics of conversion. In experiments of over four weeks duration no hint of conversion was obtained. Clearly, in this range reversibility is difficult to establish, and syntheses might therefore be correspondingly unreliable.

In a further effort to overcome the difficulty, the indirect method of

measuring the solubilities of the polymorphs in a suitable solvent has been attempted. The results obtained to date are set out below.

Experimental

Fused cryolite (Na_3AlF_6) is well known as a solvent of alumina, in which capacity it has long been used for the electrolytic preparation of aluminum. Preliminary experiments indicated that it is also a powerful solvent of aluminosilicates.

Various mixtures in the Al_2SiO_5-Na_3AlF_6 system were sealed in

TABLE I. COMPOSITIONS OF MELTS IN EQUILIBRIUM WITH CORUNDUM AND ANDALUSITE, KYANITE, AND SILLIMANITE AT 1010° C., 1 ATMOSPHERE (FIGURES FOR KYANITE ARE ONLY LIMITING VALUES DUE TO THE GROWTH OF MULLITE). ANDALUSITE FROM MINAS GERAIS, BRAZIL; KYANITE FROM BUNCOMBE COUNTY, N. CAROLINA; SILLIMANITE FROM BENSON MINES, N. Y.

Polymorph	Solution: SiO_2/Na_3AlF_6 wt. ratio	Component	Composition wt. %		Composition mole %	
Andalusite	2.19±0.09	Al_2O_3	14.0	17.0	11.0±0.1	13.5±0.1
		SiO_2	59.0±0.8	57.0±0.7	78.8±0.4	76.5±0.5
		Na_3AlF_6	27.0±0.8	26.0±0.7	10.2±0.4	10.0±0.5
Kyanite	3.17±0.17	Al_2O_3	14.0	17.0	10.3±0.1	12.7±0.1
		SiO_2	65.3±0.8	63.1±0.8	82.3±0.5	80.1±0.5
		Na_3AlF_6	20.7±0.8	19.9±0.8	7.4±0.4	7.2±0.5
Sillimanite	1.75±0.06	Al_2O_3	14.0	17.0	11.4±0.1	14.1±0.1
		SiO_2	54.7±0.7	52.8±0.7	76.1±0.4	73.9±0.5
		Na_3AlF_6	31.3±0.7	30.2±0.7	12.5±0.4	12.0±0.5

platinum tubes, taken to 1,010° C. at atmospheric pressure, held unde these conditions for 200–1,000 hours, quenched and examined under th polarizing microscope and with x-ray diffraction with a view to obtainin the composition of the solution. The composition of the mixture at whic the Al_2SiO_5 polymorphs just disappeared into the melt could be easil determined in this fashion. These compositions are in the range 80–90% Al_2SiO_5 by weight. The x-ray diffractometer technique is sensitive to 5% or even less Al_2SiO_5. The compositions thus measured are accurate t better than 1%. Microscopic examination yields an even closer toler ance. The dissolution process is incongruent resulting in the forma tion of corundum and liquid, so that our measurements give only th SiO_2/Na_3AlF_6 ratio in the liquid phase resulting from the melting of eac

of the polymorphs. The compositon of the liquid phase in equilibrium with each of the polymorphs was then determined by taking mixtures in the SiO_2–Na_3AlF_6–Al_2SiO_5 system (using the SiO_2/Na_3AlF_6 ratios previously determined) and observing at which composition corundum completely disappeared into the melt. Runs varying in duration from 200–1,000 hours gave consistent results. Since the region studied is at the Al_2O_3-poor corner of the ternary system, the accuracy of these latter determinations is no better than $\pm 1.5\%$. According to Rolin (1960) the Al_2O_3liquidus in the Al_2O_3-Na_3AlF_6 system at 1,010° C. lies at 13–14% Al_2O_3 by weight. This is within 2 to 3 per cent of that measured in this study at SiO_2/Na_3AlF_6 weight ratios varying from 1.7 to 3.3. The addition of SiO_2 in the ternary system seems to have very little effect on the weight percentage of Al_2O_3 in the melt in equilibrium with corundum. It follows that in comparisons of the equilibrium melt compositions for the three polymorphs, the Al_2O_3 content cannot vary the full range (14–17%) given in Table I. SiO_2 and Na_3AlF_6 content are therefore given for each of the limiting values of Al_2O_3 content.

Discussion

The thermodynamics of the incongruent solution may be approached as follows. For andalusite (A) in equilibrium with melt:

$$\mu^{(A)} = \mu^{0}_{SiO_2} + RT \ln \frac{a^{(sol\ A)}_{SiO_2}}{a^{0}_{SiO_2}} + \mu^{(sol\ A)}_{Al_2O_3} \qquad 1.$$

Similar expressions may be written for kyanite (K) and sillimanite (S). Corundum is in equilibrium with the melt in each case so that:

$$\mu^{(sol\ A)}_{Al_2O_3} = \mu^{(sol\ K)}_{Al_2O_3} = \mu^{(sol\ S)}_{Al_2O_3} \qquad 2.$$

Subtracting expressions of type 1 from each other and making use of 2, the free energy relations between the polymorphs are summarized as follows:

$$\mu^{(A)} - \mu^{(K)} = RT \ln \frac{a^{(sol\ A)}_{SiO_2}}{a^{(sol\ K)}_{SiO_2}};\ \mu^{(A)} - \mu^{(S)} = RT \ln \frac{a^{(sol\ A)}_{SiO_2}}{a^{(sol\ S)}_{SiO_2}};\ \text{and}\ \mu^{(K)} - \mu^{(S)} = RT \ln \frac{a^{(sol\ K)}_{SiO_2}}{a^{(sol\ S)}_{SiO_2}} \qquad 3.$$

From the data in Table I we conclude that

$$a^{(sol\ K)}_{SiO_2} > a^{(sol\ A)}_{SiO_2} > a^{(sol\ S)}_{SiO_2},$$

and therefore at 1,010° C., 1 atm.

$$\mu^{(K)} > \mu^{(A)} > \mu^{(S)}$$

so that the most stable polymorph is sillimanite. This does not mean that sillimanite necessarily is stable relative to mullite+silica. It should be

noted also that kyanite dissolved in cryolite was rapidly converted to well crystallized mullite, indicating the potential of fused salts for silicate synthesis. Entropy data for andalusite and sillimanite according to Kelley (1950 and 1960) show that in the range 127–1,327° C., $S_A > S_S$ Since $(\partial\mu/\partial T)_P = -S$ we conclude from the solubility and entropy data that andalusite is metastable with respect to sillimanite in this temperature range. According to x-ray measurements made by the writers from calibrated Weissenberg photographs: $V_A = 51.43 \pm 0.10$cc/mole and $V_S = 49.78 \pm 0.10$cc/mole. The thermal expansion of the phases in question would be most anomalous if the sign of ΔV were to change over the range of metamorphic temperatures. Thus if the compressibility is neglected, from $(\partial\mu/\partial P)_T = V$ we might conclude that andalusite has no true stability field with respect to sillimanite at metamorphic pressures and temperatures.

It must be stressed that the preceding treatment is valid only for the phases which do not deviate appreciably from the ideal composition Al_2SiO_5. The effect of compositional variations on the stability fields of the three minerals cannot be discounted.

While more data at lower temperatures are essential, the possibility that andalusite is metastable in nature need not be considered improbable because of the common geological occurrence of the mineral. The persistence of unstable phases in geologic environments is well established (*e.g.* order-disorder in feldspars, cristobalite, boehmite, etc.). In fact the lack of reactivity of the polymorphs makes such metastable persistence probable.

Estimates of the free energy differences between the three polymorphs of Al_2SiO_5 could be made if the nature of the species in solution as well as their activity coefficients were known. It is hoped that the accumulation of more data will make such a quantitative approach possible.

Acknowledgments

Dr. Adolf Pabst of the University of California Department of Geology kindly assisted the writers in the single crystal x-ray work. The research was supported by The National Science Foundation and The Petroleum Research Fund, American Chemical Society.

References

Clark, S. P., Robertson, E. C., and Birch, F. (1957), Experimental determination of kyanite sillimanite equilibrium relations at high temperatures and pressures: *Am. Jour. Sci.*, **255**, 628–640.

Kelley, K. K. (1950), Entropies of inorganic substances. Revision (1948) of data and method of calculation: *U. S. Bur. Mines, Bull.* **477**.

Kelley, K. K. (1960), High-temperature heat-content, heat-capacity, and entropy data for the elements and inorganic compounds: *U. S. Bur. Mines, Bull.* **584**.
Rolin, M. (1960), Binary diagram of cryolith-aluminium, Part I, Experimental: *Bull. Soc. Chim. France,* 1201–1203.

THE AMERICAN MINERALOGIST, VOL. 46, SEPTEMBER-OCTOBER, 1961

NATROLITE FROM HOUDAILLE INDUSTRIES QUARRY BOUND BROOK, SOMERSET COUNTY, N. J.

John Sinkankas

Compared to other quarries in the first Watchung sill of Northern New Jersey, the Houdaille Industries Quarry located 1.7 miles northwest of Bound Brook, Somerset County, New Jersey, produces few specimens of interest to the collector. A visit to the quarry in early summer of 1960 in company with Mr. Gene Vitali of North Haledon, N. J., produced specimens of ordinary calcite and, unexpectedly, natrolite crystals of unusual size and transparency. The latter are quite unlike any hitherto reported from New Jersey localities.

The Houdaille Quarry, commonly called the Chimney Rock quarry, is an oval opening approximately one third mile in length penetrating the thick basalt sill of the First Watchung Mountain. An excellent map of basalt and diabase outcrops, including the Watchung sills, plus descriptions of New Jersey trap minerals, appears in Mason (1). Current quarrying is confined (1960) to the west wall where enormous slopes of broken basalt are searched for minerals by local collectors. The exposed section of sill is divided by parallel, vertical joints, the most prominent of which are oriented in a north-south direction. Thin calcite-filled veins are emplaced in joints, and, in favorable sites, open into lenticular cavities lined with good crystals of calcite and occasionally other minerals.

Due to chloritization of wall rock, vein material separates readily from basalt and entire sections may be found in the blast rubble. One such mass revealed several small cavities lined with large rhombohedral crystals of calcite with open spaces criss-crossed by prismatic crystals of natrolite as shown in Fig. 1. Natrolite prisms were found coated almost completely by very small scalenohedral crystals of calcite of uniform size and habit. Underneath each such coating was found a layer of minute colorless gypsum crystals, simple in habit, and perfectly transparent except for a slight pearly luster upon the $b(010)$ faces. Beneath this layer and immediately in contact with the natrolite was found more gypsum as a white spongy inner layer consisting of numerous

interlocked, partly-developed crystals. Centers of cavities were filled almost entirely by rhombohedral calcite which also enclosed the crystals of natrolite. Where exposed in openings, rhombohedral calcite formed crystals of about one and a half inches in length of simple habit but with curved faces. No other minerals were recognized from the vein.

Natrolite developed at an early stage within the fissure opening but possibly was not the first mineral to form in the entire fissure system in

FIG. 1. Natrolite calcite-gypsum vein filling, Houdaille Quarry. The section shown is approximately 6 inches in height. The formless mass in the center is a remnant of calcite filling remaining behind after acid treatment.

view of the presence of gypsum. The latter is known to form from anhydrite in other basalt occurrences, especially in the quarries near Montclair, Great Notch and Paterson some miles north of Bound Brook. However, in this instance at least, there was no valid evidence of the presence of anhydrite. After formation of natrolite, gypsum deposited upon its crystals and was in turn succeeded by rhombohedral calcite. The last mineral to form was scalenohedral calcite.

Natrolite prisms range in size from extremely slender individuals scarcely as thick as a sewing needle to a few stout prisms one quarter inch in diameter and two inches in length. The majority are deeply etched on surfaces not coated with gypsum and lightly etched under-

neath such coatings. Although hydrochloric acid had to be used to dissolve much of the obstructing calcite, its effect upon the natrolite was not very pronounced when prism sections were compared before and after acid treatment. Many of the natrolite crystals were broken into segments and later cemented together with gypsum. A very few terminated crystals were found, each termination displaying a number of pale grayish-green phantoms (chlorite?) corresponding to pyramidal faces. The majority of crystals and fragments are absolutely colorless and transparent while a great many are free of inclusions of any kind.

In addition to *m*(110) and *o*(111), *b*(010) is present on almost all larger crystals which are not so severely corroded as to destroy all plane surfaces. This latter form bevels the edges between *m* faces selectively, some bevels being scarcely more than a trace but others being as broad as adjacent *m* faces. Upon a single crystal there may be several *b* faces, each of widely varying width.

Readings obtained upon the natrolite, using a Rayner refractometer and a polished prism section of a natrolite crystal, are as shown below compared to Hey values kindly supplied by Brian Mason (2).

Natrolite, Houdaille Quarry	Natrolite (M. H. Hey)
Biaxial, positive	Biaxial, positive
$\alpha=1.479$	$\alpha=1.479$
$\beta=1.481$	$\beta=1.482$
$\gamma=1.491$	$\gamma=1.491$
$\gamma-x=$ .012	$\gamma-x=$ .012

Additional optical tests by Brian Mason (2) show that the Houdaille quarry material exhibited straight extinction, $Z=c$, while an x-ray check produced a pattern for natrolite.

References

1. Mason, Brian H., Trap Rock Minerals of New Jersey; *Bulletin 64, Bureau of Geology & Topography, State of N. J.* Department of Conservation and Economic Development; Trenton, 1960.
2. Personal communication.

THE AMERICAN MINERALOGIST, VOL. 46, SEPTEMBER-OCTOBER, 1961

MONOCLINIC KAOLINITE FROM KOČEVJE MINE, YUGOSLAVIA

ILIJA KRSTANOVIĆ, *Department of Mineralogy and Petrology, University of Beograd*, AND STANIŠA RADOŠEVIĆ, *Zavod za ispitivanje nuklearnih sirovina, Beograd, Yugoslavia.*

During the field work in the Kočevje coal mine, p.r.Slovenia, one of the authors (S. Radoševič) found, in a lens of sand below the coal seam, crystals of a mineral which was considered at first to be normal kaolinite. DTA and dehydration curves showed characteristics identical with the other members of the kaolin group, but the powder diagram, taken in a 19 cm. camera using Cu filtered radiation, differed from that of kaolinite (Brindley and Robinson, 1946).

Single crystal Laue, oscillation and Weissenberg photographs were taken using Cu, Co and Fe filtered radiation, on many crystals and they clearly revealed monoclinic symetry. The length of the axis are:

$$a = 5.13 \pm 0.02 \text{ Å} \qquad b = 8.90 \pm 0.02 \text{ Å} \qquad c = 21.5 \pm 0.5 \text{ Å}$$

with the angle β lying close to 90°.

The chemical analysis of the carefully selected crystals and the calculated structural formula given below, show that this mineral is kaolinite in which aluminium is partly substituted by ferric iron.

SiO_2	44.62	CaO	0.07
Al_2O_3	35.46	MgO	0.72
Fe_2O_3	4.51	K_2O	0.51
TiO_2	0.20	Na_2O	0.05
MnO	0.07	H_2O^+	13.51
			100.35

$$(Al_{1.84}\overset{+3}{Fe}_{0.15})Si_{1.96}O_{5.04}(OH)_{3.96}$$

REFERENCE

1. BRINDLEY, G. W. AND ROBINSON, K., *Min. Mag.*, **27**, (1946).

SYMPOSIUM

The Geological Society of Czechoslovakia and the Faculty of Natural Sciences, Charles University, Prague, will arrange under the auspices of the Czechoslovak Academy of Sciences a symposium on "Problems of the origin of postmagnetic ore deposition (with special reference to the geochemistry of ore veins) in Prague, Czechoslovakia, September 16–21, 1963.

The symposium will consist of two parts: (1) Short written contributions and (2) Invited papers. Excursions will be held both before and after the symposium.

The Chairman of the organizing committee is J. Kutina, and the General Secretary M. Štemprok. Correspondence should be addressed to

General Secretary of the Symposium,
Ústřední ústav geologický
19. Malonstranské nám.,
Praha 1, Malá Strana, Czechoslovakia

ERRATUM

On page 567 of the May-June 1961 issue of the *American Mineralogist*, in the optical properties of nobleite, the correct orientation should read $Y = b$, and not $Y > b$ as printed.

Dr. Esper S. Larsen, III, a Fellow of the Mineralogical Society of America, died on October 9, 1961.

NEW MINERAL NAMES

Gutsevichite

E. A. Ankinovich. Gutsevichite, a new mineral. *Sbornik Nauch. Trudy Kazakh. Gornomet Inst.* No. **18,** 125–130 (1959); from an abstract by E. M. Bonshted-Kupletskaya in *Zapiski Vses. Mineral. Obshch.*, **90,** 104 (1961).

The mineral occurs as irregular crusts and concretions and as cavity-filling in the zon of oxidation of V-containing shales of the Middle Cambrian in northwestern Kazakhstan Color yellow-olive, tobacco-green, to dark brown, in sections greenish-yellow to yellov brown. Isotropic, n 1.560–1.575 (olive), 1.575–1.590 (tobacco-green), 1.595–1.606 (brown). Luster waxy to dull, H. $2\frac{1}{2}$, G. 1.90–2.00.

Analyses by S. I. Potok and T. L. Vileshina of yellow-olive and dark brown varietie gave, resp., MgO 1.2, 1.4; CaO 2.7, 2.3; BaO 1.5, 1.1; Al_2O_3 25.9, 24.4; Fe_2O_3 2.0, 4.7; V_2O 2.3, 2.9; V_2O_5 11.7, 14.1; P_2O_5 17.6, 15.9; SO_3 1.2, 1.2; SiO_2 1.1, 2.8; H_2O^+ 14.7, 14.3; H_2O 18.2, 15.2, sum 100.1, 100.3%, stated to correspond to $(Al, Fe)_3[(P, V)O_4]_2(OH)_3 \cdot 7\frac{1}{2}$–8 H_2O. Easily soluble in cold dilute acids. In the closed tube gives much water, having weakly acid reaction. The heating curve shows endothermal effects at 190° and 820–840 and an exothermal effect at 520–560°.

The most intense x-ray lines (yellow-olive) are 4.082 (10), 2.506 (9), 1.820 (8), 1.44 (7), 3.510 (5).

The name is for V. P. Gutsevich, geologist, of Kazakhstan.

Discussion.—The abstractor comments that 10% and 11.7% of the first and secon analyses were discarded in calculating the formula, without any statement of what im purities were present, and that the "composition needs to be made more precise." Th mineral appears to differ from al'vanite, satpaevite, and steigerite, previously describe from the same locality, and from schoderite, all aluminum vanadates.

Michael Fleischer

Fynchenite

E. M. Bonshtedt-Kupletskaya, abstract in *Zapiski Vses. Mineral. Obshch.*, **90,** 10 (1961).

This is the Russian transliteration of the name Feng-huang shih (fenghuanglite), se *Am. Mineral.* **45,** 754–755 (1961).

M. F.

Arsenothorite

E. M. Bonshtedt Kupletskaya, abstract in *Zapiski Vses. Mineral. Obshch.*, **90,** 1C (1961).

This name is given to the material named Shen-t'u-shih (or Shen-t'u-lite) in the origin (See *Am. Mineral.* **45,** 755 (1960)). Arsenothorite is the translation of the Chinese name.

M. F.

Yanshainshynite

Cheng-Chi Kuo. Jiningite, a new variety of thorite. *Kexue Tonghao* (*Scientia*) **1959,** N 6, 206–207 (in Chinese), from an abstract by E. M. Bonshtedt-Kupletskaya, *Zapisi Vses. Mineral. Obshch.* v. **90,** 108 (1961).

A calcium thorium phosphate-silicate. An incomplete analysis gave SiO_2 10.04, $P_2($

11.77, ThO_2 42.84, CaO 14.31, TR_2O_3 0.24, MgO 0.23, MnO 0.06, PbO not detd., Fe_2O_3 4.31, Al_2O_3 0.48, H_2O 9.19, total 93.47%.

DISCUSSION.—Insufficient data.

M. F.

Redledgeite

H. STRUNZ. "Chromrutil" von der Red Ledge Mine ist kein Rutil. Redledgeit: *Neues Jahrb. Mineral., Monatsh.* **1961**, p. 107–111.

Chromrutile was described by Gordon and Shanon in 1928 (*Am. Mineral.*, **13**, 69, Dana's System, 7th Ed., Vol. I, p. 560). Analysis by Shannon gave CaO 0.76, MgO 5.52, Al_2O_3 0.57, Fe_2O_3 0.80, Cr_2O_3 16.61, SiO_2 5.51, TiO_2 69.71, loss on ign. 1.48, sum 100.96%.

Weissenberg photographs of type material show it to be tetragonal, space group $I4_1/a$, a 20.32, c 5.84 Å. G (suspension) 3.72. From Shannon's analysis the unit cell contains

$$Ca_{0.70}Mg_{7.06}Cr_{11.27}Fe_{0.52}Al_{0.58}Ti_{44.99}Si_{4.73}H_{8.47}O_{130}$$

or nearly

$$Mg_8Cr_{12}Ti_{46}Si_4O_{122}(OH)_8$$

or, if TiO_4 is replaced by $(OH)_4$,

$$Mg_8Cr_{12}Ti_{48}Si_4O_{130}$$

An indexed x-ray powder pattern (31 lines) is given. The strongest lines are 3.199 (10), 2.454 (8), 1.583 (8), 2.215 (7), 1.882 (7), 1.391 (7), 3.551 (6), 1.681 (6).

Since the mineral is not a variety of rutile, the new name redledgeite is suggested for the locality, the Red Ledge Mine, Nevada County, California.

M. F.

Five new unnamed minerals

JOSEPH A. MANDARINO AND SCOTT J. WILLIAMS. Five new minerals from Moctezuma, Sonora, Mexico: *Science,* **133,** no. 3469, 2017 (1961).

The following preliminary data are given. Mackayite, emmonsite, tellurite, native Te, and paratellurite have also been found in the deposit.

(1) Minute yellow plates with high adamanitine luster give x-ray powder data agreeing with those of Bystrom (Arkiv Kemi, Mineral., Geol. 24A (1947) for synthetic Pb_2OF_2.

(2) Zinc tellurite or tellurate occurs as small, brown, hexagonal prismatic crystals terminated by a bipyramid. Spectrographic analysis gave only Zn and Te as major constituents. Uniaxial, positive, with ω1.85±0.01, ϵ1.93±0.01. The x-ray powder pattern does not match that of any known Te mineral; the strongest lines (Å.) are 8.1 (vs), 4.04 (s), 2.75 (s).

(3) Manganese-zinc tellurite or tellurate is a red to purple mineral occurring in platy masses. Spectrographic analysis showed only Mn, Zn, and Te as major constituents. G. (on 20 mg.) 5.01±0.02. Optically biaxial, positive, β1.89, γ>2.10, 2V 60° (estimated). The x-ray powder data differ from those of known Te minerals; the strongest lines (Å) are 2.98 (vs), 3.30 (s), 1.62 (s), 4.00 (s-), 4.93 (ms), 2.21 (ms).

(4) Manganese tellurite or tellurate occurs as pale green to colorless platy masses and occasionally as small euhedral platy crystals, of octagonal shape. Spectrographic analysis shows major Mn and Te, less Zn. The physical properties are variable, indicating an isomorphous series. Average values are G. 5.05, α and β approximately 1.89, γ about 2.0, 2V 15° (estimated), optically biaxial, positive. The strongest x-ray spacings (Å) are 2.03 (s), 3.36 (s-), 2.61 (s-).

(5) Iron tellurite or tellurate occurs as red-brown botryoidal coatings. Spectrographic analysis showed only Fe and Te as major constituents. Amorphous to *x*-rays. G. about 3.7. Optically very weakly anisotropic with mean n 1.885 ± 0.005.

M. F.

Carbocernaite

A. G. Bulakh, V. V. Kondrat'eva, and E. N. Baranova. Carbocernaite, a new rare earth carbonate: *Zapiski Vses. Mineralog. Obshch.*, **90**, 42–49 (1961) (in Russian).

Analysis was made by E. N. B. on a 0.4 g. sample containing not more than 2–3% total of impurities (chlorite, pyrite, sphalerite, and hydrous Fe oxides). It gave CaO 15.10, SrO 12.43, BaO 3.20, rare earths 26.10, Na_2O 5.11, CO_2 31.82, H_2O^+ 2.10, H_2O^- 0.30, F, Cl, not found, Fe_2O_3 1.50, Al_2O_3 0.30, insol. 1.40, sum 99.36%. Spectrographic analysis showed also Mn and Zn about 0.01%. Chromatographic analysis by K. A. Baklanova of the rare earths gave La_2O_3 42.40, CeO_2 42.40, Nd_2O_3 8.50, Sm_2O_3 4.25, Y_2O_3 2.90, sum 100.05%. The analysis corresponds to the formula $(Ca_{0.37}\ Na_{0.23}\ TR_{0.22}\ Sr_{0.16}\ Ba_{0.03})_{1.01}\ CO_3$, neglecting the water. The mineral is easily soluble in dilute HCl. A D.T.A. curve, by V. P. Ivanova, shows two sharp endothermal effects at 650° and 950°, a small endothermal effect at 700°, and a minimum at 1200°. The double endothermal effect suggests that the mineral may be a double salt like dolomite.

Goniometric study shows carbocernaite to be orthorhombic with {100} most prominent, {010}, {001}, {021}, {540}, and {210} minor, {305} and {210} vicinal. Laue and oscillation photographs showed the mineral to be orthorhombic, space group not given, a 6.39 ± 0.01, b 7.27 ± 0.02, c 5.21 ± 0.01 kX, $a:b:c = 0.8791:1:0.7166$, $Z = 4(RCO_3)$. Cleavage poor in three directions: {100}, {021}, {010}.

Indexed *x*-ray powder data are given (59 lines) (on coarse material; fine grinding caused poor reflections). The strongest lines are 3.00 (10)(021), 2.015 (9)(202), 1.813 (8)(231), 1.174 (8, diffuse) (252), 2.60 (7, diffuse) (002), 2.29 (7, diffuse)(112), 1.278 (7)(500).

Colorless, transparent, but turbid white, yellowish, rose, or brown when altered. Luster vitreous on crystal faces, greasy on fractures. H. 3, brittle. G (pycnometer) 3.53, calcd. 3.53. Optically biaxial, negative, ns α 1.569, β 1.679, γ 1.708 (all ± 0.002), 2V (calcd.) 52°, dispersion marked $r > v$, $X = b$, $Y = a$.

The mineral occurs in dolomite-calcite carbonatite veins 0.5–1 m. in width in pyroxenites and ijolites of the Vuorjärvi massif, Kola Peninsula, as accessory grains and as crystals on walls of cavities, closely associated with chlorite and ankerite. Other associated minerals are sphalerite, galena, pyrite, and barite, and in the cavities alstonite, anatase, quartz, and zeolites.

The name is for the chemical composition.

Discussion. Very close in composition to burbankite (Pecora and Kerr, *Am. Mineral.* **38**, 1169–1183 (1953)), and the structures may be related (burbankite has a 10.53 Å = nearly twice c of carbocernaite, and c 6.47 Å = nearly a of carbocernaite). It would be interesting to study the thermal relationship further. The differences in optical properties (birefringence of burbankite = 0.012) suggest a very different arrangement of the carbonate groups.

M. F.

Vlasovite

R. P. Tikhonenkova and M. E. Kazakova. Vlasovite, a new zirconium silicate from the Lovozero massif. *Doklady Akad. Nauk S.S.S.R.*, **137**, no. 4, 944–946 (1961) (in Russian).

Analysis by M.E.K. gave SiO_2 55.76, ZrO_2 28.11 (including HfO_2 1.7), TiO_2 trace, Nb_2O_5 0.33, Al_2O_3 0.20, Fe_2O_3 0.10, FeO none, MgO 0.06, MnO trace, CaO 0.49, rare earth

none, Na_2O 14.03, K_2O 0.68, H_2O^- 0.09, H_2O^+ 0.32, F 0.20, sum 100.37−(0=F_2 0.08) =100.29%, corresponding closely to $Na_2ZrSi_4O_{11}$. Spectrographic analysis showed traces of Be, Pb, Cu, and Sn. The mineral is nearly insoluble in HCl and HNO_3, dissolves easily in a mixture of HF and H_2SO_4.

Vlasovite is colorless; the border zones of large grains (up to 0.5×1×1.5 cm.) are light-brown due to the presence of numerous dust-like inclusions. Luster vitreous to pearly on the cleavage, greasy elsewhere, Hardness 6 (770 kg/mm² on the PMT-3 apparatus). G. 2.97 (suspension), altered material had G. 2.95. Colorless material does not luminesce in UV light, altered parts luminesce a strong orange-yellow. Optically biaxial, negative, with *n*s: α 1.607, β 1.623, γ 1.628, 2V 50–56°, plane of optic axes parallel to a distinct cleavage on (010). Disperision distinct, $r>v$.

X-ray study by N. G. Batalieva and A. A. Voronkov showed vlasovite to be monoclinic, space group not given, a 10.98±0.04, b 10.00±0.04, c 8.52±0.03 Å, β 100°24′±10′, Z=4. Unindexed *x*-ray powder data are given (52 lines); the strongest lines are 3.26 (100), 2.966 (94), 5.02 (72), 3.37 (61), 2.173 (61), 2.723 (49), 1.951 (49), 3.68 (45). Cleavages (010) distinct, a second imperfect cleavage at an angle of 88° to the first was observed under the microscope. Fracture irregular to conchoidal.

Vlasovite occurs near Mt. Vavnbed, Lovozero massif, Kola Peninsula, in the contact zone between pegmatites and fenites (arfvedsonitic alkalic syenites with eudialyte). It was formed in areas of strongly microclinized and albitized rock by replacement of eudialyte. Associated minerals include microcline, albite, arfvedsonite, aegirine, eudialyte, apatite, and fluorite.

The name is for K. A. Vlasov, Russian mineralogist and geochemist, who has done much work on the Lovozero Massif.

Discussion.—This is the Zr analogue of narsarsukite; the latter is tetragonal, however.

M. F.

Kilchoanite

S. O. Agrell, and P. Gay. Kilchoanite, a polymorph of rankinite. *Nature*, **189**, No. 4766, 743 (1961).

The mineral was found in limestones thermally metamorphosed by gabbro at Kilchoan, Ardnamurchan, Scotland, and Carlingford, Eire. It corresponds to phase Z (3 $Ca_3Si_2O_7 . H_2O$) synthesized by D. M. Roy (*Am. Mineral.* **43,** 1009 (1958) and described by Roy and others (*Nature*, **188,** 1187 (1960)). The mineral is colorless, optically biaxial, positive, *n*s α 1.647, γ 1.650, 2V 60°, dispersion distinct, $r>v$. In thin section the interference colors are commonly weak ultra-blue and ultra-brown.

X-ray data show it to be orthorhombic, space group *Imam* or *Ima*2, a 11.42, b 5.09, c 21.95 Å (all ±0.05 Å) *X*-ray powder data are given; the strongest lines are 2.89 (s), 2.68 (s), 3.07 (s), 3.56 (ms), 2.36 (ms), 1.964 (ms). When heated at 1000° C. for 10 hours, it inverts to rankinite.

Analysis of material containing no rankinite gave, after deducting all CO_2 as spurrite, the unit cell content

$$(Ca_{23.47}Mn_{0.03}Fe'''_{0.05})_{23.55}(Si_{15.71}Al_{0.35})_{16.06}O_{55.53}OH_{0.47}, \quad \text{or} \quad 8(Ca_3Si_2O_7).$$

Kilchoanite is associated with rankinite, which it replaces, spurrite, melilite, cuspidine, grossular, wollastonite, and vesuvianite.

The name is for the locality.

M. F.

Spencite

Clifford Frondel. Two yttrium minerals: spencite and rowlandite: *Canadian Mineralogist*, **6**, Pt. 5, 576–581 (1961).

The mineral was collected by H. S. Spence in 1934 from a prospect pit in Cardiff Township, Haliburton County, Ontario. It occurs as masses in a narrow pegmatite stringer in a vuggy pyroxenite, associated with calcite, red apatite crystals, diopside, purple fluorite, and wernerite. About 24 pounds of pure material was obtained. Cracks in the mineral contain a fine-grained white carbonate high in yttrium.

Analysis by C. O. Ingamells on 15 g. gave SiO_2 24.89, B_2O_3 10.04, P_2O_5 0.02, TiO_2 0.27, Al_2O_3 (including very little BeO) 3.87, Fe_2O_3 (total Fe) 3.22, MnO 0.60, MgO 0.50, CaO 7.81, SrO 0.05, Na_2O 0.11, K_2O 0.01, ΣY_2O_3 28.20, Ce_2O_3 1.44, ΣLa_2O_3 4.16, ThO_2 2.44, Cl 0.45, F 0.44, H_2O^+ 9.82, H_2O^- 1.93, sum $100.27-(O=F_2, Cl_2)0.28=99.99\%$. Spectrographic analysis by H. Bastron gave 10.0% B_2O_3. *X*-ray spectrographic analysis showed that ΣY_2O_3 is nearly all Y with very small amounts of the other elements, mainly Gd, Er, and Ho, and ΣLa_2O_3 shows only small amounts of the other elements, chiefly Nd. Optical and *x*-ray spectrographic analysis showed traces of U, Sn, Cu, Pb, Ni, Co, Zr, and Sc.

Calculating all the iron as divalent, Frondel recasts the analysis as

$$(Ca_{1.36}Fe_{0.39}Mg_{0.12}Mn_{0.09}Na_{0.04})_{2.0}(Y_{2.56}Ce_{0.09}La_{0.26}Th_{0.09})_{3.0}(Si_{4.25}B_{2.95}Al_{0.78}Ti_{0.03})_{8.0} \cdot (O_{18.21}(OH)_{1.42}F_{0.24}Cl_{0.13})_{20.0}$$

or in the structural form of the datolite group, as

$$(Ca, etc.)_{2.0}(Y, etc.)_{3.0}(B_{2.95}Si_{1.02}Ti_{0.03})_4(Si_{3.22}Al_{0.78}O_4)_4O_{16}(O_{2.21}(OH)_{1.42}F_{0.24}Cl_{0.13})_4.$$

The mineral is dark reddish brown to brownish-black, translucent in thin splinters, powder greenish gray. Luster weakly vitreous. Metamict, gives no *x*-ray diffraction pattern. Isotropic, *n* 1.627–1.653, mostly near 1.630. H. $3\frac{1}{2}$, G. 3.05. When heated in air at 325° for 46 hours was still isotropic, gave no diffraction pattern and the average *n* increased to 1.640 and G. to 3.20. The mineral decomposes at about 450–550°; heated in N_2 at 700–900° gave a light porous to slaggy mass; heated at 1050° gave a yellowish-white sintered mass; the *x*-ray pattern of the latter could not be identified.

The name is for Hugh S. Spence, Canadian Mineralogist.

M. F.

Hexastannite

Paul Ramdohr. Die Erzmineralien und ihre Verwachsungen, 3rd Ed., 1960, p. 514–515.

Name given, in analogy to the isotropic "isostannite" (of which a complete description has not yet been published), to "Zinnkies?" I, one of the many varieties of "stannite" recognized in microscopic work. Occurs partly as a product of unmixing, partly as a replacement of stannite with addition of Cu, rarely independently. Hexagonal, wurtzite structure, *a* 3.84, *c* 12.6 A, formula $Cu_3Fe_2SnS_6$. Optical data are given.

Discussion.—It would have been preferable not to name the mineral until more data were obtained.

M. F.

GEORGE BANTA COMPANY, INC., MENASHA, WISCONSIN, U